Investigation of the hepatotoxic potency of selected genotoxic pyrrolizidine alkaloids and the significance of the DNA damage response

D 386

vom Fachbereich Chemie der Technischen Universität Kaiserslautern zur Verleihung des akademischen Grades „Doktor der Naturwissenschaften“ genehmigte

Dissertation

von

Manuel Haas

geboren in Wiesbaden

Betreuer: Prof. Dr. Jörg Fahrer

Datum der wissenschaftlichen Aussprache: 14.05.2025

Der experimentelle Teil dieser Arbeit wurde im Zeitraum vom 01.11.2019 bis 31.03.2023 am Fachbereich Chemie, Fachrichtung Lebensmittelchemie und Toxikologie der Rheinland-Pfälzischen Technischen Universität (RPTU) Kaiserslautern Landau in der Arbeitsgruppe von Prof. Dr. Jörg Fahrer absolviert.

Eröffnung des Promotionsverfahrens: 19.04.2023

Promotionskommission

Vorsitzender:	Prof. Dr. Stefan Kubik
1. Berichterstatter:	Prof. Dr. Jörg Fahrer
2. Berichterstatter:	Prof. Dr. Dieter Schrenk

Für meine engstehende Familie, Feyza, Fabio und Florian,
die mich immer in schweren Zeiten unterstützt hatten

Table of contents

Abstract

Pyrrolizidine alkaloids (PAs) are secondary plant metabolites, which can occur as contaminants in predominantly plant-based foods. Only 1,2-unsatured PAs are bioactivated by cytochrome P450 (CYP450) enzymes, especially CYP3A4, into DNA reactive metabolites, which are known to be genotoxic and hepatoxic *in vivo*. The PA toxicity is strongly influenced by the chemical structure as demonstrated by several *in vitro* studies. However, quantitative genotoxicity data are needed, particularly in primary human hepatocytes (PHH). The organic cation transporter 1 (OCT1) has been identified as a key player in cellular uptake of cyclic diester, although little is known about a structure-dependent transport of PAs.

A major objective of the thesis was the investigation of the relationship between PA structure and the toxicity of PAs with different degree of esterification in human liver models (HepG2-CYP3A4 and PHH). An *in vitro* genotoxicity battery, consistently demonstrated the DNA damage markers γH2AX and p53, as well as the alkaline comet assay, confirmed a structure-toxicity relationship in HepG2-CYP3A4 cells. The data were subject to benchmark dose (BMD) modeling to derive the genotoxic potential of each PA. BMD modeling yielded values in the range of 0.1–10 µM for most cyclic and open diesters, with monoesters displaying lower genotoxic potency. Cyclic diesters such as retrorsine and seneciphylline showed the highest genotoxic potential. Furthermore, cyclic and open diesters showed comparable cytotoxic potentials with effective concentrations at 50% cell viability (EC_{50}) between 10 and 70 µM, with lasiocarpine at the top followed by seneciphylline. Besides, heliotrine and monocrotaline exhibited marked cytotoxic and genotoxic potentials, which were not comparable to other congeners within their degrees of esterification. Among the PA monoesters, only heliotrine was cytotoxic with an EC_{50} above 400 µM. Furthermore, heliotrine and monocrotaline exhibited significantly higher or lower toxic potentials, respectively, compared to PA congeners with the same esterification degree. Notably, the similar ranking was confirmed in PHH, with lasiocarpine exhibiting the highest genotoxic potential and approximately 3-4 times higher EC_{50} values for all PAs.

The second objective of the thesis was to study the role of OCT1 in the transport of structurally different PAs, i. e. riddelliine (cyclic diester), lasiocarpine (open diester) and heliotrine (monoester), in metabolically competent human liver cell models (HepG2-CYP3A4 and PHH) and hamster fibroblasts. Using pharmacological inhibitors against OCT1, we observed that the OCT1-mediated uptake is crucial for PA-induced cytotoxicity and genotoxicity, which was independently on PA structure. Both cell models, HepG2-CYP3A4 and V79-CYP3A4 revealed strongly attenuated cytotoxicity upon OCT1 inhibition. Notable, the reduced OCT1 expression in V79-CYP3A4 cells correlated well with their reduced susceptibility to PA-induced cytotoxicity. PHH confirmed the results in combination with OCT1 inhibition. Furthermore,

OCT1 inhibition reduced γH2AX and p53 levels, indicating less genotoxic stress. Consistently, OCT1 inhibition suppressed the DDR activation, as indicated by decreased checkpoint kinase phosphorylation during PA exposure.

Our findings strongly support the concept of grouping PAs into potency classes for risk assessment. Furthermore, the metabolic activation by CYP3A4 as well as OCT1 as uptake transporter play a major role for PA toxicity.

Zusammenfassung

Pyrrolizidinalkaloide (PAs) sind sekundäre pflanzliche Metaboliten, die als Kontaminanten vorwiegend in pflanzlichen Lebensmitteln vor. Nur 1,2-ungesättigte PAs werden durch CYP450-Enzyme, insbesondere CYP3A4, zu DNA-reaktiven Metaboliten bioaktiviert, die *in vivo* als genotoxisch und hepatotoxisch bekannt sind. Die PA-Toxizität wird jedoch stark von ihrer chemischen Struktur beeinflusst, wie einige *in vitro* Studien gezeigt haben. Allerdings sind quantitative Genotoxizitätsdaten erforderlich, insbesondere in primären menschlichen Hepatozyten (PHH). Darüber hinaus gibt es Hinweise, dass OCT1 eine Schlüsselrolle bei der zellulären Aufnahme von zyklischen Diestern einnimmt.

Ziel der Arbeit war die Untersuchung der Beziehung zwischen PA-Struktur und der Toxizität von PAs mit unterschiedlichem Veresterungsgrad in menschlichen Leberzellen (HepG2-CYP3A4 und PHH). Eine *in vitro* Genotoxizitätsbatterie, die aus den DNA-Schadensmarker γH2AX und p53 sowie den alkalischen Comet Assay einbezog, demonstrierte eine klare Struktur-Toxizitäts-Beziehung in HepG2-Zellen mit CYP3A4-Überexpression. Die Daten wurden einer Benchmark-Dosis (BMD)-Modellierung unterzogen, um das genotoxische Potenzial jedes PA abzuleiten. Die BMD-Modellierung ergab Werte im Bereich von 0,1–10 µM für die meisten zyklischen und offenen Diester, wobei Monoester eine geringere genotoxische Potenz zeigten. Zyklische Diester wie Retrorsin und Seneciphyllin wiesen das stärkste genotoxische Potenzial auf. Darüber hinaus demonstrierten zyklische und offene Diester vergleichbare zytotoxische Potenziale mit effektiven Konzentrationen bei 50% Zellviabilität (EC50) zwischen 10 und 70 µM, wobei Lasiocarpin an der Spitze lag, gefolgt von Seneciphyllin. Unter den Monoestern war nur Heliotrin zytotoxisch, wobei der EC_{50} über 400 µM betrug. Außerdem zeigten Heliotrin und Monocrotalin im Vergleich zu PA-Kongeneren mit demselben Veresterungsgrad ein deutlich höheres bzw. niedrigeres toxisches Potenzial auf. Interessanterweise wurde die gleiche Rangordnung in PHH bestätigt, wobei Lasiocarpin das höchste genotoxische Potenzial aufwies und 3 bis 4-fach höhere EC_{50}-Werte aller PAs bestimmt wurden.

Ein weiteres Ziel der Arbeit war die Untersuchung der Rolle des OCT1 im PA-Transport von struktur-abhängigen PAs, darunter Riddelliin (zyklischer Diester), Lasiocarpin (offener Diester) und Heliotrin (Monoester), in metabolisch kompetenten menschlichen Leberzellmodellen (HepG2-CYP3A4 und PHH) und Hamsterfibroblasten (V79-CYP3A4). Die Untersuchungen zeigten, dass die OCT1-vermittelte Aufnahme entscheidend für die PA-induzierte Zytotoxizität und Genotoxizität, unabhängig von der PA-Struktur, unter Verwendung pharmakologischer Inhibitoren gegen OCT1 ist. Beide Zellmodelle, HepG2-CYP3A4 und V79-CYP3A4, offenbarten stark abgeschwächte Zytotoxizität bei OCT1-Hemmung. Bemerkenswerterweise korrelierte die OCT1-Proteinexpression in V79-CYP3A4 mit ihrer reduzierten Anfälligkeit für

PA-induzierte Zytotoxizität überein. PHH bestätigten die Ergebnisse in Kombination mit OCT1-Hemmung. Darüber hinaus reduzierte die OCT1-Hemmung die γH2AX- und p53-Spiegel, was auf weniger genotoxischen Stress hinweist. Übereinstimmend hierzu unterdrückte die OCT1-Hemmung die DDR-Aktivierung, wie durch verringerte Checkpoint-Kinase-Phosphorylierung während der PA-Exposition angezeigt.

Unsere Ergebnisse unterstützen stark das Konzept, PAs in Potenzklassen für die Risikobewertung einzuteilen. Darüber hinaus spielen die metabolische Aktivierung durch CYP3A4 sowie OCT1 als Aufnahmetransporter eine wichtige Rolle für die PA-Toxizität.

Abbreviations

A	
ABC	ATP-binding cassette
A-T	Ataxia-telangiectasia
ATM	*Ataxia-telangiectasia* mutated
ATR	ATM- and Rad3-related
ATRIP	ATR-interacting protein
B	
BER	Base excision repair
BfR	Bundesinstitut für Risikobewertung
BMD	Benchmark dose
BMDL/U	Benchmark dose lower/ upper boundary
BMR	Benchmark response
Bw	Body weight
C	
cdc25	Cyclin division cycle 25 phosphatase
Cdks	Cyclin dependent kinases
CHK1	Checkpoint kinase 1
CHK2	Checkpoint kinase 2
CHO	Chinese hamster ovary
CI	Confidence interval
COT	Committee on Toxicity
CPDs	Cyclobutane pyrimidine dimers
CS	Cockayne syndrome
CYP450	cytochrome P450
D	
DNA-PK	DNA-dependent protein kinase
DSB	Double strand break
D-THP	D-Tetrahydropalmatine
E	
EC_{50}	Effective concentration at 50% cell viability
EDI	Estimated daily intake
EFSA	European Food Safety Authority
EMA	European Medicines Agency
F	
FA	Fanconi Anaemia
FMOs	Flavin-containing monooxygenases
G	
GG-NER	global genomic-NER
H	
HBGV	Health-based guidance value
HMPC	Committee on Herbal Medicinal Products
HR	Homologous recombination
HSOS	Hepatic Sinusoidal Obstruction Syndrome
I	
i.p.	Intraperitoneal
i.v.	Intravenous
IARC	International Agency for Research on Cancer
IARC	International Agency for Research on Cancer
iREP	Interim relative potency
J	
K	
L	

LD_{50}	Lethal dose at 50 % of the test population died
LOAEL	Lowest observed adverse effect level
LOD	Limit of detection
LPS	Lipopolysaccharides
M	
MCM	Minichromosome maintenance
MDCK	Madin-Darby canine kidney
Mdm2	Mouse double minute 2
MDR1	multi-drug resistance protein
MMEJ	Microhomology-mediated end joining
MMR	Mismatch repair
N	
NHEJ	Non-homologous end-joining
NOAEL	No observed adverse effect level
NTCP	Na^+/taurocholate co-transporting polypeptide
NTP	National toxicology programme of the U.S. Department of Health and Human Services
O	
OCT	Organic cation transporter
P	
P53	Tumor protein P53
PANOs	PA *N*-oxides
PAs	Pyrrolizidine alkaloids
PCE	Polychromatic erythrocytes
PCNA	Proliferating cell nuclear antigen
PCNA	Proliferating cell nuclear antigen
P-gp	P-glycoprotein
PHH	Primary human hepatocytes
PIG-A	Phosphatidylinositol glycan class A
Q	
qPCR	Quantitative real-time polymerase chain reaction
R	
RBC	Red blood cells
RFC	Replication factor
RPA	Replication protein A
S	
SLC	Solute carrier
SSB	Single strand break
ssDNA	Single-stranded DNA
T	
TC-NER	Trancription coupled-NER
TFIIH	Transcription factor IIH complex
TopBP1	Topoisomerase II binding protein
TP53	Tumor suppressor gene p53
U	
UDS-Assay	Unscheduled DNA-synthesis-Assay
UV	Ultraviolet
V	
W	
WHO	World Health Organization
X	
XP	Xeroderma pigmentosum
Y	
Z	
γH2AX	Phosphorylated Histon 2AX (Serine 139)

List of figures

List of tables

1 Introduction

PAs are a common group of phytotoxins produced as secondary metabolites in plants as defence against herbivores. Compared to other known phytotoxins, PAs are considered as the most widespread group (Fu et al. 2004). In the last centuries, PA outbreaks caused acute and sub-acute poisonings in animals by consumption of PA-forming plants and in humans by consumption of contaminated food such as herbal tea (Dusemund et al. 2017). Nowadays, acute PA intoxications occur rarely among humans, but commonly due to traditional herbal medicines or teas containing PA-plants (Colegate et al. 2015; Stegelmeier et al. 2016). Chronic PA intoxications have never been described in European countries, but they are more likely to occur due to long-term consumption of contaminated food and dietary supplements (Wiedenfeld 2011; Lis-Cieplak et al. 2024). Chronic PA toxicity studies in rodents report predominantly liver tumors, whereas extra-hepatic tumors of lung, pancreas and intestine are additionally observed (EFSA 2011). To date, only lasiocarpine, monocrotaline and riddelliine are classified as possible carcinogenic in humans (Group 2B) based on long-term carcinogenicity studies in in rats and mice (IARC 1983, 1987, 2002). Several lines of evidence demonstrate that 1,2-unsaturated PAs are both hepatotoxic and genotoxic. Notably, their genotoxic effects include DNA damage, chromosomal aberrations, sister chromatid exchanges and mutations. (Chen et al. 2010). PAs can be classified based on their structural features, *i.e.* the necine base or necine acids. It is commonly known that PAs with a higher degree of esterification are more toxic, whereby latest *in vitro* studies have shown exceptions. For instance, monocrotaline exhibited lower genotoxic effects compared to heliotrine (Louisse et al. 2019; Gao et al. 2020; Rutz et al. 2020). Moreover, a study discovered a link between PA exposure and liver cancer, particularly in Asia, by detecting pyrrole-protein adducts in 32% of hepatocellular carcinoma (HCC) patients and identifying a distinct PA-associated mutational signature. They confirmed through experimental models, including retrorsine-exposed mice and human liver cells, that PA exposure induces specific DNA damage and mutational patterns consistent with those observed in human liver cancer (He et al. 2021c). Given that liver cancer ranks as the 6th most common cancer globally and the 4th leading cause of cancer-related deaths, the chronic hepatotoxic and genotoxic effects of PAs warrant significant attention. HCC represents the most common form of liver cancer and is mainly induced by viral infections, followed by chronic alcohol consumption, diabetes, obesity or food carcinogens such as aflatoxins (IARC 2020; Llovet et al. 2021). The repeated oral exposure to PAs and insufficient detoxification mechanisms are particularly concerning due to their potential role in promoting the risk of HCC in humans (He et al. 2021c; Schrenk et al. 2022)

2 Theoretical backround

2.1 Occurrence and distribution of PA-producing plants and PAs

PA-producing plants are distributed globally and comprise about 3% of all flowering plants, with up to 13 known plant families (Wiedenfeld et al. 2008). More than 6,000 PA-producing plants exist, with plant families such as Asteraceae, Boraginaceae, and Fabaceae comprising the highest number of PA-producing species (Peloso et al. 2023). Only the families including *Asteraceae* (Compositae), *Apocynaceae*, *Boraginaceae*, *Fabaceae* (Leguminosae), *Ranunculaceae* and *Scrophulariaceae* produce 1,2-unsatured PAs, which are the toxicological point of interest (Mattocks 1986; Wiedenfeld et al. 2008). Exemplary pictures of PA-producing plants are shown in figure 2.1. Furthermore, PA monoesters and open-chained diesters are mainly found in Boraginaceae, whereby cyclic diesters are commonly produced in *Senecio* species of Asteraceae and Fabaceae (Hartmann and Witte 1995). Up to the 1990s, comprehensive investigations were carried out on the occurrence of different PAs in various plant species (Mattocks 1986). Exemplary PAs found in plant genera or subspecies are listed in table 2.1 (Mattocks 1986; Teschke et al. 2021; Tábuas et al. 2024). Nowadays, only a few plant species, such as *Borago officinalis* (borage) or *Tussilago farfara* (coltsfoot), are screened for the sum of PAs due to their use in food such as salad, herbal tea or oil-based supplements (Mulder et al. 2015; Avila et al. 2020). It is important to note that PAs are commonly found in plant genera, such as *Crotalaria*, *Cynoglossum*, *Eupatorium*, *Heliotropium*, *Petasites*, *Senecio* and *Symphytum* (Wiedenfeld 2011).

PAs are present in various organs of PA-producing plants. The highest PA amount is found in the roots, which is due to the predominant biosynthesis of PAs in this organ (Tábuas et al. 2024). As example, in many *Senecio* subspecies PA concentrations are up to 100-fold higher in roots as compared to aerial parts (Muetterlein and Arnold 1993). In addition, the PA content varies from species to species, as well as in response to environmental conditions and according to the geographical location (Peloso et al. 2023). A great variability in the PA amount and pattern can be triggered by abiotic or biotic stress such as root damage (Boppré 2011). Factors such as soil properties, nutrients, water quantity, herbivore infestations and climate changes also have an impact on the PA content (Schramm et al. 2019). Furthermore, a transfer of PAs in soil and surface water is promoted during raining events (Hama and Strobel 2021). It should be noted that plant species do not provide only a single PA, but contain a plethora of structurally diverse PAs (Hartmann and Witte 1995). Additionally, PAs exist in plants both as free base and the corresponding *N*-oxide (PANO) (Stegelmeier 2011). For example, *S. jacobaea* contains up to 30 PAs and PANOs, whereby *E. plantagineum* comprises only up to 14 as sum of both (Weston et al. 2013; Hama and Strobel 2021).

PA-forming plants can be found as a weed or crop plant along rivers, in fields, meadows, or at different altitudes, regardless of the prevailing climatic or local conditions. For example, *S. jacobea*, commonly known as 'ragwort', grows along streets and forest edges, or in areas where natural vegetation has been disrupted by floods or fires. It is predominantly found in Asian and European countries (Günthardt et al. 2020; Hama and Strobel 2021). In contrast, *H. indicum* ("hatisur") is mainly found in gardens, roadsides and waste lands and is widespread in tropical parts of Asia and Africa (Sarkar et al. 2021). Consequently, PA-producing plants are globally distributed across diverse habitats, allowing for their accessibility to humans and animals (EFSA 2011).

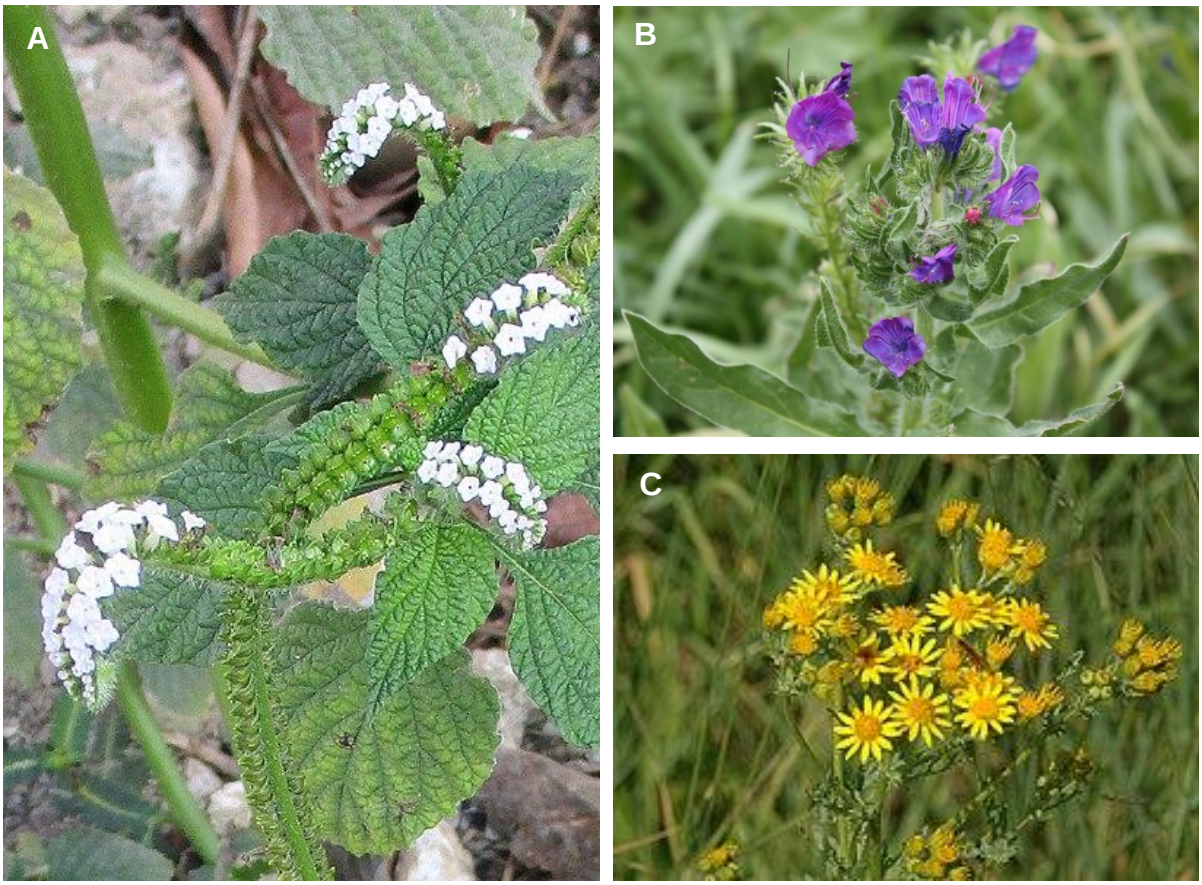

Figure 2.1: Examples of PA-producing plants. A: *Heliotropium indicum*[1]. **B**: *Echium plantagineum*[2], **C**: *Senecio jacobea*[3]

[1] By David E Mead- Own work, public domain, https://commons.wikimedia.org/wiki/File:Indian_heliotrope_(Heliotropium_indicum)_La%27ea_Buton_Island_2.jpg
[2] By Phil41 – Own work, public domain, https://commons.wikimedia.org/w/index.php?curid=9893486
[3] By Gary Houston Ghouston- Own work, public Domain, https://commons.wikimedia.org/wiki/File:20050716-008-ragwort.jpg

Table 2.1: **Examples of PAs synthesized in specific plant genera and their subspecies**

PAs (selected)	Plant families	Plant genera and their subspecies
Echimidine	Asteracea, Boraginaceae	*Eupatoriae, Echium, Symphytum*
Europine	Boraginaceae	*Heliotropium, Trichodesma africana*
Heliotrine	Boraginaceae	*Heliotropium*
Indicine	Apocynaceae, Boraginaceae	*Parasonsia, Heliotropium*
Lasiocarpine	Boraginaceae	*Heliotropium, Lappula intermedia, Symphytum*
Lycopsamine	Asteraceae, Apocynaceae, Boraginaceae	*Parasonsia, Amsinckia, Anchusa officinalis, Borago officinalis, Heliotropium steudneri, Messerschmidia sibirica, Symphytum uplandicum, Eupatorium compositifolium, Lithospermum canescens*
Monocrotaline	Boraginaceae, Fabaceae	*Lindelofia spectabilis, Crotalaria*
Retrorsine	Asteraceae, Fabaceae	*Brachyglottis*, *Senecio, Tussilago farfara, Crotalaria*
Riddelliine	Asteraceae, Fabaceae	*Senecio, Crotalaria juncea*
Senecionine	Asteraceae, Fabaceae Ranunculaceae, Scrophulariaceae	*Brachyglottis, Emilia flammea, Erechtites heiracifolia, Petasites, Senecio, Crotalaria, Caltha, Castillega rhexifolia*
Seneciphylline	Asteraceae, Fabaceae	*Adenostyles, Cineraria*, *Erechtites heiracifolia, Tussilago farfara, Senecio, Crotalaria juncea*

2.2 Chemical structure of PAs

PAs are composed of a 1-hydroxymethyl pyrrolizidine (necine base) and one or two esterified acids (necine acids) (Figure 2.2). At the chemical level, the necine base represents a pyrrolizidine backbone with a hydroxymethyl group at C1 and a hydroxyl group at C7. One or both hydroxyl groups can be esterified with mono or dicarboxylic acids to form PAs with different degrees of esterification. Based on the stereoselectivity and composition of both main compartments, a high structural diversity is present among PAs. To have a comprehensive overview and understanding of the structure of PAs, they are classified according to their necine base or the degree of esterification (Mattocks 1986; Wiedenfeld et al. 2008).

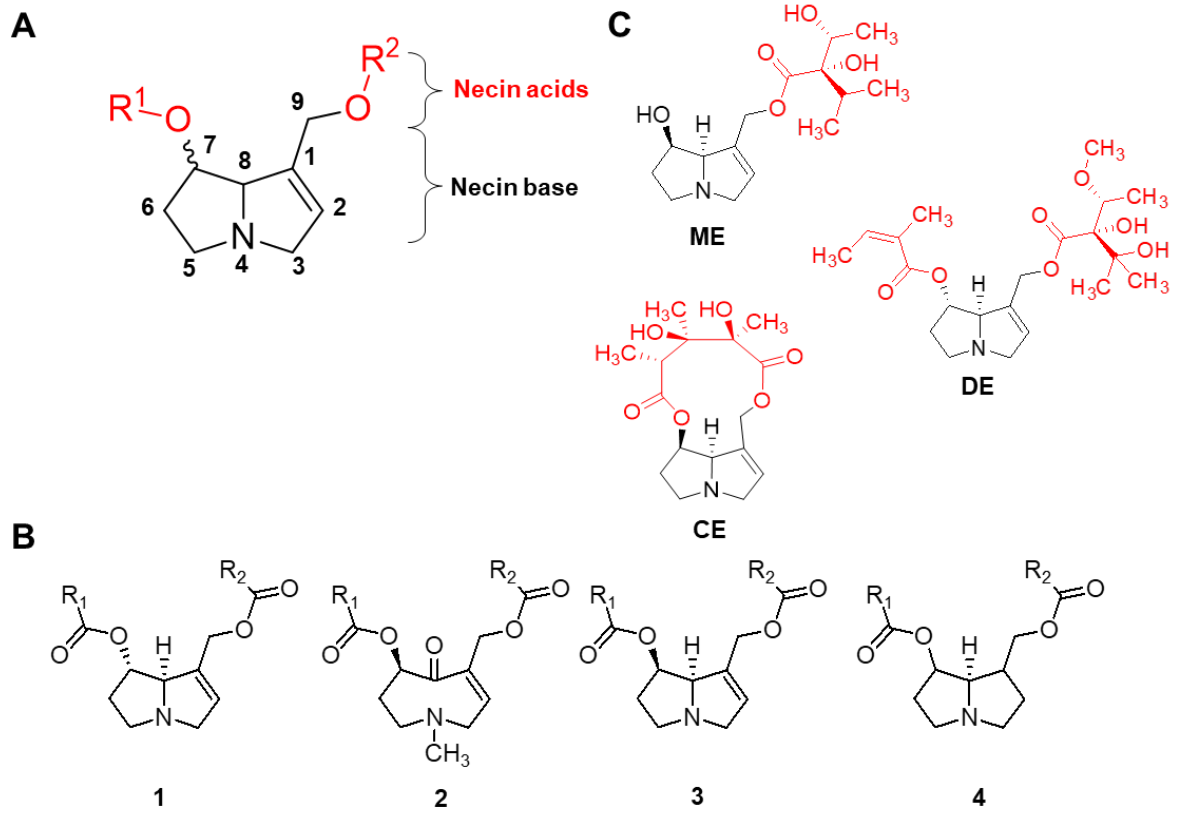

Figure 2.2: Chemical structure and structural features of PAs. **A**: Hetereocyclic structure of PAs composed of a necin base and one or two esterified necin acids. **B**: Classification of PAs based on the necin base: (1) heliotridine-type, (2) otonecine-type, (3) retronecine-type and (4) platynecine-type PAs. **C**: Classification of PAs based on the degree of esterification: ME: monoesters, DE: open diesters. CE: cyclic diesters (modified by Mattocks 1986, Fu et al 2004).

In terms of the necine base, PAs can be divided into four groups, known as retronecine-, heliotridine-, otonecine- and platynecine-type PAs (Figure 2.2B). Furthermore, the retronecine- , heliotridine and platynecine-type PAs occur mostly in an oxidized form in PA-producing plants). Retronecine- and heliotridine-type PAs such as lycopsamine and heliotrine are enantiomers according to the carboxyl group at C7. Otonecine-type PAs including e.g. clivorine, contain a carbonyl group in the ring system. Only platynecine-type PAs like platyphylline do not possess a double bond at the C1-C2 position. It is noteworthy, that only

1,2-unsatured PAs are of interest due to their bioactivation via CYP450 enzymes into DNA and protein reactive agents (Mattocks 1986; Wiedenfeld et al. 2008). The chapter 2.3.3 describes the metabolization of 1,2-unsaturated PAs in more detail.

On the other hand, PAs can be classified by their degree of esterification as monoesters, open-chained diesters and cyclic diesters (Figure 2.2C), whereas the latter are formed by the double esterification with dicarboxylic acids such as riddellic acid or isatinecic acid (Mattocks 1986). In general, the esterification of necine bases takes place at the C7 and C9 hydroxy groups. Most of the monoesters show an esterified acid on C9, except 7-angelyl heliotridine/ retronecine or 7-senecioyl retronecine (Mattocks 1986). The term “necine acid” is used to distinguish between monocarboxylic acids and dicarboxylic acids, as well as between aromatic monocarboxylic acids (e.g. benzoic acid) and dicarboxylic acids with eleven and/or twelve members (Schramm et al. 2019). Necine acids differ in their carbon chain length, acidity, branching degrees or in their functional groups, resulting in a structural complexity among PAs (Wiedenfeld et al. 2008). In addition, some necine acids, such as angelic or trachelanthic acid, are commonly found in different PAs, and there are also PA-specific necine acids such as senecic acid. Angelic acid consists of an α,β-unsaturated carbonyl group, whereas the monocrotalic acid is saturated and loaded exclusively with hydroxyl groups (Mattocks 1986). Interestingly, monocrotalic acid does not contain an α,β-unsaturated carbonyl group, unlike senecic, seneciphyllic, riddelliic or isatenecic acid (Tábuas et al. 2024). A detailed overview of the structure of exemplary PAs is given in Table 2.2 and Figure 2.3.

Table 2.2: Examples of PAs and their chemical composition (Tabuas et al 2024, Mattocks 1986)

PAs	Necine base	Necine acids
Clivorine	Otonecine	Clivonenic acid (dicarboxylic)
Echimidine	Retronecine	C7-angelic acid; C9-echimidenic acid
Europine	Heliotridine	C9-lasiocarpic acid
Heliotrine	Heliotridine	C9-heliotric acid
Indicine	Retronecine	C9-(–)-trachelanthic acid
Lasiocarpine	Heliotridine	C7-angelic acid; C9-lasiocarpic acid
Lycopsamine	Retronecine	C9-(–)-viridofloric acid
Monocrotaline	Retronecine	Monocrotalic acid (dicarboxylic)
Platyphylline	Platynecine	Senecic acid (dicarboxylic)
Retrorsine	Retronecine	Isatinecic acid (dicarboxylic)
Riddelliine	Retronecine	Riddellic acid (dicarboxylic)
Senecionine	Retronecine	Senecic acid (dicarboxylic)
Seneciphylline	Retronecine	Seneciphyllic acid (dicarboxylic)

Several studies have shown that the classification of 1,2-unsatured PAs based on the degree of esterification is the most meaningful, as it recognizes distinct differences in PA toxicokinetic and toxicity. For instance, *in vitro* and *in vivo* studies have demonstrated that cyclic esters and open diesters exhibit considerably higher toxicity than monoesters. Furthermore, PA individuals within an esterification group, such as monocrotaline or heliotrine, also differ in toxicokinetic and toxicity (Louisse et al. 2019; Gao et al. 2020; Rutz et al. 2020; To et al. 2024). In the following chapters, shared and individual PA characteristics in toxicokinetic and toxicity are given in detail.

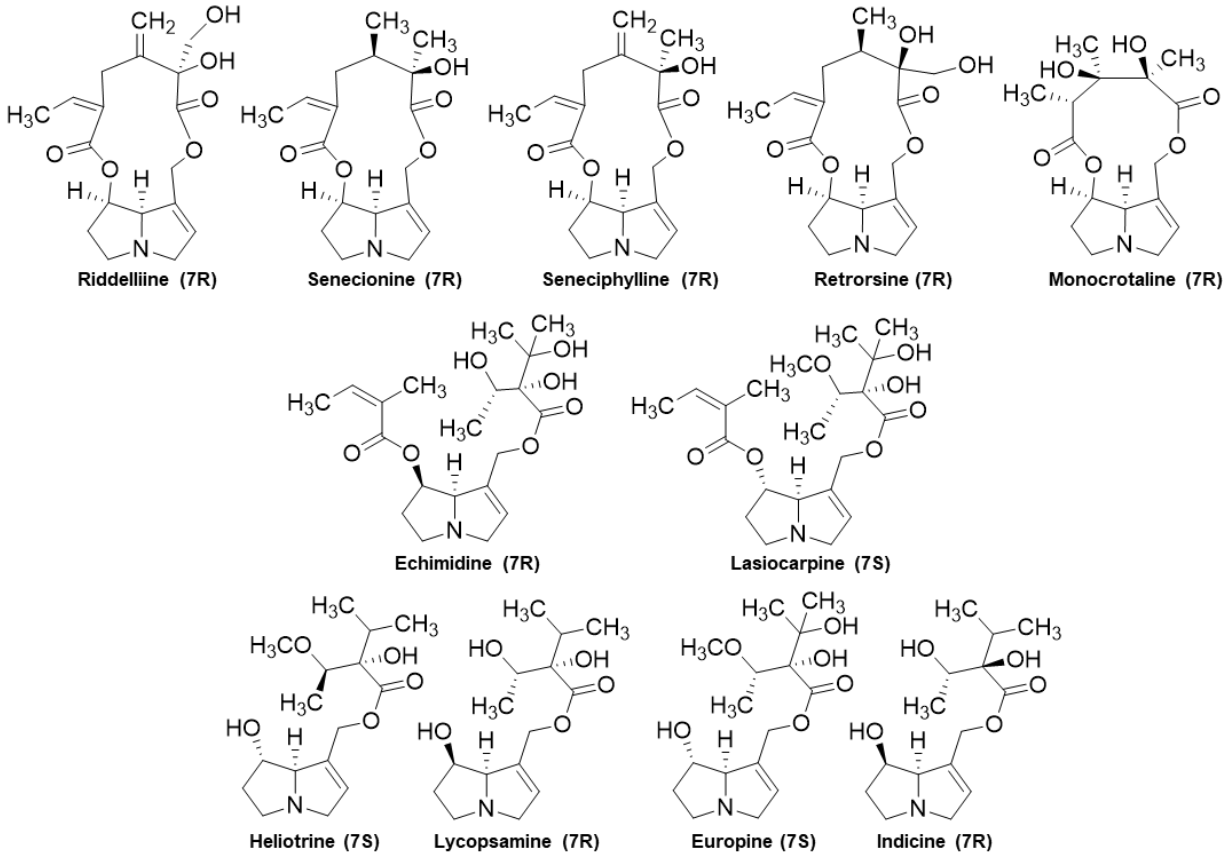

Figure 2.3: Chemical structures of selected PAs. PA cyclic diester (riddelliine, senecionine, seneciphylline, retrorsine, monocrotaline), PA open diester (lasiocarpine, echimidine) and PA monoester (heliotrine, lycopsamine, europine, indicine) are displayed.

2.3 Toxicokinetic aspects / ADME

2.3.1 Absorption

2.3.1.1 Dermal and oral bioavailability

PA bioavailability is primarily determined by two distinct exposure routes: dermal and oral(Prakash et al. 1999; Stickel and Seitz 2000). PAs intake occurs primarily via the oral route, although dermal uptake of PAs is also possible due to herbal medicinal products derived from plant parts such as *Crotalaria sessiliflora L*. for topical applications (Roeder 2000; Jedlinszki et al. 2017). The dermal absorption of PAs is considered low, although the available data is sparse. As example, lycopsamine showed a dermal absorption between 0.11 - 0.72% within 24 h through a synthetic membrane and 0.04 – 0.22% through human epidermis after 24 h exposure (Jedlinszki et al. 2017). In contrast, PAs are rapidly absorbed within the first hour (10-70 min) after oral administration, as shown by plasma peak concentrations (EFSA 2011; Yang et al. 2017). It is noteworthy that predominantly cyclic diesters were tested *in vivo*, yet they are showing different toxicokinetics among the esterification class (Williams et al. 2002; Wang et al. 2011; To et al. 2024). As example, the bioavailability of monocrotaline was over 3-fold higher compared to retrorsine (83% vs 25%) in rats after oral administration for 12 h (To et al. 2024). Based on the numbers, it seems that monocrotaline is more readily absorbed and systematically available as compared to retrorsine. However, a lower bioavailability can result from a first-pass effect or reduced gastrointestinal absorption. Retrorsine showed almost three times higher pyrrole protein adduct formation in the red blood cell fraction as compared to monocrotaline, indicating that its lower bioavailability is likely due to faster and more extensive metabolic activation, which correlates with higher PA toxicity (To et al. 2024).

Wang and colleagues found similar results with senecionine and adonifoline, two cyclic diester, in rats after oral administration. Adonifoline exhibited an absolute bioavailability four times greater than senecionine (33.4% vs. 8.2%), while the combined levels of senecionine and its *N*-oxides were 2.7 times higher than those of adonifoline and its *N*-oxides (Wang et al. 2011). The authors attributed this to a higher rate of senecionine *N*-oxide formation by intestinal microflora. This study is in line with a recently published rodent study (Long et al. 2021). Rats were orally treated with single doses of senecionine and senecionine *N*-oxide and blood samples were collected at specific time-points. Subsequently, oral bioavailabilites between 5.43 - 10.31% and 37.85 - 42.51% were calculated depending on the dose for senecionine and senecionine N-oxide (Long et al. 2021).

Li et al showed a bioavailability of 81.8% for retrorsine in mice after oral administration up to 24 h, indicating that the bioavailability differs between rats and mice (Li et al. 2022; To et al. 2024). However, the bioavailability of monocrotaline in rats (83%) is comparable to that in mice (88.3%), showing no inter-species differences in contrast to retrorsine (Chen et al. 2018; To et

al. 2024). Over the years, only one study investigated the bioavailability of an open diester (lasiocarpine) and a monoester (heliotrine) *in vivo*, showing an absolute bioavailability of 0.5% for lasiocarpine and 23.3% for heliotrine in rats (Lin et al. 2023a).

Moreover, PAs as free bases show a significantly greater intestinal absorption compared to their respective *N*-oxides, explaining the lower hepatotoxicity of *N*-oxides, as shown in plasma and blood measurements (Yang et al. 2020). Furthermore, free bases are more lipophilic based on calculated Log P octanol/water coefficients and show a significantly greater absorption in Caco-2 monolayer model compared to their respective *N*-oxides (Yang et al. 2020). Although the intestinal uptake of PAs is considered to be low, both PAs and their *N*-oxides are capable of inducing Hepatic Sinusoidal Obstruction Syndrome (HSOS) (Yang et al. 2017). Furthermore, there is evidence that rat intestinal microbiota reduces PANOs to their free bases, which affects the level of PA uptake through the intestine and transport to the liver (Yang et al. 2019). The biotransformation of several PANOs such as riddelliine *N*-oxide has been studied *in vitro* and *in vivo*, showing a NADPH-dependent conversion of *N*-oxides to free bases, which is mainly catalyzed by CYP1A2 and CYP2D6 enzymes (Yang et al. 2019).

Several *in vitro* studies investigated the uptake of different PAs in cell models including human colon and liver cells to explain inter-species differences and find common characteristics, which will be briefly summarized in the following subchapter.

2.3.1.2 Passive diffusion versus transporter-mediated absorption

The transport across cellular membranes can occur via passive diffusion or transporter-mediated uptake. Passive diffusion represents the major route by which molecules move across the intestinal barrier without the aid of transport proteins, driven by a concentration gradient without the use of energy (Sugano et al. 2010; Yang and Hinner 2015). According to Lipinski's "Rule of 5", the membrane permeability of a substance for passive diffusion can be predicted by polarity, size and lipophilicity (Lipinski et al. 2001). Consequently, a successful penetration through the cellular membrane via passive diffusion is possible if the molecule is small, nonpolar and lipophilic. The diffusion rate is influenced by the solute concentration gradient, osmosis, electrical potential difference and pressure across the cell membrane (Sahoo et al. 2014). It has recently been demonstrated that PAs as free bases such as senecionine, seneciphylline, retrorsine, riddelliine, lycopsamine can cross from apical to basolateral side in Caco-2 cells via passive diffusion. Furthermore, each PA showed different permeabilities and had a significantly greater permeability than their respective *N*-oxides in Caco-2 cells (Yang et al. 2020). It is possible that transporters may play a minor role in the uptake and release of PAs with a high permeability rate, as passive diffusion is the predominant mechanism (Kell and Oliver 2014). The mode of uptake is also influenced by the pH level. A study conducted with monocrotaline in genetically modified Madin-Darby canine kidney

(MDCK) cells expressing human OCT1 revealed that, in the protonated state, organic cation transporter 1 (OCT1) plays a more significant role in uptake (Tu et al. 2013).

Transporters are proteins embedded in the cell membrane that facilitate the uptake and release of substances often against their concentration gradient. This process requires energy either directly from ATP hydrolysis (primary active transport) or from the electrochemical gradient of another molecule (secondary active transport) (Liu and Pan 2019). Around 10% of all human genes are related to transporters and are involved in drug absorption, distribution and excretion, highlighting their important role (Hediger et al. 2013). The two superfamilies of transporters that are of interest in this context are the solute carrier (SLC) and ATP-binding cassette (ABC) transporters. A large number of transporter subfamilies, such as *SLC10A* or *SLC22A*, belong to the SLC superfamily, which in total comprises over 300 transporter subtypes. Only seven subfamilies are known in the ABC family, which share up to 40 transporter subtypes. In general, both SLC and ABC transporter can be found in the same tissue including intestine, liver, kidney and brain, and interact together with phase I or II metabolism (Liu and Pan 2019). The figure 2.4 illustrates the expression of SLC and ABC transporter in human hepatocytes. However, the transporter superfamilies can be distinguished in their mode of action.

SLC transporters primarily mediate the influx of substrates into cells via facilitated transport or as secondary active transporter. For example, the *SLC22A* subfamily comprise organic cation transporters (OCTs), which allow the influx of cationic substrates such as active pharmaceutical ingredients (e.g. oxaliplatin), endogenous substrates (e. g. acetylcholine), nutrients (e. g. Vitamin B1) and the neurotoxin 1-methyl-4-phenyl-pyridinium (Koepsell 2013; Liu and Pan 2019; Zeng et al. 2023). The main members OCT1-OCT3 (*SLC22A1*-*SLC22A3*) share common substrates, which allow for the substitution of each transporter (Brosseau and Ramotar 2019). Nevertheless, the OCT expression is tissue- and species-dependent. For example, OCT1 is primarily found in hepatocytes and OCT2 is mainly located in renal tubular cells (Brosseau and Ramotar 2019; Morse et al. 2021). On the other hand, OCT3 expression is located in many tissues such as liver, intestine and heart (Roth et al. 2012). For instance, the highest OCT1 expression levels are found in humans and monkeys compared to rodents and dogs (Morse et al. 2021). In the past, some studies found evidence that cyclic diester including monocrotaline and retrorsine are taken up into genetically engineered MDCK cells with human OCT1 expression and in primary rat hepatocytes (Tu et al. 2013, 2014). Furthermore, it was shown that both OCT1 and Na^+/taurocholate co-transporting polypeptide (*SLC10A1*, NTCP) are responsible for the uptake of retrorsine and senecionine in HepaRG cells (Enge et al. 2021, 2022). So far, it remains unclear whether the chemical structure of PAs has an impact on the OCT1-mediated uptake into human hepatocytes.

In contrast, ABC transporters use ATP to actively export substances out of cells. The ABC transporter *ABCB1*, also known as P-glycoprotein (P-gp) or multi-drug resistance protein (MDR1), is known for the efflux transport of hydrophobic substrates such as colchicines or aristolochic acid or drugs including doxorubicin or irinotecan (Liu and Pan 2019). P-gp is expressed in several tissues including capillary endothelial cells of testis and brain, in bile canalicular membrane of hepatocytes and intestine (Leschziner et al. 2007). Two studies confirmed the relevance of *ABCB1* as efflux transporter for PAs with different degree of esterification (senecionine *N*-oxide, echimidine and heliotrine) in Caco-2 cells (Hessel et al. 2014; Yang et al. 2020). Another *study* highlighted the role of *ABCB1* as an efflux transporter for the cyclic diesters retrorsine and senecionine by demonstrating that cyclosporine A acts as a competitive inhibitor of the *ABCB1* transporter in HepaRG cells, leading to significantly increased cell viability (Enge et al. 2021).

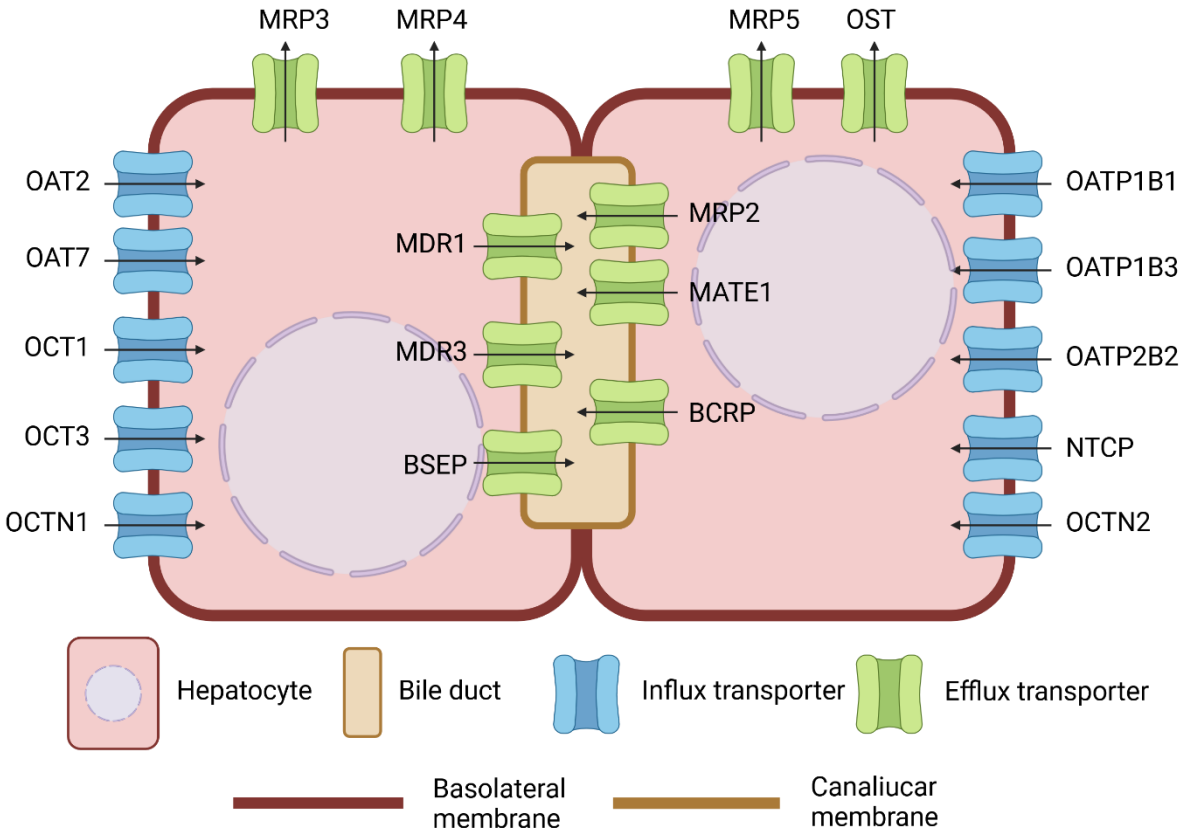

Figure 2.4: Influx and efflux transporter located in basolateral and canalicular membrane of hepatocytes (modified by Liu and Pan 2019, created in https://BioRender.com)

2.3.2 Distribution and Excretion:

In the last decades, only a limited number of new findings on the distribution and excretion of PAs in animals were reported. To date, no studies have been conducted to investigate the distribution and excretion of structurally different PAs in a cell system. It was demonstrated in rodent studies that cyclic diesters such as monocrotaline, riddelliine and senecionine were detected in organs including the liver, lung, kidney, erythrocytes, plasma and brain (EFSA 2011; Silva et al. 2023). Furthermore, it has been observed that more than 80% of a given dose of PA is eliminated within 24 h via urine and bile in mice and rats (EFSA 2011).

In terms of tissue distribution, two studies were conducted using monocrotaline in rats (Estep et al. 1990; Lamé et al. 1997). The results demonstrated that following a single subcutaneous or intravenous administration of 5 and 60 mg/kg ^{14}C-labelled monocrotaline, monocrotaline equivalents were present in different tissues and covalently attached to proteins in various organs, including red blood cells, liver, lungs, kidney and plasma. In general, the level of radioactivity declined in most of the tissues and proteins following a 24-hour period, with the exception of erythrocytes. The authors suggested that erythrocytes may play a role as carrier of monocrotaline or its metabolites between organs (Estep et al. 1990; Lamé et al. 1997).

It was demonstrated *in vivo* after oral PA administration that metabolites of monocrotaline, retrorsine, or riddelliine bind to erythrocytes and disrupt the oxygen-carrying capacity (Xiao et al. 2019; Song et al. 2020). Xia and colleagues concluded that in venous blood, low oxygen pressure allows monocrotaline pyrroles to bind on hemoglobin. In the lungs, higher oxygen pressure displaces these metabolites, releasing them into pulmonary capillaries. This targeted release leads to pulmonary artery damage, characterized by endothelial injury and smooth muscle layer thickening (Xiao et al. 2019). However, PA adducts were found predominantly in the liver rather than in lungs regardless of the PA individual such as riddelliine or retrorsine. Notably, only monocrotaline showed almost the same adduct level in both organs (Song et al. 2020).

To and colleagues determined the toxicokinetic parameters of three cyclic diesters (monocrotaline, retrorsine and clivorine) in rats following a single intravenous and oral administration of 20 mg/ kg bw of the respective PA. The half-lifes were found to be approximately 1 h, with no significant differences between the administration routes. Nevertheless, monocrotaline followed by clivorine and retrorsine exhibited the slowest elimination based on clearance (To et al. 2024).

Wang et al. conducted a comparative study on the pharmacokinetics of two cyclic diesters, senecionine and adonifoline, in rats. After a single i.v. dose of 1.5 and 4.0 m g/ kg body weight (bw) of the respective PAs, an initial rapid decline in concentration was observed, which slowed down between 4-6 h. The plasma concentrations of senecionine and adonifoline fell below the

detection limits within 12 h. Following oral administration of 5.7-22.9 mg/ kg bw senecionine or 16-64 mg/ kg bw adonifoline, half-lives of less than 1 h and their metabolites of approximately 2 h were determined (Wang et al. 2011). Furthermore, the first evidence of an enterohepatic recirculation with senecionine N-oxide as the main metabolite in bile was demonstrated (Wang et al. 2011). An enterohepatic circulation was also observed in mice with retrorsine, which was responsible for the formation of HSOS in mice (Xiao et al. 2019).

The distribution and excretion of unmetabolized PAs and their metabolites in the physiological body depend on their lipophilicity, affinity to erythrocytes and proteins in whole blood or cellular compartments such as F-actin (Deleve et al. 2003a, b, c; Widjaja et al. 2022). Furthermore, the distribution of PAs and their metabolites in human body could be affected by membrane associated influx and efflux transporter such as OCT1 or *ABCB1* (Widjaja et al. 2022). It is known that monocrotaline has a higher affinity to red blood cells (RBC) than to plasma proteins, as shown via H-NMR in incubated human blood samples (Yang et al. 2011). Recent studies have indicated that pyrrole-protein adducts (PPA), which are PA metabolites covalently bound to proteins such as haemoglobin or albumin, can be found circulating in the body and therefore represent potential biomarkers (Ma et al. 2019). In general, PPA levels bound to erythrocytes are higher than those on plasma proteins for PAs including retrorsine, monocrotaline and clivorine (To et al. 2024). This can be explained by the longer life span of erythrocytes compared to plasma (115 days vs. $T_{1/2}$ = 19 days) and by the nucleophilic sites of haemoglobin compared to albumin (Franco 2012; Mishra and Heath 2021).

2.3.3 Metabolism

The metabolism of PAs and PANOs has been extensively studied *in vitro*, *ex vivo* and *in vivo* (JECFA 2020). Upon oral ingestion of PA-contaminated foods, PAs are rapidly absorbed through the small intestine and transported via portal vein blood into the liver (NTP 2003). The biotransformation of PAs takes place predominantly in the liver and include several phase I and II metabolic pathways. The involvement of phase I or phase II enzymes in the bioactivation of PAs is dependent of the necine-base type and steric hindrance of ester groups (He et al. 2021d). The major metabolic pathways including hydrolysis (I), *N*-oxidation (II), *N*-glucuronidation (III) and *C*-oxidation (IV) for PA bioactivation are demonstrated in Figure 2.5.

Retronecine-, heliotridine- and otonecine type PAs undergo hydrolysis of the ester groups at the C7 and C9 position mainly by liver microsomal carboxylesterases to form their respective necine bases and necine acids (Fu et al. 2004). This pathway is regarded as a detoxification pathway, facilitating the rapid excretion of metabolites from the urine without the involvement of Phase II metabolism (Hosokawa et al. 1990). Another known detoxification pathway is the *N*-oxidation of the necine bases. This pathway is initiated by hepatic CYP450 monooxygenases and flavin-containing monooxygenases (FMO), which are located in the endoplasmatic reticulum of the hepatocytes (Fu et al. 2004; Hodgson 2010). As example, senecionine or retrorsine are catalysed to the respective *N*-oxide by hepatic CYP2B and FMO in guinea pigs (Ramsdell and Buhler 1987; Miranda et al. 1991; Chung et al. 1995; Duringer et al. 2004). However, the *N*-oxidation of otonecine-type PAs is not feasible due to the methylated nitrogen in the pyrrole moiety (Fu et al. 2004). Furthermore, the *N*-oxidation of PAs by CYPs and FMOs is dependent on both species and organ. For instance, the *N*-oxidation of senecionine is induced by FMOs from rat liver microsomes and pig liver, lung and kidney microsomes, whereby rabbit lung FMOs are not capable for the formation of PANOs (Miranda et al. 1991). Although *N*-oxides are frequently regarded as a detoxification product, they can be transformed into the reduced form and further oxidized by intestinal and hepatic CYP enzymes, resulting in the formation of DNA-reactive metabolites that subsequently induce toxicity (Yang et al. 2017, 2019). The *N*-glucuronidation of PAs (senecionine and senecionine *N*-oxide) mediated by glucuronosyltransferases was identified as a third detoxification pathway, giving rise to a PA *N*-glucuronic acid (GluA) conjugate in (UGT)1A4-humanised mice and in presence of human liver microsomes (He et al. 2010; Chen et al. 2022b, 2023).

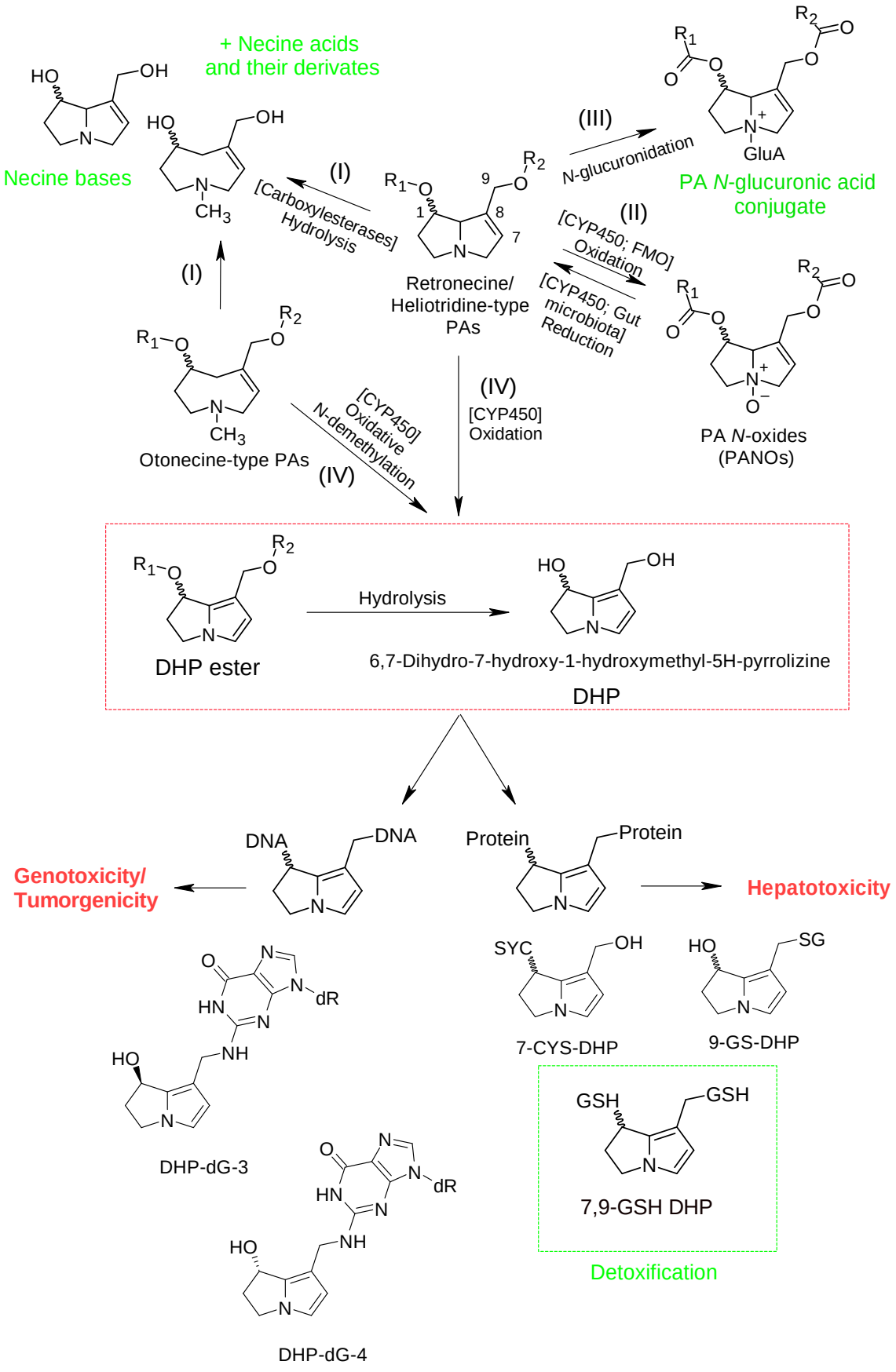

Figure 2.5: Metabolism of retronecine-, heliotridine- and otonecine-type PAs. Important metabolic pathways for detoxification and metabolic activation to DNA-reactive metabolites are shown (modified by He et al. 2021a; Xiao et al. 2022)

The last pathway, the so-called *C*-oxidation, is mediated by several CYPs, but not FMO, and includes the hydroxylation of only 1,2-unsatured PAs into DNA- or protein-reactive metabolites (Prakash et al. 1999; Fu et al. 2004). Ruan et al. showed that structural diverse PAs in presence of human recombinant CYPs are predominantly metabolized by CYP3A4, 3A5 and CYP2A6 (Ruan et al. 2014b). Whereas retronecine-type PAs were predominantly activated by CYP3A4 and 3A5, monocrotaline (retronecine-type) was shown to be predominantly converted by CYP2A6 and minor CYP2E1 (Ruan et al. 2014b). It is noteworthy that not only one, but several CYP enzymes are involved in PA bioactivation as shown in a genetically engineered TK6 cells (Li et al. 2020). The subfamilies CYP3A and CYP2B were mainly responsible for the bioactivation of PAs in rodents (Chung et al. 1995; Huan et al. 1998). The hepatic metabolism of PAs is also dependent on gender, species and age, whereby males and sensitive species including human, rat, horse show a higher biotransformation and lower degradation rate of PAs. Children are more vulnerable due to the proportionally higher intake of PA relative to their body weight. (Wiedenfeld et al. 2008; Kolrep et al. 2018).

The PAs of the retronecine- and heliotridine-type PAs are hydroxylated at the C3 and C8 positions by CYP enzymes, resulting in the formation of 3- or 8-hydroxynecine derivatives. These derivatives undergo spontaneous dehydrogenation, leading to the generation of (±)-6,7-dihydro-7-hydroxy-1-hydroxymethyl-5H-pyrrolizine esters (DHP ester). Otonecine-type PAs undergo *N*-demethylation mediated by CYP enzymes, followed by ring closure and spontaneous dehydration to form DHP ester (Fu et al. 2004; Xia et al. 2004). Platynecine-type PAs do not contain a C1-C2 double bond position and undergo oxidation via CYP3A4 to form dehydro-platyphylline carboxylic acid, which is readily excreted via urine (Ruan et al. 2014a). DHP esters can subsequently release a carboxylate leaving group from C7 or C9 position to form intermediates with carbocations. These carbenium ions interact through an SN1 mechanism at nucleophilic sites, which contain amino, thiol, or hydroxyl groups, located on nucleotides (e.g., DNA), proteins (e.g., ATP5B, glutathione), or amino acids, leading to the formation of respective adducts (Mattocks 1986; Prakash et al. 1999; Fu et al. 2004; Li et al. 2015b). This pathway is considered as primary toxification pathway (Xu et al. 2019). Fu and colleagues provided evidence for the formation of DHP-dG-1, DHP-dG-2, DHP-dG-3, DHP-dG-4, DHP-dA-1, DHP-dA-2, DHP-dA-3, and DHP-dA-4 adducts with dehydroretronecine in the presence of calf thymus DNA (Fu et al. 2010a). Similar findings were reported by Zhao and coworkers, who observed the same DHP-DNA adducts with riddelliine following rat liver microsomal metabolism in presence of calf thymus DNA (Zhao et al. 2012). However, only DHP-dG3/4 and DHP-dA3/4 adducts were formed in the livers of rats after oral treatment with daily doses up to 5.0 mg/ kg bw riddelliine or monocrotaline for three consecutive days (Fu et al. 2010a). The same set of DHP-dG and -dA adducts were measured in liver samples of rats from a NTP study, which were orally treated with doses up to 1.0 mg/ kg bw riddelliine for six

months. The same set of DHP-dG-3/4 and DHP-dA-3/4 adducts was detected in the livers of rats and mice treated with various PAs and PANOs, such as retrorsine, lasiocarpine, riddelliine, monocrotaline and riddelliine *N*-oxide, with each PA exhibiting distinct total adduct levels (Xia et al. 2013; Zhu et al. 2017). In addition, the DHP-dG-3/4 adduct levels were higher than DHP-dA-3/4 levels, potentially due to differences in steric accessibility or adduct stability. Notably, the formation of DHP-derived DNA adducts correlated with the order of liver tumor potency (Yang et al. 2001; Fu et al. 2010a; Xia et al. 2013; Zhu et al. 2017). Subsequently, the DHP-DNA adducts, characterised as DHP-dG-3/4 and DHP-dA-3/4, are proposed as potential biomarkers for PA and PANO exposure and as indicators of PA-induced liver tumor initiation (He et al. 2019).

DHP esters can be further hydrolyzed into (±)-6,7-dihydro-7-hydroxy-1-hydroxymethyl-5H-pyrrolizine (DHP), which are less reactive and unstable in water, but showing bifunctional alkylating activity too (Wiedenfeld et al. 2008). The DHP derived adducts are mainly protein adducts, also known as secondary metabolites. Over the past few years, a total of 11 distinct secondary pyrrolic metabolites such as 7- and 9-glutathione-DHP, 7-cysteine-DHP or 7-N-acetylcysteine-DHP have been identified, which have the capacity to bind to DNA and form the same set of DHP-dG3/4 and DHP-dA3/4 adducts (Chen et al. 2016; Fu 2017; Xia et al. 2018; He et al. 2019, 2020a). It should be noted, that the total DHP-DNA adduct levels vary between the secondary metabolites, whereby 9-ethoxy-DHP and 7-cysteine-DHP showed the highest total DHP-DNA adduct levels (Xia et al. 2018). The covalent binding of glutathione, cysteine or *N*-acetylcysteine (NAC) on both C7 and C9 positions of pyrrolic metabolites resulted in undetectable total DHP-DNA adduct levels in HepG2 cells and significant low levels compared to other secondary metabolites in presence with calf thymus DNA (Xia et al. 2018). For instance, the dual binding of glutathione to pyrrolic metabolites is facilitated by enzymes such as glutathione S-transferase (GSTA1) or glutathione peroxidase (GPX1), thus enabling their detoxification and subsequent excretion through bile (Yan and Huxtable 1995; Yan et al. 2016). Besides DNA-adducts, PAs can also trigger genotoxic outcomes such as clastogenic effects or mutations (Chen et al. 2010).

2.4 Toxicity

2.4.1 Acute and chronic toxicity

The liver is the primary target of PA toxicity due to the bioactivation in situ. PA intoxication can be clinically categorized into three distinct types: acute, subacute and chronic intoxication. The type of poisoning can be triggered by the duration of PA exposure or the PA amount ingested and differ in their respective clinical symptoms or manifestations (He et al. 2021d).

The ingestion of high PA amounts (mg PA/ kg food) in a short time interval is the primary cause of acute PA intoxication in humans (Dusemund et al. 2018). This is characterized by abdominal pain and swelling, hemorrhagic necrosis, hepatomegaly, sinusoidal endothelial hyperplasia, medial hypertrophy and ascites. Furthermore, liver necrosis and dysfunction are observed, which may result in liver failure or even death (Stegelmeier et al. 2016; He et al. 2021d). The most well-documented acute cases of PA intoxication in humans were observed in two children, who died within days due to PA levels ingested between 0.8-1.7 and 3 mg/ kg bw per day (WHO-IPCS 1988). One child developed a hepatic sinusoidal obstruction syndrome (HSOS), which is known as the most prevalent clinical manifestation for PA poisoning (EFSA 2011). Studies on acute toxicity in rodents, using intraperitoneal or intravenous PA administration, reported letal doses at which 50% of animals died (LD_{50}) ranging from 5 to 1500 mg/ kg bw for retrorsine, the most potent PA in rats (Merz and Schrenk 2016). Nevertheless, acute PA intoxications are less common in the modern era, although occasional cases do exist due to highly contaminated food or the use of PA containing herbs as traditional Chinese medicines (Schrenk et al. 2022; Lu et al. 2024).

The HSOS is classified as an intrinsic liver injury, whereby the risk of developing the syndrome is dependent on the PA dose, the frequency of intake and the cumulative dose (Moreira et al. 2018; Teschke et al. 2021). HSOS outbreaks were observed around the world, predominantly in subtropical, tropical and eastern countries, due to the consumption of PA-containing herbs as traditional medicines or contaminated grains. So far, HSOS can only be linked to the consumption of high amounts of PAs (Teschke et al. 2021). Clinically, HSOS is described with hyperbilirubinaemia, hepatomegaly, and weight gain due to ascites (Helmy 2006). HSOS is characterized by the occlusion of small hepatic veins, primarily in zone 3 of the liver acinus, which can progress to liver failure in severe cases (Mohty et al. 2015; Valla and Cazals-Hatem 2016; Teschke et al. 2021). The pathogenesis of HSOS, driven by pyrrolic-protein adducts, is well understood. Here, pyrrolic metabolites enter the Dissé space and the sinusoidal lumen, leading to the destruction of sinusoidal endothelial cells (Prakash et al. 1999; Dusemund et al. 2018; Xu et al. 2019). Recent findings have indicated that PAs, which undergo enterohepatic circulation and interact with gut bacteria, contributed to the pathogenesis of HSOS in mice, as shown by significant lipopolysaccharides (LPS) levels in the liver (He et al. 2021d; Xiao et al.

2022). The PA treatment led to reduced goblet cell density and disrupted intestinal tight junction proteins, leading to increased intestinal permeability and significant elevated hepatic LPS levels (He et al. 2021b). LPS, also known as endotoxins, are produced by gram-negative bacteria in the gut. When the gut barrier is compromised, LPS can translocate into the bloodstream and reach the liver, triggering hepatocyte death and liver inflammation. LPS also act as a critical cofactor in the progression of liver diseases, contributing to hepatopathogenesis (Altin and Bygrave 1988; Rao 2009).

Furthermore, pneumotoxicity caused by PAs is another event discovered *in vivo*. Animal studies showed that PAs are capable to cause pulmonary arterial hypertension (PAH), changes in vascular smooth muscle and endothelial-smooth muscle interactions in the lungs after intravenous or subcutaneous injections of single PA doses over the course of the subsequent two weeks (Huxtable 1990; Xiao et al. 2019). Song and coworkers observed acute liver and lung injuries within 48 h in rats after oral administration of single doses of PAs such as riddelliine, retrorsine and monocrotaline. Pyrrole-protein adducts were predominantly found in the liver rather than the lungs of the treated rats. The highest pyrrole-protein adduct level in the lung was observed with monocrotaline, which is well-known among 1,2-unsatured PAs for its pneumotoxicity (Song et al. 2020). Although animal studies have confirmed the pneumotoxicity of certain PAs, no observations in humans have been published to date.

The chronic toxicity of PAs is a more significant concern in relation to human health in comparison to the acute toxicity, due to the fact that their genotoxic effects can accumulate over a period of time, if not adequately or incorrectly repaired, and result in irreversible liver damage or cancer. Conversely, chronic PA intoxication in humans has not been documented in literature so far, largely due to the absence of comprehensive epidemiological data (Schrenk et al. 2022). A recent study with mutational signature analyses in > 1,000 liver cancer genomes reported a correlation between PA exposure and liver cancer predominantly in Asian countries, raising significant concerns (He et al. 2021c). In animals, chronic intoxications are caused from repeated low PA uptake and associated with hepatic fibrosis, nodular regeneration and cirrhosis. In the most severe cases, liver failure, liver cancer or death are reported too (Merz and Schrenk 2016; Dusemund et al. 2018; Chen et al. 2023). A 2-year carcinogenicity study with orally administrated riddelliine in rats revealed a no-observed-adverse-effect-level (NOAEL) of 0.01 mg/ kg bw per day for hepatocyte cytomegaly as non-neoplastic effects (NTP 2003; BfR 2020). Furthermore, 2-year carcinogenicity studies demonstrated that PAs including riddelliine and lasiocarpine can induce liver haemangiosarcoma, liver cell carcinoma or adenoma and pulmonary adenocarcinoma. (NTP 1987, 2003)

2.4.2 Hepatotoxicity and cytotoxicity

The hepatotoxicity of PAs is a complex process involving multiple biochemical pathways. After metabolic activation of 1,2-unsatured PAs such as retrorsine, pyrrolic metabolites can initiate oxidative stress indirectly via reduced mitochondrial ATP synthesis or lipid peroxidation, apoptosis or bile acid metabolism dysfunction, which are all linked to PA-induced hepatoxicity (Waizenegger et al. 2018; Xu et al. 2019; He et al. 2021d).

Lu and coworkers demonstrated that retrorsine lead to the formation of pyrrolic-ATP5B adducts in rat liver, hepatic sinusoidal endothelial cells and HepaRG cells (Lu et al. 2018). ATP5B is a key subunit of mitochondrial ATP synthase with the function of catalysing ATP synthesis. The interaction of ATP5B can result in reduced mitochondrial ATP synthesis (Deng et al. 2018). HepaRG cells showed significantly decreased ATP synthase activity and intracellular ATP levels followed by a decrease in mitochondrial membrane potential and respiration (Li et al. 2015b; Lu et al. 2018). It is known that a reduced ATP synthase activity in mitochondria goes hand in hand with excessive reactive oxygen species (ROS) formation (Roy et al. 2008). Intracellular ROS are commonly located in mitochondria and the cellular redox balance is normally maintained by enzymes such as glutathione peroxidase and nonenzymatic antioxidants such as vitamin E. However, if the balance is disturbed for example by a depletion of glutathione, it can result in an overproduction of ROS, which bind to macromolecules such as DNA or proteins, causing cellular damage (Skoryk and Horila 2023). The development of HSOS can be considered a classic consequence of glutathione depletion. The rapid depletion of sinusoidal glutathione levels by DHP results in an increase of matrix metalloproteinase activity and therefore supporting the risk of HSOS (DeLeve et al. 2002; Deleve et al. 2003b, c). The occurrence of HSOS is characterised by the presence of necrotic lesions, which are indicative of uncontrolled cell death. These observations have been documented in HSOS patients (Tan and Zheng 2023). Necrosis, defined as an uncontrolled form of cell death that is energy-independent, can be triggered by severe damage or stress (D'Arcy 2019). Furthermore, it was shown that DNA-reactive metabolites such as trans-4-hydroxyl-2-hexenal through lipid peroxidation are formed and cause cellular damage in hepatocytes (Griffin and Segall 1987; Zhu et al. 2024).

It is noteworthy that Lu and colleagues further investigated the distinction between apoptosis and necrosis and concluded that retrorsine primarily induces apoptosis (Lu et al. 2018). Their findings revealed no significant lactate dehydrogenase increase, but a significant increase in caspase-8, -9, and -3 activity and pronounced apoptotic cell numbers after 18 h retrorsine treatment in HepaRG cells. Moreover, recent studies have shown that certain PAs induce apoptosis in liver cells through either the intrinsic (mitochondrial) pathway, the extrinsic (death receptor) pathway, or both by measuring the expression of related genes via quantitative real-

time polymerase chain reaction (qPCR) and whole genome microarray analysis *in vitro* and *in vivo* (Li et al. 2015b; Yang et al. 2017; Waizenegger et al. 2018; Ebmeyer et al. 2020; Glück et al. 2021; Zhu et al. 2024). For example, retrorsine was identified as a candidate that activates both pathways in primary rat hepatocytes, as confirmed by western blot and immunofluorescence microscopic analyses (Zhu et al. 2024). Furthermore, oxidative stress was reduced and both apoptosis and autophagy were normalized in retrorsine-treated primary rat hepatocytes with NAC as an antioxidant, indicating that oxidative damage is involved in PA-induced hepatotoxicity (Zhu et al. 2024). Pan and colleagues screened the hepatotoxicity of nine PAs including lasiocarpine, retrorsine, monocrotaline and heliotrine as well as PANOs in zebrafish after single oral administration of individual 0.3 mmol/ kg PA for 6 h (Pan et al. 2023). Notably, zebrafish CYP3A65 and CYP2Y3 are orthologous to human CYP3A4 and CYP2A6/ CYP2E1. The rank order in hepatotoxicity (plasma alanine transaminase, hepatocellular vacuolation and fatty droplets accumulation) was structure-dependent, showing the strongest effects bv lasiocarpine and retrorsine equally, followed by monocrotaline, clivorine, heliotrine and PANOs. Furthermore, inflammation- and apoptosis-associated genes such as IL-6 or IL-8 and p53 or *bax* were upregulated regulated measured by qPCR analysis (Pan et al. 2023).

Additionally, pyrrolic metabolites of 1,2-unsatured PAs can interact with DNA, leading to the formation of DNA adducts, DNA-DNA crosslinks, and DNA-protein crosslinks, which contribute to their genotoxicity (Chen et al. 2010). Although hepatocytes possess efficient detoxification mechanisms, prolonged or excessive PA exposure can overwhelm these systems. This may result in DNA damage that remains unrepaired, is incorrectly repaired, or triggers apoptosis. Persistent DNA damage can also lead to mutations, increasing the risk of carcinogenesis (Fu et al. 2002; Fu 2017; He et al. 2021d). Evidence from animal studies has demonstrated that chronic low-dose PA exposure is associated with the development of hepatic fibrosis, nodular regeneration, and cirrhosis. In addition, megalocytosis, obliteration of central and sub-lobular veins, and bile duct proliferation have been reported as characteristic pathological changes resulting from repeated low-level PA exposure or a single sublethal dose (Dusemund et al. 2018).

Over the years, the cytotoxicity of different PAs was investigated in human or rat liver cells to study the structure-dependent toxicity. The relative cytotoxicity expressed as the effective concentration at 50% cell viability (EC_{50}) of each PA was assessed. Surprisingly, EC_{50} values could not be determined after 24 h treatment with any tested PA in HepaRG cells, indicating a moderate sensitivity of HepaRG cells to PA-induced cytotoxicity (Waizenegger et al. 2018; Louisse et al. 2019; Glück et al. 2021). For example, HepaRG cells revealed a cell viability of 53% after 24 h at the highest concentration (250 µM) of lasiocarpine (Glück et al. 2021). In comparison, Gao and coworkers observed a greater PA cytotoxicity in primary rat hepatocytes (Gao et al. 2020). Furthermore, they discovered that the duration of pre-incubation of rat

hepatocytes had a negative impact on CYP activity, with a time-dependent decrease in activity attenuated PA cytotoxicity. Thus, the PA cytotoxicity would have a greater impact on cell viability if the CYP activity would be stable in primary rat hepatocytes after cultivation (Gao et al. 2020). More importantly, all studies confirmed a structure-dependent toxicity, implicating cyclic and open diester are more cytotoxic compared to monoesters and goes in line with the classification based on acute toxicity studies in rodents (Merz and Schrenk 2016). Recently, it was shown that DHP-derived protein adducts in primary mouse hepatocytes correlated with the cytotoxicity caused by PAs such as senecionine, retrorsine and senecionine *N*-oxide, indicating DHP-protein adducts are associated with hepatotoxicity (Xiong et al. 2020).

2.4.3 Genotoxicity and mutagenicity

PAs have been widely studied for their genotoxic effects across various biological systems and are known to form DNA adducts *in vivo* (JECFA 2020). The formation of DNA adducts requires the metabolic activation of 1,2-unsatured PAs, such as by CYP3A4, to generate DNA-reactive metabolites including DHP ester and DHP. Pyrrolic metabolites are bifunctional nucleophiles, which are capable on binding to DNA and proteins to form DNA-DNA and DNA-protein cross-links as well (Fu et al. 2004). Furthermore, PAs can lead to clastogenicity and gene mutations both *in vitro* and *in vivo*, contributing to genomic instability and the potential development of tumors in exposed organisms (Chen et al. 2010; EFSA 2011; Allemang et al. 2018; Rutz et al. 2020). In the following, selected studies are described for the genotoxicity and mutagenicity of PAs.

2.4.3.1 DNA damage

The unscheduled DNA synthesis (UDS) assay was used to investigate the repair of primary DNA damage after PA incubation in different cell models. PAs such as senecionine, seneciphylline or retrorsine were tested positive in primary rat liver cells using the UDS assay (Griffin and Segall 1986). Rodent studies and cultured rat or mice hepatocytes treated with riddelliine as model PA also showed significant positive results, confirming the induction of DNA repair synthesis in the liver cells through the incorporation of labelled nucleosides in cells that are not undergoing scheduled (S-phase) DNA synthesis (Mirsalis 1987; Mirsalis et al. 1993; NTP 2003).

DHP-DNA adducts were characterized using riddelliine in *in vitro* and *in vivo* studies. A set of two enantiomers of DHP-7-deoxyguanosin-2N-yl adducts and DHP-modified dinucleotides were formed *in vitro* and in rat liver (Yang et al. 2001; Xia et al. 2003; Chou et al. 2003). Further studies with selected heliotridine-, retronecine- and otonecine-type PAs as well as PA-containing herbs generated the same set of DHP-derived DNA adducts with rat and human liver microsomes with calf thymus DNA and in rodents (rats and mice), indicating a common mode of action by PAs (JECFA 2020). Rodent studies demonstrated that the DHP-derived DNA

adduct level correlated with tumorigenic potency after administration with doses in a range of 0.01 – 1.0 mg/ kg bw and 1 – 3 mg/ kg bw riddelliine in rats and mice. Furthermore, the DHP-DNA adduct levels were higher in endothelial cells than in parenchymal liver cells, consistent with the observed haemangiosarcoma formation (Yang et al. 2001; Xia et al. 2004). Fu and colleagues reported that *in vivo*, the formation of DHP-dG-3/4 and DHP-dA-3/4 adducts (Figure ***2.6***) is more prevalent compared to the additional DHP-dG-1/2 and DHP-dA-1/2 adducts observed in the reaction of dehydroretronecine with calf thymus DNA. Similar outcomes were reported by Zhao et al. in rats following oral exposure to riddelliine. This variation between both test models is presumably attributable to the rapid repair of DHP-dG-1/2 and DHP-dA-1/2 adducts *in vivo* (Fu et al. 2010b; Zhao et al. 2012).. Besides, the levels of DHP-dG and -dA adducts varied between PAs tested in rats after three consecutive days of treatment, with retrorsine followed by lasiocarpine, riddelliine, monocrotaline and riddelliine *N*-oxide, showing the highest levels (Xia et al. 2013). Lester and coworkers found similar results in rat sandwich-culture hepatocytes, which were incubated over 6 and 24 h with different PAs. In the sum, the DHP-DNA adducts levels as well as the concentration versus time curve for the depletion of parent PA from extracellular media (AUC) for nine PAs were studied in rat hepatocytes. The highest DHP-DNA adducts per AUC were formed by lasiocarpine followed by echimidine, riddelliine and heliotrine after 24 h incubation in rat hepatocytes (Lester et al. 2019). The DHP-dG3/4 and -dA3/4 adducts are seen as biomarker for PA exposure and being associated with development of liver tumors (Fu et al. 2010a; Xia et al. 2013). In a more recent study, Louisse and colleagues used a high-throughput western assay to examine the formation of γH2AX, a well-established DNA damage marker (Nikolova et al. 2014), in HepaRG liver cells in response to various PAs. The findings indicated that the PA genotoxicity was structure-dependent, with PAs such as monocrotaline or heliotrine showing either lower or higher toxicity compared to other PAs in the same esterification group. The highest γH2AX levels were observed with open and cyclic diester (Louisse et al. 2019).

Furthermore, there is evidence that DHP-derived protein adducts can also give rise to DHP-dG and -dA adducts, as shown in the reaction of pyrrolic metabolites with calf thymus DNA and in HepG2 cells (Xia et al. 2018). To date, 10 DHP-protein adducts were identified, which are DNA-reactive and form the same set of DHP-dG3/4 and -dA3/4 adducts, suggesting their role in PA-induced liver cancer initiation (He et al. 2016, 2017, 2020b; Fu 2017; Xia et al. 2018). Exemplary DHP-protein adducts are depicted in Figure ***2.6***. DHP was found to bind on amino acids and proteins such as cysteine (7-CYP-DHP), *N*-acetylcysteine (7-NAC-DHP) and glutathione (7-GS-DHP) (Fu 2017). In addition, the pyrrolic metabolite, 1-formyl-7-hydroxy-6,7-dihydro-5*H*-pyrrolizine (1-CHO-DHP), was capable to react with cysteine to generate three DNA-reactive metabolites *in vitro* (He et al. 2020b). Moreover, there is evidence that the formation of different DHP glutathione conjugates is dependent on species and the individual

PA, which was demonstrated with glutathione using human and rat liver microsomes (Geburek et al. 2020). For example, senkirkine induced a greater amount of mono- and di-glutathione-coupled DHP conjugates with rat liver microsomes, whereas senecionine generated more glutathione conjugates with human liver microsomes. In contrast, lasiocarpine formed similar levels of glutathione DHP conjugates in both liver microsomes (Geburek et al. 2020).

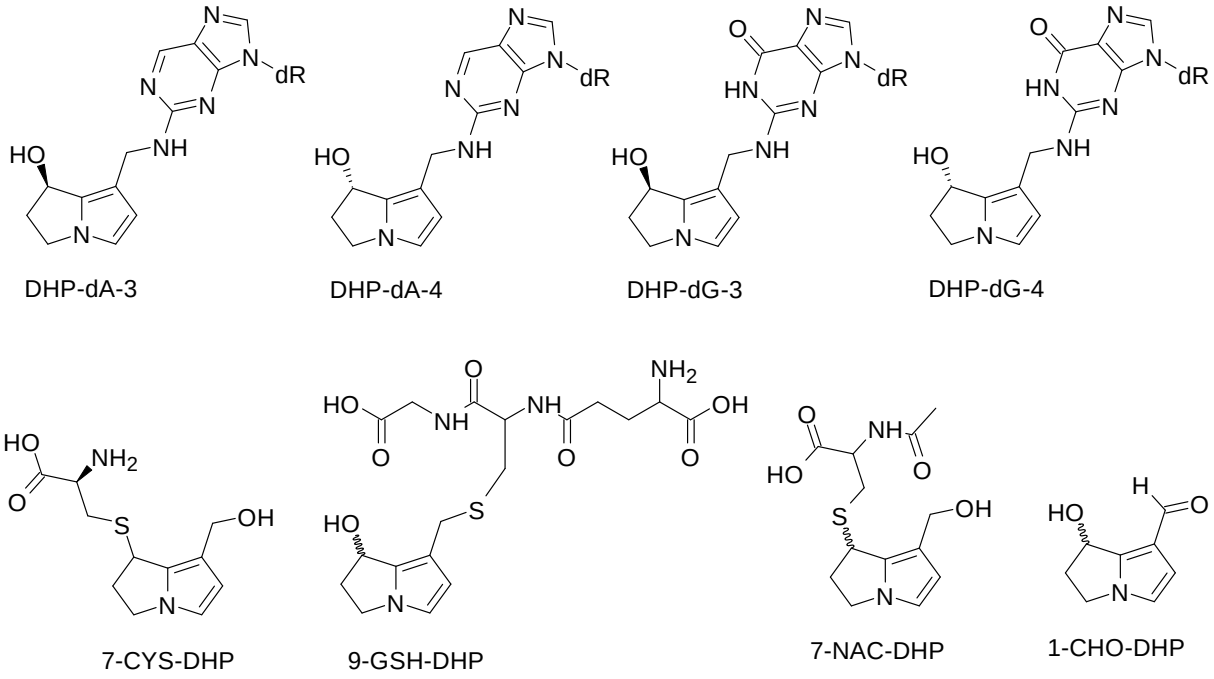

Figure 2.6: Structures of DHP-DNA adducts and secondary reactive metabolites. Shown are the main DHP-DNA adducts including DHP-dG3/4 and -dA3/4 as well as exemplary secondary metabolites such as 7-CYS-, 9-GSH-, 7-NAC- and 1-CHO-DHP formed by 1,2-unsatured PAs *in vivo* (modified by Fu 2017, Chen et al 2016).

Pyrrolic metabolites possess multiple reactive sites within their necine backbone, specifically at the C5, C7 and C9 position of the necine base. These sites facilitate binding to two distinct sites of DNA or protein to form respective DNA-DNA or DNA-protein crosslinks (Kim et al. 1995, 1999; Coulombe et al. 1999). Studies using cells or isolated nuclei showed that pyrrolic PAs like dehydrosenecionine induced DNA-protein crosslinks, making up to 50% of total cellular DNA crosslinks. Furthermore, the crosslinking potency of PAs *in vitro* is comparable with the toxicity in animals (Petry et al. 1984; Kim et al. 1995; Coulombe et al. 1999). On the other hand, DNA-DNA crosslinking was investigated with monocrotaline in rats via intraperitoneal administration and *in vitro*. Both DNA-DNA and DNA-protein crosslinks were formed *in vivo* (Pereira et al. 1998). Furthermore, Coulombe and colleagues demonstrated that all tested PAs are capable to induce DNA crosslinks, with the degree of induction varying considerably. The order of DNA crosslinking activity is decreasing as follows: seneciphylline, riddelliine, and retrorsine (Coulombe et al. 1999).

2.4.3.2 Chromosomal damage

DNA strand breaks caused by PAs can lead to chromosomal damage and the formation of micronuclei. Micronuclei are small, extranuclear structures formed when lagging chromosomes or chromosome fragments fail to integrate into the primary nucleus during mitosis or meiosis. These fragments are encapsulated by a nuclear envelope and persist into interphase. Micronuclei often arise from errors in chromosome segregation, such as defective kinetochore-microtubule attachments or chromatin bridges, and are associated with genomic instability, chromothripsis, and tumor progression (Krupina et al. 2021). Several lines of evidence showed that certain PAs, predominantly cyclic di-ester, were clastogenic *in vivo* and *in vitro* (Chen et al. 2010; Allemang et al. 2018; Rutz et al. 2020; Hadi et al. 2021). The studies revealed chromosomal damage including micronuclei, sister chromatid exchanges and chromosomal aberrations *in vivo* or *in vitro*.

Isatidine, monocrotaline and retrorsine induced micronuclei in cultured rat hepatocytes. Furthermore, rodent studies confirmed the evidence of polychromatic erythrocytes (PCE) in mouse bone marrow and fetal liver as well as micronucleated PCE in adult and fetal tissues after PA and PA mixture administration (Sanderson and Clark 1993; Chan et al. 1994; Mueller-Tegethoff et al. 1995, 1997). Recent studies showed the induction of micronuclei caused by various PAs in HepaRG, HepG2 with CYP3A4 overexpression or wild type HepG2 with rifampicin pretreatment (Allemang et al. 2018; Rutz et al. 2020; Hadi et al. 2021). Notably, rifampicin is used for CYP3A4 mRNA upregulation in wild type HepG2 cells, that usually display low CYP3A4 expression (Berger et al. 2016). In two studies, various PAs including monoesters, open diesters and cyclic diesters were chosen to study the structure-dependent genotoxicity in a dose-dependent manner for 24 h in HepaRG and HepG2-CYP3A4 (Allemang et al. 2018; Rutz et al. 2020). The cells were incubated for 72 h in fresh medium and micronuclei were counted at the end. Both studies showed that cyclic diesters and open diesters exhibited the most pronounced genotoxic potential, except monocrotaline, followed by monoester. Monocrotaline was similar genotoxic compared to monoesters such as europine and indicine, whereby heliotrine caused a likewise rate of micronuclei compared to open and cyclic diester. The results of both studies indicated that the highest rate of micronuclei was induced by lasiocarpine followed by various cyclic esters, including senecionine, seneciphylline, retrorsine and riddelliine (Allemang et al. 2018; Rutz et al. 2020). Similar findings were found by another study, showing micronuclei formation caused by various PAs in HepG2 cells pretreated with rifampicin. Lasiocarpine followed by riddelliine, echimidine and retrorsine showed the highest rate of micronuclei formation, whereby monoester including europine and lycopsamine exhibited the lowest genotoxic potency (Hadi et al. 2021).

In addition, several PAs such as riddelliine, lasiocarpine or monocrotaline caused chromosomal aberrations in mammalian cells like Chinese hamster ovary (CHO) or V79 cells

together with S9 mix (Takanashi et al. 1980; NTP 2003). Muller and coworkers found chromosomal aberrations caused by monocrotaline, retrorsine and isatidine in V79 cells and primary hepatocytes only in presence of S9 mix (Mueller et al. 1992). According to the literature, only integerrimine as a cyclic diester was tested for chromosomal aberrations *in vivo*. Mice of both sexes revealed interchromosomal exchanges in a dose-dependent manner with the highest frequency of chromosomal aberrations 12 h after treatment (Gimmler-Luz et al. 1990). Chromosomal aberrations were also found in blood cells of children, which suffered from HVOD (Martin et al. 1972).

Besides, PAs were tested positive for sister chromatid exchange in CHO and V79 cells after S9 activation (Bruggeman and Van Der Hoeven 1985; NTP 2003). Sister chromatid exchanges were also found in chick embryo hepatocytes and varied in the amount among the tested PAs. The highest mutant frequencies were measured with seneciphylline followed by senkirkine, heliotrine and monocrotaline (Bruggeman and Van Der Hoeven 1985).

2.4.3.3 Gene Mutations

The formation of mutations depends on the failure of DNA repair mechanisms or the absence of cell death (Carusillo and Mussolino 2020). Mutagenicity assays with PAs such as retrorsine, heliotrine or lasiocarpine in bacteria, especially *Salmonella typhimurium*, yielded inadequate results. For example, retrorsine was tested positive in presence of S9 mix, showing both basepair substitutions and frameshift mutations in strains TA1535 and TA1537 with *S. typhimurium* (Wehner et al. 1979). Riddelliine showed positive mutagenic responses in *S. typhimurium* strains TA98, TA100, TA1535 and TA1537 after S9 activation too (White et al 1984). Furthermore, heliotrine and lasiocarpine were positive in TA100 with metabolic activation via S9-mix too (Yamanaka et al 1979). However, other studies observed no or weak mutagenicity of PAs such as retrorsine, riddelliine seneciphylline in *S. typhimurium* strains. Due to the controversial results in *S. typhimurium,* it was considered that the test system was not suitable for the assessment of PA mutagenicity. (Clark 1976; Rubiolo et al. 1992; NTP 2003). Recently, a study confirmed the negative results of PAs in the ames fluctuation assay with and without rat liver S9 fraction. Rutz et al investigated the mutagenicity of eleven PAs such as lasiocarpine, retrorsine or heliotrine in *S. typhimurium* TA98 and TA100 strains. It was observed that all PAs were negative up to a concentration that resulted in more than a 50% reduction in bacterial viability, as assessed by resazurin reduction. Moreover, the inclusion of rat liver S9-mix did not influence the results of the fluctuation assay. Therefore, the reactive metabolites of PA could exert bactericidal activity by attacking the outer bacterial wall or membrane (Rutz et al. 2020).

On the other side, several PAs such as heliotrine, seneciphylline, retrorsine or monocrotaline were tested positive as mutagens in the wing spot assay or sex-linked recessive lethal test of

Drosophila melanogaster (Clark 1959; Candrian et al. 1984; Frei et al. 1992). Frei et al. investigated the structure-dependent mutagenicity of 15 PAs like heliotrine, indicine, monocrotaline and indicine *N*-oxide in the wing spot of *D. melanogaster*. The most potent PAs were senkirkine followed by monocrotaline, seneciphylline and senecionine. The only negative tested PA was the monoester supinine. Furthermore, the author observed structure-dependent differences among the tested PAs, with cyclic and open diesters identified as the most potent groups (Frei et al. 1992).

Furthermore, riddelliine was tested for its mutagenicity via transgenic mutation assay in rat liver. Rats were gavaged with 0.1, 0.3 and 1.0 mg riddelliine per kg bw five days a week for 12 weeks. The author found liver tumors at middle and high doses as well as significant dose-dependent mutant frequencies in endothelial, but not parenchymal cells. Riddelliine induced G:C to T:A transversions and tandem base substitutions, such as GG to TT and GG to AT (Mei et al. 2004b, a). Moreover, the administration of riddelliine in mice has been demonstrated to induce mutations in the *k-ras* proto-oncogene as well as *p53* tumour suppressor gene in the context of liver hemangiosarcomas. The study revealed that 58% of riddelliine-induced tumors showed a *k-ras* codon 12 G to T mutation and 75% unspecified *p53* mutations (Hong et al. 2003).

2.4.4 Tumorigenicity

In the last centuries, several rodent carcinogenicity studies with PAs such as heliotrine, monocrotaline, lasiocarpine or riddelliine were carried out, consistently showing liver tumor formation in rats. However, most of the studies were non-standard assays, lacking dose-response data due to testing only a single dose, though they still produced positive results (Fu 2017; Dusemund et al. 2018; Hartwig et al. 2020). The National Cancer Institute (NCI) and U.S. National Toxicology Program (NTP) conducted two-year carcinogenicity assays in rodents (mice and/ or rat) to investigate the carcinogenicity of lasiocarpine and riddelliine. The results indicated that both PAs were rodent carcinogens (NCI 1978; NTP 2003). Shumaker et al showed the induction of liver cell carcinomas and pulmonary adenocarcinomas in rats exposed to monocrotaline (Shumaker et al. 1976). Furthermore, the set of four DHP-DNA adducts is suggested as marker for PA-induced liver tumor development (Xia et al. 2013). The IARC has classified three PAs, namely riddelliine, lasiocarpine and monocrotaline, as 2B possibly carcinogenic for humans (IARC 1976, 1983, 1987, 2002).

Lasiocarpine was evaluated in rats, both sexes, through the administration of daily dietary doses at 7, 15 and 30 ppm for a duration of 104 weeks. The high-dose group experienced significantly lower body weights throughout most of the study, while the mid-dose group had reduced body weights only in the second year. In addition, a dose-related increase in mortality

in both sexes was seen. None of the high-dose animals survived to the end of the study. For females, more deaths occurred at higher doses. In male rats, a significant dose-related increase in angiosarcoma of the liver was observed. In comparison, the incidences of angiosarcoma were significant in the low- and mid-dose groups, but not in the high-dose group of females, likely due to early mortality. For both sexes, angiosarcomas were found predominantly in the liver, with some metastasis the lungs. Furthermore, there was a positive dose-related trend in the combined incidence of hepatocellular carcinoma and adenoma in both sexes, especially in the high-dose groups. Finally, a significant induction of leukaemia or lymphoma was observed in the low- and mid-dose groups of female rats. In summary, the study with lasiocarpine provided evidence of carcinogenicity, predominantly in the liver, with findings of both dose-dependent tumor development and a significant gender impact (NCI 1978).

Riddelliine was tested in rats and mice, both sexes, using oral administration with doses ranging from 0.1 to 1 mg/ kg bw for rats and 0.1 to 3 mg/ kg bw in mice five days per week for a total of 105 weeks. The body weights of the rats and mice in the high-dose groups were significantly reduced compared to controls. The administration of 1 mg/ kg bw to male rats resulted in a high mortality rate, which led to an early termination of this part of the study. The majority of rats succumbed before reaching week 70. Furthermore, significant inductions of non-neoplastic lesions were found in the liver and kidneys for both rats and mice, with liver hyperplasia and cytomegaly being common. Both species revealed a distinct tumor development linked with riddelliine exposure. As example, a high rate of liver hemangiosarcoma was found, with 86% of male and 76% of female rats in the high-dose groups developing these tumors, indicating the liver as primary target organ. The development of liver tumors was investigated through the analysis of DNA adducts in the liver tissues. Furthermore, a significant increase in mononuclear cell leukemia in male and female rats was observed, implying systemic carcinogenic effects. Besides, female mice showed a notable increase in alveolar/ bronchiolar neoplasm predominantly in high-dose groups. In summary, riddelliine induced liver tumors in rats and both liver and lung tumors in mice (NTP 2003).

The European Food Safety Authority (EFSA) reviewed both studies and applied the Benchmark dose (BMD) model averaging approach on the data sets regarding the incidence of liver hemangiosarcoma in both sexes. A benchmark dose lower confidence interval (BMDL) of 73 µg kg bw per day was determined based on liver tumors from the 2-year carcinogenicity study with lasiocarpine. On the other side, a BMDL of 237 µg/ kg bw per day based on the formation of liver haemangiosarcoma as the most sensitive neoplastic endpoint was assessed for retrorsine (EFSA 2011, 2017a, b). The BMD_{10} confidence intervals of both PAs were compared and used to evaluate the reference point for chronic risk assessment. Riddelliine was favoured over lasiocarpine because of the adequate number of animals tested per dose

group, ensuring more reliable data. Additionally, the narrower BMD_{10} confidence interval for riddelliine indicated less uncertainty in the modelling compared to lasiocarpine (EFSA 2017b).

2.4.5 Reproductive and developmental toxicity

Several rodent studies were conducted in the 20th century to investigate the capability of PAs to induce embryotoxicity and teratogenicity since it was shown that senecionine was capable crossing the placenta in pregnant rats, resulting in litters born prematurely as well as offspring deaths (Sundareson 1942; Mattocks 1986). The LD_{50} in fetuses *in utero* was up to three times higher than in adult rats, indicating lower metabolic activity. In addition, embryos from PA-treated rats showed only minor liver damage after birth (Sundareson 1942). The metabolism of retrorsine to pyrrolic esters in both maternal and fetal liver microsomes revealed higher activity in maternal liver. Furthermore, the formation of pyrrolic-protein adducts was greater in maternal than fetal liver of rats from both sexes (Li et al. 2018). Besides, the PA-induced toxicity in fetal and maternal livers was different among the tested PAs. Only lasiocarpine equally damaged both maternal and fetal liver, leading to liver necrosis or haemorrhage (Mattocks 1986). Recently, Guo and coworkers investigated the effects of prenatal exposure to retrorsine and monocrotaline on fetal rats. Pregnant rats were administrated via gavage with 20 mg/ kg bw of either retrorsine or monocrotaline once daily from gestational day 9 to 20 and fetuses were collected after day 20 for analysis. The study resulted in both maternal and fetal growth retardation, congestion, vacuolization or hemorrhage as well as oxidative stress expressed in a decrease of GSH/GSSG ratio in both liver and lungs of fetuses. Fetal rats could be more impacted by PA-induced toxicity than maternal rats likely due to the accumulation and missing elimination of DHP-derived protein adducts (Guo et al. 2019). Green and Christie found dose-related fetal abnormalities including retardation of development, musculo-skeletal defects in ribs, hyperplasia of the jaw and cleft palate, in rats during their second week of pregnany after single i. p. injections of heliotrine. Furthermore, heliotrine showed teratogenic effects such as morphological abnormalities in adult abdomen of *Drosophila* larvae too (Mattocks 1986). The findings of Lin and colleagues in zebrafish larvae indicated that echimidine has a deleterious impact on the development and functionality of the cardiac system. It would represent the first case of an open diester to report organ toxicity outside of the liver (Lin et al. 2023b).

In conclusion, the figure 2.7 demonstrate a comprehensive overview of the toxicological endpoints induced by 1,2-unsaturated PAs in both animal models and *in vitro* models.

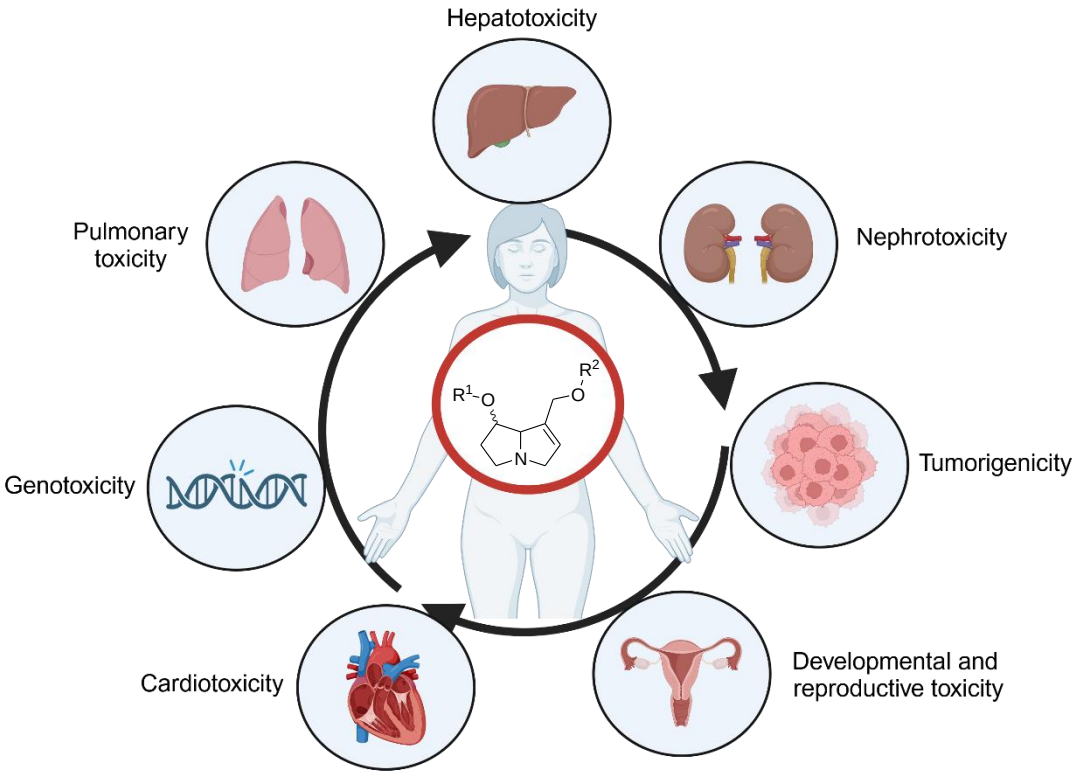

Figure 2.7: Impact of 1,2-unsatured PAs on different organs based on *in vivo* and *in vitro* findings (created in https://BioRender.com)

2.5 Health risks of PAs and legal framework

2.5.1 PA uptake through the consumption of contaminated food

PA intoxications occurred worldwide in both animals and humans. Compared to humans, animals were poisoned mainly by the consumption of PA plants on the field. Conversely, the consumption of plant-based foods such as herbal teas or wheat contaminated with PA is associated with reported cases of PA intoxication in humans (Wiedenfeld and Edgar 2011; Tamariz et al. 2018). It is well-known that a PA transfer into animal-derived products including milk or eggs occurs; however, the quantities involved are negligible. For example, the PA levels in milk and eggs were found to be 0.17 µg/ kg and 0.12 µg/ kg, respectively, while the average level in herbal tea was 454 µg/ kg (Mulder et al. 2018). The contamination of plant-based food with PAs takes place through several pathways. These include the unconscious harvesting of PA plants next to crops on the field, the carry-over from PA contaminated food and the horizontal transfer of PAs from PA producing plants to non-PA plants via their roots (Teschke et al. 2021).

In recent years, many studies have been carried out to determine the PA content in plant-based foods. In summary, the major food products contaminated with excessive levels of PA include herbal teas, honey, food supplements and spices (Lu et al. 2024). A study was conducted to screen herbal teas of diverse varieties from six European countries for the presence of PAs. The analysis revealed that 92% of the samples tested positive, with a maximum value of 4805 µg/ L and an average value of 454 µg/ L. Rooibos, followed by peppermint, black tea, and green tea, exhibited the highest concentration of PAs (Mulder et al. 2018). The analysis of vegetable and spice samples from the Netherlands revealed that artichokes exhibited the highest contamination levels of PAs, followed by fennel and dandelion with average levels between 793 and 2385 µg/ kg PAs. Oregano, rosemary and mint exhibited levels between 151 and 235 µg/ kg (EFSA 2017b). Compared to the results of the Bundesinstitut für Risikobewertung (BfR) study, PA levels in spices were found to reach up to 5000 µg/ kg, with approximately 78% of the samples containing no more than 100 µg/ kg of PAs (BfR 2016). The concentration of PAs in honey varies depending on the country of origin. The mean PA levels in local honey from northern Germany and Ghana were found to be 73 µg/ kg and 283 µg/ kg, respectively, with maximum values of 3313 µg/ kg PA and 2639 µg/ kg (Letsyo et al. 2017; Gottschalk et al. 2020). The PA levels in local honey from Ghana are comparable to those observed in bee pollen. The average PA content was 382 µg/ kg, with a maximum of 3356 µg/kg (De Jesus Inacio et al. 2020). The interest in bee pollen products e.g. as dietary supplement increased in the last years (Lu et al. 2024).

Furthermore, there is evidence that PA transfer into streams, ground water, soil or in non-PA-producing plants like maize is possible (Günthardt et al. 2020; Kisielius et al. 2020; Letsyo et

al. 2024). PA amounts of up to 70 ng/ L in stream water and up to 230 ng/ L in seepage water from groundwater wells were measured in Denmark due to the contamination of the invasive butterbur (Kisielius et al. 2020). Moreover, it was demonstrated that during rain events, the PA concentration in ragwort areas increased significantly in both soil and surface water (Hama and Strobel 2021). The PA uptake into non-producing PA plants through contaminated soil has been demonstrated in maize, although only trace amounts were detectable. It is hypothesised that an increased concentration of copper in soil may damage roots of both PA plants and food crops, enhancing the uptake of PA in non-PA-producing plants (Letsyo et al. 2021).

2.5.2 Chronic PA intake and human health risk

Especially the chronic PA toxicity is of interest due to its hepatotoxic and genotoxic potentials *in vivo*, leading to irreversible organ damage or cancer (EFSA 2011). For substances that are both genotoxic and carcinogenic, the margin of exposure (MoE) approach is used for risk characterisation. The MoE represents a dimensionless ratio between an appropriate toxicological reference point and the estimated daily intake (EDI) in a human population (Hartwig et al. 2020; Schrenk et al. 2022). The reference point can be derived from epidemiological studies or rodent carcinogenicity studies using the benchmark dose (BMD) approach. The BMD approach requires a benchmark response (BMR) comparable to the tumour incidence in a carcinogenicity study. In addition, the BMR includes a percentage (typically 10%) of the incidence above backround tumour rates (US EPA 1995). In general, a lower incidence rate of e.g. 5% is associated with a greater degree of uncertainty (Barlow et al. 2006). However, the BMR should be chosen according to the data set, typically 5% for continuous data (5%) and 10% for quantitative data due to the change in mean response and extra risk (EFSA 2017a). Moreover, in consideration of statistical uncertainty, the 95% confidence interval (CI) was employed to assess the lower boundary for the BMD value (BMDL). No human health concern is expected if the MoE value is above 10,000 (Lachenmeier and Rehm 2015).

In 2017, the CONTAM panel of the EFSA published a new $BMDL_{10}$ of 237 µg/ kg bw per day based on the formation of liver haemangiosarcoma as the most sensitive neoplastic endpoint (see chapter 2.4.4). This reference point was estimated based on the data from the riddelliine carcinogenicity study, which is more reliable compared to the 2-year carcinogenicity study with lasiocarpine (EFSA 2017b). It was estimated that the chronic PA exposure resulting from the consumption of herbal and rooibos tea was slightly above 10,000 for high consumers (EFSA 2017b). Chen and colleagues evaluated MoE values for 21 types of teas and found evidence of concern for the daily consumption of tephroseris, borage and lemon balm as tea during a lifetime (Chen et al. 2022a). Due to data gaps only model scenarios for herbs and spices were performed to investigate the human health risk. The model scenarios showed that even a low

consumption of herbs or spices such as oregano or thyme could lead to a potential PA exposure and health concern in adults or children (Kaltner et al. 2020). According to model scenarios from the BfR, MoE values below 10,000 are achieved for regular consumer and high consumer (adults) by the consumption of 3,000 µg and 1000 µg 1,2-unsatured PA per kg contamined spices, respectively (BfR 2020).

It should be noted that one or more PAs are found in food, but the MoE approach is performed on the $BMDL_{10}$ value of riddelliine. Several lines of evidence observed a structure-dependent toxicity of PAs *in vitro*, showing a greater toxic potential for PAs with a higher degree of esterification. Furthermore, some PAs like heliotrine or monocrotaline are not equally toxic within the same esterification group (Allemang et al. 2018; Louisse et al. 2019; Gao et al. 2020; Rutz et al. 2020). Accordingly, the MoE approach may result in an over- or underestimation of the risks, depending on the PAs found in food (Schrenk et al. 2022). Merz and Schrenk proposed interim relative potency (iREP) factors to evaluate PAs based on their chemical structure. The iREP factors describe the toxic potential of each PA, whereby additional literature data were used to compare the PAs. The data include acute toxicity in rodents, *in vitro* cytotoxicity and genotoxicity in drosophila of each PA. The data allowed the derivation of iREP factors of 1.0, 0.3, 0.1 and 0.01, whereby a lower factor is associated with a decreased toxic potential. The researchers concluded that cyclic di-esters, followed by open di-esters, are the most toxic PAs compared to mono-esters. Furthermore, PAs with a 7S configuration are more toxic than those with a 7R configuration (Merz and Schrenk 2016). However, the BfR declined the congener-specific approach due to insufficient data and upheld the recommendation that all 1,2-unsaturated PAs should be classified as equally toxic (BfR 2020).

2.5.3 PA regulations and recommendations

In addition to chronic PA toxicity, acute intoxication manifests as non-neoplastic damage such as liver necrosis, if high PA amounts are orally ingested and metabolized within a short time (Dusemund et al. 2017). The BfR established a health-based guidance value (HBGV) of 0.1 µg PA/ kg bw per day derived from a NOAEL of 10 µg/ kg bw per day from a 2-year rat carcinogenicity study with riddelliine, which showed non-neoplastic damage, and applied an extrapolation factor of 100 based on interspecies (10) and intraspecies (10) differences. The HBGV is used as a reference point for assessing the risk of non-carcinogenic damage (BfR 2020). In comparison, this reference point is 8000-fold lower (0.8-1.7 mg/ kg bw per day) compared to the lowest known acute dose associated with adverse liver effects in children after 4-14 days PA-contaminated tea exposure. Furthermore, the HBGV is 150-fold lower compared to the lowest known dose associated with long-term toxicity (6 months) in humans (15 µg/ PA/ kg bw per day) (WHO-IPCS 1988; EFSA 2011).

In the past, the BfR and the Committee on Toxicity of Chemicals in Food, Consumer Products and the Environment (COT) recommended a maximum daily intake of 0.007 µg/ kg bw per day for PAs based on the $BMDL_{10}$ of 73 µg kg bw per day based on liver tumors from the two-year carcinogenicity study with lasiocarpine. The maximum daily intake of 0.007 µg/ kg bw per day is derived by allowing a MoE of 10,000 (EFSA 2011; Lu et al. 2024). The European Medicines Agency (EMA) Committee on Herbal Medicinal Products (HMPC) referenced the EFSA risk assessment and agreed that an oral intake, including for contamination in medicinal products, of 1.0 µg/ day for an adult is not a cause for concern based on the acceptable intake of 0.0237 µg/ kg bw for a 50 kg person based on the two-year carcinogenicity study with riddelliine (EMA 2021). Furthermore, the regulation (EC) No. 2023/ 915 provides maximum limits of the sum of 21 PAs/ PANOs and 14 co-eluated isomers in food such as oregano or herbal teas (EC Regulation 2023/ 915).

Moreover, it is recommended that manufacturers in the European Union pursue continuous optimisation of their cultivation, harvesting and cleaning methods with the objective of reducing the content of 1,2-unsaturated PAs in food as far as is technically feasible (ALARA principle – as low as reasonably achievable) (BfR 2020).

2.6 DNA damage and its cellular response

Cells are constantly exposed to DNA damage from both endogenous and exogenous sources (Marechal and Zou 2013). While endogenous damage arises from normal cellular processes, such as metabolic by-products or spontaneous chemical reactions, exogenous sources comprise ultraviolet (UV) and ionizing radiation, environmental chemicals or dietary carcinogens. Spontaneous errors during DNA replication and repair as well as chemical instability of DNA including depurination, deamination and hydrolysis are examples for endogenous DNA damage. Exogenous sources such as UV radiation can cause thymine dimers, while ionizing radiation can induce double-strand breaks and complex DNA lesions (Giglia-Mari et al. 2011; Yousefzadeh et al. 2021).

It is estimated that each cell experiences up to 10,000 single-strand breaks (SSB) and spontaneous base losses in its DNA daily. When accounting for all types of spontaneous damage, the total number can reach up to 100,000 lesions per cell each day (Lindahl 1993; Sander et al. 2004). On the other side, UV-A and -B exposure can cause up to 100,000 lesions in a cell per hour (Ward 1988).

To manage with this constant threat, cells have developed a sophisticated DDR system. The DDR is of crucial importance for the preservation of genomic integrity in the face of constant DNA damage from both internal and external sources (Smith et al. 2020). Failure to properly repair DNA damage can lead to mutations, genomic instability, and cancer (Roos et al. 2016).

2.6.1 DNA damage response

In response to genotoxic stress, cells have developed complex mechanisms that subsequently determine whether the cell will survive or undergo cell death. The cellular response is controlled and orchestrated by the DDR signaling pathway. The DDR is activated in presence of DNA strand breaks or replication stress, such as stalled replication forks, and allows removal of lesions to be completed before replication or cell division (Roos and Kaina 2013; Blackford and Jackson 2017). The DDR signaling pathway involves protein kinases and mediator proteins, which facilitate phosphorylation events within the DDR network. In mammalian cells, the kinases *ataxia-telangiectasia* mutated (ATM), ATM- and Rad3-related (ATR) and DNA-dependent protein kinase (DNA-PK) are pivotal components of the DDR. These serine/ threonine kinases belong to the phosphatidylinositol-3-kinase-like kinase (PI3K) family and are essential for maintaining genomic stability (Jackson and Bartek 2009; Maréchal and Zou 2013). While ATR is primarily activated in response to stalled DNA replication forks, ATM and DNA-PK are both recruited to DSBs (Figure 2.8). However, there is ample evidence for crosstalk between all three PI3K kinases with each other through DNA end resection or post-translational modifications on shared proteins such as Histone H2AX, which is essential for maintaining genomic stability (Maréchal and Zou 2013). The apical phosphokinases are activated via autophosphorylation, except ATR, and phosphorylate numerous downstream-targets like checkpoint kinases (CHKs), H2AX or the tumorsurpressor protein p53 (Blackford and Jackson 2017). There is evidence that certain PAs like lasiocarpine lead to an activation of both CHK1 and CHK2 as well as p53 signaling pathways in liver cells or TK6 cells (Ebmeyer et al. 2020; Li et al. 2021). The DDR either halts the cell cycle to allow for repair or triggers apoptosis if the DNA damage is irreparable, depending on the severity, to prevent potential mutations. The phosphorylation on both CHKs and p53 is essential for initiating signal cascades that result in cell cycle arrest (Roos et al. 2016). Abdelfatah and coworker showed that cyclic and open diester lead to the up- and downregulation of several genes involved in cell phase arrest through G1/S and G2/M transition in liver cells (Abdelfatah et al. 2022). Furthermore, p53 plays a crucial role as transcription factor by initiating the transcription of genes involved in DNA repair, cell cycle arrest and apoptosis, hence being referred to as “guardian of the genome” (Silva et al. 2020; Chen et al. 2020).

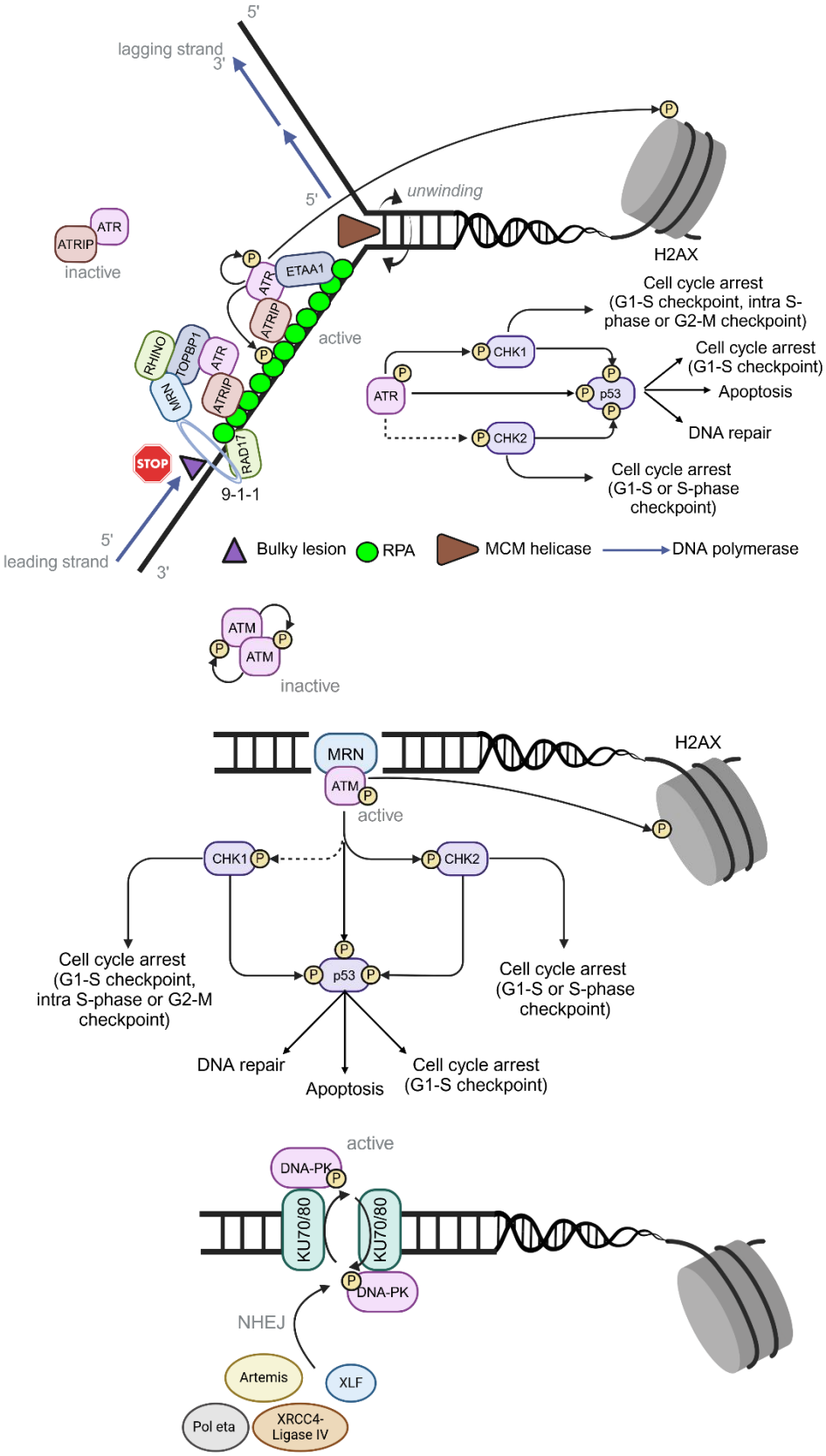

Figure 2.8: The DNA damage response. ATR, ATM and DNA-PK recruitment to DNA strand breaks and their respective activation pathway (modified by Blackford and Jackson 2017, Saldivar et al 2017, created in https://BioRender.com)

In presence of replications stress and single-stranded DNA (ssDNA) regions, the ATR signaling pathway is activated. In the first step, the leading strand polymerase is blocked and the minichromosome maintenance (MCM) helicase continues unwinding DNA ahead of the replication fork. This process results in substantial stretches of ssDNA, which are rapidly coated by replication protein A (RPA) (Byun et al. 2005; Nickoloff et al. 2022). In general, RPA is coated at ssDNA through nucleolytic processing due to damaged DNA or by helicase-polymerase uncoupling at stalled replication forks (Zou and Elledge 2003; Byun et al. 2005). Next, ATR is recruited by its partner, the ATR-interacting protein (ATRIP), on the RPA-coated ssDNA. The RAD9-RAD1-HUS1 (9-1-1) is structurally similar to the proliferating cell nuclear antigen (PCNA) and is loaded by the RAD17-replication factor C subunits 2-5 (RFC2-5 or RAD17) clamp loader at the single-stranded and double-stranded DNA junction close to the ssDNA (Bermudez et al. 2003; Ellison and Stillman 2003; Zou et al. 2003; Zou and Elledge 2003). Both complexes form sliding clamps at or near sites of DNA damage (Abraham 2001). The 9-1-1-complex interact with the RAD9-HUS1-RAD1-interacting nuclear orphan (RHINO) and the MRN complex to recruit the ATR activator topoisomerase II binding protein (TOPBP1). The TOPBP1 binds to the ATR-ATRIP complex and lead to ATR activation (Cotta-Ramusino et al. 2011; Lindsey-Boltz et al. 2015). Besides, the Ewing tumor-associated antigen 1 (ETAA1) can bind to RPA and activate ATR in a parallel pathway (Bass et al. 2016; Haahr et al. 2016; Lee et al. 2016). It is known, that both TOPBP1 and ETAA1 induce a conformational change in ATR, enhancing its kinase activity against its substrates (Mordes et al. 2008). In the meanwhile, RPA is phosphorylated by the ATR-ATRIP complex, which is essential for recruiting downstream targets to the stalled replication fork and minimize ssDNA generation (Kang et al. 2023). Activated ATR can autophosphorylate itself on Thr1989 for enhanced activity and phosphorylates downstream targets including CHK1 at Ser345. The activation of CHK1 is only in presence of claspin possible (Kumagai and Dunphy 2000). Furthermore, ATR and CHK1 are capable both to phosphorylate p53 at Ser15 and Ser20, leading to p53 accumulation. The activation of both, CHK1 and p53, is necessary to regulate cell cycle progression and DNA repair (Blackford and Jackson 2017). Besides, the histone H2AX is phosphorylated (γH2AX) at Ser139 by ATR as well, which is a known DNA damage marker at SSB and DSB (Shiloh and Ziv 2013).

When two SSBs occur close to each other or when the DNA replication machinery encounters a SSB or certain other lesions, DSBs are formed. In response to DSBs, both ATM and DNA-PK become activated, but each apical phosphokinase is recruited on site by different sensor proteins. While the MRE11/RAD50/NBS1 (MRN) complex is needed for ATM recruitment, the heterodimer KU70/80 is necessary for DNA-PK assembly (Blackford and Jackson 2017). The latter is further described in the chapter “DNA repair pathways”, as NHEJ plays a major role following DNA-PK activation. In general, ATM relies as a Dimer in undamaged cells. After MRN

recruitment at DSB sites, ATM undergoes autophosphorylation at serine residues (Ser 367, 1893 and 1981) to activate itself and its substrates (Kozlov et al. 2011). Common downstream targets including CHK2 (Thr68), p53 (Ser15/ 20) and H2AX (Ser139) are phosphorylated after ATM activation, which in turn affect cell cycle progression at G1/S and G2/M cell cycle checkpoint and DNA repair (Shiloh and Ziv 2013). Phosphorylated CHK2 leads to its dimerization and autophosphorylation, which is required for full activation (Zannini et al. 2014). Besides ATR, ATM and DNA-PK lead to a RPA32 phosphorylation at specific residues in response to replication stress (Liu et al. 2012). ATM phosphorylates RPA32 at serine residues 4, 8, and 12, while DNA-PK targets the same sites with an additional phosphorylation at serine 21. Notably, it is suggested that the phosphorylation at serine 4 and 8 is mainly mediated by DNA-PK. In contrast, ATR specifically phosphorylates serine 33 at RPA32 (Liu et al. 2012; Maréchal and Zou 2015). RPA32 phosphorylation can have an impact on the stabilization of replication forks, facilitates the recruitment of repair proteins and suppresses DNA replication, ensuring proper cell cycle arrest and repair processes (Feng et al. 2009; Liu et al. 2012; Kang et al. 2023). Furthermore, H2AX phosphorylation belongs to the most prominent DDR-associated histone modification in response to DNA damage (Giglia-Mari et al. 2011). The ubiquitination of γH2AX by E3 ubiquitin ligases including RNF8 and RNF168 promotes the DSB repair. RNF8 ubiquitinates proteins at the damage site directly to γH2AX, creating a platform for RNF168 to dock. RNF168 amplifies the signal by ubiquitinating histone H2A at lysines 13 and 15 (H2AK13/K15). This process allows the recruitment of DNA repair proteins such as 53BP1 and BRCA1 to the site and is necessary for chromatin remodeling (Giglia-Mari et al. 2011; Sekiguchi and Matsushita 2022). On the other hand, the deubiquitination is essential for resolving the DDR and restoring chromatin to its original state. Specifically, USP3 and USP49 are responsible for the deubiquitination of γH2AX, ensuring proper regulation of the repair process and preventing prolonged signaling (Sharma et al. 2014; Sekiguchi and Matsushita 2022).

2.6.2 Cell cycle regulation and arrest

The eukaryotic cell cycle is comprised of four phases: G1 (first gap phase), S (DNA synthesis), G2 (second gap phase) and M (mitosis) (Figure 2.9). Checkpoints regulate the progression between these phases, ensuring the correct sequence of events and halting the cycle if issues such as DNA damage or spindle defects arise, allowing time for resolution (Huang and Zhou 2020). The cell cycle can be halted at the G1/S transition, during the S-phase, or at the G2/M transition, depending on the type of DNA damage and the cell cycle stage when the lesion is detected (Figure 2.9). Key proteins, such as cyclins and cyclin-dependent kinases (CDKs), promote cell cycle progression, while inhibitors like p21 can halt progression in response to DNA damage (Zhou and Elledge 2000).

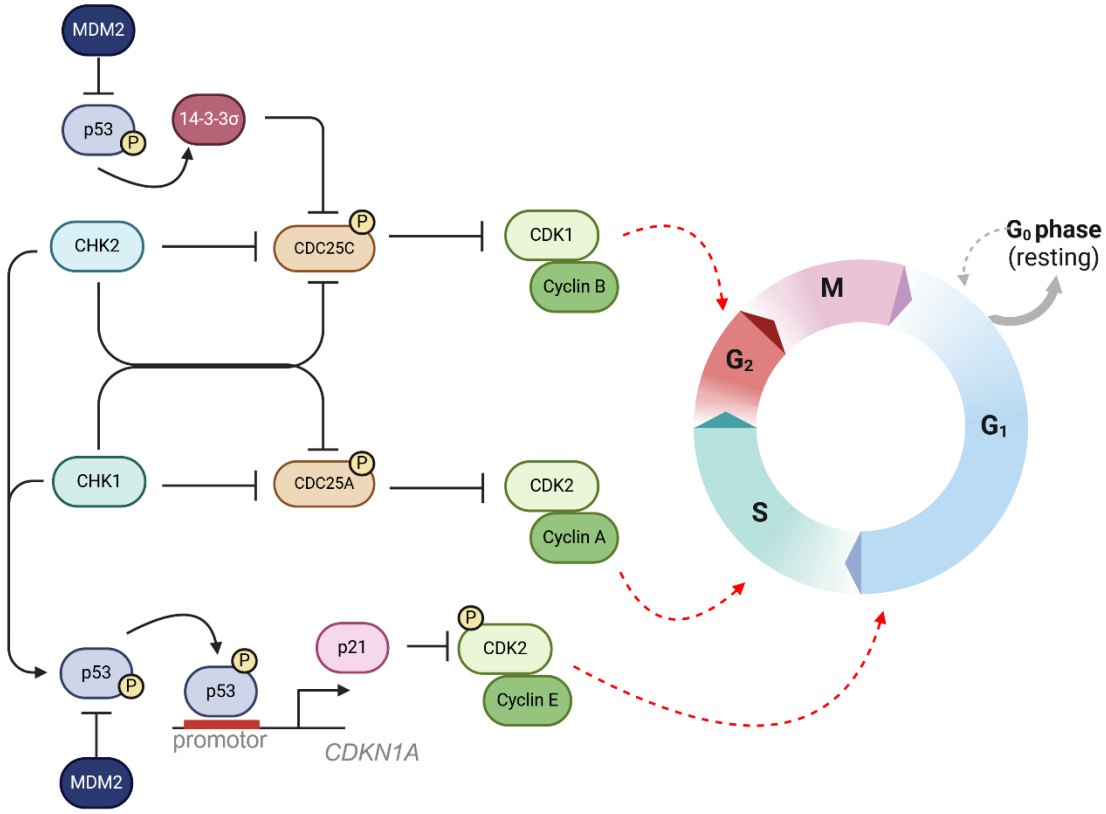

Figure 2.9: Cell cycle regulation after phosphorylation of p53, CHK1 and CHK2 (modified by Smith et al. 2020; Gorecki et al. 2021; Vlatkovic et al. 2022, created in https://BioRender.com)

The TP53 gene encodes the tumor suppressor protein p53, which is a key regulator of the cell cycle. In response to DNA damage, p53 is phosphorylated by apical phosphokinases or checkpoint kinases at e.g. Ser15 or Ser20, leading to a dissociation of mouse double minute 2 (MDM2) and p53 accumulation (Chen et al. 2020). In general, low levels of p53 are present in non-transformed cells due to the E3 ubiquitin ligase MDM2. The transcription of MDM2 is activated by p53, which in turn block the transcriptional activity of p53 and mediate its degradation via the 26S proteasome through ubiquitination (Jung et al. 2020). The negative feedback loop of both proteins is interrupted if p53 is phosphorylated at specific residues. Stabilized p53 binds to specific p53-response elements of the cyclin-dependent kinase inhibitor 1A (*CDKN1A*) promotor region, leading to its transcriptional activation of p21/WAF1. Subsequently, p21 can bind to cyclin-dependent kinases (CDK) 2 and 4, inhibiting their activity and preventing their association with cyclins E and D, respectively. This inhibition leads to cell cycle arrest at the G1 phase(Harper et al. 1995; Roos and Kaina 2013; Huang and Zhou 2020). The G1 cell cycle arrest prevents the phosphorylation of the retinoblastoma protein (Rb), allowing it to bind to the transcription factor E2F1, thereby repressing the expression of genes required for DNA replication and cell-cycle progression. Furthermore, p21 also interact with the proliferating cell nuclear antigen (PCNA), assisting to block DNA replication and reinforce the

cell cycle arrest (Luo et al. 1995; Huang and Zhou 2020). Besides, p53 further controls the cell cycle at the G2/M phase, preventing cell proliferation. Other p53 target genes like 14-3-3σ and the cell division cycle 25 (cdc25) are linked with a p53-induced G2/M arrest in response of DNA damage (Hermeking et al. 1997; Badie et al. 2000). In cases of sustained damage, stabilized p53 induces the transcription of pro-apoptotic genes like PUMA and BAX, resulting in apoptosis (Bieging et al. 2014).

Activated CHK1 and CHK2 can phosphorylate and inactivate cdc25A and cdc25C phosphatases, preventing them from removing the inhibitory phosphorylation on CDK1 (Lewis et al. 2017; Rundle et al. 2017). The phosphorylation of cdc25A leads to its degradation during the S phase, while phosphorylation of cdc25C causes it to associate with 14-3-3 signaling proteins, resulting in its sequestration in the cytoplasm (Saldivar et al. 2017). The inhibition of CDK1 stops entry into mitosis, whereas inhibiting CDK2 prevents entry into and progression through the S-phase. Furthermore, both checkpoint kinases phosphorylate p53 at specific sites, leading to its accumulation and activation of the p53-p21 axis (Smith et al. 2020).

2.6.3 DNA repair pathways

DNA repair is crucial for genomic stability since deficiencies can lead to diseases like xeroderma pigmentosum (XP), Cockayne syndrome (CS), ataxia-telangiectasia (A-T) or Seckel syndrome. These conditions are linked to distinct risks: XP (caused by mutations in XPA-XPG) is associated with an increased risk of skin cancer, while Li-Fraumeni syndrome (p53 mutations) predisposes to breast and brain tumors. Defects in homologous recombination (BRCA1/2 mutations) elevate breast cancer risk, and A-T (ATM mutation) is linked to lymphoma. In contrast, neurodegenerative disorders are primarily associated with CS, Seckel syndrome (ATR mutation), and A-T (Jackson and Bartek 2009; Coon and Benarroch 2018). In mammalian cells, several repair pathways are crucial for addressing different types of DNA damage. For example, the base excision repair (BER) is responsible for removing oxidative base modifications, while the mismatch repair (MMR) identifies and correct base-base mismatches that arise from errors during DNA replication (Jiricny 2006; Modrich 2006; Wilson and Bohr 2007). The nucleotide excision repair (NER) responds to bulky or UV-induced adducts, while the non-homologous end-joining (NHEJ) and homologous recombination (HR) are activated in the presence of DSBs (Schärer 2013; Kowalczykowski 2015; Seol et al. 2018). Each DNA repair pathway relies on specific proteins for the recognition, removal, and repair of DNA lesions. A comprehensive overview of the various DNA repair pathways and their associated proteins is provided in table 2.3.

In the context of the NER, two distinct sub-pathways have been characterised for the detection of DNA damage. The global genome NER (GG-NER) is triggered by helix-distorting DNA damage, such as UV-induced cyclobutane pyrimidine dimers (CPDs) and (6-4) photoproducts,

and is active throughout the entire genome. On the other hand, the transcription-coupled NER (TC-NER) is triggered only to RNA polymerase II stalling at lesions on the transcribed strand. Furthermore, each sub-pathway differs in their recognition proteins: The GG-NER is initiated by XPC and RAD23B, whereas the TC-NER involves CSA and CSB (Mullenders 2015; Nastasi et al. 2020). After the recognition of the DNA lesion, both pathways recruit the transcription factor IIH complex (TFIIH), including helicases XPB and XPD, to open the DNA duplex, followed by exonucleases and XP proteins for damage removal (Coon and Benarroch 2018). The helicase XPB is responsible for the recruiting of TFIIH, while XPD is necessary for the damage verification. The damaged DNA segment is removed as a 22-30 base oligonucleotide by XPF-ERCC1 and XPG. The correct incision of the oligonucleotide requires the organization of the proteins XPA, XPG and RPA. At the end, the DNA resynthesis and ligation is carried out by proliferating cell nuclear antigen (PCNA), replication factor (RFC) and DNA polymerases δ/ε to fill the gap, whereby the nick is sealed by either the XRCC1–ligase 3 or flap endonuclease 1–ligase 1 complex (Schärer 2013).

The NER operates throughout the cell cycle, whereas the NHEJ or HR is limited to cell division phases. The NHEJ is the predominant pathway for DSBs during the G1 phase in both post-mitotic and cycling cells, though it is known to be error-prone (Zha et al. 2011). The error-prone nature of microhomology-mediated end joining (MMEJ) arises when the classical non-homologous end joining (NHEJ) pathway fails, prompting the activation of an alternative repair mechanism mediated by DNA polymerase θ. The polymerase θ plays a crucial role in MMEJ, an alternative pathway for repairing DSBs (Beagan and McVey 2016). It promotes MMEJ by aligning short microhomologous sequences at the ends of processed DNA, filling in gaps, and displacing DNA strands during the repair process. Unlike most other polymerases, Pol θ can synthesize DNA from single-stranded templates and 3' overhangs, making it particularly suited for MMEJ (Beagan and McVey 2016). MMEJ can result in the induction of mutations and cancer progression (Van Schendel et al. 2015). The NHEJ starts with the recognition and binding to the broken DNA ends by the KU70/80 protein complex without needing a repair template. The recruitment of DNA-PK to KU70/80 allows the aligning of DSB ends for repair. It was shown that the autophosphorylation at both Ser2056 and Thr2609 are necessary for DNA-PK activation. Next, the endonuclease Artemis is recruited by DNA-PK to process the DNA ends, making them suitable for ligation (Blackford and Jackson 2017). Finally, the XRCC4-Ligase IV complex, along with XLF, joins the DNA ends together for completing the repair (Giglia-Mari et al. 2011; Coon and Benarroch 2018). On the other hand, the HR is restricted to the S and G2 phases since homologous sister chromatids are needed. HR also helps to restart stalled replication forks and fix interstrand DNA crosslinks, which involves the Fanconi Anaemia (FA) protein complex (Jackson and Bartek 2009). The MRN complex initially recognizes and binds to DSBs, facilitating the recruitment of ATM. Afterwards, ATM

phosphorylates several substrates including CtIP, BRCA1 and H2AX, which lead to the recruitment of additional repair proteins (Coon and Benarroch 2018). The MRN complex, along with CtIP and BRCA1, initiates DNA end resection, creating a ssDNA overhang (Smith et al. 2020). RPA binds to ssDNA, preventing secondary structure formation. RAD51 is then loaded onto the ssDNA, displacing RPA with the help of BRCA2 and other mediators, forming a nucleoprotein filament that invades the homologous DNA sequence. At the end, DNA synthesis and ligation complete the repair (Giglia-Mari et al. 2011). A key factor in selecting the DSB repair pathway is the initiation of 5′-3′ resection of DNA ends to form ssDNA segments, followed by a coating with the recombinase RAD51 (Kowalczykowski 2015). Furthermore, BRCA1 interacts with DNA-PKs during the S phase to block its autophosphorylation, facilitating DNA end resection and HR factor loading (Davis et al. 2014).

Table 2.3: Overview of exemplary DNA repair mechanism (modified by Jackson and Bartek 2009, Nastasi et al 2020)

Repair mechanism	Causes / Type of DNA damage	Key proteins
MMR	DNA mismatches and insertion/deletion loops arising from DNA replication	Sensors MSH2-MSH6 and MSH2-MSH3 plus MLH1-PMS2, MLH1-PMS1, PLH1-MLH3, EXO1, polymerases δ and ε, PCNA, RFC, RPA, ligase I
BER	Abnormal DNA bases, simple base adducts	DNA glycosylases as sensor, AP endonuclease, polymerase (β, δ, ε) FEN1, DNA ligase I or ligase III, XRCC1
NER	Lesions that disrupt the DNA double-helix, such as bulky base adducts and UV photo-products	Sensors elongating RNA polymerase, XPC-HR23B and DDB1/2, plus XPA, XPE, XPF/ERCC1, XPG, CSA, CSB, TFIIH (containing helicases XPB and XPD), DNA polymerases and associated factors, RPA, ligase I
Trans-lesion bypass	Base damage blocking replication fork progression	“Error-prone” DNA polymerases, including polymerases (η, ι, κ), REV3 and REV1; plus associated factors
NHEJ	Radiation- or chemically-induced DSBs plus V(D)J and CSR intermediates	Sensors Ku70/80 and DNA-PKs plus XRCC4, XLF/ Cernunnos and ligase IV Can also employ the MRE11-RAD50-NBS1 complex, Artemis nuclease, PNK, Aprataxin and polymerases (μ and λ)
HR	DSBs, stalled replication forks, inter-strand DNA cross-links and sites of meiotic recombination and abortive Topoisomerase II action	RAD51, RAD51-related proteins (XRCC2, XRCC3, RAD51B, RAD51C, RAD51D, DMC1), RAD52, RAD54, BRCA2, RPA, FEN1, DNA polymerase and associated factors. Promoted by MRN, CtIP, BRCA1, and the ATM signalling pathway
MMEJ	DSB, UV or chemotherapy, ROS	PARP1, CtIP, Mre11 complex, BLM/ EXO1, MHs, RPA, XPF/ ERCC1 nuclease, polymerase θ and ligation by Ligases I/III

3 Objectives

Currently, PAs in food are assessed using the MoE approach, which is based on the $BMDL_{10}$ value of riddelliine. However, several lines of evidence indicate that PAs exhibit structure-dependent toxicity, with a greater toxic potential for PAs with a higher degree of esterification. Moreover, PAs within the same esterification group, such as heliotrine and monocrotaline, can differ in toxicity, leading to potential over- or underestimation of risks depending on the specific PAs found in food. To refine PA risk assessment, Merz and Schrenk reviewed existing literature on PA toxicity and proposed iREP factors, classifying PAs based on their chemical structure and toxic potential. These factors, ranging from 1.0 to 0.01, account for acute toxicity in rodents, *in vitro* cytotoxicity, and genotoxicity in Drosophila, suggesting that cyclic di-esters are the most toxic, followed by open di-esters and then mono-esters. Additionally, PAs with a 7S configuration show higher toxicity than those with a 7R configuration. Despite these insights, the BfR rejected a congener-specific approach due to insufficient data, maintaining the classification of all 1,2-unsaturated PAs as equally toxic.

Although the literature provides valuable insights into PA toxicity, current data on PA effects in liver cells are limited. Further studies are required to comprehensively evaluate structure-dependent PA toxicity and improve risk assessment strategies. This project aims to address these gaps by providing a refined toxicity assessment of structurally diverse PAs, supporting the development of a more precise risk evaluation framework. Through systematic potency ranking and a detailed investigation of PA transport mechanisms, this research offers valuable data that can contribute to a reworked PA risk assessment strategy.

Publication I: It is commonly known that a higher PA toxicity is related to a higher degree of esterification. Previous studies have indicated that individual PA congeners within esterification groups, including monoesters, open diesters, and cyclic diesters, display distinct cytotoxic and genotoxic effects. This highlights the importance of distinguishing these congeners from others within the same group, as they cannot be regarded as equivalent (Louisse et al. 2019; Gao et al. 2020; Rutz et al. 2020). This study employs human HepG2 cells with CYP3A4 overexpression and PHH to assess PA-induced genotoxicity and cytotoxicity. The following research questions are addressed:

- What is the cytotoxic potential of structurally distinct PAs in HepG2-CYP3A4 cells and PHH, and how do their toxic effects correlate with their chemical structures?
- Can genotoxicity markers, such as γH2AX and p53, be used to establish a potency ranking for PAs based on structure-dependent effects?
- How do BMD approaches support the classification of PAs into potency classes for risk assessment?

- Can the observed cytotoxic and genotoxic effects be confirmed in PHH, considering their full metabolic competence compared to HepG2-CYP3A4 cells?

Publication II: The hepatotoxic potential of PAs is influenced not only by metabolic activation but also by their intracellular accumulation via transporters such as OCT1. It remains to be clarified whether OCT1 transport is relevant for PAs, irrespective of their esterification group. This study examines the impact of the OCT1-mediated uptake of selected PAs, representing one congener from each esterification group, on PA toxicity in wildtype HepG2 and V79, CYP3A4- overexpression HepG2 and V79 cells as well as PHH. The following research questions are explored:

- How does OCT1 influence the cellular uptake of structurally different PAs in human liver cell and hamster lung fibroblasts?
- Can pharmacological inhibition of OCT1 prevent PA-induced cytotoxicity and genotoxicity in liver cell models?
- Does the inhibition of OCT1 affect the activation of the DDR, as indicated by reduced phosphorylation of checkpoint kinases?

In summary, this project aims to elucidate the structure-dependent toxicity of PAs and the role of OCT1-mediated transport in modulating their hepatotoxic effects. The findings will contribute to a more refined risk assessment framework for PAs and help establish mechanistic insights into their toxicological profiles.

4 Cumulative Part: Publications

4.1 Publication I

The publication I describes the investigation of the cytotoxic and genotoxic potential of 11 pyrrolizidine alkaloids using the Alamar blue assay and an *in vitro* genotoxicity battery in HepG2-CYP3A4 cells and PHH. The *in vitro* test battery includes assays to assess the DNA damage, including the alkaline comet assay as well as the determination of DNA damage markers γH2AX and p53. The aim was to rank the potency of different PAs based on their genotoxic and cytotoxic effects.

Reference: Haas, M., Wirachowski, K., Thibol, L., Küpper, J.-H., Schrenk, D., Fahrer, J., *Potency ranking of pyrrolizidine alkaloids in metabolically competent human liver cancer cells and primary human hepatocytes using a genotoxicity test battery.* Arch Toxicol 97, 1413–1428 (2023).

The publication, along with the supplementary data, is free available in the journal “Archives of Toxicology”. The following link provides full access to the article and the data.

DOI: 10.1007/s00204-023-03482-8

Contributions to this publication:

I contributed in the investigation, methodology and formal analysis as well as the writing of the original draft and its editing. Furthermore, I performed cytotoxicity and genotoxicity experiments of nine out of eleven PAs in HepG2-CYP3A4 cells and all PAs in cryoconserved human hepatocytes. Ms. Wirachowski investigated the genotoxic and cytotoxic potential of two PAs, echimidine and heliotrine, as part of her master’s thesis. Additionally, I conducted and managed the cell culture and treatment, experiments including western-blot analysis, alkaline comet-assay, confocal immunofluorescence microscopic analysis and resazurin reduction assay. I was primarily responsible for comet analysis, with Ms. Thibol assisting in evaluation. Furthermore, I determined the relative cytotoxicity, the genotoxicity by BMD modelling and statistical analysis with the data. The HepG2-CYP3A4 cells were generated by Küpper’s group at the Department of Environment and Nature Science in Brandenburg University of Technology Cottbus-Senftenberg. Cryopreserved PHH pooled from five Caucasian donors were purchased from Thermo Fisher Scientific.

Archives of Toxicology (2023) 97:1413–1428
https://doi.org/10.1007/s00204-023-03482-8

GENOTOXICITY AND CARCINOGENICITY

Potency ranking of pyrrolizidine alkaloids in metabolically competent human liver cancer cells and primary human hepatocytes using a genotoxicity test battery

Manuel Haas[1] · Karina Wirachowski[1] · Lea Thibol[1] · Jan-Heiner Küpper[2] · Dieter Schrenk[1] · Jörg Fahrer[1]

Received: 20 January 2023 / Accepted: 2 March 2023 / Published online: 16 March 2023

Abstract
Pyrrolizidine alkaloids (PAs) occur as contaminants in plant-based foods and herbal medicines. Following metabolic activation by cytochrome P450 (CYP) enzymes, PAs induce DNA damage, hepatotoxicity and can cause liver cancer in rodents. There is ample evidence that the chemical structure of PAs determines their toxicity. However, more quantitative genotoxicity data are required, particularly in primary human hepatocytes (PHH). Here, the genotoxicity of eleven structurally different PAs was investigated in human HepG2 liver cells with CYP3A4 overexpression and PHH using an in vitro test battery. Furthermore, the data were subject to benchmark dose (BMD) modeling to derive the genotoxic potency of individual PAs. The cytotoxicity was initially determined in HepG2-CYP3A4 cells, revealing a clear structure–toxicity relationship for the PAs. Importantly, experiments in PHH confirmed the structure-dependent toxicity and cytotoxic potency ranking of the tested PAs. The genotoxicity markers γH2AX and p53 as well as the alkaline Comet assay consistently demonstrated a structure-dependent genotoxicity of PAs in HepG2-CYP3A4 cells, correlating well with their cytotoxic potency. BMD modeling yielded BMD values in the range of 0.1–10 µM for most cyclic and open diesters, followed by the monoesters. While retrorsine showed the highest genotoxic potency, monocrotaline and lycopsamine displayed the lowest genotoxicity. Finally, experiments in PHH corroborated the genotoxic potency ranking, and revealed genotoxic effects even in the absence of detectable cytotoxicity. In conclusion, our findings strongly support the concept of grouping PAs into potency classes and help to pave the way for a broader acceptance of relative potency factors in risk assessment.

Keywords Cytotoxicity · Genotoxicity · Benchmark dose modeling · Pyrrolizidine alkaloids · Primary human hepatocytes · Potency ranking · γH2AX · p53 · DNA damage

Introduction

Pyrrolizidine alkaloids (PAs) are toxins, which are formed in 3% of the worldwide flowering plants as a defence against herbivores (Chen et al. 2010). More than 660 individual PAs and *N*-oxide derivatives were identified in over 6000 plants, with *Asteraceae*, *Boraginaceae*, *Heliotropiaceae* and *Fabaceae* as major PA-producing plant families (Fu et al. 2004; Mattocks 1986; Yang et al. 2019). In the last decades, intoxications in lifestock and wildlife were reported due to the consumption of PA producing plants and in humans by consumption of PA-contaminated foods (e.g., contaminated herbal teas or wheat flours) (Tamariz et al. 2018; Wiedenfeld and Edgar 2010). PA-contaminated food led to several outbreaks of acute liver disease in countries of the Global South like Afghanistan, South Africa and Tajikistan, characterized by hepatomegaly, ascites and liver failure, which are known symptoms for acute and sub-acute PA intoxications (Moreira et al. 2018). Although chronic PA intoxications are not documented (Merz and Schrenk 2016), a recent study with mutational signature analyses in > 1,000 liver cancer genomes revealed a link between PA exposure and liver cancer prevalent in Asian countries (He et al. 2021b).

✉ Jörg Fahrer
fahrer@chemie.uni-kl.de

[1] Division of Food Chemistry and Toxicology, Department of Chemistry, RPTU Kaiserslautern-Landau, Erwin-Schroedinger-Str. 52, 67663 Kaiserslautern, Germany

[2] Division of Molecular Cell Biology, Department of Environment and Nature Science, Brandenburg University of Technology Cottbus-Senftenberg, 01968 Senftenberg, Germany

At the chemical level, PAs are heterocyclic structures composed of a pyrrolizidine backbone (necine base) and one or two esterified acids (necine acids). Necine acids can be mono- or dicarboxylic acids, which show high structural diversity and differ in the length of the carbon chain, acidities and branching degrees (Wiedenfeld et al. 2008). Despite their high structural diversity, PAs can be classified according to the necin-base type and degree of esterification. There are four known necine base types, namely retronecine-, heliotridine-, otonecine- and platynecine-type. Only retronecine-, heliotridine- and otonecine-type PAs possess a double bond at the C1-C2 position (1,2-unsatured) within the necin base (Wiedenfeld et al. 2008). Depending on their degree of esterification, PAs can be classified as monoester, open diester or cyclic diester.

Only the 1,2-unsatured PAs are of toxicological concern, since they can undergo metabolic activation giving rise to genotoxic and potentially carcinogen species (Chen et al. 2010; Fu et al. 2004; Prakash et al. 1999). The liver is the primary target organ for PA toxicity, since the compounds are activated by hepatic cytochrome P450 (CYP) monooxygenases (mostly CYP3A, but also CYP2B subfamilies) (Edgar et al. 2015). This biotransformation results in the generation of reactive dehydro-pyrrolizidine derivatives (dehydro-PAs), which can quickly hydrolyse into another reactive intermediate (±)-6,7-dihydro-7-hydroxy-1-hydroxymethyl-5H-pyrrolizine (DHP). Both metabolites bind covalently to DNA and cellular proteins, thereby forming adducts and crosslinks (Edgar 2014; Fu 2017). Furthermore, PAs can induce gene mutations (e.g., in *p53* and *Kras*), sister chromatid exchange, chromosomal aberrations and micronuclei (Chen et al. 2010). In the liver, PAs not only damage hepatocytes, but also proximate liver sinusoidal endothelial cells (LSEC), which was attributable to the efflux of reactive metabolites from the hepatocytes and uptake into LSEC (Hessel-Pras et al. 2020). This has recently also been demonstrated using a co-culture model of HepG2 liver cells and metabolically deficient HeLa cells (Hadi et al. 2023). It is further noteworthy that PAs can also be transported to other organs such as the lungs, where they can cause toxicity (He et al. 2021a; Song et al. 2020).

PAs in food and herbal medicinal products are currently regulated as a sum parameter independent of their chemical structure and genotoxic potential. However, several studies were conducted in recent years using various liver cell models, which provided evidence for a clear structure–toxicity relationship (Allemang et al. 2018; Gao et al. 2020; Louisse et al. 2019; Rutz et al. 2020). The data strongly support the concept to classify PAs according to their genotoxic and cytotoxic potential as previously suggested (Merz and Schrenk 2016). Nevertheless, a systematic potency ranking in human liver models, particularly primary human hepatocytes, based on a comprehensive genotoxicity data set for benchmark dose (BMD) analysis is still missing.

Thus, we analyzed the cytotoxicity and genotoxicity of up to eleven structurally diverse PAs in human HepG2-CYP3A4 liver cells and in primary human hepatocytes (PHH). The cytotoxic potential was investigated by the resazurin reduction assay in both liver cell models and EC_{50} values were calculated to assess the relative cytotoxicity. The genotoxic potential was determined using the alkaline Comet assay as well as western blot analysis of the DNA damage markers γH2AX and p53 in HepG2-CYP3A4 cells and confocal immunofluorescence microscopy of γH2AX in PHH. Furthermore, the comprehensive data sets were subject to benchmark dose (BMD) modelling via PROAST to derive BMD values for assessing the relative genotoxic potential. Finally, the obtained data sets were used for potency ranking in HepG2-CYP3A4 cells vs. PHH.

Results

HepG2-CYP3A4 cells reveal clear impact of PA structure and cell proliferation on PA-triggered cytotoxicity

First, we determined the cytotoxicity of eleven different PAs, representative for PA monoesters, cyclic diesters and open diesters (SI Fig. 1), using genetically engineered HepG2 cells with CYP3A4 overexpression. In these cells, CYP3A4 enzyme activity is comparable to that of PHH as shown previously (Herzog et al. 2015). HepG2-CYP3A4 cells were exposed to increasing PA concentrations (0 µM up to 500 µM, depending of the PA) for 24 h and cell viability was assessed by the resazurin reduction assay. All experiments included appropriate solvent controls as negative control and 0.1% saponine as technical positive control. No or only a slight decrease in cell viability was observed for the monoesters indicine (92%), lycopsamine (85%) and europine (77%) (Fig. 1A and SI Fig. 2A, B), whereas a strong decrease was seen for the monoester heliotrine (44%) in HepG2-CYP3A4 cells (Fig. 1B). The open diester echimidine and the cyclic diesters senecionine, retrorsine and riddelliine showed stronger cytotoxicity than all monoesters (Si Fig. 2C, D, Fig. 1C, D). Lasiocarpine and seneciphylline exerted the highest cytotoxicity with a decrease in cell viability to 21% at 40 µM and 24% at 100 µM, respectively (Fig. 1E and SI Fig. 2E). Interestingly, the cyclic diester monocrotaline was an exception among the tested cyclic diesters and caused only weak cytotoxicity at a concentration of 500 µM (77%) (SI Fig. 2F).

Next, we determined the relative cytotoxicity of each PA by calculating the effective concentration at 50% cell viability (EC_{50}) from the concentration–response data,

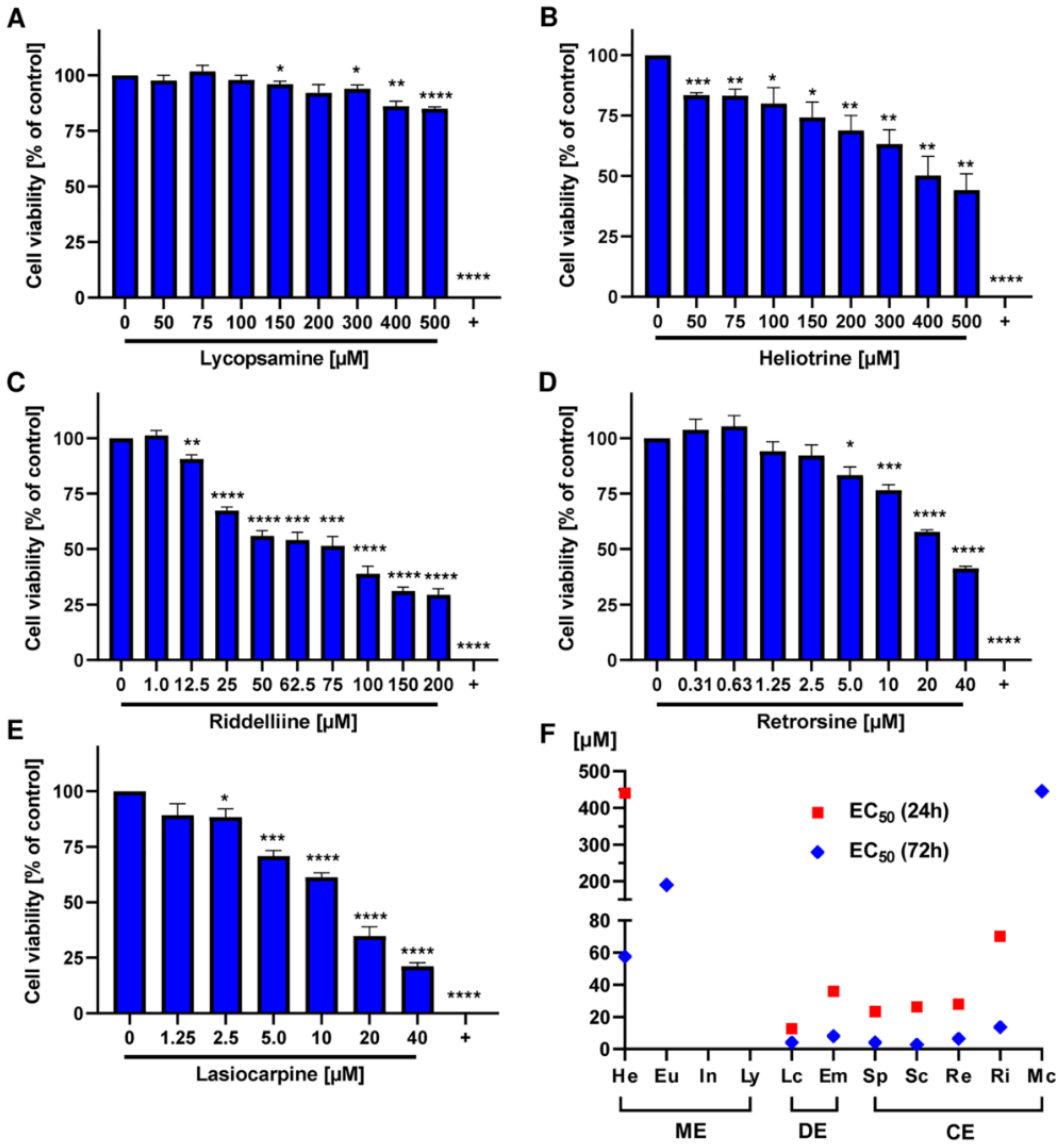

Fig. 1 Cytotoxicity in HepG2-CYP3A4 cells triggered by structurally different PAs. A-E: Viability of HepG2-CYP3A4 cells 24 h after treatment with increasing concentrations of lycopsamine (**A**), heliotrine (**B**), riddelliine (**C**), retrorsine (**D**) and lasiocarpine (**E**). Saponin (0.1%) was used as a positive control (+) and solvent (0) as a negative control. Mean + SEM are shown for each incubation ($n = 3$, each measured as triplicates). Statistical analyses were performed using unpaired two-tailed Student's t-test with respect to the negative control. $^{*}P \leq 0.05$, $^{**}P \leq 0.01$, $^{***}P \leq 0.001$, $^{****}P \leq 0.0001$. **F** EC_{50} values of HepG2-CYP3A4 after 24 and 72 h incubations with monoesters (ME), open diesters (DE), and cyclic diesters (CE). EC_{50} couldn't be determined for Eu, In, Ly, and Mc, because the cytotoxic effects weren't strong enough. *He* Heliotrine, *Eu* Europine, *In* Indicine, *Ly* Lycopsamine, *Lc* Lasiocarpine, *Em* Echimidine, *Sp* Seneciphylline, *Sc* Senecionine, *Re* Retrorsine, *Ri* Riddelliine, *Mc* Monocrotaline

which was used to rank the PAs according to their cytotoxic potential (SI Fig. 3). The EC_{50} values of each PA after 24 h exposure in HepG2-CYP3A4 cells are shown in Fig. 1F. It should be noted that EC_{50} values could not be determined for europine, indicine, lycopsamine and monocrotaline due to their weak cytotoxicity. EC_{50} values between 10 and 70 µM were calculated for lasiocarpine, echimidine, seneciphylline, senecionine, retrorsine and riddelliine, whereby no striking differences in the cytotoxicity between cyclic and open diesters were observed. Furthermore, lasiocarpine displayed the highest cytotoxic potential with an EC_{50} of 12.6 µM in HepG2-CYP3A4 cells after 24 h exposure, followed by seneciphylline with an EC_{50} of 26.2 µM.

Subsequently, we wished to know how longer exposure might affect the cytotoxic potential of PAs in HepG2-CYP3A4 cells. To this end, cells were challenged with increasing concentrations (0 µM up to 500 µM, depending of the PA) for 72 h. Generally, we observed a higher concentration-dependent cytotoxicity in HepG2-CYP3A4 cells as compared to the shorter incubation period of 24 h. A moderate concentration-dependent decrease in cell viability was observed for lycopsamine and indicine, while a stronger drop in viability was seen for europine and heliotrine after 72 h exposure (SI Fig. 4A–D). Both lasiocarpine and senecionine showed the highest cytotoxicity after 72 h in HepG2-CYP3A4 cells (Fig. S4E and F), followed by the other diesters (SI Fig. 4G and H and SI Fig. 5A and B). Once again, the cytotoxicity of monocrotaline was comparable with the other tested monoesters, but not with the open or cyclic diesters (SI Fig. 5C). The EC_{50} values of the PAs were then calculated from the concentration–response data obtained in HepG2-CYP3A4 with 72 h PA exposure (SI Fig. 6). The EC_{50} values were consistently lower after 72 h as compared to 24 h (Fig. 1F). Indicine and lycopsamine showed the lowest cytotoxic potential and EC_{50} values could not be determined even after 72 h exposure. However, we were able to calculate the EC_{50} values of europine and monocrotaline after 72 h, which ranged between 200 and 500 µM. The other EC_{50} values were between 2 and 60 µM, including senecionine, seneciphylline, lasiocarpine, retrorsine, echimidine, riddelliine and heliotrine.

In summary, the panel of eleven representative PAs revealed a clear structure-dependent cytotoxicity and the following rank order with decreasing cytotoxic potential: lasiocarpine > seneciphylline = senecionine = retrorsine > echimidine > riddelliine > > heliotrine > > europine > monocrotaline > indicine = lycopsamine. In addition, our findings demonstrate that longer exposure enhances the cytotoxic effects induced by PAs in HepG2-CYP3A4 cells.

Studies in PHH confirm the structure–dependent PA toxicity and potency ranking obtained in HepG2-CYP3A4 cells

PHH are the gold standard in toxicological and pharmacological studies to investigate ADME profile and hepatotoxic effects of substances (Fraczek et al. 2013; Ruoss et al. 2020). PHH display full metabolic competence, express numerous influx and efflux transporters and exhibit no mutations in critical tumor suppressor genes or proto-oncogenes (Fraczek et al. 2013; Ruoss et al. 2020). Therefore, we were eager to analyze the cytotoxicity of PAs in PHH. The tested PAs were selected according to their relevance as contaminants in herbal medicinal products, different structure types and existing toxicological datasets in other cell models. In all assays, solvent served as negative control and 0.1% saponine as positive control. PHH were exposed to increasing PA concentrations (0 µM–500 µM, depending on the PA) for 24 h. The cytotoxicity was measured as described before and the relative potency of each PA was determined by calculating the EC_{50} from the concentration–response data. The results showed similar weak cytotoxic effects of heliotrine, lycopsamine and monocrotaline, with a cell viability of above 75% at 500 µM (Fig. 2A–C). Due to the low cytotoxicity of these PAs, it was not possible to calculate an EC_{50}. In contrast to that, a significant dose-dependent decrease in cell viability was observed after treatment of PHH with lasiocarpine, retrorsine and riddelliine, with cell viabilities below 35% at the highest concentrations tested (Fig. 2D–F). Lasiocarpine showed the strongest cytotoxic effect with an EC_{50} of 45 µM, followed by retrorsine with a twofold higher EC_{50} value (98 µM) and riddelliine with a sevenfold higher EC_{50} value (292 µM) (SI Fig. 7A–C). The findings in PHH were supported by phase contrast microscopy, whereby higher concentrations led to decreased cell density, cell detachment and morphological changes (SI Fig. 8A-D). Altogether, the panel of six representative PAs showed a clear structure-dependent cytotoxicity and the following rank order with decreasing cytotoxic potential: lasiocarpine > retrorsine > riddelliine > > heliotrine = monocrotaline = lycopsamine.

Structure-dependent genotoxicity of different PAs shown by an in vitro genotoxicity test battery in HepG2-CYP3A4 cells

Next, we investigated the impact of the PA structure on genotoxicity in HepG2-CYP3A4 cells using the established DNA damage markers γH2AX and p53 (Fahrer et al. 2015; Nikolova et al. 2014). The histone variant H2AX is phosphorylated (γH2AX) in response to DNA double-strand breaks and replication stress by apical DNA damage response (DDR) kinases (Kinner et al. 2008). The tumor suppressor protein p53 is known to be activated by genotoxic stress, resulting in its accumulation and p53-dependent regulation of downstream pathways such as DNA repair, cell cycle and cell death (Brady and Attardi 2010). HepG2-CYP3A4 cells were incubated with increasing PA concentrations for 24 h. The PA concentrations were chosen according to the determined EC_{50} values, with the highest concentration not exceeding the EC_{50} value. Solvent treated cells were used as negative control and the anticancer drug etoposide (10 µM) was included as positive control. Retrorsine induced a more than twofold induction of γH2AX already at the lowest tested concentration of 0.05 µM, whereas lasiocarpine and heliotrine showed a more than twofold increase in γH2AX at 1.3 µM and 10 µM, respectively (Fig. 3A–F). Comparable genotoxic effects were seen for p53 accumulation (SI Fig. 9A–C). A structure-dependent genotoxicity was also demonstrated for other PA congeners (SI Fig. 10–12). For

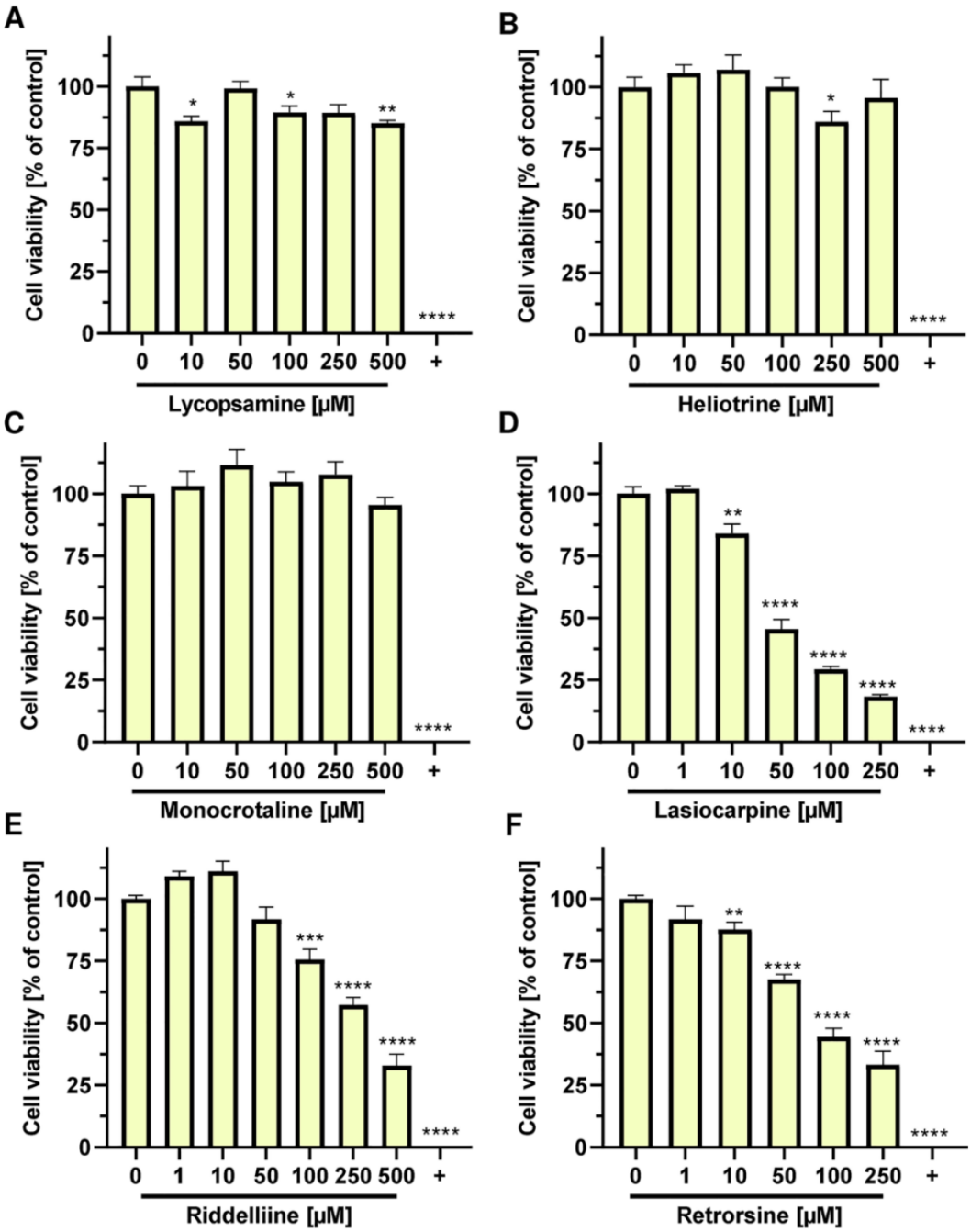

Fig. 2 Structure-dependent cytotoxic effects of PAs in primary human hepatocytes. Viability of primary human hepatocytes after 24 h incubation with lycopsamine (**A**), heliotrine (**B**), monocrotaline (**C**), lasiocarpine (**D**), riddelliine (**E**), retrorsine (**F**). Saponin (0.1%) was used as a positive control (+) and solvent (0) as a negative control. Mean + SEM are shown (pooled hepatocytes from 5 donors, $n = 2$, each performed as triplicate). Statistical analyses were performed using unpaired two-tailed Student's t-test with respect to the negative control. $^{*}P \leq 0.05$, $^{**}P \leq 0.01$, $^{***}P \leq 0.001$, $^{****}P \leq 0.0001$. *He* Heliotrine, *Ly* Lycopsamine, *Lc* Lasiocarpine; *Re* Retrorsine, *Ri* Riddelliine, *Mc* Monocrotaline

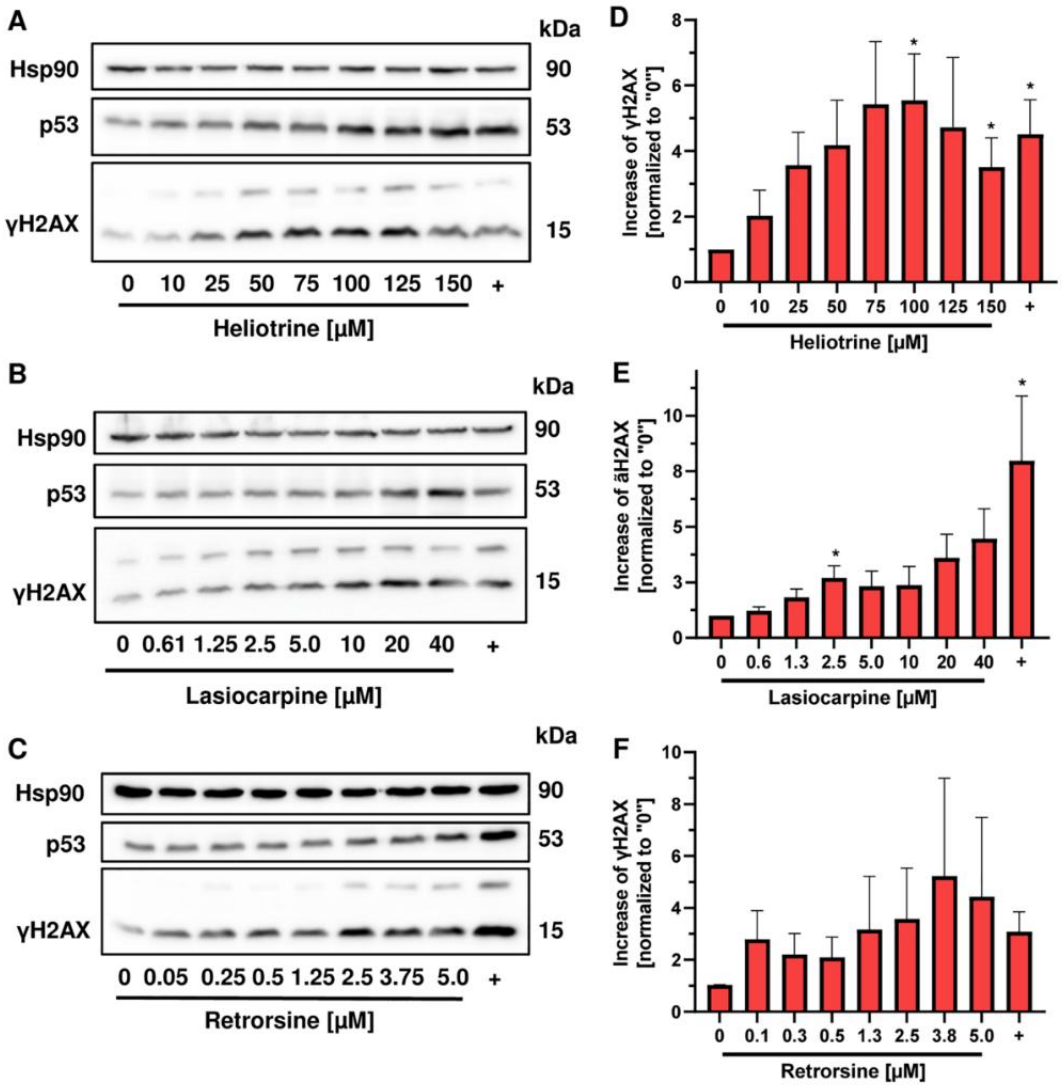

Fig. 3 Structure-dependent γH2AX and p53 formation in HepG2-CYP3A4 cells triggered by different PAs. A-C: Representative western blots of γH2AX and p53 after 24 h incubation with heliotrine (**A**), lasiocarpine (**B**) and retrorsine (**C**) in HepG2-CYP3A4 cells. Etoposid was used as a positive (+) and solvent as a negative control (0). **D–F**: Densitometric evaluations of γH2AX after 24 h incubation with heliotrine (**D**), lasiocarpine (**E**) and retrorsine (**F**) in HepG2-CYP3A4. Hsp90 served as loading control. γH2AX level relative to the loading control and normalized versus the negative control. Mean + SEM of three independent experiments ($n = 3$). Statistical analyses were performed using unpaired two-tailed Student's t-test with respect to the negative control. $^{*}P \leq 0.05$, $^{**}P \leq 0.01$, $^{***}P \leq 0.001$, $^{****}P \leq 0.0001$

example, seneciphyilline showed at 0.4 µM a significant increase of γH2AX (SI Fig. 10E and SI Fig. 12D), while a comparable effect was not observed below and at 100 µM europine (SI Fig. 10B and SI Fig. 11B). In general, most of the PAs showed a concentration-dependent increase in γH2AX and p53. However, lycopsamine (SI Fig. 11G and H) and monocrotaline (SI Fig. 12A and B) caused no clear concentration-related accumulation of both genotoxicity markers. Intriguingly, heliotrine provoked a more than twofold induction of both γH2AX and p53 at a concentration of 10 and 25 µM respectively, whereas the other monoesters europine and indicine showed the same effects at fivefold higher concentrations (50–150 µM) (SI Fig. 11A–D). The open diesters lasiocarpine and echimidine were equally genotoxic, with a twofold induction of γH2AX and p53 between 1.3 and 2.5 µM (Fig. 3B, SI Fig. 9B, SI Fig. 11E and F). With regard to the cyclic diesters, a wide concentration range between 0.05 and 12.5 µM depending on the

individual PA was required for a twofold induction of the DNA damage markers (SI Fig. 11 and 12). Interestingly, the genotoxic effects of the open diesters were detected at the same concentration range as for cyclic diesters.

The concentration–response data were used for benchmark dose (BMD) modeling to derive relative genotoxic potencies (Fig. 4, SI Figs. 13 and 14). To this end, a critical effect size (CES) of one, i.e., a doubling of the measured γH2AX and p53 levels as compared to controls, was used as benchmark response with a confidence interval of 90%. Interestingly, the calculated critical effect dose (CED; represents BMD) and the respective critical effect dose lower boundary (CEDL, represents the BMDL) values of γH2AX and p53 were almost in the same concentration range for most of the PAs (Tables S1 and S2; SI Fig. 15). Moreover, the BMDL values of the cyclic diesters and open diesters were all below 1 µM, except for riddelliine (Tables S1 and S2). Retrorsine showed the strongest genotoxic potency with a BMDL of 0.01 µM, which is between 42- and 93-fold lower compared to the BMDL values of the open diesters and 409 and 2050-fold lower as those of monoesters (SI Fig. 15, Tab. S1 and S2). BMD modeling for lycopsamine and monocrotaline could not be performed due to lack of a significant genotoxic response. Taken together, the individual genotoxic potency of the tested PAs was shown to be structure dependent and correlated very well with their cytotoxic potency (Fig. 4A, B). BMD modeling of the γH2AX and p53 data resulted in the following rank order with decreasing genotoxicity: retrorsine > > seneciphylline > lasiocarpine > senecionine = echimidine > riddelliine = heliotrine > indicine > europine > lycopsamine = monocrotaline.

Furthermore, we performed the alkaline Comet assay as additional genotoxicity endpoint with the same set of PAs. The alkaline Comet assay detects DNA single-strand breaks and double-strand breaks as well as alkali labile sites (Azqueta and Collins 2013; Moller et al. 2020). Thus, HepG2-CYP3A4 cells were incubated with increasing concentrations of PAs for 24 h. The PA concentrations were selected according to the determined EC_{50} values and comparable to those used for the determination of the genotoxicity markers p53 and γH2AX. Solvent treated cells were used as negative control and 200 µM tBOOH was applied as positive control. In agreement with the p53 and γH2AX data, retrorsine was very potent and caused a statistically significant increase in the OTM already at 0.05 µM, whereas a significant increase in OTM was detected at 0.6 µM lasiocarpine and 10 µM heliotrine (Fig. 5A–F). Importantly, a significant, concentration-dependent increase in OTM was observed for all tested PAs, including lycopsamine and monocrotaline (Fig. 5 and SI Fig. 16). The comet assay data were used for BMD modeling to derive relative genotoxic potencies. To this end, a CES of 0.5, which corresponds to a 1.5-fold increase of OTM as compared to controls, was used as benchmark response with a confidence interval of 90%. The calculated BMDL values of the cyclic and open diesters were in a range of 0.14 and 40 µM, whereas the BMDL values of the monoesters were between 6.2 and 62 µM (SI Fig. 17 and Tab. S3). Retrorsine and seneciphylline were

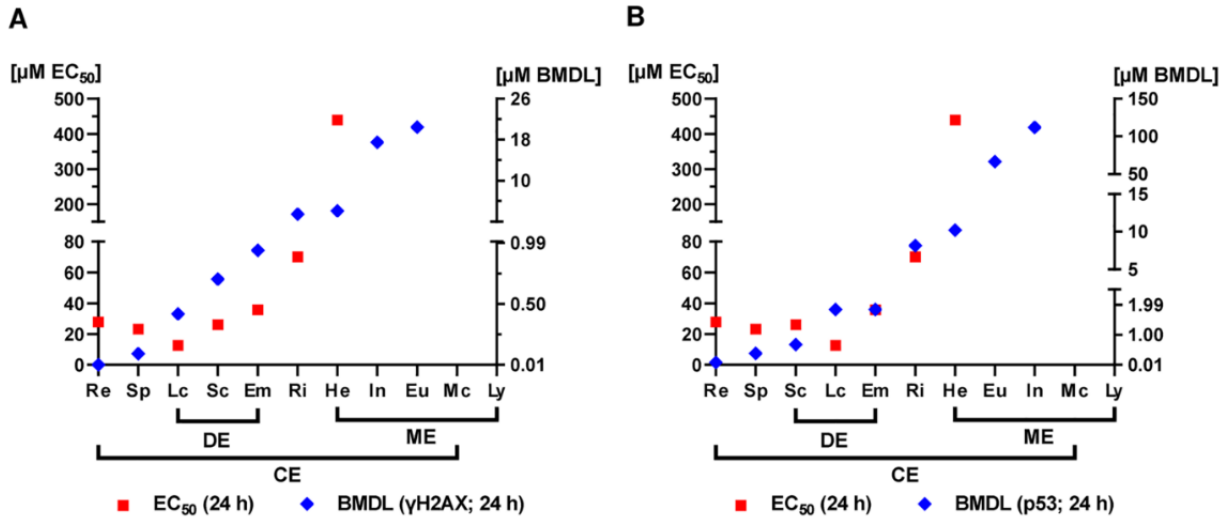

Fig. 4 Genotoxic potency ranking of all tested PAs using the p53 and γH2AX data. A-B: BMDL values of γH2AX (**A**) and p53 (**B**) from western blot analysis and EC_{50} values of the 11 PAs including monoesters (Eu, He, In, Ly), open diesters (Em, Lc), and cyclic diesters (Mc, Re, Ri, Sc, Sp). BMDL values of the PAs depicted according to genotoxic potency. *He* Heliotrine, *Eu* Europine, *In* Indicine, *Ly* Lycopsamine, *Lc* Lasiocarpine, *Em* Echimidine, *Sp* Seneciphylline, *Sc* Senecionine, *Re* Retrorsine, *Ri* Riddelliine, *Mc* Monocrotaline

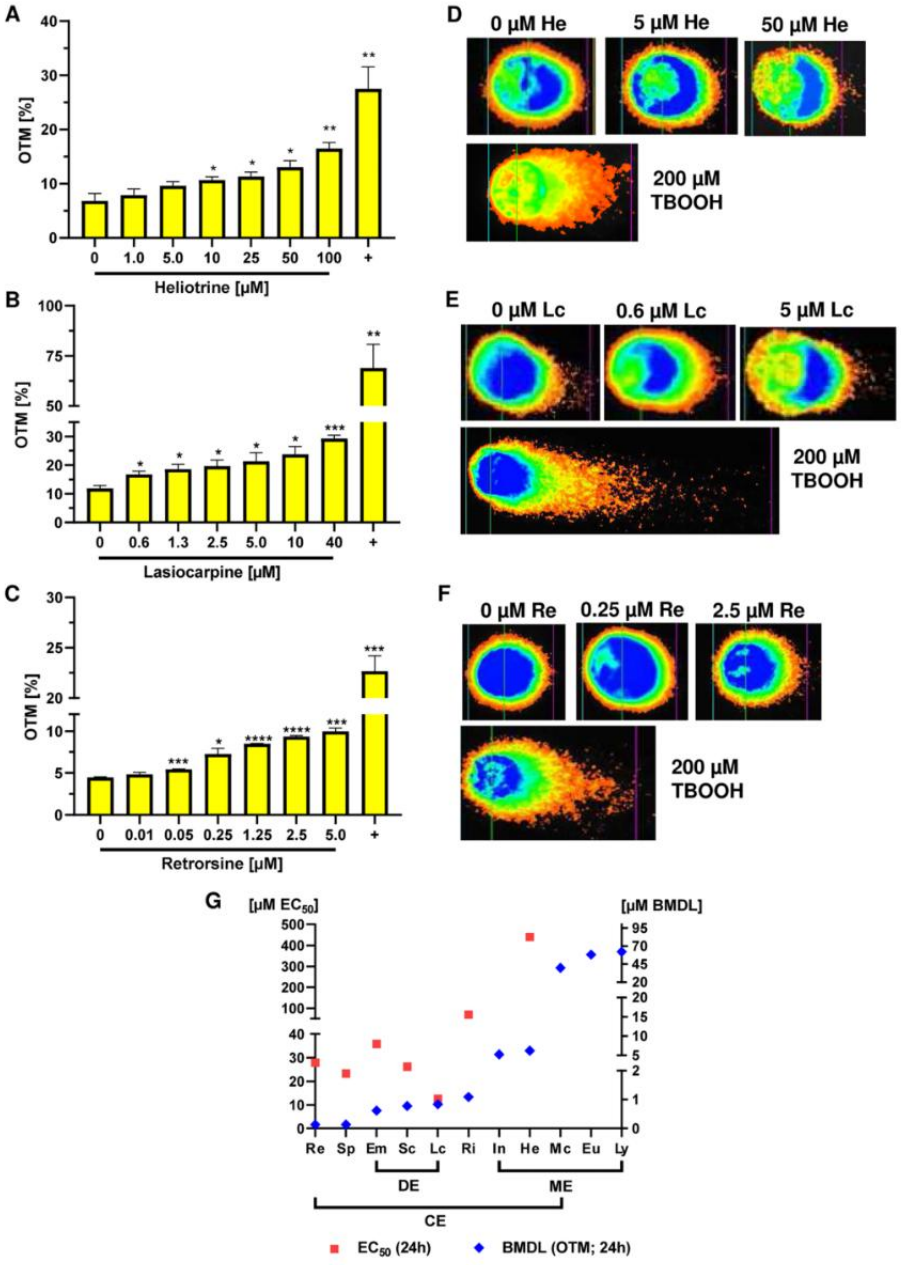

Fig. 5 Structure-dependent DNA strand break formation in HepG2-CYP3A4 cells caused by different PAs. **A–C** Olive tail moments (OTM), which represents DNA strand break formation, in HepG2-CYP3A4 cells after 24 h incubation with heliotrine (**A**), lasiocarpine (**B**) and retrorsine (**C**). tBOOH was used as a positive (+) and solvent as a negative control (0). The alkaline Comet assay was performed as described. Mean + SEM are depicted ($n = 3$, except for heliotrine and europine $n = 4$). At least 50 comets per slide were counted and OTM was calculated by the software Comet Assay IV. Statistical analyses were performed using unpaired two-tailed Students t-test with respect to the negative control. $^{*}P \leq 0.05$, $^{**}P \leq 0.01$, $^{***}P \leq 0.001$, $^{****}P \leq 0.0001$. **D–F** Representative images of comets. **G** BMDL values derived from Comet data and EC_{50} values of the 11 PAs including monoester (Eu, He, In, Ly), open diester (Em, Lc), and cyclic diester (Mc, Re, Ri, Sc, Sp). BMDL values of the PAs shown according to genotoxic potency. *He* Heliotrine, *Eu* Europine, *In* Indicine, *Ly* Lycopsamine, *Lc* Lasiocarpine, *Em* Echimidine, *Sp* Seneciphylline, *Sc* Senecionine, *Re* Retrorsine, *Ri* Riddelliine, *Mc* Monocrotaline

the most genotoxic PAs with BMDL values of 0.14 µM (SI Fig. 17 and Tab. 1). Both PAs showed a three- to fivefold higher genotoxic potency as compared with the open diesters and a 38 – 444-fold higher genotoxic potency as monoesters. Among those, heliotrine and indicine displayed the highest genotoxicity, with BMDL values being about tenfold higher than those of europine and lycopsamine. Interestingly, the BMDL value of monocrotaline was in the same range as those of europine and lycopsamine (SI Fig. 17 and Tab. S3). In summary, the structure-dependent genotoxicity of the PAs was confirmed by the alkaline Comet assay. The calculated BMDL values were in very good agreement with those determined with the p53 and γH2AX assay (SI Fig. 13 and 14 vs. SI Fig. 17; Tab. S1–S3), providing the following rank order with decreasing genotoxic potential: retrorsine = seneciphylline > echimidine > senecionine = lasiocarpine > riddelliine > indicine > heliotrine > monocrotaline > europine > lycopsamine.

PHH corroborate the genotoxic potency ranking performed in HepG2-CYP3A4 cells and reveal genotoxic effects in the absence of detectable cytotoxicity

Finally, we challenged PHH with increasing concentrations of the selected PAs lycopsamine, heliotrine, lasiocarpine, monocrotaline, retrorsine and riddelliine, which were also used in the cytotoxicity studies. Solvent treated cells served as negative control and 20 µM *cis*-platin was used as positive control. Importantly, every tested PA caused a concentration-dependent increase of γH2AX foci. PHH treated with 1 µM lasiocarpine showed on average 23 γH2AX foci per nucleus, whereas treatment with 5 µM retrorsine induced 27 γH2AX foci per nucleus (Fig. 6A–C). Twofold higher concentrations of heliotrine, fivefold higher concentrations of riddelline and 10- to 20-fold higher concentrations of monocrotaline and lycopsamine were required to cause the same γH2AX levels (Fig. 6D–G). It is noteworthy to mention that lycopsamine, although being weakly cytotoxic in PHH, induced γH2AX formation already at the lowest concentration tested, which was not observed in HepG2-CYP3A4 cells. Furthermore, monocrotaline was also genotoxic in PHH at the lowest concentration tested (50 µM), whereas in HepG2-CYP3A4 cells significant genotoxic effects were only detected at 200 µM using the alkaline Comet assay. Next, the relative genotoxicity of these PAs in PHH was determined by BMD modeling. To this end, a CES of 0.5, which corresponds to a 1.5-fold increase of γH2AX foci as compared to control, was used as benchmark response with a confidence interval of 90%. The calculated BMDL value of lasiocarpine was sixfold lower than the BMDL of retrorsine and 28-fold lower as compared to that of riddelline (SI Fig. 17 and Tab. S4). Heliotrine was as potent as riddelliine, but threefold more genotoxic than monocrotaline and even 15-fold more genotoxic than lycopsamine (SI Fig. 18 and Tab. S4). To summarize, all BMDL values were below 7 µM except for lycopsamine and were overall comparable with the results obtained in HepG2-CYP3A4, but with a six- to tenfold higher genotoxicity for monocrotaline and lasiocarpine in PHH. The following rank order with decreasing genotoxic potential was revealed in PHH: lasiocarpine > riddelliine > retrorsine > heliotrine > monocrotaline > lycopsamine.

Discussion

In this study, we investigated the structure-dependent toxicity of up to 11 PAs in human HepG2-CYP3A4 cells and PHH, which are a gold standard in pharmaco-toxicokinetic in vitro studies of the human liver. Importantly, we used an in vitro test battery consisting of three different genotoxicity endpoints that were combined with cytotoxicity testing side-by-side. Our findings in HepG2-CYP3A4 cells showed that cyclic and open diesters are highly cytotoxic already after 24 h, which is further potentiated after 72 h. These findings may be due to a higher sensitivity of proliferating cells and/or an accumulation of cell damage events over time. In contrast to that, monoesters with the exception of heliotrine exerted no cytotoxicity after 24 h incubation and were moderately cytotoxic after 72 h. The cytotoxic effects of the PAs were much higher than those reported in HepaRG cells, in which an EC_{50} calculation was not possible due to a lack of cytotoxicity (Glück et al. 2020). For example, lasiocarpine was the most cytotoxic PA in our cell model with an EC_{50} of 12 µM after 24 h. In HepaRG cells, a concentration of 250 µM reduced viability by 50% only (Glück et al. 2020), indicating a moderate sensitivity of HepaRG cells towards the cytotoxic effects of PAs. Furthermore, the PA-triggered cytotoxic effects were also stronger in PHH as compared to HepaRG cells, although PHH do not proliferate at all. Our study demonstrated that the ranking of PAs according to their cytotoxicity in PHH is comparable with that in HepG2-CYP3A4 cells, although the cytotoxic potency was generally lower in PHHs. An attenuated cytotoxicity was also observed in primary rat hepatocytes (pRH) (Gao et al. 2020). Most of the EC_{50} values in pRH were almost twofold higher as in PHH and between four- and ninefold higher than in HepG2-CYP3A4 (Fig. 7A). Intriguingly, a comparable rank order was observed for all tested PAs in both rodent and human liver cell models. The lower cytotoxicity in primary hepatocytes is most likely attributable to the lack of cell proliferation, but other processes like the expression of transporters, their extensive metabolic capacity and the effect of cryopreservation (in case of pHH) on CYP activity could also be relevant (Fraczek et al. 2013; Ruoss et al. 2020; Kammerer and Küpper 2018). Senecionine was an exception in this regard and showed a similar cytotoxicity in pRH and in HepG2-CYP3A4 (Fig. 7A). Interestingly, a recent study revealed an EC_{50} value of 26 µM for senecionine in primary mouse hepatocytes (pMH) (Hessel-Pras et al. 2020), which fits very well to the EC_{50} values for senecionine determined in HepG2-CYP3A4 and pRH.

Our genotoxicity test battery with the endpoints γH2AX, p53 and DNA strand break induction demonstrated a clear structure-dependent toxicity of the tested PAs in HepG2-CYP3A4 cells, which was consistent with the results obtained in PHH. The determined BMDL values revealed a higher genotoxic potency for diesters compared to monoesters, except for monocrotaline (Fig. 7B). Retrorsine showed the strongest genotoxic potential with a BMDL value of 0.01 µM followed by seneciphylline based on the γH2AX data (Fig. 7B). A similar pattern of γH2AX induction was obtained in another study conducted in HepaRG cells, which included PAs and PA N-oxides (Louisse et al. 2019). However, the BMDL values determined in HepaRG

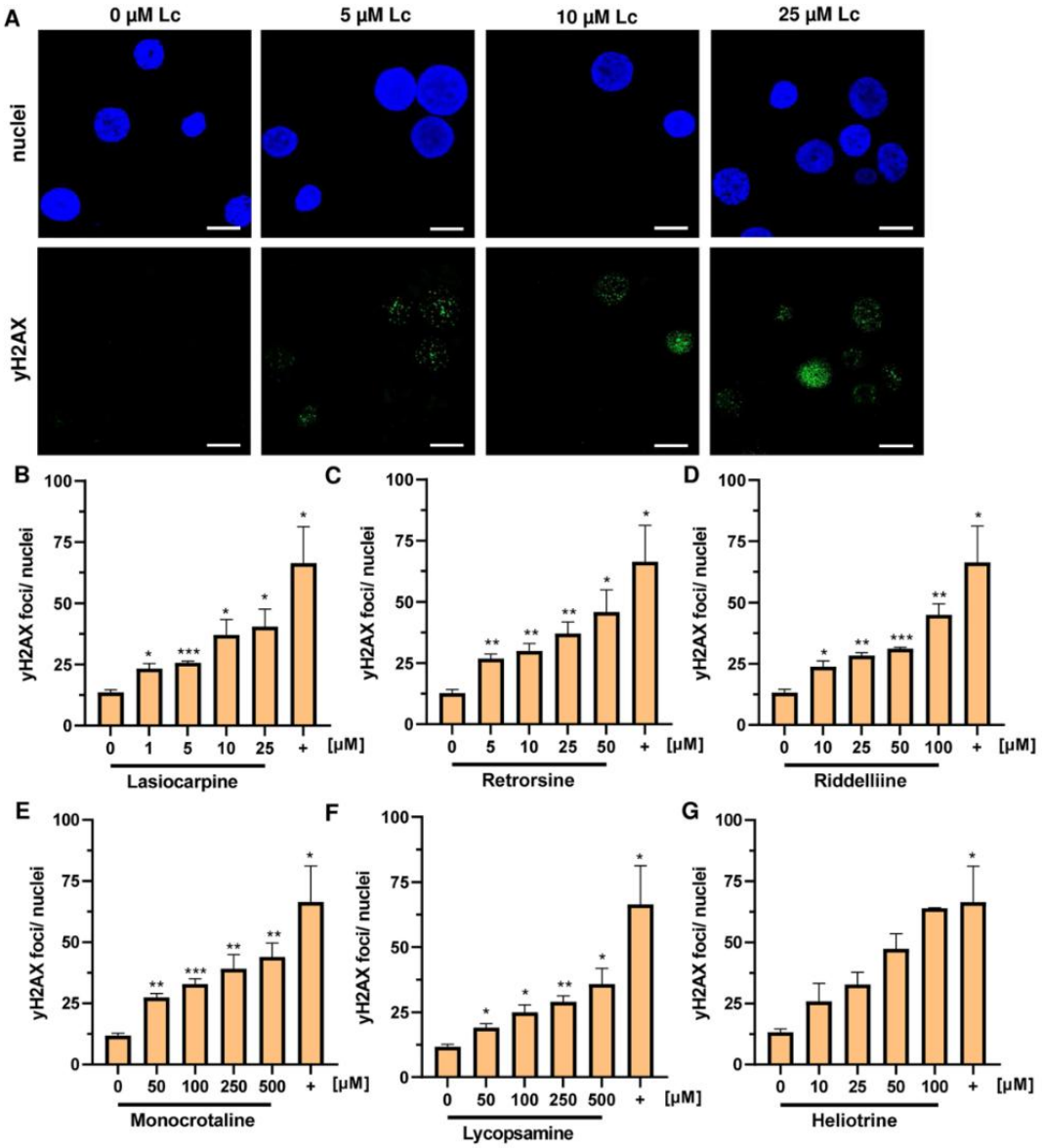

Fig. 6 Formation of γH2AX foci in primary human hepatocytes by structurally different PAs. A: Representative images of primary human hepatocytes after 24 h incubation with 0–25 µM lasiocarpine. γH2AX was stained as described and detected by high resolution confocal microscopy (scale bar: 10 µm). **B–G** γH2AX foci in primary human hepatocytes after 24 h incubation with lasiocarpine (**B**), retrorsine (**C**), riddelliine (**D**), monocrotaline (**E**), lycopsamine (**F**) and heliotrine (**G**). *cis*-platin was served as positive control (+) and solvent as negative control (0). Mean + SEM are shown (pooled hepatocytes from 5 donors, $n = 3$), except for heliotrine (pooled hepatocytes from 5 donors, $n = 2$). At least 40 nuclei per sample were counted for γH2AX foci formation and evaluated with Zen 3.6 software. Statistical analyses were performed using unpaired two-tailed Students t-test with respect to the negative control. $^{*}P \leq 0.05$, $^{**}P \leq 0.01$, $^{***}P \leq 0.001$, $^{****}P \leq 0.0001$

cells were 1.3- to 440-fold lower as compared to those found in HepG2-CYP3A4 cells (Fig. 7B). This might be explained by differences in cell proliferation, expression of influx/efflux transporters or other factors that influence the cellular sensitivity. Consistent with our findings in PHH, both human liver cell models provided comparatively high BMDL values for the diester monocrotaline, which was even higher than those of most monoesters. The weak genotoxic potency of monocrotaline might be due to lack of efficient bioactivation or other toxicokinetic parameters, such as hepatocyte uptake or efflux. Interestingly, monocrotaline was found to be mainly metabolized by rat liver S9 and only to a small

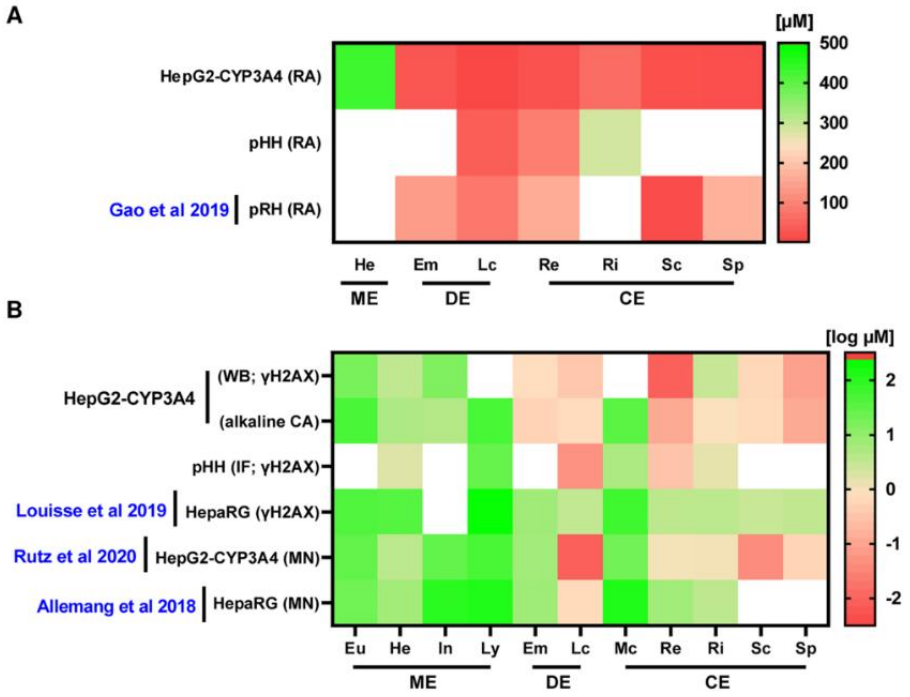

Fig. 7 Comparison of BMD and EC_{50} values determined for structurally different PAs in various liver cell models. Comparison of cytotoxic (24 h) and genotoxic (24–48 h) potency of different PAs based on data in HepG2-CYP3A4, primary human hepatocytes (pHH), rat hepatocytes (pRH) as well as HepaRG cells. **A:** The cytotoxic effects of the PAs were measured by resazurin reduction assay. EC_{50} values were calculated to derive the relative cytotoxicity. Only PAs with existing EC_{50} value, i.e., sufficient cytotoxicity, are shown in the heatmap. Cytotoxicity is colour graded from high (dark red) to low (bright green). **B:** The genotoxic potentials were derived from γH2AX, Comet and micronuclei (MN) data, whereby data were transformed into BMDL values by PROAST. The BMDL values are shown in logarithmic concentrations [µM], i.e., a lower value represents a higher genotoxic potency. Data collected from the present work and published studies (Gao et al. 2020; Louisse et al. 2019; Allemang et al. 2018 and Rutz et al. 2020)

extent by lung S9 fractions (Song et al. 2020). Nevertheless, the ratio of pyrrole-protein adducts in lung vs. liver was significantly higher for monocrotaline than that of other tested PAs, which might indicate a preferential lung toxicity of monocrotaline. A recent in vivo study confirmed that bioactivation of monocrotaline by liver CYPs and transport of the reactive metabolites via the blood stream is required for its lung toxicity (He et al. 2021a).

Furthermore, our study provided evidence that p53 is a valuable and sensitive genotoxicity marker for PAs, which allows BMD modeling to derive the genotoxic potency. The BMDL values based on the γH2AX and p53 data sets were almost equal among the tested open diesters and cyclic diesters, but differed to some extent within the monoesters. All monoesters showed a 2.5- to eightfold higher BMDL value with p53 as endpoint, which might indicate differences in the genotoxic mode of action of monoesters as compared to diesters. The observed concentration-dependent accumulation of p53 after treatment of HepG2-CYP3A4 cells with all 11 tested PAs is in line with transcriptome studies performed in the same cell model, which revealed an upregulation of the p53 pathway (Abdelfatah et al. 2022). An activation of the p53 signaling pathway in rat liver was also found in a 28-day feeding study (Ebmeyer et al. 2020), highlighting the relevance of p53 as genotoxicity marker for PAs.

As third genotoxicity endpoint, we investigated the PA triggered DNA damage using the alkaline Comet assay. The obtained BMDL values matched very well to those determined with the two other endpoints (i.e., γH2AX and p53). Moreover, we were able to derive BMDL values for the weakly genotoxic PAs lycopsamine and monocrotaline, highlighting the sensitivity of the Comet assay. PA-triggered DNA strand breaks can result in chromosomal damage and formation of micronuclei. This has also been investigated in a structure-dependent manner using metabolically competent HepG2-CYP3A4 cells and HepaRG cells (Rutz et al. 2020; Allemang et al. 2018) as well as HepG2 cells with CYP induction by rifampicin pretreatment (Hadi et al. 2021). The two studies in metabolically competent cells revealed BMDL values in the range of 0.01–8.5 µM for the tested cyclic and open diesters as well as heliotrine, whereas the BMDL values for monoesters and monocrotaline ranged between 25

and 154 µM (Fig. 7B) (Rutz et al. 2020; Allemang et al. 2018). These results are in good agreement with our findings obtained by a genotoxicity test battery, in particular the alkaline Comet assay (Fig. 7B).

Since our used HepG2 cell model was genetically engineered only for CYP3A4 expression, we conducted further genotoxicity experiments in PHH, which express the whole array of phase I and phase II enzymes (Fraczek et al. 2013). It is noteworthy that PAs are not exclusively metabolized via CYP3A4, but bioactivation also involves CYP3A5 (e.g., lasiocarpine) and CYP3A7 (e.g., riddelliine) to some extent as shown in a panel of genetically engineered TK6 cells (Li et al. 2020). Previous studies with recombinant human CYP supersomes revealed that the vast majority of tested PAs are substrates for CYP3A4 (Ruan et al. 2014). One exception was monocrotaline, which was predominantly metabolized via CYP2A6 (Ruan et al. 2014). This CYP isoform plays also an important role for the metabolism of retrorsine together with CYP3A4 (Ruan et al. 2014). In PHH, we analyzed nuclear γH2AX formation using high-resolution confocal microscopy, which requires less cells than the western blot analysis used in HepG2-CYP3A4 cells. Our findings showed that lasiocarpine and retrorsine were the most potent genotoxic PAs in PHH with BMDL values between 0.06 and 0.4 µM. Furthermore, the genotoxic potencies of the tested PAs in PHH were generally comparable with those obtained in HepG2-CYP3A4 cells, but revealed a six- to tenfold higher genotoxicity for monocrotaline and lasiocarpine in PHH. This may be attributable due to the presence of further CYP enzymes in PHH, such as CYP2A6 and CYP3A5, which contribute to the metabolic activation of those PAs as pointed out above. Interestingly, lasiocarpine followed by riddelliine and heliotrine caused the highest DHP-DNA adduct levels in a rat sandwich-culture hepatocytes (Lester et al. 2019), which is in line with our findings in PHH.

Finally, we made an integrated approach for potency ranking using all genotoxicity data and depicted the determined BMD values with the confidence intervals (BMDL and BMDU) to account for data variability. To this end, PAs were ranked according to their genotoxic potency based on the mean of the BMD values from all genotoxicity endpoints in HepG2-CYP3A4 cells (Fig. 8). Retrorsine showed the highest and lycopsamine the lowest genotoxic potency from all tested PAs, which was consistent with the rank order observed in PHH (Fig. 8). Interestingly, the BMD values of monocrotaline determined in HepG2-CYP3A4 and PHH were two- to 40-fold lower as compared to the BMD values of riddelliine, which is in good agreement with a previous study in HepaRG cells (Louisse et al. 2019).

In 2016, Merz and Schrenk introduced the concept of relative (toxicity) potency (REP) factors to group PAs with respect to their toxicity (Merz and Schrenk 2016). This was based on available data comprising acute toxicity in rodents, cytotoxicity in hepatocellular carcinoma cells and

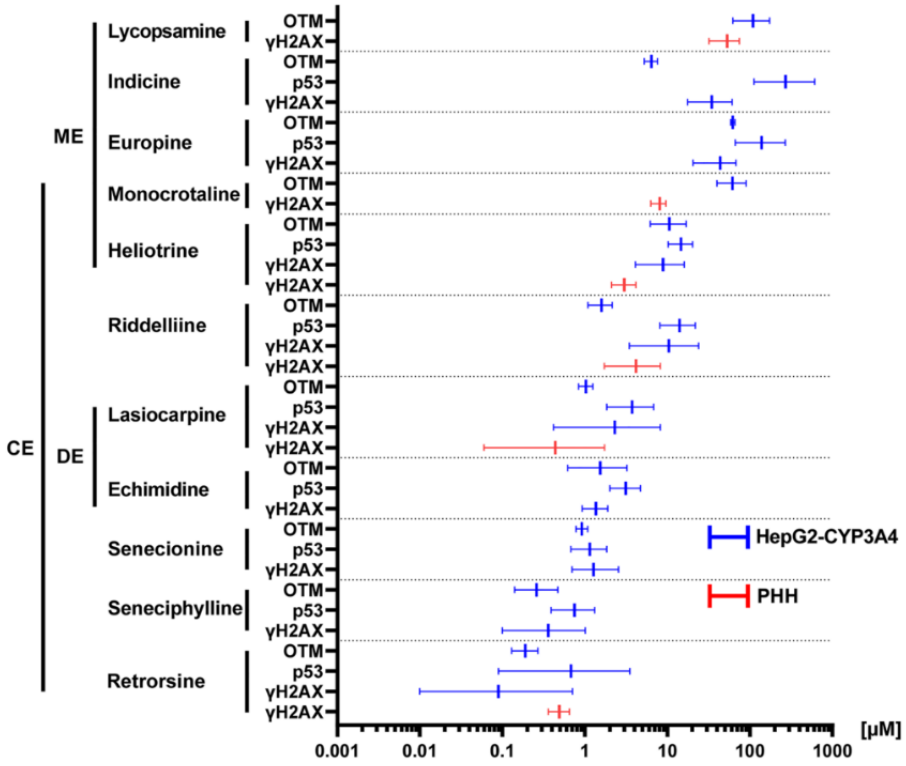

Fig. 8 Comprehensive genotoxic potency ranking of PAs in HepG2-CYP3A4 cells and PHH. The concentration–response data for the endpoints γH2AX, p53 and Comet assay (OTM) were used to derive BMD values including the 90% confidence intervals (BMDL, BMDU) by PROAST. PAs were then ranked according to their genotoxic potency based on their mean of all derived BMD values (equally weighted) determined in HepG2-CYP3A4 cells. Depicted are the BMD confidence interval plots for the different endpoints in HepG2-CYP3A4 cells (blue) and PHH (red)

genotoxicity in *Drosophila*. In the meantime several in vitro studies have been performed in rodent and human liver cell models (Allemang et al. 2018; Gao et al. 2020; Louisse et al. 2019; Rutz et al. 2020), largely corroborating the suggested interim REPs within one order of magnitude (Schrenk et al. 2022). Our comprehensive analysis of different genotoxicity endpoints in human HepG2-CYP3A4 cells and PHH as gold standard in preclinical toxicity testing reinforced the existing database and provisional iREPs. Particularly, we were able to demonstrate the structure-dependent toxicity of PAs in PHH with a similar potency ranking as observed in metabolically competent liver cancer cell lines (i.e., HepG2-CYP3A4 and HepaRG). Furthermore, our study highlights that genotoxic effects in PHH occur already at PA concentrations that cause no cytotoxicity. Our data contribute to a broader database on cyto- and genotoxic effects and their concentration–response relationships for various PAs in mammalian cell culture. It is not surprising that the various tests did not and will not result in identical BMDs due to the complexity and diversity of the endpoints tested. Attempts are currently under way to harmonize the methodology for benchmark derivation between tests including data from other laboratories. Such a comprehensive inventory will allow carrying out a density distribution (probability) analysis over all available and relevant concentration–response relationships to derive the most consolidated (likely) REP factors. Altogether, this will help to pave the way for a broader acceptance of REPs in PA risk assessment.

Material and methods

Cell culture and treatment

HepG2-CYP3A4 cells were generated as previously described (Herzog et al. 2015). CYP3A4 expression was confirmed by western blot analysis (Data not shown). HepG2-CYP3A4 cells were maintained in DMEM high glucose supplemented with 10% FCS, 1% P/S and 3 µg/mL blasticidin S hydrochloride (Carl Roth, Karlsruhe, Germany). HepG2-CYP3A4 cells were cultured at 37 °C in humidified atmosphere of 5% CO_2. Cell culture medium and supplements were obtained from Gibco Life Technologies (Darmstadt, Germany) and Pan Biotech (Aidenbach, Germany). Cell lines were mycoplasma negative, as demonstrated by routine PCR testing using Venor®GeM OneStep (Berlin, Germany). Cryopreserved primary human hepatocytes (PHH) pooled from five Caucasian donors were obtained from Thermo Fisher Scientific (Massachusetts, USA). The primary cells were thawed and plated according to the protocol provided by Invitrogen. All reagents were from Thermo Fisher. Cells were thawed at 37 °C in the water bath, transferred to 45 mL hepatocyte thaw media, centrifuged at 500 *g* for 5 min at room temperature (RT) and re-suspended in plating medium. The cell viability was assessed using trypan blue exclusion and cells with a viability of ≥ 90% were used for experiments. Before seeding, the wells were coated with 50 µg/ mL Collagen type I for at least 1 h (Herzog et al. 2016). Cells were cultured at 37 °C in humidified atmosphere of 5% CO_2 for 6 h. Afterwards, the cells were attached and ready for exposure. The plating medium was replaced with incubation medium mixed with the test compounds and cells were treated for 24 h. Collagen type I (rat) was purchased from Corning (New York, USA) and sterile-filtered 50 µg/mL stock solution in 0.8 M acetic acid was prepared for coating.

Compounds and treatment

The investigated PAs (indicine, heliotrine, lycopsamine, europine, echimidine, lasiocarpine, riddelliine, retrorsine, monocrotaline, senecionine, seneciphylline) were of highest purity and obtained from Phytolab (Vestenbergsgreuth, Germany). Stock solutions of PAs were prepared in suitable solvents (50–150 mM) and stored at −20 °C. Heliotrine, lycopsamine, echimidine, lasiocarpine, riddelliine, monocrotaline were dissolved in DMSO, whereas senecionine and seneciphylline were dissolved in a 1:1 mixture (v:v) of DMSO and acetonitrile. Retrorsine was dissolved in ethanol. Stock solutions were diluted in cell culture medium to reach final concentrations in the cell experiments.

Analysis of cell viability and determination of EC_{50} values

HepG2-CYP3A4 cells (45,000 cells/ well) were seeded on 96-well plates, grown overnight and then treated with increasing PA concentrations. PHH were seeded on collagen type I coated 96-well plates at density of 62,500 cells/ well and treated as described above. Saponine (0.1%) served as positive control and solvent as negative control. Cell viability was determined as described previously (Carlsson et al. 2022). After 24 h and 72 h, cells were washed with PBS and incubated for 1 h with DMEM low glucose (-FCS; -P/S) or William's E Medium (1X) supplemented with 10% 440 µM Resazurin-NaCl-Pi-solution (0,1% dimethylformamide; 1.1 mM KH_2PO_4, 154 mM NaCl, 3.7 mM Na_2HPO_4) at 37 °C in humidified atmosphere of 5% CO_2. Cell viability was measured using a microplate reader (Fluoroskan HSCENT FL, ThermoScientific and Spark®, Tecan) at 544 nm for absorbance and 590 nm for emission. The effective concentration, at which cell viability was reduced by 50% (EC_{50}), was calculated by semi-logarithmic transformation of the data and fitting with sigmoidal, non-linear curve using GraphPad Prims software (Version 9).

SDS-PAGE and western blot analysis

HepG2-CYP3A4 cells (500,000 cells/ plate) were seeded on 3.5 cm plates, grown overnight and treated with increasing PA concentrations for 24 h. Cells were directly harvested with 1 × Laemmli loading buffer as described (Fahrer et al. 2014). Western blot analysis was then conducted as reported (Fahrer et al. 2013). Briefly, proteins were separated by SDS-PAGE and transferred onto a nitrocellulose membrane (PerkinElmer, Rodgau, Germany) with wet blot technique. The membrane was blocked with 5% nonfat dry milk in Tris-buffered saline (TBS)/ 0.1% Tween-20 (TBS-T) for 1 h at RT. Afterwards, primary antibody incubation was started overnight at 4 °C. The membranes were washed three times with TBS-T and incubated with appropriate secondary antibodies coupled with horseradish peroxidase for 1 h at RT. After additional washing steps, the membranes were incubated with Western Lighting® Plus-ECL (PerkinElmer, Rodgau, Germany) and proteins detected using a c300 chemiluminescence imager (Azure biosystems, Dublin, CA, USA). The primary antibodies directed against Hsp90 (F8, sc-13119) p53 (DO-1, sc-126) were obtained from Santa Cruz Biotechnology (Heidelberg, Germany). The primary antibody directed against γH2AX (phospho S139, ab81299), was from Abcam (Cambridge, UK). Secondary antibodies conjugated with horseradish peroxidase were purchased from Santa Cruz Biotechnology (sc-516102, Heidelberg, Germany) and Cell Signaling Technology (#7074, Danvers, Massachusetts, USA).

Alkaline comet-assay

HepG2-CYP3A4 cells (500,000 cells/ plate) were seeded on 3.5 cm plates and exposed to PAs for 24 h. tBOOH (200 µM, 1 h) was used as positive control and solvent as negative control. The alkaline Comet assay was essentially performed as described (Dörsam et al. 2018), with slight modifications. Cell lysis was conducted for 60 min, followed by 20 min denaturation and electrophoresis for 30 min. The slides were stored under light exclusion before DNA staining with propidium iodide. At least 50 comets per slide were scored using an Axioskop 2 fluorescence microscope (Zeiss, Jena, Germany) and Comet Assay IV software (Perceptive Instruments, Bury St Edmunds, UK).

Confocal immunofluorescence microscopy of γH2AX in PHH

PHH were seeded on collagen type I coated 12-well chamber slides at density of 10,000 cells/ well. The 12-well chamber slides were obtained from Ibidi® (Gräfelfing, Germany) and used according to the manufacturer`s protocol. Cells were exposed to different concentrations of PAs (heliotrine, lasiocarpine, lycopsamine, monocrotaline, retrorsine and riddelliine) for 24 h. C*is*-platin were used as positive control and solvent as negative control. γH2AX immunofluorescence staining was essentially performed as described (Mimmler et al. 2016). After fixation with methanol for 10 min at − 20 °C, cells were washed with PBS and blocked with 5% BSA in PBS/ 0.3% Triton X-100 for 1 h at RT. Afterwards, incubation with primary antibody directed against γH2AX (1:1000 in PBS/ 0.3% Triton X-100; Millipore, Burlington, Massachusetts, USA) was performed overnight at 4 °C. Cells were washed with PBS and PBS/ 0.4 M NaCl and subsequently incubated with a secondary antibody labeled with Alexa Fluor 488 (1:400 in PBS/ 0.3% Triton X-100) for 1 h at RT. Cells were washed as mentioned before and embedded with Vectashield® (Vector Labs, Burlingame, CA, USA). The samples were then analyzed using a Zeiss Axio Observer 7 microscope equipped with a 63x oil objective (plan-apochromat 63x/1.40 DIC M27) and LSM 900 confocal laser scanner (Carl Zeiss Microscopy, Jena, Germany). At least 40 nuclei per sample were analyzed for γH2AX foci by Zen 3.6 software (Carl Zeiss Microscopy, Jena, Germany). High resolution images were obtained using the Zeiss Airyscan.

Determination of relative genotoxicity by Benchmark dose modelling

To derive the relative genotoxic potencies based on the western blot, Comet assay and immunofluorescence data, a free software available from the European Food and Safety Agency (EFSA), called PROAST, was used. Hereby, concentration–response relationships were modelled to determine the benchmark dose (BMD) at a defined benchmark response (BMR) and its related 90% lower and upper confidence limits (BMDL and BMDU). The software determined best fits out of different algorithms and the best four fits were summarized as mean as long as they fulfilled the requirements (lowest AIC value). The BMR were chosen according to the outcome of data, so that a higher threshold was set for the more semi-quantitative western blot data. A lower BMR for comet assay and immunofluorescence data were chosen, because 50 comets or > 40 cells per sample in each biological replicate were evaluated. Therefore, a 2.0-fold increase of γH2AX intensity from western blot data (BMD_{100}, CES = 1.0) and 1.5-fold increase (BMD_{50}; CES = 0.5) of OTM and γH2AX foci per nuclei were used as a benchmark response (CES, critical effect size). The means of BMDL and BMDU were calculated by averaging the four models.

Statistical analysis

All experiments were performed independently at least three times, except otherwise stated. Results are presented as means ± standard error of the means (SEM) from representative experiments. Statistics were carried out by Graphpad Prism software (Version 9), statistical significance was defined as $P < 0.05$ and statistical analyses were performed using unpaired two-tailed Student's t-test with respect to the negative control.

Supplementary Information The online version contains supplementary material available at https://doi.org/10.1007/s00204-023-03482-8.

Acknowledgements We are grateful to Melanie-Abel Beckmann (Division of Food Chemistry and Toxicology, Department of Chemistry, RPTU Kaiserslautern-Landau) for performing mycoplasm detection in routine cell culture. Furthermore we thank Prof. Dr. Elke Richling (Division of Food Chemistry and Toxicology, Department of Chemistry, RPTU Kaiserslautern-Landau) for access to the Axioskop 2 fluorescence microscope used for Comet analysis.

Funding Open Access funding enabled and organized by Projekt DEAL. This project was supported by Kooperation Phytopharmaka GbR, Bonn, Germany (TU-KL #2) and the German Research Foundation [DFG] (INST 248/331–1 FUGG).

Data availability All datasets generated and analyzed during this study were included in the manuscript and the supplementary information. They are also available from the corresponding author upon reasonable request.

Declarations

Conflict of interest The authors declare no conflict of interest.

References

Abdelfatah S, Nass J, Knorz C, Klauck SM, Kupper JH, Efferth T (2022) Pyrrolizidine alkaloids cause cell cycle and DNA damage repair defects as analyzed by transcriptomics in cytochrome P450 3A4-overexpressing HepG2 clone 9 cells. Cell Biol Toxicol 38(2):325–345. https://doi.org/10.1007/s10565-021-09599-9

Allemang A, Mahony C, Lester C, Pfuhler S (2018) Relative potency of fifteen pyrrolizidine alkaloids to induce DNA damage as measured by micronucleus induction in HepaRG human liver cells. Food Chem Toxicol 121:72–81. https://doi.org/10.1016/j.fct.2018.08.003

Azqueta A, Collins AR (2013) The essential comet assay: a comprehensive guide to measuring DNA damage and repair. Arch Toxicol 87(6):949–968. https://doi.org/10.1007/s00204-013-1070-0

Brady CA, Attardi LD (2010) p53 at a glance. J Cell Sci 123(Pt 15):2527–2532. https://doi.org/10.1242/jcs.064501

Carlsson MJ, Vollmer AS, Demuth P et al (2022) p53 triggers mitochondrial apoptosis following DNA damage-dependent replication stress by the hepatotoxin methyleugenol. Cell Death Dis 13(11):1009. https://doi.org/10.1038/s41419-022-05446-9

Chen T, Mei N, Fu PP (2010) Genotoxicity of pyrrolizidine alkaloids. J Appl Toxicol 30(3):183–196. https://doi.org/10.1002/jat.1504

Dörsam B, Seiwert N, Foersch S et al (2018) PARP-1 protects against colorectal tumor induction, but promotes inflammation-driven colorectal tumor progression. Proc Natl Acad Sci U S A 115(17):E4061–E4070. https://doi.org/10.1073/pnas.1712345115

Ebmeyer J, Rasinger JD, Hengstler JG et al (2020) Hepatotoxic pyrrolizidine alkaloids induce DNA damage response in rat liver in a 28-day feeding study. Arch Toxicol 94(5):1739–1751. https://doi.org/10.1007/s00204-020-02779-2

Edgar JA (2014) Food contaminants capable of causing cancer, pulmonary hypertension and cirrhosis. Med J Aust 200(2):73–74. https://doi.org/10.5694/mja13.10227

Edgar JA, Molyneux RJ, Colegate SM (2015) Pyrrolizidine Alkaloids: potential role in the etiology of cancers, pulmonary hypertension, congenital anomalies, and liver disease. Chem Res Toxicol 28(1):4–20. https://doi.org/10.1021/tx500403t

Fahrer J, Schweitzer B, Fiedler K, Langer T, Gierschik P, Barth H (2013) C2-streptavidin mediates the delivery of biotin-conjugated tumor suppressor protein p53 into tumor cells. Bioconjug Chem 24(4):595–603. https://doi.org/10.1021/bc300563c

Fahrer J, Huelsenbeck J, Jaurich H et al (2014) Cytolethal distending toxin (CDT) is a radiomimetic agent and induces persistent levels of DNA double-strand breaks in human fibroblasts. DNA Repair (amst) 18:31–43. https://doi.org/10.1016/j.dnarep.2014.03.002

Fahrer J, Frisch J, Nagel G et al (2015) DNA repair by MGMT, but not AAG, causes a threshold in alkylation-induced colorectal carcinogenesis. Carcinogenesis 36(10):1235–1244. https://doi.org/10.1093/carcin/bgv114

Wiedenfeld H, Roeder E, Bourauel T, Edgar J (2008) Pyrrolizidine Alkaloids: Structure and Toxicity. V and R Unipress

Fraczek J, Bolleyn J, Vanhaecke T, Rogiers V, Vinken M (2013) Primary hepatocyte cultures for pharmaco-toxicological studies: at the busy crossroad of various anti-dedifferentiation strategies. Arch Toxicol 87(4):577–610. https://doi.org/10.1007/s00204-012-0983-3

Fu PP (2017) Pyrrolizidine Alkaloids: metabolic activation pathways leading to liver tumor initiation. Chem Res Toxicol 30(1):81–93. https://doi.org/10.1021/acs.chemrestox.6b00297

Fu PP, Xia Q, Lin G, Chou MW (2004) Pyrrolizidine alkaloids–genotoxicity, metabolism enzymes, metabolic activation, and mechanisms. Drug Metab Rev 36(1):1–55. https://doi.org/10.1081/dmr-120028426

Gao L, Rutz L, Schrenk D (2020) Structure-dependent hepato-cytotoxic potencies of selected pyrrolizidine alkaloids in primary rat hepatocyte culture. Food Chem Toxicol 135:110923. https://doi.org/10.1016/j.fct.2019.110923

Glück J, Waizenegger J, Braeuning A, Hessel-Pras S (2020) Pyrrolizidine alkaloids induce cell death in human hepaRG cells in a structure-dependent manner. Int J Mol Sci. https://doi.org/10.3390/ijms22010202

Hadi NSA, Bankoglu EE, Schott L et al (2021) Genotoxicity of selected pyrrolizidine alkaloids in human hepatoma cell lines HepG2 and

Huh6. Mutat Res Genet Toxicol Environ Mutagen. https://doi.org/10.1016/j.mrgentox.2020.503305

Hadi NSA, Bankoglu EE, Stopper H (2023) Genotoxicity of pyrrolizidine alkaloids in metabolically inactive human cervical cancer HeLa cells co-cultured with human hepatoma HepG2 cells. Arch Toxicol 97(1):295–306. https://doi.org/10.1007/s00204-022-03394-z

He Y, Lian W, Ding L et al (2021a) Lung injury induced by pyrrolizidine alkaloids depends on metabolism by hepatic cytochrome P450s and blood transport of reactive metabolites. Arch Toxicol 95(1):103–116. https://doi.org/10.1007/s00204-020-02921-0

He Y, Shi M, Wu X et al (2021b) Mutational signature analysis reveals widespread contribution of pyrrolizidine alkaloid Exposure to human liver cancer. Hepatology 74(1):264–280. https://doi.org/10.1002/hep.31723

Herzog N, Katzenberger N, Martin F, Schmidtke K-U, Küpper J-H (2015) Generation of cytochrome P450 3A4-overexpressing HepG2 cell clones for standardization of hepatocellular testosterone 6β-hydroxylation activity. J Cell Biotechnol 1(1):15–26. https://doi.org/10.3233/JCB-15002

Herzog N, Hansen M, Miethbauer S et al (2016) Primary-like human hepatocytes genetically engineered to obtain proliferation competence display hepatic differentiation characteristics in monolayer and organotypical spheroid cultures. Cell Biol Int 40(3):341–353. https://doi.org/10.1002/cbin.10574

Hessel-Pras S, Braeuning A, Guenther G et al (2020) The pyrrolizidine alkaloid senecionine induces CYP-dependent destruction of sinusoidal endothelial cells and cholestasis in mice. Arch Toxicol 94(1):219–229. https://doi.org/10.1007/s00204-019-02582-8

Kammerer S, Küpper J-H (2018) Human hepatocyte systems for *in vitro* toxicology analysis. J Cell Biotechnol 3(2):85–93. https://doi.org/10.3233/JCB-179012

Kinner A, Wu W, Staudt C, Iliakis G (2008) Gamma-H2AX in recognition and signaling of DNA double-strand breaks in the context of chromatin. Nucleic Acids Res 36(17):5678–5694. https://doi.org/10.1093/nar/gkn550

Lester C, Troutman J, Obringer C et al (2019) Intrinsic relative potency of a series of pyrrolizidine alkaloids characterized by rate and extent of metabolism. Food Chem Toxicol 131:110523. https://doi.org/10.1016/j.fct.2019.05.031

Li X, He X, Chen S et al (2020) Evaluation of pyrrolizidine alkaloid-induced genotoxicity using metabolically competent TK6 cell lines. Food Chem Toxicol. https://doi.org/10.1016/j.fct.2020.111662

Louisse J, Rijkers D, Stoopen G et al (2019) Determination of genotoxic potencies of pyrrolizidine alkaloids in HepaRG cells using the gammaH2AX assay. Food Chem Toxicol. https://doi.org/10.1016/j.fct.2019.05.040

Mattocks AR (1986) Chemistry and toxicology of pyrrolizidine Alkaloids. Academic Press

Merz K-H, Schrenk D (2016) Interim relative potency factors for the toxicological risk assessment of pyrrolizidine alkaloids in food and herbal medicines. Toxicol Lett 263:44–57. https://doi.org/10.1016/j.toxlet.2016.05.002

Mimmler M, Peter S, Kraus A et al (2016) DNA damage response curtails detrimental replication stress and chromosomal instability induced by the dietary carcinogen PhIP. Nucleic Acids Res 44(21):10259–10276. https://doi.org/10.1093/nar/gkw791

Moller P, Azqueta A, Boutet-Robinet E et al (2020) Minimum Information for reporting on the comet assay (MIRCA): recommendations for describing comet assay procedures and results. Nat Protoc 15(12):3817–3826. https://doi.org/10.1038/s41596-020-0398-1

Moreira R, Pereira DM, Valentao P, Andrade PB (2018) Pyrrolizidine Alkaloids: chemistry, pharmacology toxicology food safety. Int J Mol Sci. https://doi.org/10.3390/ijms19061668

Nikolova T, Dvorak M, Jung F et al (2014) The gammaH2AX assay for genotoxic and nongenotoxic agents: comparison of H2AX phosphorylation with cell death response. Toxicol Sci 140(1):103–117. https://doi.org/10.1093/toxsci/kfu066

Prakash AS, Pereira TN, Reilly PE, Seawright AA (1999) Pyrrolizidine alkaloids in human diet. Mutat Res 443(1–2):53–67. https://doi.org/10.1016/s1383-5742(99)00010-1

Ruan J, Yang M, Fu P, Ye Y, Lin G (2014) Metabolic activation of pyrrolizidine alkaloids: insights into the structural and enzymatic basis. Chem Res Toxicol 27(6):1030–1039. https://doi.org/10.1021/tx500071q

Ruoss M, Vosough M, Konigsrainer A et al (2020) Towards improved hepatocyte cultures: progress and limitations. Food Chem Toxicol. https://doi.org/10.1016/j.fct.2020.111188

Rutz L, Gao L, Kupper JH, Schrenk D (2020) Structure-dependent genotoxic potencies of selected pyrrolizidine alkaloids in metabolically competent HepG2 cells. Arch Toxicol 94(12):4159–4172. https://doi.org/10.1007/s00204-020-02895-z

Schrenk D, Fahrer J, Allemang A et al (2022) Novel insights into pyrrolizidine alkaloid toxicity and implications for risk assessment: occurrence, genotoxicity, toxicokinetics risk assessment-a workshop report. Planta Med 88(2):98–117. https://doi.org/10.1055/a-1646-3618

Song Z, He Y, Ma J, Fu PP, Lin G (2020) Pulmonary toxicity is a common phenomenon of toxic pyrrolizidine alkaloids. J Environ Sci Health C Toxicol Carcinog 38(2):124–140. https://doi.org/10.1080/26896583.2020.1743608

Tamariz J, Burgueno-Tapia E, Vazquez MA, Delgado F (2018) Pyrrolizidine alkaloids. alkaloids. Chem Biol 80:1–314. https://doi.org/10.1016/bs.alkal.2018.03.001

Wiedenfeld H, Edgar J (2010) Toxicity of pyrrolizidine alkaloids o humans and ruminants. Phytochem Rev 10:137–151

Yang M, Ma J, Ruan J, Ye Y, Fu PP, Lin G (2019) Intestinal and hepatic biotransformation of pyrrolizidine alkaloid N-oxides to toxic pyrrolizidine alkaloids. Arch Toxicol 93(8):2197–2209. https://doi.org/10.1007/s00204-019-02499-2

Supplementary Figures

Figure S1

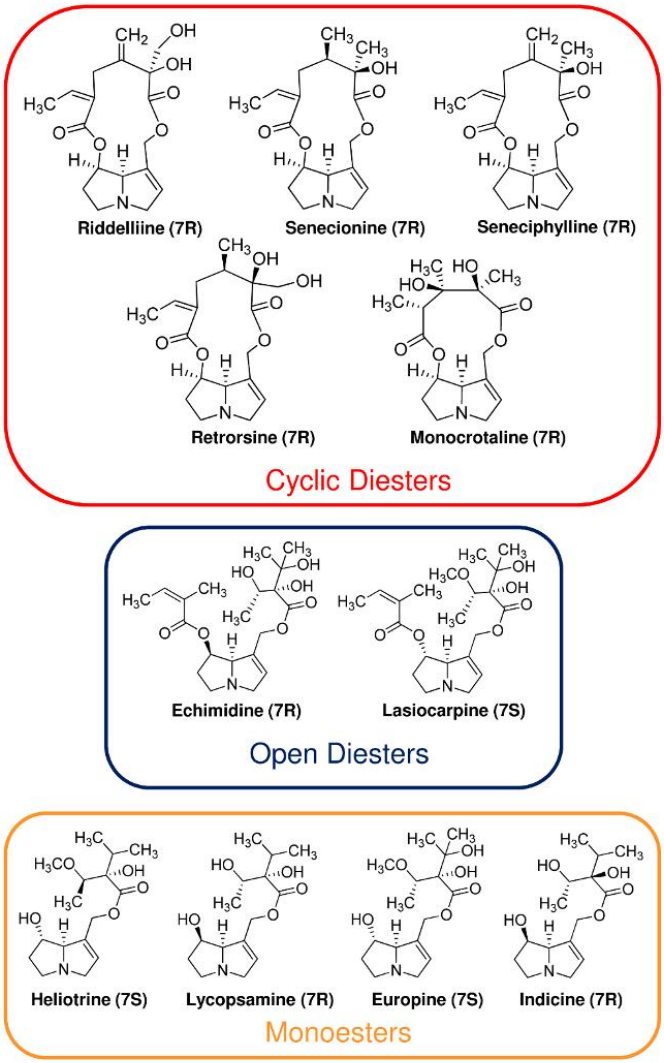

Figure S1: Chemical structures of the eleven PAs tested in human liver cells. As cyclic di-esters monocrotaline (7R), retrorsine (7R), riddelliine (7R), senecionine (7R) and seneciphylline (7R) were selected. Echimidine (7R) and lasiocarpine (7S) were chosen as open di-esters. Four mono-esters including europine (7S), heliotrine (7S), indicine (7R) and lycopsamine (7R) were tested.

Figure S2

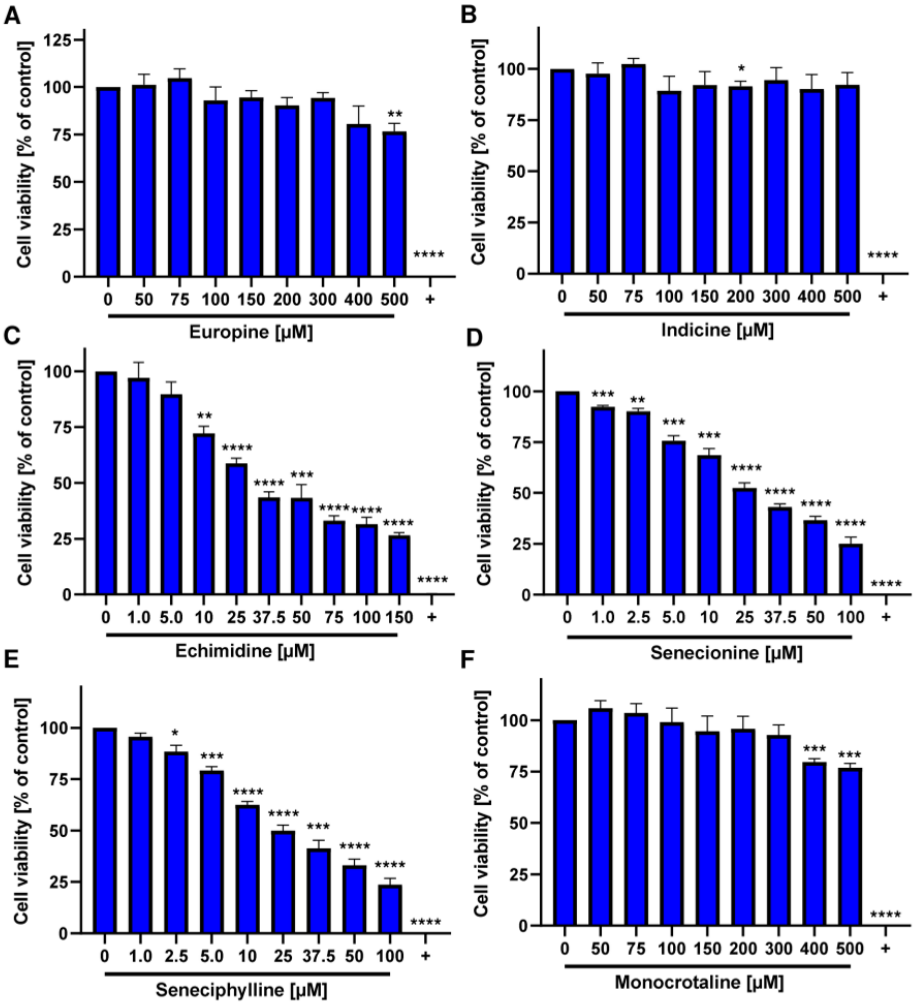

Figure S2: Structure-dependent cytotoxic effects in HepG2-CYP3A4 cells triggered by different PAs. Viability of HepG2-CYP3A4 cells 24 h after treatment with increasing concentrations of europine (**A**), indicine (**B**), echimidine (**C**), senecionine (**D**), seneciphylline (**E**), and monocrotaline (**F**)**.** Saponin was used as a positive control (+) and solvent as a negative control (0). Mean + SEM are shown for each incubation (n=3, each measured as triplicates). Statistical analyses were performed using unpaired Students t-test with respect to the negative control. "*" P≤0.05, "**" P ≤0.01, "***" P ≤0.001, "****" P ≤0.0001.

Figure S3

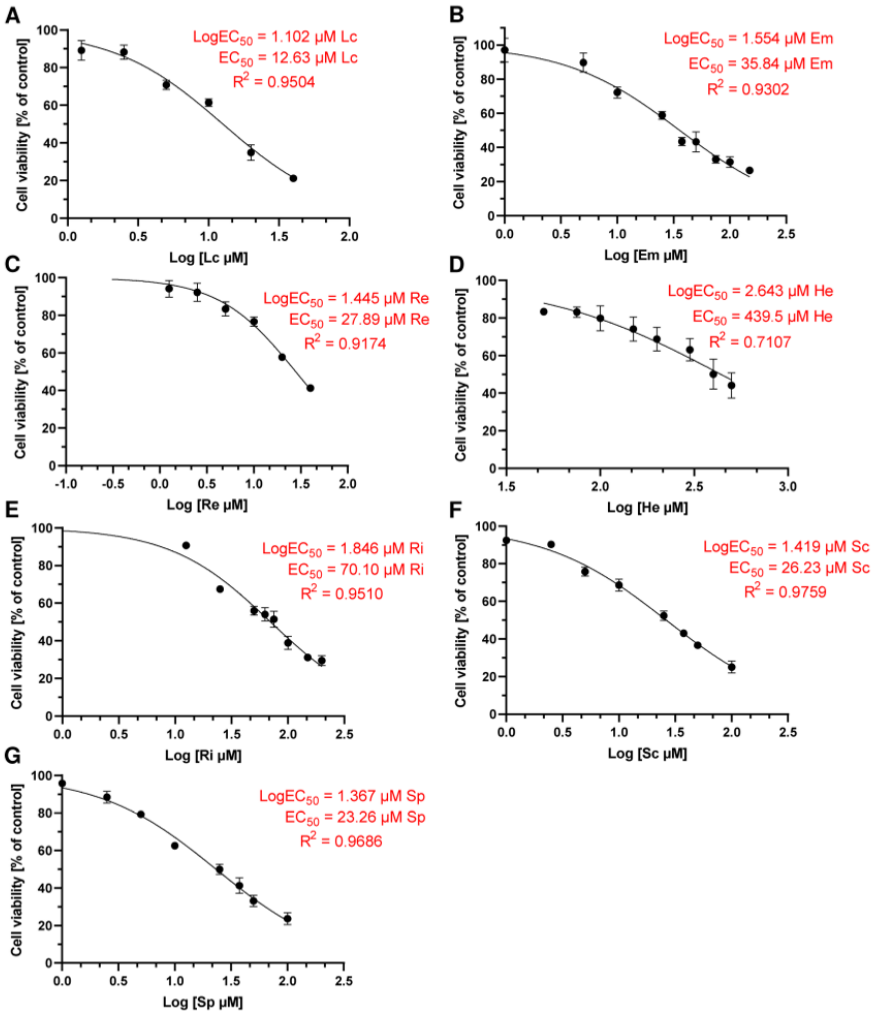

Figure S3: Determination of EC_{50} values from PA concentration-response data in HepG2-CYP3A4 cells after 24 h exposure. The data were transformed via GraphPad and fitted with a sigmoidal, non-linear model to determine the relative cytotoxicity for lasiocarpine (**A**), echimidine (**B**), retrorsine (**C**), heliotrine (**D**), riddelliine (**E**), senecionine (**F**) and seneciphylline (**G**). The relative cytotoxicity was calculated as the effective concentration, at which cell viability was reduced by 50 % (EC_{50}).

Figure S4

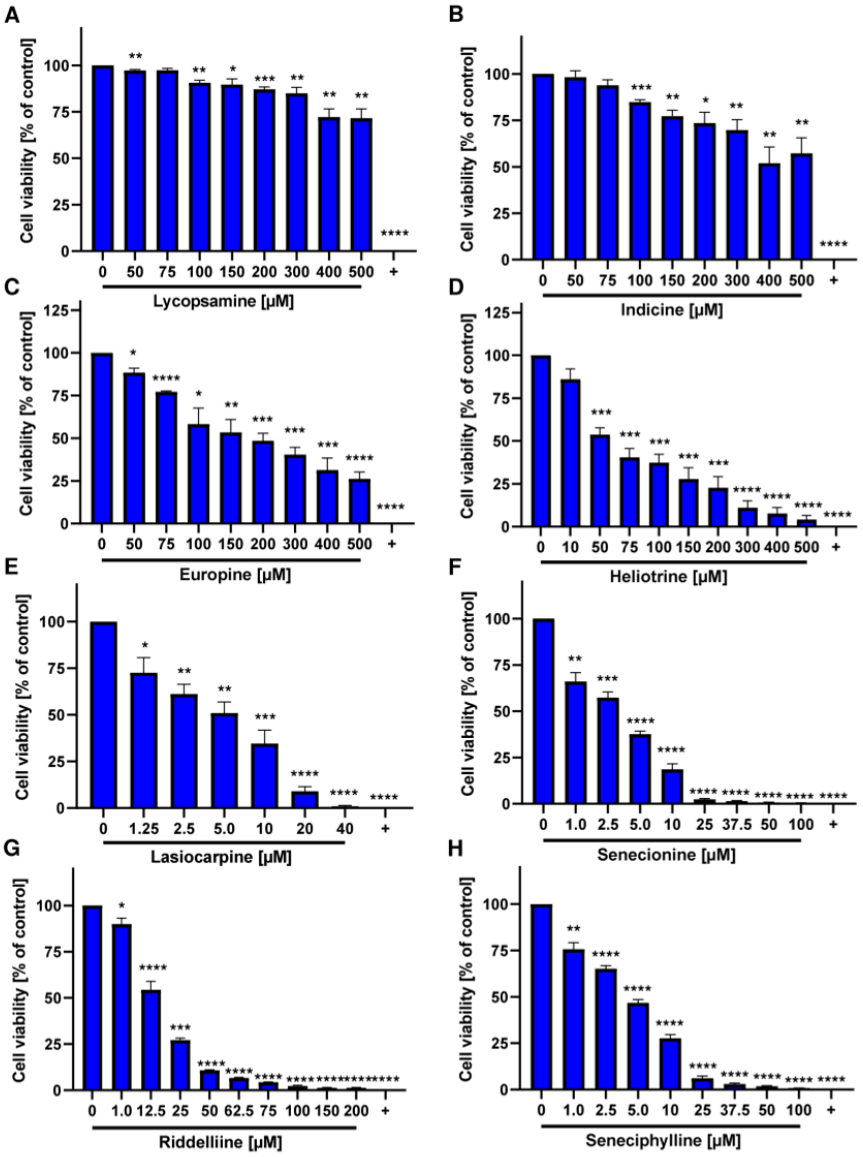

Figure S4: Structure-dependent cytotoxic effects in HepG2-CYP3A4 cells triggered by different PAs. Viability of HepG2-CYP3A4 cells 72 h after treatment with increasing concentrations of lycopsamine (**A**), indicine (**B**), europine (**C**), heliotrine (**D**), lasiocarpine (**E**), senecionine (**F**), riddelliine (**G**) and seneciphylline (**H**). Saponin was used as a positive control (+) and solvent as a negative control (0). Mean + SEM are shown for each incubation (n=3,

each measured as triplicates). Statistical analyses were performed using unpaired Students t-test with respect to the negative control. * P≤0.05, ** P ≤0.01, *** P ≤0.001, **** P ≤0.0001.

Figure S5

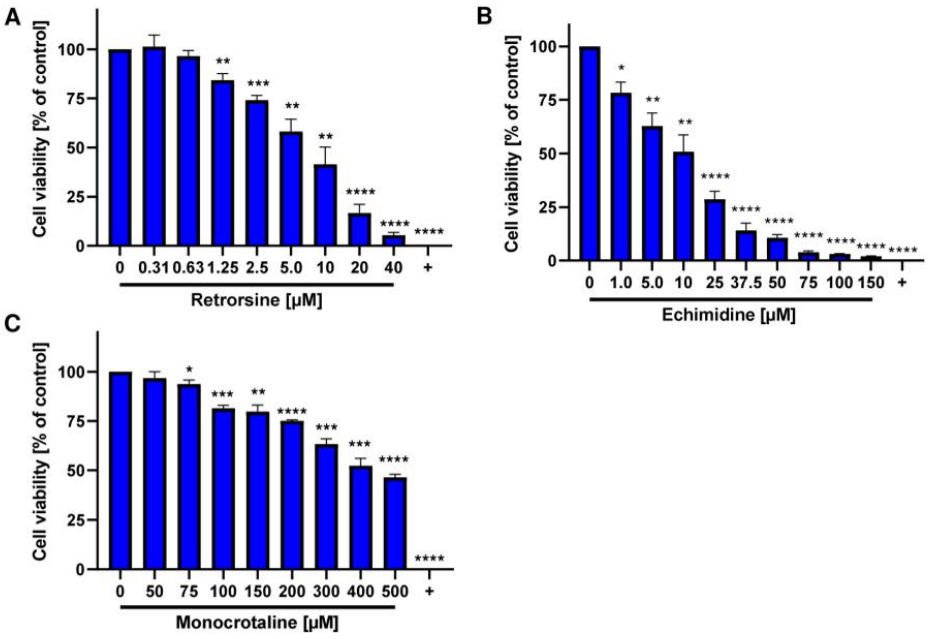

Figure S5: Structure-dependent cytotoxic effects in HepG2-CYP3A4 cells triggered by different esterified PAs. Viability of HepG2-CYP3A4 cells 72 h after treatment with increasing concentrations of retrorsine (**A**), echimidine (**B**) and monocrotaline (**C**). Saponin was used as a positive control (+) and solvent as a negative control (0). Mean + SEM are shown for each incubation (n=3, each measured as triplicates. Statistical analyses were performed using unpaired Students t-test with respect to the negative control. * P≤0.05, ** P ≤0.01, *** P ≤0.001, **** P ≤0.0001.

Figure S6

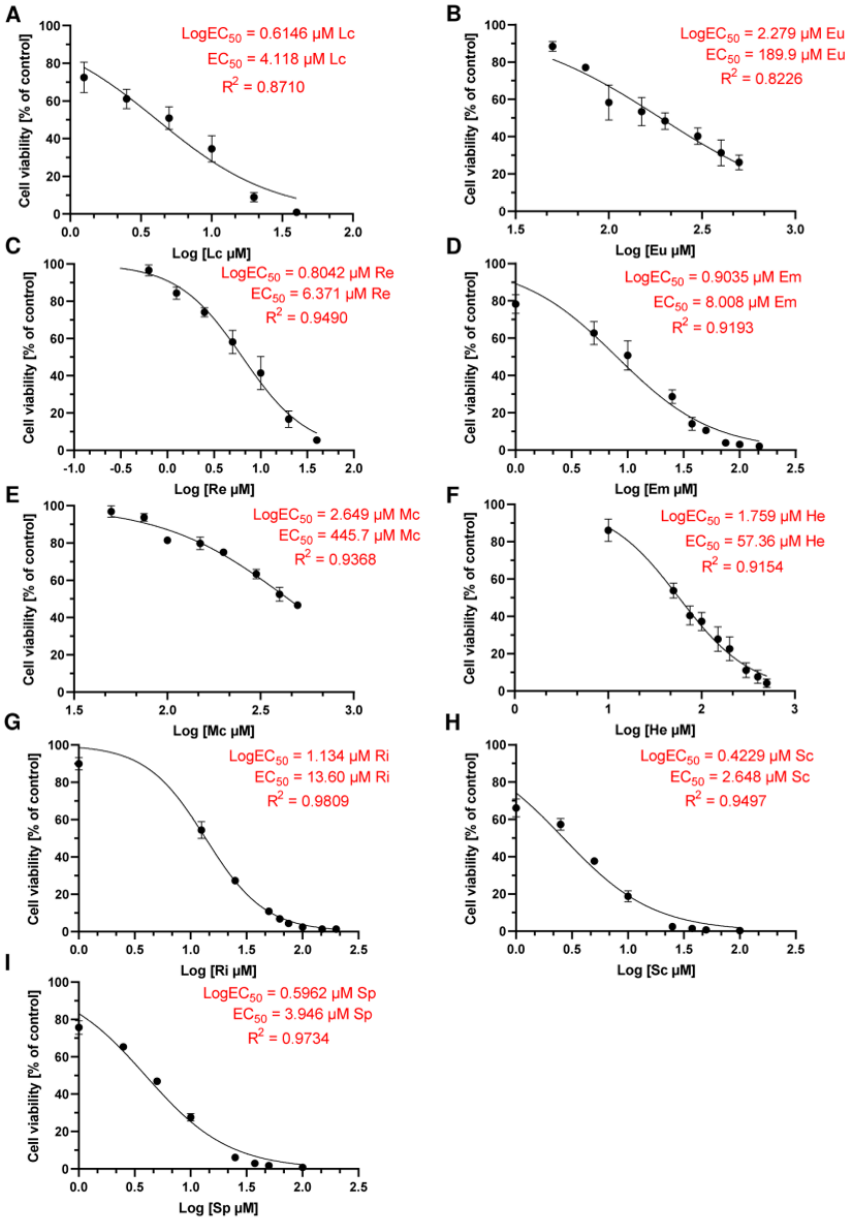

Figure S6: Determination of EC_{50} values from PA concentration-response data in HepG2-CYP3A4 cells after 72 h exposure. The data were transformed via GraphPad and fitted with a sigmoidal, non-linear model to determine the relative cytotoxicity for lasiocarpine (**A**), europine (**B**), retrorsine (**C**), echimidine (**D**), monocrotaline (**E**), heliotrine (**F**), riddelliine

(**G**), senecionine (**H**) and seneciphylline (**I**). The relative cytotoxicity was calculated as the effective concentration, at which cell viability was reduced by 50 % (EC_{50}).

Figure S7

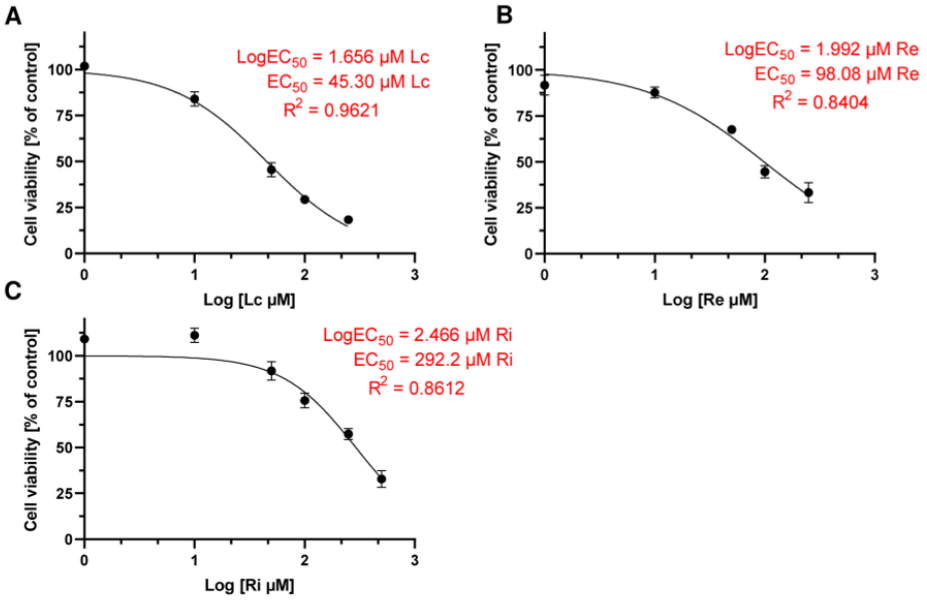

Figure S7: Determination of EC_{50} values from PA concentration-response data in primary human hepatocytes after 24 h exposure. The data were transformed via GraphPad and fitted with a sigmoidal, non-linear model to calculate the relative cytotoxicity for lasiocarpine (**A**), retrorsine (**B**) and riddelliine (**C**). The relative cytotoxicity was calculated as the effective concentration, at which cell viability was reduced by 50 % (EC_{50}).

Figure S8

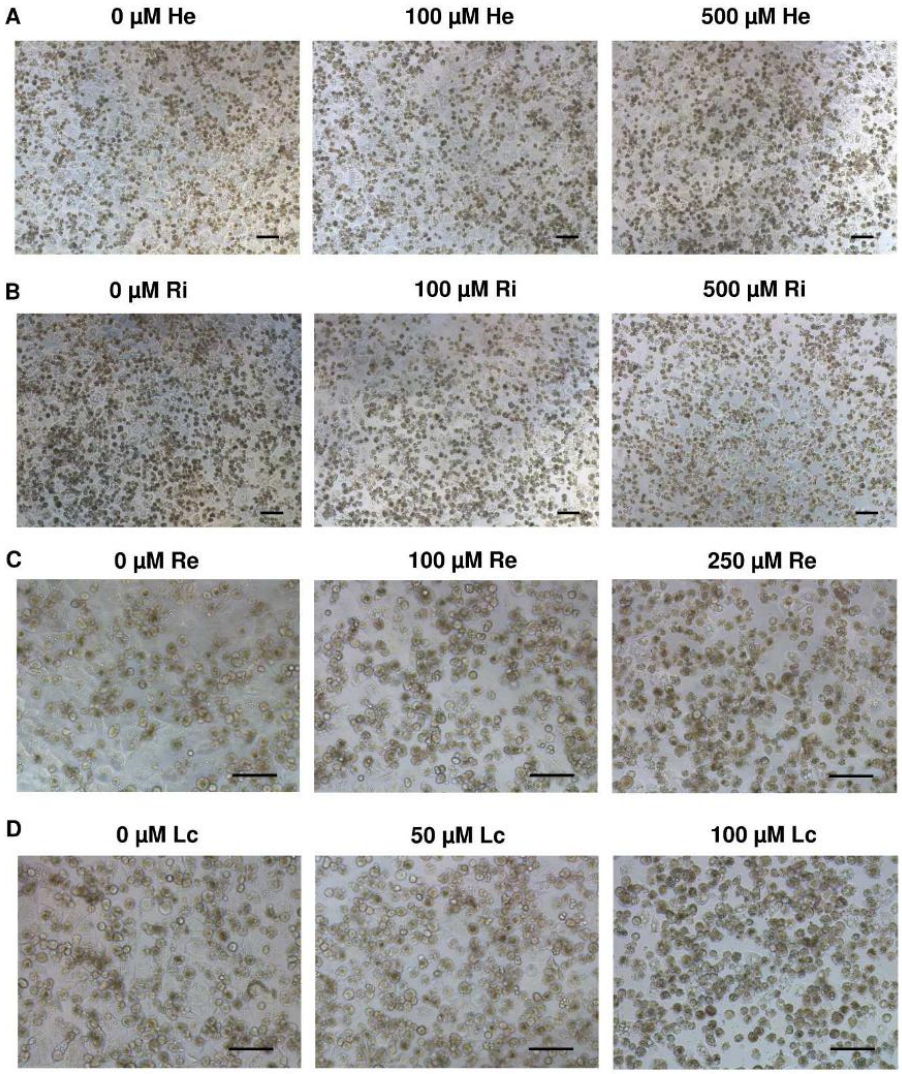

Figure S8: Cell morphology of primary human hepatocytes exposed to increasing PA concentrations. A-D: Representative microscopic images of primary human hepatocytes after 24 h incubation with different concentrations of heliotrine (**A**), riddelliine (**B**), retrorsine (**C**) and lasiocarpine (**D**). Representative images are shown. Scale bar: 100 µm.

Figure S9

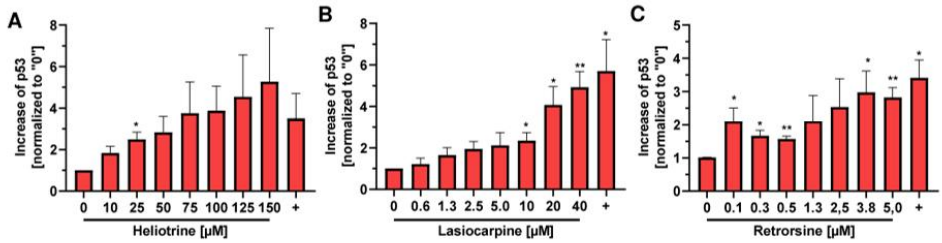

Figure S9: Structure-dependent p53 accumulation in HepG2-CYP3A4 cells triggered by different PAs. Densitometric evaluations of p53 after 24 h incubation with heliotrine (**A**), lasiocarpine (**B**) and retrorsine (**C**) in HepG2-CYP3A4. Etoposide was used as a positive (+) and solvent as a negative control (0). HSP90 served as loading control. p53 level relative to the loading control and normalized versus the negative control. Data depicted as mean + SEM (N=3). Statistical analysis was performed by unpaired Student's t test on negative control. * P≤0.05, ** P ≤0.01, *** P ≤0.001, **** P ≤0.0001.

Figure S10

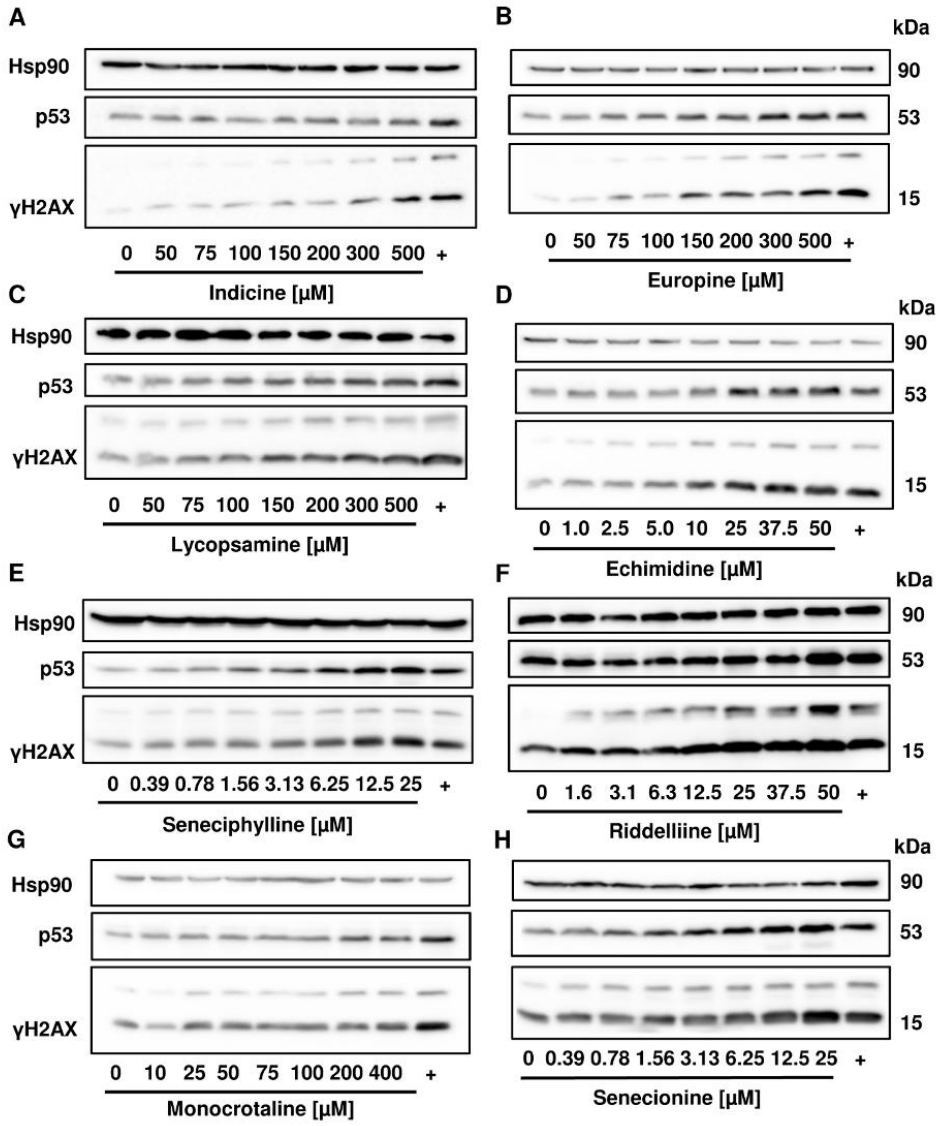

Figure S10: Structure-dependent γH2AX and p53 formation in HepG2-CYP3A4 cells triggered by different PAs. Representative western blots of γH2AX and p53 after 24 h incubation with indicine (**A**), europine (**B**), lycopsamine (**C**), echimidine (**D**), seneciphylline (**E**), riddelliine (**F**), monocrotaline (**G**) and senecionine (**H**) in HepG2-CYP3A4 cells. Etoposide was used as a positive (+) and solvent as a negative control (0). HSP90 served as loading control.

Figure S11

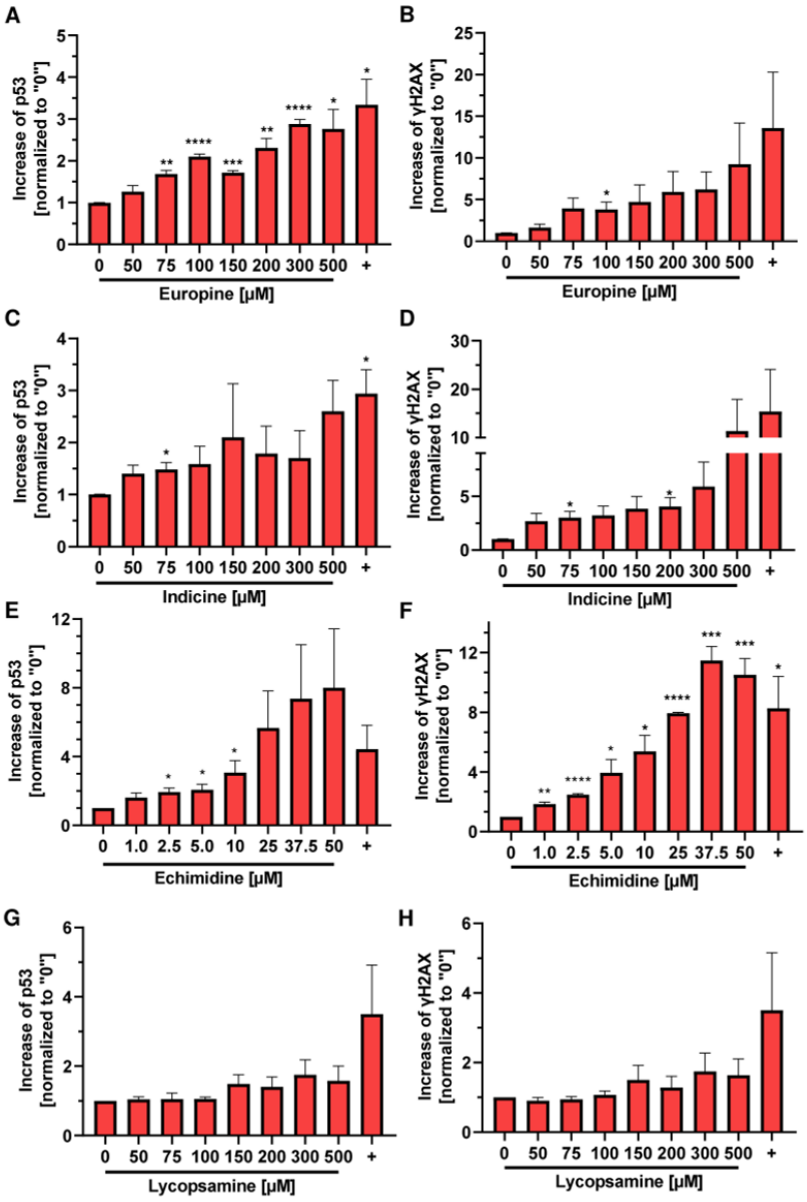

Figure S11: Structure-dependent γH2AX and p53 formation in HepG2-CYP3A4 cells triggered by different PAs. Densitometric evaluations of γH2AX and p53 after 24 h incubation with europine (**A-B**), indicine (**C-D**), echimidine (**E-F**) and lycopsamine (**G-H**) in HepG2-CYP3A4. Etoposide was used as a positive (+) and solvent as a negative control (0). HSP90

served as loading control. γH2AX and p53 levels relative to the loading control and normalized versus the negative control. Data depicted as mean + SEM (N=3). Statistical analysis was performed by unpaired Student's t test on negative control. “*” P≤0.05, “**” P ≤0.01, “***” P ≤0.001, “****” P ≤0.0001

Figure S12

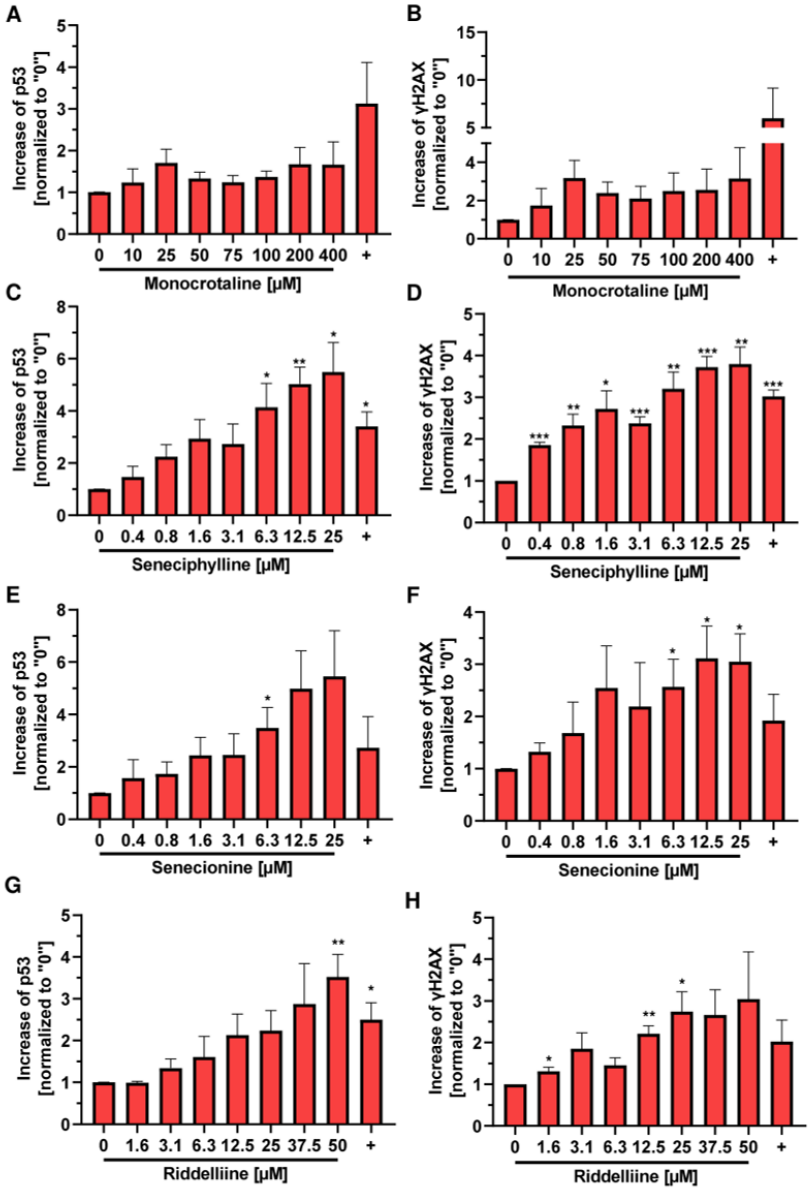

Figure S12: Structure-dependent γH2AX and p53 formation in HepG2-CYP3A4 cells triggered by different esterified PAs. Densitometric evaluations of γH2AX and p53 after 24 h incubation with monocrotaline (**A-B**), seneciphylline (**C-D**), senecionine (**E-F**) and riddelliine (**G-H**) in HepG2-CYP3A4. Etoposide was used as a positive (+) and solvent as a negative

control (0). HSP90 served as loading control. γH2AX and p53 levels relative to the loading control and normalized versus the negative control. Data depicted as mean + SEM (N=3). Statistical analysis was performed by unpaired Student's t test on negative control. * P≤0.05, ** P ≤0.01, *** P ≤0.001, **** P ≤0.0001.

Figure S13

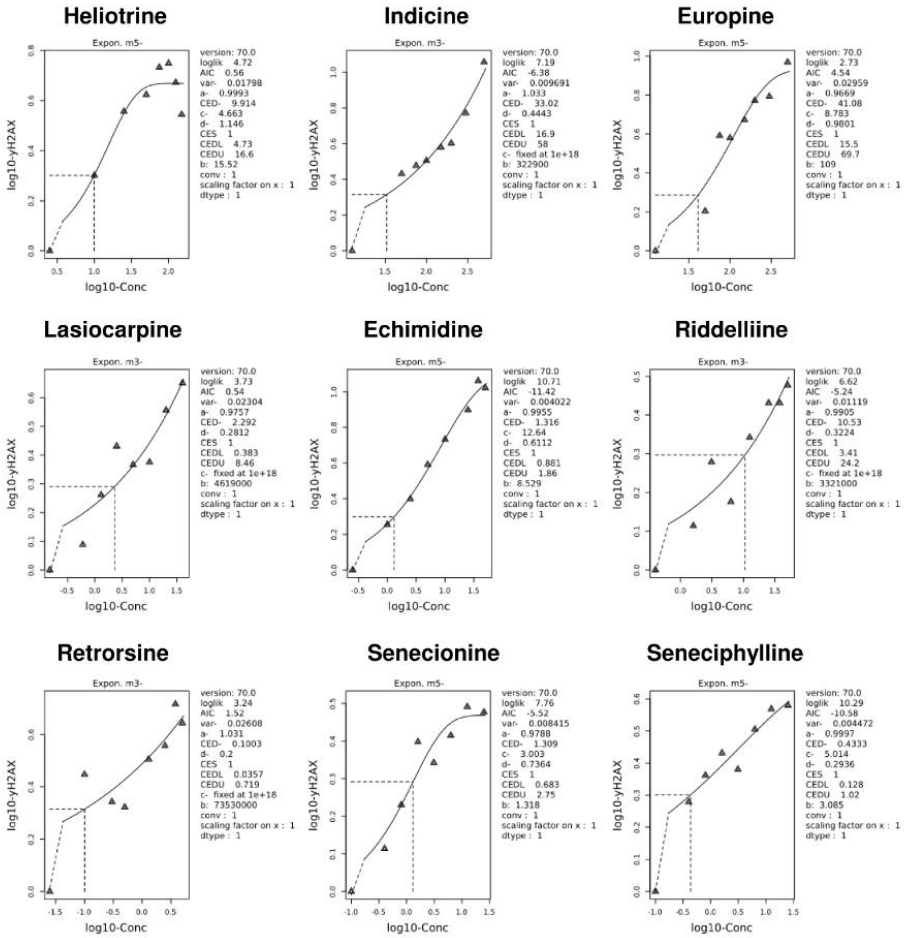

Figure S13: BMD modeling of γH2AX data from heliotrine, indicine, europine, lasiocarpine, echimidine, riddelliine, retrorsine, senecionine and seneciphylline in HepG2-CYP3A4.

Figure S14

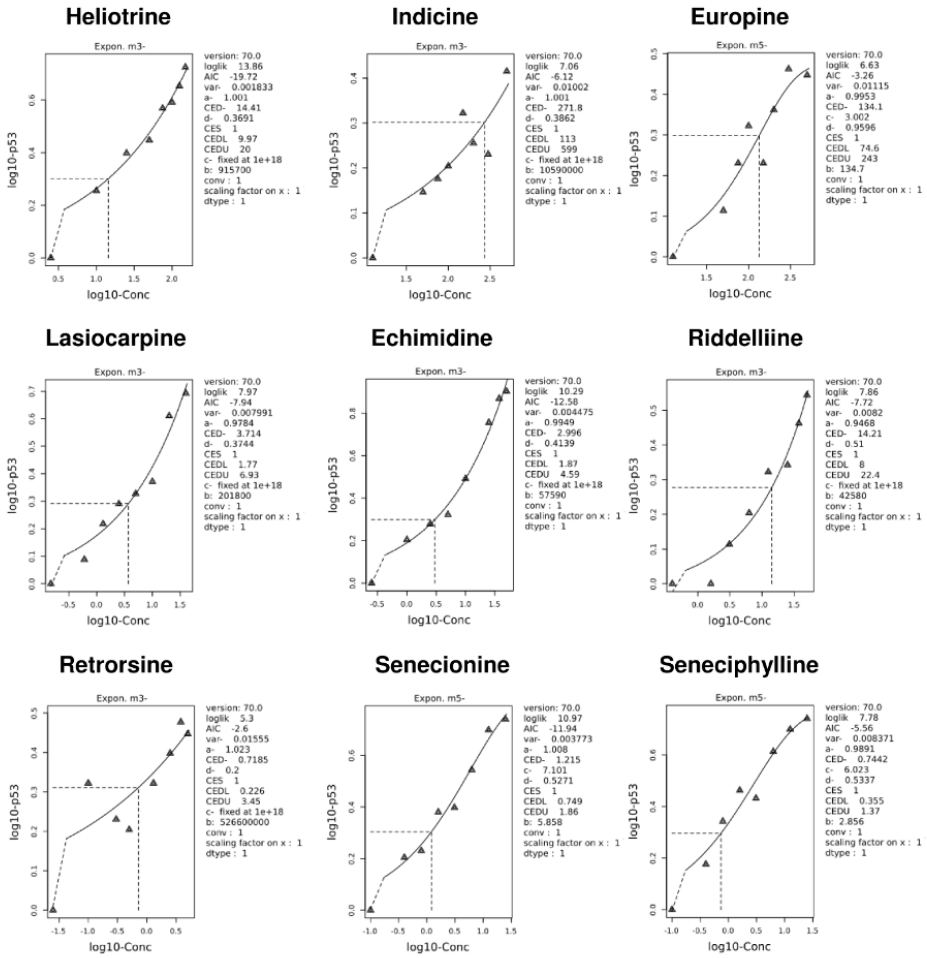

Figure S14: BMD modeling of p53 data from heliotrine, indicine, europine, lasiocarpine, echimidine, riddelliine, retrorsine, senecionine and seneciphylline in HepG2-CYP3A4.

Figure S15

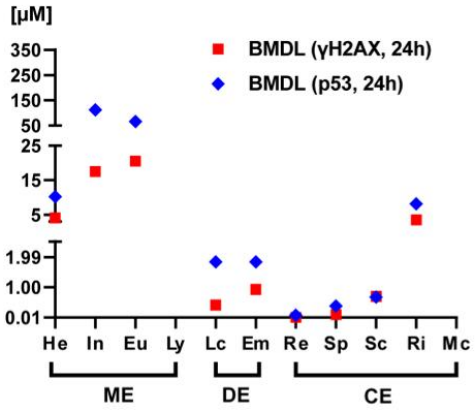

Figure S15: BMDL values for different PAs based on γH2AX and p53 data. BMD modeling was performed with concentration-response data using PROAST from EFSA with a CES of 1.0. ME: monoester; DE: open diester; CE: cyclic diester.

Figure S16

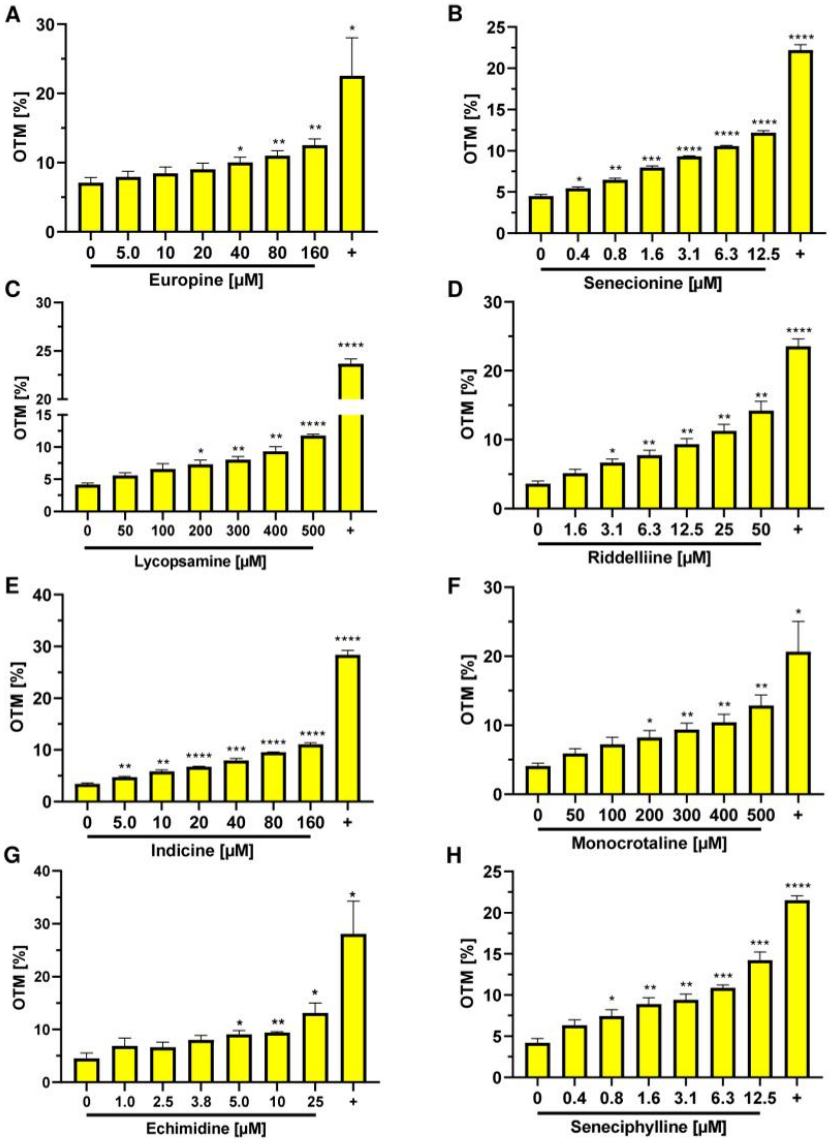

S16: Structure-dependent DNA strand break induction in HepG2-CYP3A4 by different PAs. Olive tail moments (OTM), which represents DNA strand break formation, in HepG2-CYP3A4 after 24 h incubations with europine (A), senecionine (B), lycopsamine (C), riddelliine (D), indicine (E), monocrotaline (F), echimidine (G) and seneciphylline (H). tBOOH was used as a positive (+) and solvent as a negative control (0). Data are shown as mean + SEM (N=3,

except for heliotrine and europine N=4). At least 50 comets per slide were counted. Statistical analyses were performed using unpaired two-tailed Students t-test with respect to the negative control. * P≤0.05, ** P ≤0.01, *** P ≤0.001, **** P ≤0.0001.

Figure S17

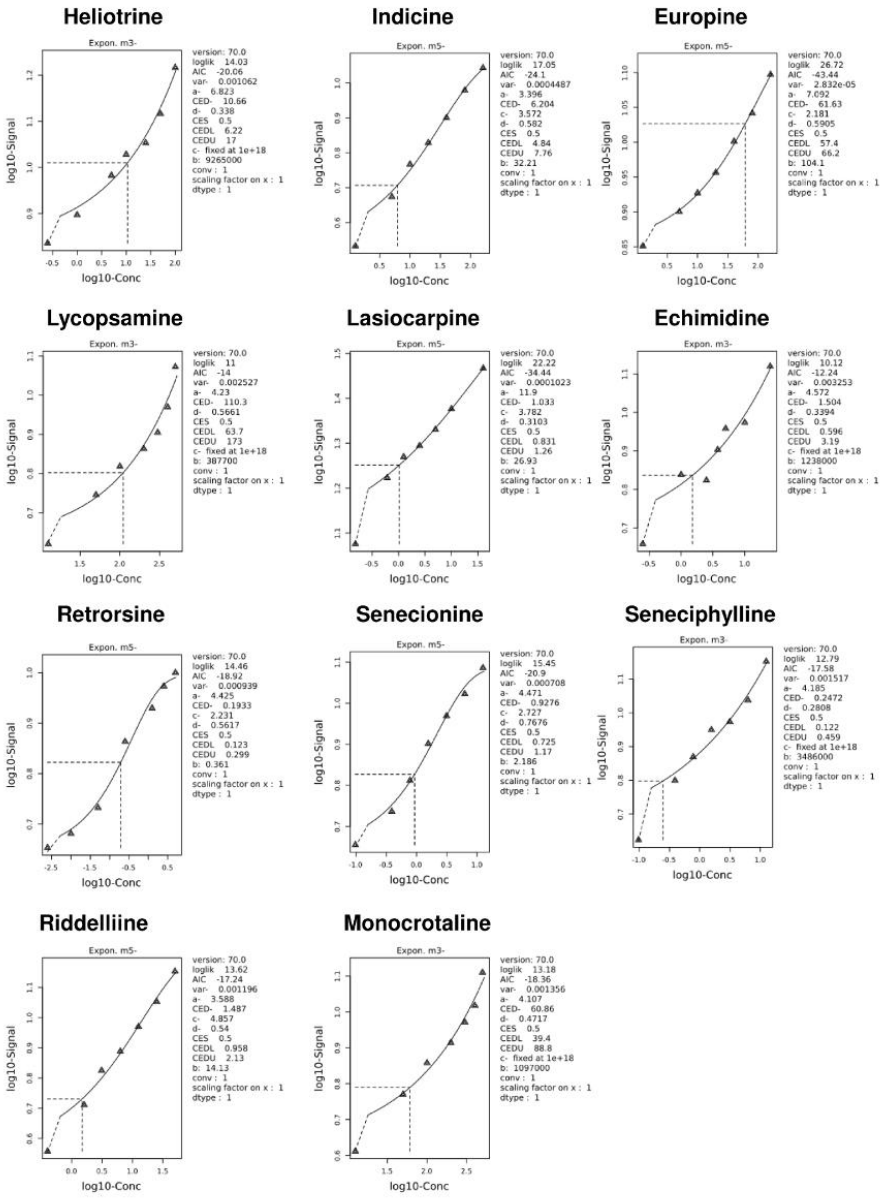

Figure S17: BMD modeling of Comet data for heliotrine, indicine, europine, lycopsamine, lasiocarpine, echimidine, riddelliine, retrorsine, monocrotaline, senecionine and seneciphylline in HepG2-CYP3A4.

Figure S18

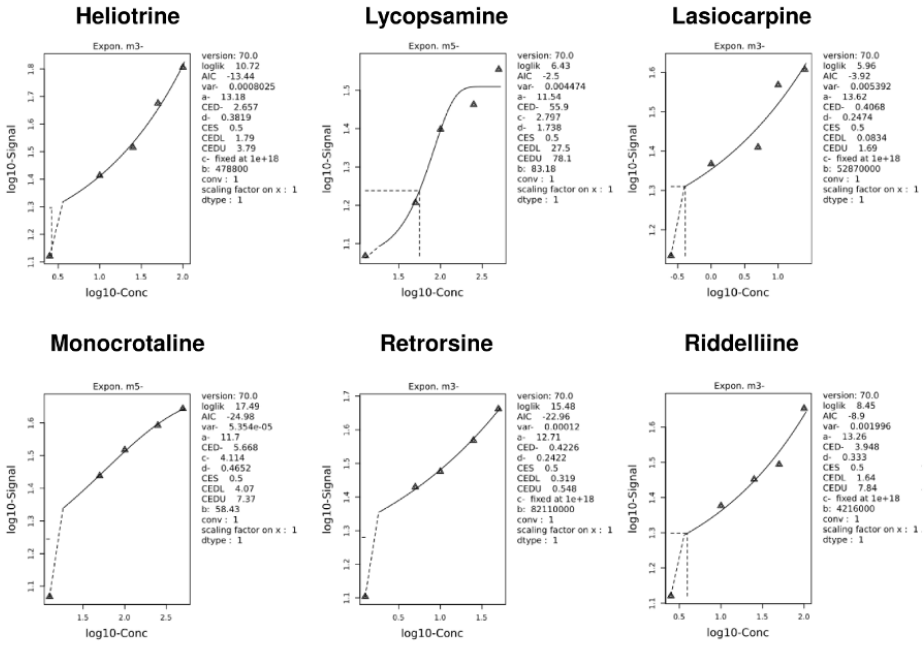

Figure S18: BMD modeling of γH2AX data for heliotrine, lycopsamine, lasiocarpine and monocrotaline, retrorsine and riddelliine in primary human hepatocytes.

Supplementary Tables

Table S1: BMD values obtained from concentration-response data for PAs in HepG2-CYP3A4. Data from γH2AX analysis for eleven PAs in HepG2-CYP3A4 cells were used for BMD modeling as described in Material & Methods. NA: not analyzable due to weak, concentration-independent effects.

PA	BMDL (γH2AX) [µM]	BMD (γH2AX) [µM]	BMDU (γH2AX) [µM]
He	4.09	8.84	16.00
Ly	NA	NA	NA
In	17.5	34.46	60.93
Eu	20.5	43.61	67.68
Lc	0.42	2.30	8.22
Em	0.93	1.36	1.89
Sp	0.10	0.36	1.01
Sc	0.70	1.27	2.57
Re	0.01	0.09	0.71
Ri	3.48	10.43	23.98
Mc	NA	NA	NA

Table S2: BMD values obtained from concentration-response data for PAs in HepG2-CYP3A4. Data from p53 analysis for eleven PAs in HepG2-CYP3A4 cells were used for BMD modeling as described in Material & Methods. NA: not analyzable due to weak, concentration-independent effects.

PA	BMDL (p53) [µM]	BMD (p53) [µM]	BMDU (p53) [µM]
He	10.2	14.64	20.30
Ly	NA	NA	NA
In	112.3	270.08	608.75
Eu	66.7	138.55	268.00
Lc	1.84	3.74	6.84
Em	1.84	3.14	4.72
Sp	0.39	0.75	1.31
Sc	0.68	1.15	1.84
Re	0.09	0.68	3.52
Ri	8.14	14.04	21.75
Mc	NA	NA	NA

Table S3: BMD values obtained from concentration-response data for PAs in HepG2-CYP3A4. Data from Comet (OTM) analysis for eleven PAs in HepG2-CYP3A4 cells were used for BMD modeling as described in Material & Methods. NA: not analyzable due to weak, concentration-independent effects.

PA	BMDL (OTM) [µM]	BMD (OTM) [µM]	BMDU (OTM) [µM]
He	6.20	10.57	16.85
Ly	62.1	109.13	173.00
In	5.26	6.39	7.63
Eu	58.28	62.10	66.10
Lc	0.84	1.03	1.25
Em	0.62	1.54	3.23
Sp	0.14	0.26	0.47
Sc	0.78	0.92	1.08
Re	0.14	0.19	0.27
Ri	1.09	1.59	2.15
Mc	39.85	61.68	90.15

Table S4: BMD values obtained from concentration-response data for PAs in primary human hepatocytes (PHH). γH2AX data from six PAs in PHH were used for BMD modeling as described in Material & Methods.

PA	BMDL (γH2AX) [µM]	BMD (γH2AX) [µM]	BMDU (γH2AX) [µM]
He	2.1	3.00	4.16
Ly	31.9	52.85	74.63
Lc	0.06	0.44	1.73
Re	0.36	0.49	0.65
Ri	1.72	4.17	8.24
Mc	6.3	8.07	9.63

4.2 Publication II

The publication II describes the investigation of OCT1 as an uptake transporter of structurally different PAs tested in human liver and hamster lung fibroblast cells. The primary endpoints examined include genotoxicity and cytotoxicity. The aim of the work was to elucidate the mechanism by which OCT1 influences the cellular uptake of structurally diverse PAs and to assess the subsequent toxicological effects with the use of pharmacological inhibitors against OCT1. This study offers insights into the significance of OCT1 in PA toxicity and suggests that targeted pharmacological inhibition of OCT1 may play a crucial role in mitigating PA toxicity.

Reference: Haas, M., Ackermann, G., Küpper, J.-H., Schrenk, D., Fahrer, J., *OCT1-dependent uptake of structurally diverse pyrrolizidine alkaloids in human liver cells is crucial for their genotoxic and cytotoxic effects*. Arch Toxicol 97, 3259–3271 (2023).

The publication, along with the supplementary data, is free available in the journal “Archives of Toxicology”. The following link provides full access to the article and the data.

DOI: 10.1007/s00204-023-03591-4

Contributions to this publication:

I contributed in the investigation, methodology and formal analysis as well as the writing of the original draft and its editing. Furthermore, I performed cytotoxicity and genotoxicity experiments in HepG2 and V79 wild-type, HepG2- and V79-CYP3A4 cells as well in cryoconserved human hepatocytes. I conducted and managed the cell culture and treatment, experiments including western-blot analysis and resazurin reduction assay. Furthermore, I determined the relative cytotoxicity and statistical analysis with the data. Mr. Ackermann performed immunofluorescence staining of CYP3A4 via confocal microscopy in HepG2 and HepG2-CYP3A4 cells to examine the CYP3A4 status. The HepG2-CYP3A4 cells were generated by Küpper’s group at the Department of Environment and Nature Science in Brandenburg University of Technology Cottbus-Senftenberg. The V79-CYP3A4 cells were generated by Ebmeyer and colleagues (Ebmeyer et al. 2019). Cryopreserved PHH pooled from five Caucasian donors were purchased from Thermo Fisher Scientific.

Archives of Toxicology (2023) 97:3259–3271
https://doi.org/10.1007/s00204-023-03591-4

GENOTOXICITY AND CARCINOGENICITY

OCT1-dependent uptake of structurally diverse pyrrolizidine alkaloids in human liver cells is crucial for their genotoxic and cytotoxic effects

Manuel Haas[1] · Gabriel Ackermann[1] · Jan-Heiner Küpper[2] · Hansruedi Glatt[3,4] · Dieter Schrenk[1] · Jörg Fahrer[1]

Received: 17 July 2023 / Accepted: 24 August 2023 / Published online: 7 September 2023

Abstract

Pyrrolizidine alkaloids (PAs) are important plant hepatotoxins, which occur as contaminants in plant-based foods, feeds and phytomedicines. Numerous studies demonstrated that the genotoxicity and cytotoxicity of PAs depend on their chemical structure, allowing for potency ranking and grouping. Organic cation transporter-1 (OCT1) was previously shown to be involved in the cellular uptake of the cyclic PA diesters monocrotaline, retrorsine and senescionine. However, little is known about the structure-dependent transport of PAs. Therefore, we investigated the impact of OCT1 on the uptake and toxicity of three structurally diverse PAs (heliotrine, lasiocarpine and riddelliine) differing in their degree and type of esterification in metabolically competent human liver cell models and hamster fibroblasts. Human HepG2-CYP3A4 liver cells were exposed to the respective PA in the presence or absence of the OCT1-inhibitors D-THP and quinidine, revealing a strongly attenuated cytotoxicity upon OCT1 inhibition. The same experiments were repeated in V79-CYP3A4 hamster fibroblasts, confirming that OCT1 inhibition prevents the cytotoxic effects of all tested PAs. Interestingly, OCT1 protein levels were much lower in V79-CYP3A4 than in HepG2-CYP3A4 cells, which correlated with their lower susceptibility to PA-induced cytotoxicity. The cytoprotective effect of OCT1 inhibiton was also demonstrated in primary human hepatocytes following PA exposure. Our experiments further showed that the genotoxic effects triggered by the three PAs are blocked by OCT1 inhibition as evidenced by strongly reduced γH2AX and p53 levels. Consistently, inhibition of OCT1-mediated uptake suppressed the activation of the DNA damage response (DDR) as revealed by decreased phosphorylation of checkpoint kinases upon PA treatment. In conclusion, we demonstrated that PAs, independent of their degree of esterification, are substrates for OCT1-mediated uptake into human liver cells. We further provided evidence that OCT1 inhibition prevents PA-triggered genotoxicity, DDR activation and subsequent cytotoxicity. These findings highlight the crucial role of OCT1 together with CYP3A4-dependent metabolic activation for PA toxicity.

Keywords Pyrrolizidine alkaloids · Cytotoxicity · Genotoxicity · OCT1 · Transport · Primary human hepatocytes · γH2AX · p53

✉ Jörg Fahrer
fahrer@chemie.uni-kl.de

[1] Division of Food Chemistry and Toxicology, Department of Chemistry, RPTU Kaiserslautern-Landau, Erwin-Schroedinger-Str. 52, 67663 Kaiserslautern, Germany

[2] Division of Molecular Cell Biology, Department of Environment and Nature Science, Brandenburg University of Technology Cottbus-Senftenberg, 01968 Senftenberg, Germany

[3] Department Food Safety, German Federal Institute for Risk Assessment (BfR), Max-Dohrn-Strasse 8-10, 10589 Berlin, Germany

[4] Department of Nutritional Toxicology, German Institute of Human Nutrition (DIfE), Potsdam-Rehbrücke, Arthur-Scheunert-Allee 114-116, 14558 Nuthetal, Germany

Introduction

Pyrrolizidine alkaloids (PAs) are phytotoxins with a high structural diversity formed in 3% of all flowering plant species worldwide (Chen et al. 2010). PAs are frequently found as contaminants in plant-based food like herbal teas or spices (Chen et al. 2010; Fu et al. 2004). Several cases of acute and subacute PA intoxications were reported previously in humans or animals due to consumption of contaminated food or PA producing plants, which were characterized by hepatomegaly, ascites, hepatic sinusoidal obstruction syndrome (HSOS) and acute liver failure (Moreira et al. 2018; Teschke et al. 2021). More recently, exposure to PAs has

also been linked to human liver cancer formation in Asian countries (He et al. 2021a).

Chemically, PAs are composed of the necine base 1-hydroxymethylpyrrolizidine, which can be esterified with one or two necine acids, resulting in the formation of PA monoesters, open-chained diesters or cyclic diesters (He et al. 2021b; Schrenk et al. 2020). PAs with a 1,2-unsaturated necine base are known to be hepatotoxic, genotoxic and possibly carcinogenic, which is attributable to their bioactivation by cytochrome P450 (CYP) monooxygenases (mostly CYP3A4, but also CYP2B subfamilies) in the liver (Chen et al. 2010; Edgar et al. 2015; Prakash et al. 1999). This biotransformation step gives rise to dehydro-pyrrolizidine derivatives (dehydro-PAs) and, upon hydrolysis, to (±)-6,7-dihydro-7-hydroxy-1-hydroxymethyl-5H-pyrrolizine (DHP), which both react with DNA and proteins (Edgar 2014; Fu 2017). A plethora of studies performed in different liver cell models including human primary hepatocytes demonstrated a structure–toxicity relationship for PAs, supporting the concept of grouping PAs into potency classes (Allemang et al. 2018; Gao et al. 2020; Haas et al. 2023; Hadi et al. 2021; Lester et al. 2019; Louisse et al. 2019; Merz and Schrenk 2016; Rutz et al. 2020).

An important process for their hepatotoxic mode of action is the uptake of PAs into hepatocytes as well as the efflux of PAs or their metabolites. Hepatocytes express an array of influx and efflux transporters belonging to the solute carrier (SLC) and ATP-binding cassette (ABC) superfamily, respectively (Nigam 2015). The SLC22A family comprise the organic cation transporters (OCTs), which mediate the uptake of cationic compounds such as nutrients, endogenous substrates and active pharmaceutical ingredients into cells (Koepsell 2021). The main members are OCT1 (SLC22A1), OCT2 (SLC22A2) and OCT3 (SLC22A3), which share common substrates and can therefore substitute for each other (Brosseau and Ramotar 2019). However, these influx transporters differ in the tissue-specific expression levels. OCT1 is mainly expressed in hepatocytes, whereas OCT2 is primarily found in renal tubular cells. OCT3 expression is detected in many tissues (Brosseau and Ramotar 2019; Koepsell 2021). The OCT substrates include the prototypical chemical compound 1-methyl-4-phenyl-pyridinium (Koepsell 2013), endogenous compounds such as acetylcholine and catecholamine (Breidert et al. 1998; Nakata et al. 2013) as well as pharmaceuticals including metformin and imatinib (Chen et al. 2014; White et al. 2006). First evidence for the involvement of OCT1 in the uptake of PAs was obtained in a study with the cyclic PA diester monocrotaline, which was shown to be taken up into genetically engineered MDCK cells with human OCT1 expression and into primary rat hepatocytes (Tu et al. 2013). This was subsequently confirmed for retrorsine, which also belongs to the group of cyclic PA diesters (Tu et al. 2014). Two more recent studies performed in human HepaRG hepatoma cells revealed that both OCT1 and Na^+/taurocholate co-transporting polypeptide (SLC10A1) are involved in the hepatocellular uptake of retrorsine and senescionine, which are both cyclic PA diesters (Enge et al. 2021, 2022).

Up to now little information is available on the impact of the chemical structure (PA monoester vs. open-chained diester vs. cyclic diester) on the OCT1-mediated uptake into hepatocytes. Therefore, we selected three structurally diverse PAs (heliotrine, lasiocarpine and riddelliine) and analyzed their toxicity in human HepG2-CYP3A4 liver cells, primary human hepatocytes (PHH) and V79-CYP3A4 Chinese hamster fibroblasts. The impact of OCT1 was studied using the pharmacological inhibitors D-tetrahydropalmatine (D-THP) and quinidine. First, the cytotoxicity of the three PAs was investigated using the resazurin reduction assay in the absence or presence of OCT1 inhibitors. Subsequently, the genotoxic effects of the three selected PAs were determined with and without OCT1 inhibition using western blot analysis of the DNA damage markers γH2AX and p53. Furthermore, the DNA damage response markers pCHK1 and pCHK2 were assessed upon PA exposure in the absence or presence of OCT1 inhibitors.

Results

PA triggered cytotoxicity is rescued by pharmacological OCT1 inhibitors in human liver cells

To study the role of OCT1 in the hepatocellular uptake of the selected PAs (SI Fig. 1), we used quinidine and D-THP as established OCT1 inhibitors (Ingoglia et al. 2015; Tu et al. 2013). First, the cytotoxicity of these pharmacological OCT inhibitors was assessed in wild-type HepG2 cells and genetically engineered HepG2 cells with CYP3A4 overexpression (SI Fig. 2). To this end, the cells were exposed to increasing OCT inhibitor concentrations (0–1000 µM) for 24 h and viability was determined by the resazurin reduction assay. Solvent served as negative control and 0.1% saponine was included as technical positive control (not shown). In general, little differences were observed between the two HepG2 cell models. While concentrations up to 100 µM had no effects (quinidine) or little effects (D-THP) on cell viability, both inhibitors displayed strong cytotoxicity at 500 µM (SI Fig. 3A). Therefore, 100 µM was selected as final concentration for the subsequent cytotoxicity studies with the different PAs.

We first determined the cytotoxicity of the open diester lasiocarpine in HepG2-CYP3A4 cells, which were incubated with increasing PA concentrations (0–40 µM) for 24 h in the absence or presence of the OCT inhibitors (100 µM each).

As expected, lasiocarpine caused a concentration-dependent decrease in cell viability, with a reduction below 50% at a concentration of 40 µM (Fig. 1a). Strikingly, both D-THP and quinidine prevented the cytotoxic effects of lasiocarpine in HepG2-CYP3A4 cells (Fig. 1a), which was also observed by phase contrast microscopy (Fig. 1b and SI Fig. 4A). In wild-type HepG2 cells without CYP3A4 expression, lasiocarpine did not affect cell viability at all (SI Fig. 3B). We then studied the cytotoxicity of the monoester heliotrine with or without OCT inhibition. Cells were incubated with up to 500 µM heliotrine for 24 h, causing a drop in cell viability to 60% at the highest PA concentration (Fig. 1c). Both inhibitors rescued the cytotoxic effects of heliotrine, with D-THP being slightly more potent than quinidine, which was also visible by phase-contrast microscopy (Fig. 1c, d; SI Fig. 4B). Finally, the cyclic diester riddelliine was analyzed in HepG2-CYP3A4 cells in concentrations ranging from 0 to 200 µM. Cell viability was reduced by 50% at the top PA concentration, but almost completely restored to control levels upon quinidine co-treatment. D-THP was not as effective as quinidine, but nevertheless prevented the morphological changes induced by riddelliine (Fig. 1e, f; SI Fig. 4C). In

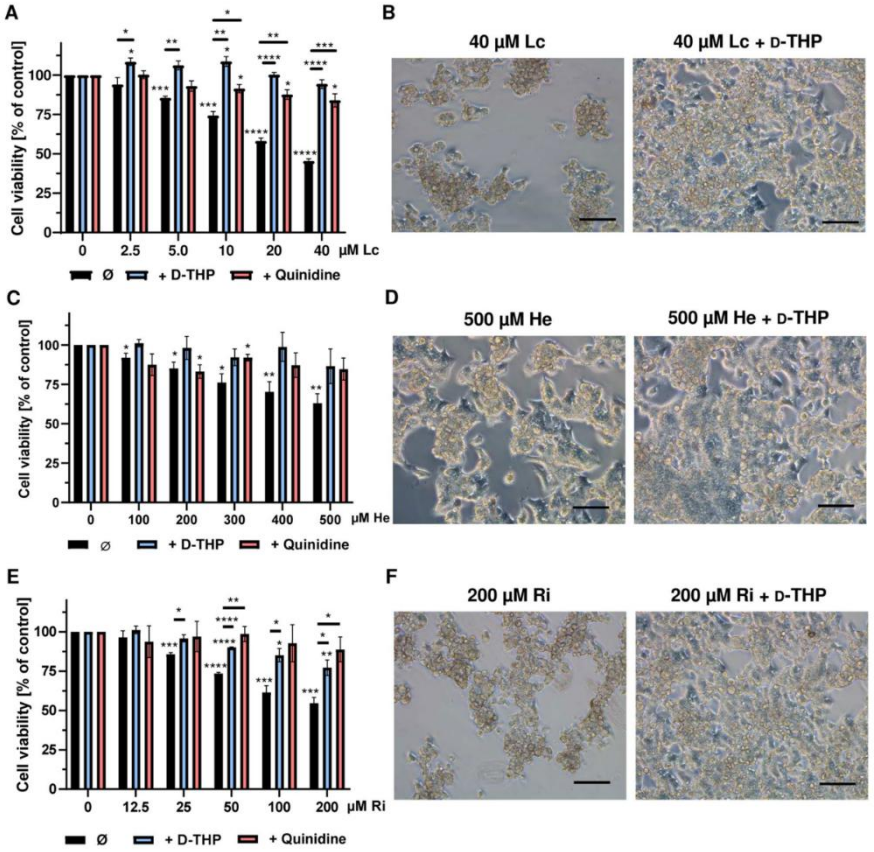

Fig. 1 Pharmacological OCT1 inhibition and impact on PA-induced cytotoxicity in HepG2-CYP3A4 cells. **a**, **c**, **e** Viability of HepG2-CYP3A4 cells 24 h after incubation with increasing concentrations of lasiocarpine (**a**), heliotrine (**c**) and riddelliine (**e**) with or without OCT1-inhibitors. Solvent (0 µM) was used as negative control. Mean + SEM are shown for each incubation (n = 3, each measured as triplicates). Statistical analyses were performed using unpaired two-tailed Students t-test with respect to the negative control or the respective PA treatment as indicated. *P < 0.05, **P < 0.01, ***P < 0.001, ****P ≤ 0.0001. **b, d, f** Representative microscopic images of HepG2-CYP3A4 cells after 24 h treatment with different concentrations of heliotrine (**b**), lasiocarpine (**d**) and riddelliine (**f**) with or without D-THP. Scale bar represents 100 µm

summary, these results reveal an OCT1-mediated uptake of lasiocarpine, heliotrine and riddelliine into human liver cells.

OCT1 and CYP3A4 as key determinants for PA-induced cytotoxicity

The role of OCT1 was further detailed in V79 Chinese hamster fibroblasts and genetically engineered V79 cells with human CYP3A4 expression. V79-CYP3A4 cells display a comparable CYP3A4 expression level as HepG2-CYP3A4 cells, which was demonstrated by western blot analysis (Fig. 2a). In contrast to that, OCT1 levels were much lower in both V79 and V79-CYP3A4 cells as compared to their HepG2 counterparts (Fig. 2b). We were thus interested how the strongly reduced OCT1 levels affect the cytotoxicity of the selected PAs. Lasiocarpine caused a concentration-dependent decrease of viability in V79-CYP3A4 cells, with a concentration of 250 µM reducing the viability by 50% as compared to control (Fig. 2c). A similar cytotoxic effect was already observed at a tenfold lower concentration in HepG2-CYP3A4 cells (see Fig. 1a). Riddelliine also exerted cytotoxicity in V79-CYP3A4 cells and decreased the viability to 70% at a concentration of 500 µM (Fig. 2d), whereas a comparable response was measured in HepG2-CYP3A4 cells upon incubation with only 50 µM riddelline (see Fig. 1e). Heliotrine displayed only little cytotoxicity in V79-CYP3A4 cells at concentrations of 250 µM and above (SI Fig. 5A), while it reduced the viability in HepG2-CYP3A4 cells to about 60% at a concentration of 500 µM (see Fig. 1c). It should also be noted here that neither lasiocarpine nor riddelline or heliotrine induced cytotoxicity in parental, metabolically incompetent V79 cells (Fig. 2c, d; SI Fig. 5A). As a next step, we tested whether OCT inhibition with D-THP or quinidine also protects V79-CYP3A4 cells against the PA-induced cytotoxicity. Our findings revealed that D-THP almost completely blocked the cytotoxic effects of lasiocarpine, riddelliine and heliotrine in V79-CYP3A4 cells (Fig. 2e, f; SI Fig. 5B). Quinidine also prevented the cytotoxicity of all three PAs, but was somewhat less active than D-THP. These results provided evidence that low OCT1 expression levels confer resistance towards the cytotoxic effects of PAs and that both OCT1 and CYP3A4 are required for PA toxicity.

OCT1 inhibition prevents PA-mediated cytotoxicity in primary human hepatocytes

Primary human hepatocytes (PHH) are the gold standard for in vitro toxicokinetic studies of the liver, since they display full metabolic competence and express a plethora of efflux and influx transporters (Fraczek et al. 2013; Ruoss et al. 2020). Up to date, no study is available that investigated the transport of PAs into PHHs. Based on our obtained results in HepG2-CYP3A4 as well as V79-CYP3A4 cells and our previous study in different human liver cell models (Haas et al. 2023), we selected lasiocarpine at a concentration of 45 µM for these experiments in PHH. Our results showed that lasiocarpine treatment decreased the viability of PHH to approximately 33% (Fig. 3a), which correlated with the morphological changes seen by phase contrast microscopy in lasiocarpine treated cells (Fig. 3b, c). D-THP itself had no effects, while quinidine caused a moderate reduction of viability in PHH (Fig. 3a). Interestingly, D-THP efficiently blocked the cytotoxic effects of lasiocarpine in PHH and restored viability almost to control levels (Fig. 3a). Quinidine also moderately increased the viability of lasiocarpine-treated cells, which was however not statistically significant as compared to the PA single exposure (Fig. 3a). The cytoprotective effects of D-THP and, to a minor degree, quinidine towards lasiocarpine were also visible using phase-contrast microscopy (Fig. 3d, e). The OCT1 inhibitors themselves did not induce changes in cell morphology (SI Fig. 6). Taken together, these findings in PHH corroborate the importance of OCT1 for hepatocellular PA uptake and toxicity.

Pharmacological inhibition of OCT1-dependent transport abolishes the genotoxic effects and DNA damage response triggered by PAs in HepG2-CYP3A4 cells

We were then interested whether the reduced cytotoxicity following OCT inhibition is related to an attenuated genotoxicity. Thus, we assessed the genotoxicity of the selected PAs (heliotrine, lasiocarpine and riddelliine) in HepG2-CYP3A4 cells using the well-established DNA damage markers γH2AX and p53 (Fahrer et al. 2015; Nikolova et al. 2014) in the presence or absence of the OCT inhibitors. HepG2-CYP3A4 cells were exposed to 5 µM lasiocarpine, 12.5 µM riddelliine and 50 µM heliotrine for 24 h. The lower PA concentrations were chosen to avoid overt cytotoxicity. The genotoxic anticancer drug and topoisomerase I inhibitor irinotecan was included as positive control (10 µM), since it was previously described as an OCT substrate (Chen et al. 2016; Hucke and Ciarimboli 2016). All tested PAs caused substantial γH2AX formation and p53 accumulation in HepG2-CYP3A4 cells (Fig. 4a–f; SI Fig. 7A–C). D-THP strongly attenuated γH2AX levels and reduced p53 levels to control levels despite PA exposure (Fig. 4a–f; SI Fig. 7A–C). Likewise, quinidine prevented the formation of both genotoxicity markers, although with differential efficacy. While p53 levels were even reduced below baseline, the effects on γH2AX induction were not as pronounced, at least in the case of lasiocarpine (Fig. 4a, c). As expected, irinotecan treatment caused strong genotoxic effects in HepG2-CYP3A4 cells, which were attenuated by D-THP (Fig. 4a–f;

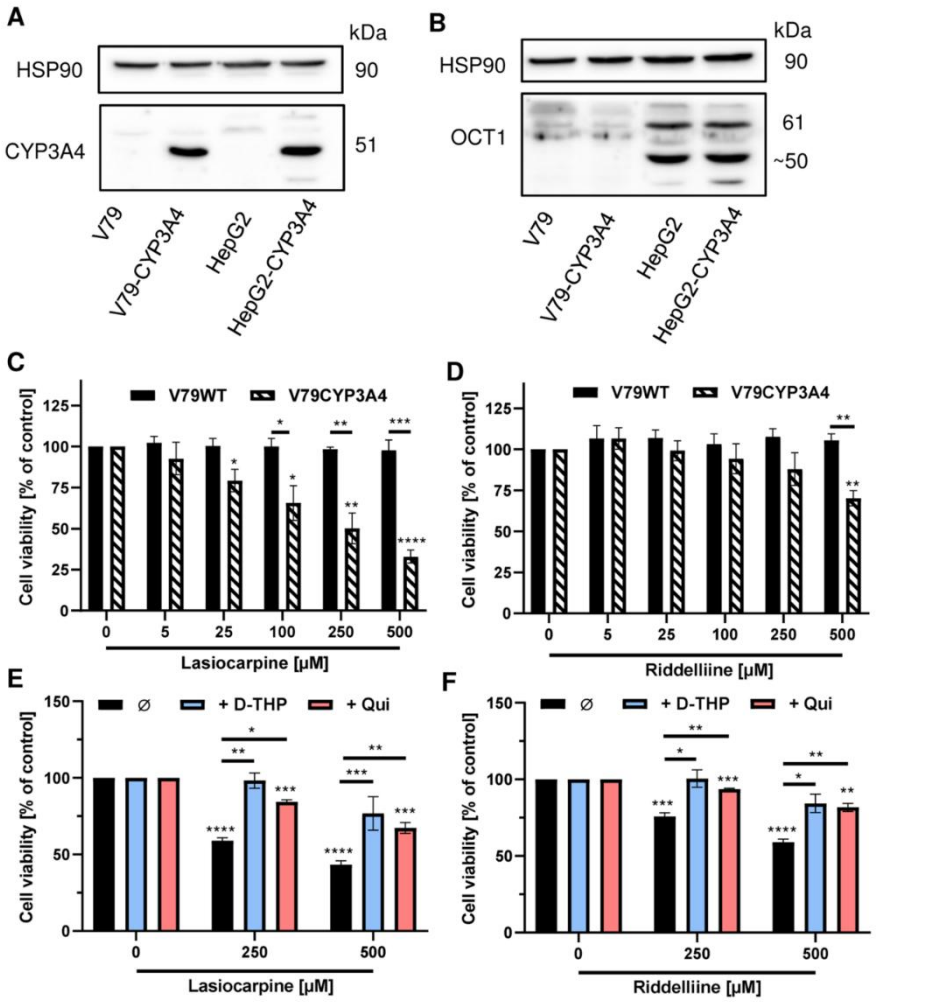

Fig. 2 PA-triggered cytotoxicity in V79 and V79-CYP3A4 hamster cells and role of OCT1. **a**, **b** Analysis of CYP3A4 (**a**) and OCT1 (**b**) protein expression in V79, V79-CYP3A4, HepG2 and HepG2-CYP3A4 cells using SDS-PAGE and western blot detection. HSP90 served as loading control. A representative blot is shown. **c**, **d** Viability of V79 and V79-CYP3A4 cells 24 h after treatment with increasing concentrations of lasiocarpine (**c**) and riddelliine (**d**). Solvent (0 µM) was used as negative control. Mean + SEM are shown for each incubation (n = 3, each measured as triplicates). Statistical analyses were performed using unpaired two-tailed Students t-test with respect to the negative control or as indicated by bars. *P < 0.05, **P < 0.01, ***P < 0.001, ****P ≤ 0.0001. **e**, **f** Viability of V79-CYP3A4 cells 24 h after treatment with 250 and 500 µM lasiocarpine (**e**) or riddelliine (**f**) in the presence or absence of OCT1 inhibitors (quinidine and D-THP, 100 µM each). Solvent (0 µM) was used as negative control. Mean + SEM are shown for each incubation (n = 3, each measured as triplicates). Statistical analyses were performed using unpaired two-tailed Students t-test with respect to the negative control or as indicated by bars. *P < 0.05, **P < 0.01, ***P < 0.001, ****P < 0.0001

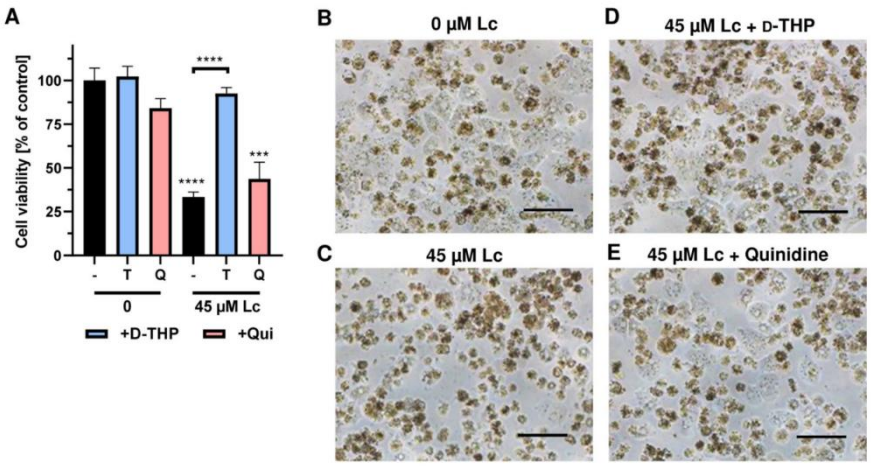

Fig. 3 Lasiocarpine triggered cytotoxicity in primary human hepatocytes and impact of OCT1-mediated transport. **a** Viability of primary human hepatocytes 24 h after incubation with 45 µM lasiocarpine with or without the OCT1 inhibitors D-THP (T) and Quinidine (Q). Solvent (0 µM) was used as negative control. Mean + SEM are shown for each incubation (pooled hepatocytes from 5 donors, n = 2, each performed as triplicate). Statistical analyses were performed using unpaired two-tailed Students t-test with respect to the negative control or as indicated with a bar. ***P < 0.001, ****P < 0.0001. **b–e**: Representative microscopic images of primary human hepatocytes after 24 h incubation with lasiocarpine in the absence or presence of the OCT1 inhibitors. The scale bar represents 100 µm

SI Fig. 7A–C). Quinidine, in turn, did not or hardly prevent γH2AX formation upon irinotecan exposure, but suppressed its p53 induction (Fig. 4a–f; SI Fig. 7A–C).

Finally, we analyzed the DNA damage response (DDR) triggered by the three selected PAs in HepG2-CYP3A4 cells and studied the impact of OCT inhibition. The DDR is coordinated by apical DDR kinases including ATM and ATR, which phosphorylate a plethora of downstream substrates such as the checkpoint kinases CHK1 and CHK2 (Marechal and Zou 2013). While CHK1 is primarily phosphorylated by ATR in response to DNA replication stress, CHK2 is mainly phosphorylated by ATM following DNA double-strand breaks (Rundle et al. 2017; Shiloh and Ziv 2013). First, HepG2-CYP3A4 cells were exposed to the three structurally diverse PAs lasiocarpine, heliotrine and riddelliine for 24 h as described above. Western Blot analysis revealed a pronounced increase in pCHK1 and pCHK2 levels upon exposure to all PAs, whereas the levels of total CHK1 and CHK2 were unchanged (Fig. 5a, b; SI Fig. 8A). Co-treatment of cells with the OCT inhibitors D-THP and quinidine reduced phosphorylation of CHK1 and CHK2 upon PA exposure (Fig. 5a–f; SI Fig. 8A–C), which is in line with the reduced genotoxicity of PAs upon OCT inhibition (see Fig. 4). The anticancer drug irinotecan also caused genotoxicity (see Fig. 4a, b) as well as CHK1 and CHK2 phosphorylation (Fig. 5a, b; SI Fig. 8A). However, the OCT inhibitors displayed little or no effects on these DDR markers induced by irinotecan. In summary, our findings show that OCT1-dependent uptake of PAs is required for PA triggered genotoxicity and activation of the ATM/ATR-driven DDR, which precedes the cytotoxic effects.

Discussion

In the present work, we investigated the relevance of OCT1 for the uptake of structurally diverse PAs in metabolically competent human HepG2-CYP3A4 cells, Chinese hamster V79-CYP3A4 cells and PHH. HepG2-CYP3A4 cells were revealed as a very useful model in our previous study, since the genotoxic and cytotoxic potency of structurally diverse PAs was in very good agreement with that obtained in PHH as gold standard (Haas et al. 2023). Furthermore, HepG2 cells were reported to display *OCT1* gene expression, although the expression levels were lower than those in PHH (Herzog et al. 2016; Rodrigues et al. 2009). Importantly, OCT1 expression was confirmed on the protein level in HepG2-CYP3A4 and wildtype HepG2 cells as shown above, thus representing a valuable model to study OCT1-mediated uptake of PAs. Here, we made use of the established pharmacological OCT1 inhibitors quinidine and D-THP (Ingoglia et al. 2015; Tu et al. 2013), which were instrumental to study the uptake of other PAs (see below). However, it should be noted that both quinidine and D-THP undergo

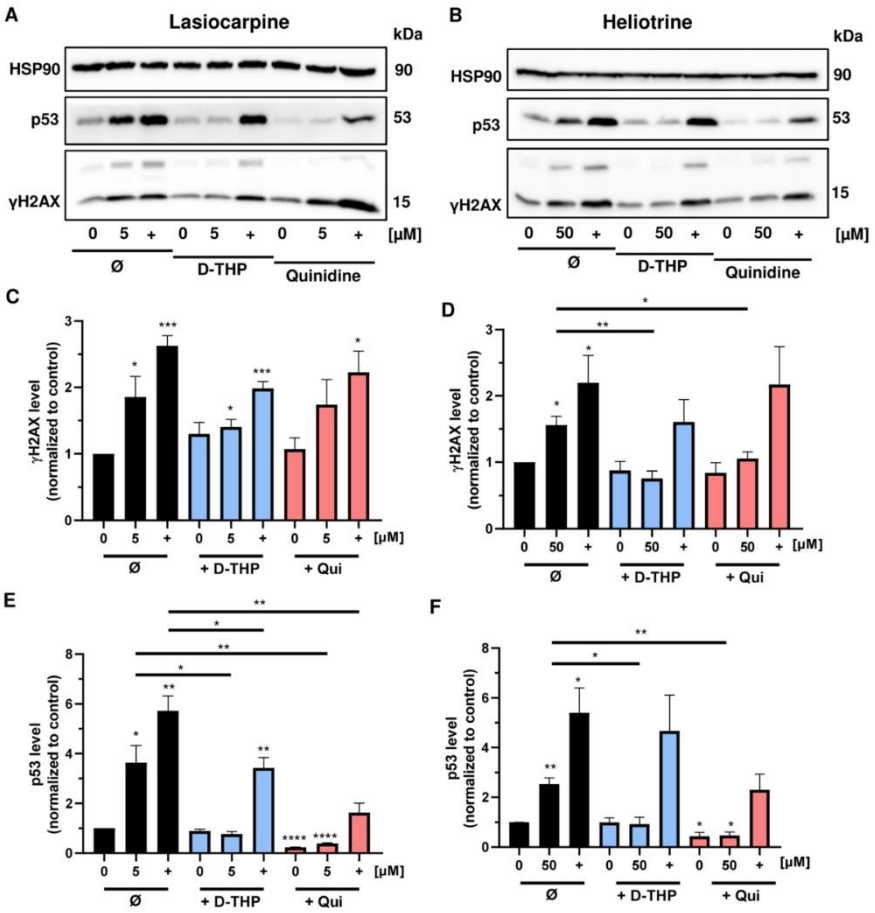

Fig. 4 Impact of OCT1-inhibition on the genotoxicity of PAs in HepG2-CYP3A4 cells. **a**, **b** Representative western blots of γH2AX and p53 after 24 h treatment with lasiocarpine (**a**) and heliotrine (**b**). The genotoxic anticancer drug irinotecan was used as a positive control (+) and solvent as a negative control (0 µM). HSP90 served as loading control. **c**, **d** Densitometric evaluation of γH2AX after 24 h incubation with lasiocarpine (**c**) and heliotrine (**d**) in HepG2-CYP3A4 cells. HSP90 served as loading control. γH2AX level relative to the loading control and normalized versus the negative control. Mean + SEM for three independent experiments (n = 3). Statistical analyses were performed using unpaired two-tailed Students t-test with respect to the negative control or as indicated with a bar. *P < 0.05, **P < 0.01, ***P < 0.001. **e**, **f** Densitometric evaluation of p53 after 24 h incubation with lasiocarpine (**e**) and heliotrine (**f**) in HepG2-CYP3A4 cells. HSP90 served as loading control. p53 level relative to the loading control and normalized versus the negative control. Mean + SEM for three independent experiments (n = 3). Statistical analyses were performed using unpaired two-tailed Students t-test with respect to the negative control or as indicated with a bar. *P < 0.05, **P < 0.01, ****P < 0.0001

CYP-mediated phase I metabolism. Quinidine is a known substrate of CYP3A4, which catalyzes its 3-hydroxylation (Nielsen et al. 1999). D-THP was reported to be a substrate for rat CYP3A1/2, the orthologue of human CYP3A4 (Zhao et al. 2012). Thus, it might be possible that the tested PAs and the inhibitors compete for CYP3A4, thereby decreasing the metabolic activation rate of PAs. Importantly, inhibitory effects of D-THP were only observed for CYP2D6 and CYP1A2 activities (Li et al. 2015).

First, we were able to demonstrate that pharmacological OCT1 inhibition by either D-THP or quinidine rescued the cytotoxic effects of all three PAs tested, i.e. lasiocarpine,

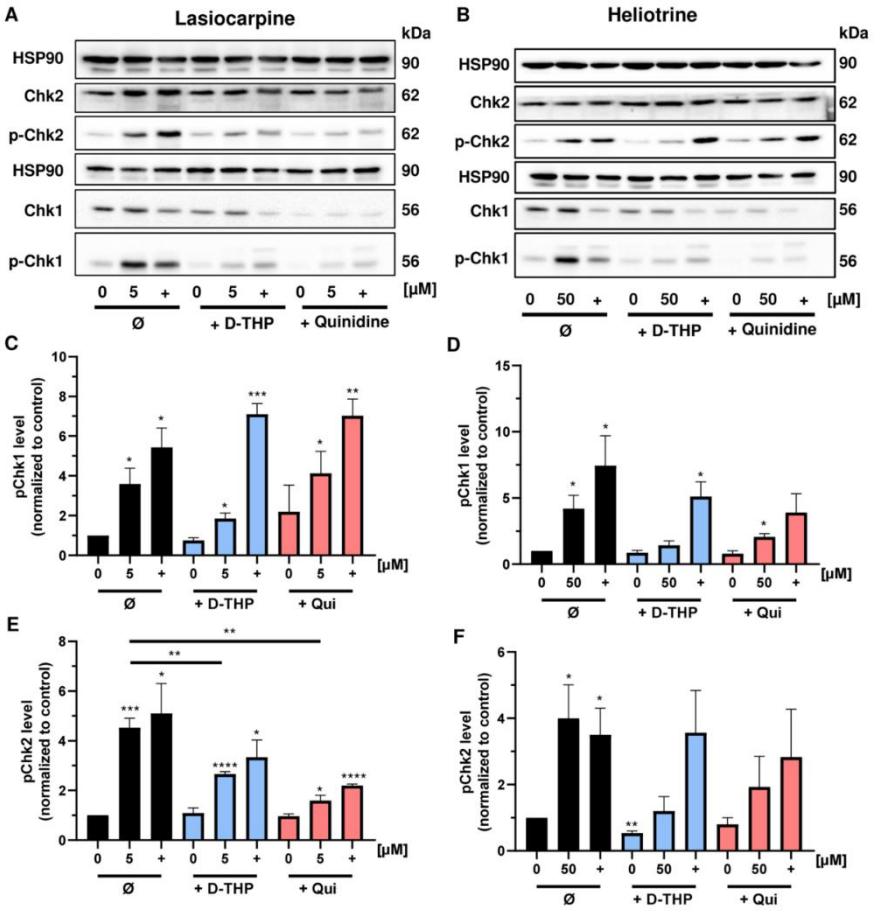

Fig. 5 OCT1-inhibition and PA-triggered DNA damage response (DDR). **a**, **b** Representative western blots of (phosphorylated) CHK1 and CHK2 as downstream targets of the apical DDR kinases ATR and ATM after 24 h treatment with lasiocarpine (**a**) and heliotrine (**b**). The genotoxic anticancer drug irinotecan was used as a positive control (+) and solvent as a negative control (0 µM). HSP90 served as loading control. **c**, **d** Densitometric evaluations of p-Chk1 (S345) after 24 h incubation with lasiocarpine (**c**) and heliotrine (**d**) in HepG2-CYP3A4 cells. Unphosphorylated CHK1 served as loading control. pCHK1 level relative to the loading control and normalized versus the negative control. Mean + SEM for three independent experiments (n = 3). Statistical analyses were performed using unpaired two-tailed Students t-test with respect to the negative control or as indicated with a bar. *P < 0.05, **P < 0.01, ***P < 0.001. **e**, **f** Densitometric evaluations of pChk2 (Thr68) after 24 h incubation with lasiocarpine (**e**) and heliotrine (**f**) in HepG2-CYP3A4 cells. Unphosphorylated CHK2 served as loading control. pCHK2 level relative to the loading control and normalized versus the negative control. Mean + SEM for three independent experiments (n = 3). Statistical analyses were performed using unpaired two-tailed Students t-test with respect to the negative control or as indicated with a bar. *P < 0.05, **P < 0.01, ***P < 0.001, ****P < 0.0001

heliotrine and riddelliine, in HepG2-CYP3A4 cells. Our results for riddelliine extend the previous findings obtained for the other cyclic PA diesters monocrotaline, retrorsine and senecione, which were shown to be taken up into kidney MDCK-hOCT1 cells, primary rat hepatocytes as well as HepaRG cells in a OCT1-dependent manner (Enge et al. 2021; Tu et al. 2013, 2014). Furthermore, our data showed for the first time that also open-chained PA diesters as well as PA monoesters are substrates for OCT1. These findings were confirmed with another set of experiments in V79-CYP3A4 cells, in which OCT1 inhibition conferred resistance towards the cytotoxic effects of the three PAs tested.

Interestingly, the cytotoxicity observed in V79-CYP3A4 cells was generally lower than that detected in HepG2-CYP3A4 cells, although both cell lines displayed similar CYP3A4 protein levels. However, OCT1 expression was revealed to be much higher in HepG2-CYP3A4 cells, which very likely explains their increased sensitivity towards PAs and further emphasizes the relevance of OCT1 for PA-triggered toxicity. Apart from that, V79 Chinese hamster fibroblasts are known to harbor a mutated and non-functional p53 (Chaung et al. 1997), whereas HepG2 cells display wild-type p53 (Müller et al. 1997).

Due to its high cytotoxic potency, lasiocarpine was selected for further analysis in PHH as gold standard for toxikokinetic studies. Consistent with the results in HepG2-CYP3A4 and V79-CYP3A4 cells, D-THP almost completely inhibited the cytotoxic effects of lasiocarpine, while quinidine only moderately increased the cell viability. The reduced effectiveness of quinidine might be attributable to its own toxicity and/or the differences in the metabolic competence of PHH vs. HepG2-CYP3A4 cells.

Then we addressed the question whether the reduced cytotoxicity upon OCT1 inhibition is associated with an attenuated genotoxicity. Our results provided evidence that OCT1 inhibition also prevents the genotoxic effects of all three selected PAs as attested by reduced DNA damage levels (γH2AX and p53). However, quinidine only partially blocked γH2AX formation triggered by lasiocarpine, whereas it strongly attenuated γH2AX formation caused by heliotrine and riddelliine. This finding might indicate that low intracellular levels of lasiocarpine are sufficient to cause substantial γH2AX formation, bearing in mind that this is an open-chained PA diester with a higher genotoxic potency than the cyclic PA diester riddelliine and the PA monoester heliotrine (Haas et al. 2023). Furthermore, we analyzed the DNA damage response markers CHK1 and CHK2. These checkpoint kinases are phosphorylated by apical DDR kinases, namely ATM, ATR and/or DNA-PK, in response to diverse genotoxic stimuli (Marechal and Zou 2013). First evidence for a DDR activation stems from a 28 day rat feeding study with different PAs. Transcriptomic analysis of liver tissue showed an enrichment of DDR pathways such as p53 and ATM signaling (Ebmeyer et al. 2020), which was further substantiated with a transcriptomics study performed in HepG2-CYP3A4 cells (Abdelfatah et al. 2021). Intriguingly, we were able to show that all three PAs (50 µM heliotrine, 5 µM lasiocarpine and 12.5 µM riddelliine) significantly increased both CHK1 and CHK2 phosphorylation in HepG2-CYP3A4 cells after 24 h. This is consistent with experiments performed in genetically engineered TK6 cells with human CYP3A4 expression, which displayed CHK1 and CHK2 phosphorylation upon exposure to lasiocarpine (5 µM) and riddelliine (20 µM) for 24 h. Moreover, our data revealed that OCT1 inhibition (D-THP > quinidine) blocked PA triggered DDR activation as evidenced by reduced pCHK1 and pCHK2 levels.

In conclusion, we demonstrated that PAs independent of their degree of esterification are substrates for OCT1-mediated uptake into human liver cells. We further provided evidence that OCT1 inhibition prevents PA triggered genotoxicity, DDR activation and subsequent cytotoxicity, highlighting the crucial role of OCT1. Our results have also implications for the toxicity of PAs in vivo, since the cell- and tissue-dependent expression of OCTs have a major effect on their susceptibility towards the detrimental effects of PAs as demonstrated herein. Finally, the better understanding of the involved hepatocellular uptake mechanisms might also open an avenue for the protection of (liver) cells in case of an acute intoxication by using i.v. administered OCT1 inhibitors.

Material and methods

Cell culture and treatment

V79 Chinese hamster cells and genetically engineered V79 cells with stable expression of human CYP3A4 (Ebmeyer et al. 2019) were grown in Dulbecco`s modified Eagle`s Medium (DMEM) high glucose supplemented with 5% fetal calf serum (FCS) and 1% penicillin/streptomycin (P/S). HepG2 cells were obtained from DSMZ (Braunschweig, Germany) and HepG2-CYP3A4 cells were generated as previously described (Herzog et al. 2015). HepG2-CYP3A4 cells were maintained in DMEM high glucose supplemented with 10% FCS, 1% P/S and 3 µg/ml blasticidin S hydrochloride (Carl Roth, Karlsruhe, Germany). All cell lines were cultured at 37 °C in humidified atmosphere of 5% CO_2. Cell culture medium and supplements were obtained from Gibco Life Technologies (Darmstadt, Germany) and Pan Biotech (Aidenbach, Germany). All cell lines were mycoplasma negative, as demonstrated by routine PCR testing using Venor®GeM OneStep (Berlin, Germany). Cryopreserved PHH pooled from five Caucasian donors were from Thermo Fisher Scientific (Massachusetts, USA) and were maintained as described recently (Haas et al. 2023). After attachment of PHH to collagen type I coated plates, the plating medium was replaced with incubation medium containing the test compounds and cells were incubated for 24 h. Collagen type I was obtained from Corning (New York, USA) and prepared as sterile-filtered 50 µg/ mL stock solution in 0.8 M acetic acid for coating.

Compounds and cell treatment with OCT1 inhibitors

The PAs used (heliotrine, lasiocarpine, riddelliine) were of highest purity and were from Phytolab (Vestenbergsgreuth,

Germany). All PAs were dissolved in DMSO to prepare stock solutions (50–150 mM), which were stored at − 20 °C. Two OCT1 inhibitors, namely D-tetrahydropalmatine (D-THP) and quinidine, were purchased from Hycultec (Beutelsbach, Germany) and dissolved in DMSO to obtain 100 mM stock solutions stored at − 20 °C. Stock solutions were diluted in cell culture medium to reach final concentrations in the experiments as indicated (typically 100 µM). For the inhibitor studies, cells were pre-incubated for 1.5 h with 100 µM D-THP or quinidine. The medium was then aspirated and fresh medium was added, which contained the PAs under investigation with or without 100 µM of the respective OCT1-inhibitor for 24 h. Cells were then analyzed as described below.

Assessment of cell viability

HepG2 and HepG2-CYP3A4 cells (45,000 cells/ well) as well as V79 and V79-CYP3A4 cells (5,000 cells/ well) were seeded on 96-well plates, grown overnight and incubated with increasing PA concentrations without or with 100 µM of each OCT1-inhibitor. PHH were seeded on collagen type I coated 96-well plates at density of 62,500 cells/well and treated as described above. Saponine (0.1%) served as positive control and solvent (DMSO) as negative control. Cell viability was determined using the resazurin reduction assay as described previously (Carlsson et al. 2022). After 24 h, cells were washed with PBS and incubated for 1 h with DMEM low glucose (-FCS; -P/S) or William's E Medium (1X) supplemented with 10% 440 µM resazurin-NaCl-Pi-solution (0.1% dimethylformamide; 1.1 mM KH_2PO_4, 154 mM NaCl, 3.7 mM Na_2HPO_4) at 37 °C in humidified atmosphere of 5% CO_2. Cell viability was determined using a microplate reader (Spark, Tecan) with 544 nm for excitation and 590 nm for emission. In addition, phase-contrast microscopy was performed using a Leica microscope (HI PLAN I 20x/0.30 PH1 or HI PLAN I 10x/0.22 PH1) equipped with Leica MC170 HD camera.

SDS-PAGE and western blot analysis

HepG2-CYP3A4 cells (500,000 cells/plate) were grown on 3.5 cm plates, incubated with increasing PA concentrations for 24 h and directly harvested with 1 × Laemmli loading buffer as described (Fahrer et al. 2014). Samples were then subject to SDS-PAGE and western blot analysis as reported (Fahrer et al. 2013). Briefly, proteins were separated by SDS-PAGE and transferred onto a nitrocellulose membrane (PerkinElmer, Rodgau, Germany) with wet blot technique. The membrane was blocked with 5% nonfat dry milk or 5% bovine serum albumine (BSA) in Tris-buffered saline (TBS)/ 0.1% Tween-20 (TBS-T) for 1 h at RT. As a next step, the membranes were incubated with the primary antibody overnight at 4 °C. The membranes were washed three times with TBS-T and incubated with appropriate secondary antibodies conjugated with horseradish peroxidase (HRP) for 1 h at RT. After additional washing steps, the membranes were incubated with Western Lighting® Plus-ECL (PerkinElmer, Rodgau, Germany) and proteins were visualized with a c300 chemiluminescence imager (Azure biosystems, Dublin, CA, USA). The primary antibodies directed against CYP3A4 (HL3, sc-53580), p53 (DO-1, sc-126) and HSP90α/β (sc-13119) were obtained from Santa Cruz Biotechnology (Heidelberg, Germany). The primary antibody raised against γH2AX (phosphor S139, ab81299) was from Abcam (Cambridge, UK). The primary antibodies p-CHK1 (phosphor S345, #2348) and p-CHK2 (phosphor Thr68, #2197) as well as CHK1 (#2360) and CHK2 (#2662) were obtained from Cell Signaling Technology (Danvers, Massachusetts, USA). The primary antibody directed against OCT-1/SLC22A1 (2C5, NBP1-51684) was obtained from Novus Biologicals LLC (Centennial, Colorado, USA). HRP-conjugated secondary antibodies conjugated were purchased from Santa Cruz Biotechnology (sc-516102, Heidelberg, Germany) and Cell Signaling Technology (#7074, Danvers, Massachusetts, USA).

Immunofluorescence and confocal microscopy

HepG2 and HepG2-CYP3A4 cells were seeded on cover slips in 3.5-cm dishes (4×10^5 per dish) and allowed to grow for 24 h. Immunofluorescence staining and confocal microscopy were essentially performed as reported (Mimmler et al. 2016). To this end, cells were rinsed with PBS and fixed with 4% paraformaldehyde (PFA) for 15 min at RT. The PFA solution was discarded and cells were fixed additionally with ice-cold methanol for 10 min at − 20 °C. Thereafter, cells were washed three times with PBS and unspecific binding sites were blocked with 5%-BSA in PBS/0.3%-Triton-X100 in PBS. The samples were then incubated with a primary antibody against CYP3A4 (1:200 in 0.3%-Triton-X100 in PBS; HL-3, sc-53580, Santa Cruz Biotechnology, Heidelberg, Germany) overnight at 4 °C. The cells were washed with PBS and PBS/0.4 M NaCl before incubation with a secondary antibody labeled with Alexa Fluor 488 (1:400 in 5%-BSA in PBS/ 0.3%-Triton-X100; Life Technologies, Darmstadt, Germany) for 1.5 h at room temperature. Cells were then washed again as described above and embedded with Vectashield-DAPI (Vector Labs, Burlingame, CA, USA). The samples were analyzed with a Zeiss Axio Observer 7 microscope equipped with 63-oil-objective (plan-apochromat 63x/1.40 DIC M27) and the LSM 900 confocal laser scanner. The images were acquired and processed with Zen Software 3.4 (Carl Zeiss Microscopy, Jena, Germany).

Statistical analysis

All experiments were performed independently at least three times, except otherwise stated. Results are presented as means + standard error of the means (SEM) from representative experiments. Statistics were carried out by Graphpad Prism software (Version 9). Statistical significance was defined as $P < 0.05$ and statistical analyses were performed using unpaired two-tailed Students t-test with respect to the negative control.

Supplementary Information The online version contains supplementary material available at https://doi.org/10.1007/s00204-023-03591-4.

Acknowledgements We are grateful to Melanie-Abel Beckmann (Division of Food Chemistry and Toxicology, Department of Chemistry, RPTU Kaiserslautern-Landau) for analysing mycoplasm detection in routine cell culture.

Funding Open Access funding enabled and organized by Projekt DEAL. This project was supported by Kooperation Phytopharmaka GbR, Bonn, Germany (TU-KL #2) and the German Research Foundation [DFG] (INST 248/331-1 FUGG).

Data availability The datasets generated and analyzed during this study were included in the manuscript and the supplementary information. They are also available from the corresponding author upon reasonable request.

Declarations

Conflict of interest The authors declare no conflict of interest.

References

Abdelfatah S, Nass J, Knorz C, Klauck SM, Kupper JH, Efferth T (2021) Pyrrolizidine alkaloids cause cell cycle and DNA damage repair defects as analyzed by transcriptomics in cytochrome P450 3A4-overexpressing HepG2 clone 9 cells. Cell Biol Toxicol. https://doi.org/10.1007/s10565-021-09599-9

Allemang A, Mahony C, Lester C, Pfuhler S (2018) Relative potency of fifteen pyrrolizidine alkaloids to induce DNA damage as measured by micronucleus induction in HepaRG human liver cells. Food Chem Toxicol 121:72–81. https://doi.org/10.1016/j.fct.2018.08.003

Breidert T, Spitzenberger F, Grundemann D, Schomig E (1998) Catecholamine transport by the organic cation transporter type 1 (OCT1). Br J Pharmacol 125(1):218–224. https://doi.org/10.1038/sj.bjp.0702065

Brosseau N, Ramotar D (2019) The human organic cation transporter OCT1 and its role as a target for drug responses. Drug Metab Rev 51(4):389–407. https://doi.org/10.1080/03602532.2019.1670204

Carlsson MJ, Vollmer AS, Demuth P et al (2022) p53 triggers mitochondrial apoptosis following DNA damage-dependent replication stress by the hepatotoxin methyleugenol. Cell Death Dis 13(11):1009. https://doi.org/10.1038/s41419-022-05446-9

Chaung W, Mi LJ, Boorstein RJ (1997) The p53 status of Chinese hamster V79 cells frequently used for studies on DNA damage and DNA repair. Nucleic Acids Res 25(5):992–994. https://doi.org/10.1093/nar/25.5.992

Chen T, Mei N, Fu PP (2010) Genotoxicity of pyrrolizidine alkaloids. J Appl Toxicol 30(3):183–196. https://doi.org/10.1002/jat.1504

Chen L, Shu Y, Liang X et al (2014) OCT1 is a high-capacity thiamine transporter that regulates hepatic steatosis and is a target of metformin. Proc Natl Acad Sci USA 111(27):9983–9988. https://doi.org/10.1073/pnas.1314939111

Chen S, Sutiman N, Zhang CZ et al (2016) Pharmacogenetics of irinotecan, doxorubicin and docetaxel transporters in Asian and Caucasian cancer patients: a comparative review. Drug Metab Rev 48(4):502–540. https://doi.org/10.1080/03602532.2016.1226896

Ebmeyer J, Braeuning A, Glatt H, These A, Hessel-Pras S, Lampen A (2019) Human CYP3A4-mediated toxification of the pyrrolizidine alkaloid lasiocarpine. Food Chem Toxicol 130:79–88. https://doi.org/10.1016/j.fct.2019.05.019

Ebmeyer J, Rasinger JD, Hengstler JG et al (2020) Hepatotoxic pyrrolizidine alkaloids induce DNA damage response in rat liver in a 28-day feeding study. Arch Toxicol 94(5):1739–1751. https://doi.org/10.1007/s00204-020-02779-2

Edgar JA (2014) Food contaminants capable of causing cancer, pulmonary hypertension and cirrhosis. Med J Aust 200(2):73–74. https://doi.org/10.5694/mja13.10227

Edgar JA, Molyneux RJ, Colegate SM (2015) Pyrrolizidine alkaloids: potential role in the etiology of cancers, pulmonary hypertension, congenital anomalies, and liver disease. Chem Res Toxicol 28(1):4–20. https://doi.org/10.1021/tx500403t

Enge AM, Kaltner F, Gottschalk C, Braeuning A, Hessel-Pras S (2021) Active transport of hepatotoxic pyrrolizidine alkaloids in HepaRG cells. Int J Mol Sci. https://doi.org/10.3390/ijms22083821

Enge AM, Kaltner F, Gottschalk C et al (2022) Organic cation transporter I and Na(+)/taurocholate co-transporting polypeptide are involved in retrorsine- and senecionine-induced hepatotoxicity in HepaRG cells. Mol Nutr Food Res 66(2):e2100800. https://doi.org/10.1002/mnfr.202100800

Fahrer J, Schweitzer B, Fiedler K, Langer T, Gierschik P, Barth H (2013) C2-streptavidin mediates the delivery of biotin-conjugated tumor suppressor protein p53 into tumor cells. Bioconjug Chem 24(4):595–603. https://doi.org/10.1021/bc300563c

Fahrer J, Huelsenbeck J, Jaurich H et al (2014) Cytolethal distending toxin (CDT) is a radiomimetic agent and induces persistent levels of DNA double-strand breaks in human fibroblasts. DNA Repair (Amst) 18:31–43. https://doi.org/10.1016/j.dnarep.2014.03.002

Fahrer J, Frisch J, Nagel G et al (2015) DNA repair by MGMT, but not AAG, causes a threshold in alkylation-induced colorectal carcinogenesis. Carcinogenesis 36(10):1235–1244. https://doi.org/10.1093/carcin/bgv114

Fraczek J, Bolleyn J, Vanhaecke T, Rogiers V, Vinken M (2013) Primary hepatocyte cultures for pharmaco-toxicological studies: at the busy crossroad of various anti-dedifferentiation strategies. Arch Toxicol 87(4):577–610. https://doi.org/10.1007/s00204-012-0983-3

Fu PP (2017) Pyrrolizidine alkaloids: metabolic activation pathways leading to liver tumor initiation. Chem Res Toxicol 30(1):81–93. https://doi.org/10.1021/acs.chemrestox.6b00297

Fu PP, Xia Q, Lin G, Chou MW (2004) Pyrrolizidine alkaloids—genotoxicity, metabolism enzymes, metabolic activation, and mechanisms. Drug Metab Rev 36(1):1–55. https://doi.org/10.1081/dmr-120028426

Gao L, Rutz L, Schrenk D (2020) Structure-dependent hepato-cytotoxic potencies of selected pyrrolizidine alkaloids in primary rat hepatocyte culture. Food Chem Toxicol 135:110923. https://doi.org/10.1016/j.fct.2019.110923

Haas M, Wirachowski K, Thibol L, Kupper JH, Schrenk D, Fahrer J (2023) Potency ranking of pyrrolizidine alkaloids in metabolically competent human liver cancer cells and primary human hepatocytes using a genotoxicity test battery. Arch Toxicol 97(5):1413–1428. https://doi.org/10.1007/s00204-023-03482-8

Hadi NSA, Bankoglu EE, Schott L et al (2021) Genotoxicity of selected pyrrolizidine alkaloids in human hepatoma cell lines HepG2 and Huh6. Mutat Res Genet Toxicol Environ Mutagen 861–862:503305. https://doi.org/10.1016/j.mrgentox.2020.503305

He Y, Shi M, Wu X et al (2021a) Mutational signature analysis reveals widespread contribution of pyrrolizidine alkaloid exposure to human liver cancer. Hepatology 74(1):264–280. https://doi.org/10.1002/hep.31723

He Y, Zhu L, Ma J, Lin G (2021b) Metabolism-mediated cytotoxicity and genotoxicity of pyrrolizidine alkaloids. Arch Toxicol 95(6):1917–1942. https://doi.org/10.1007/s00204-021-03060-w

Herzog N, Katzenberger N, Martin F, Schmidtke K-U, Küpper J-H (2015) Generation of cytochrome P450 3A4-overexpressing HepG2 cell clones for standardization of hepatocellular testosterone 6β-hydroxylation activity. J Cell Biotechnol 1(1):15–26. https://doi.org/10.3233/JCB-15002

Herzog N, Hansen M, Miethbauer S et al (2016) Primary-like human hepatocytes genetically engineered to obtain proliferation competence display hepatic differentiation characteristics in monolayer and organotypical spheroid cultures. Cell Biol Int 40(3):341–353. https://doi.org/10.1002/cbin.10574

Hucke A, Ciarimboli G (2016) The role of transporters in the toxicity of chemotherapeutic drugs: focus on transporters for organic cations. J Clin Pharmacol 56(Suppl 7):S157–S172. https://doi.org/10.1002/jcph.706

Ingoglia F, Visigalli R, Rotoli BM et al (2015) Functional characterization of the organic cation transporters (OCTs) in human airway pulmonary epithelial cells. Biochim Biophys Acta 1848(7):1563–1572. https://doi.org/10.1016/j.bbamem.2015.04.001

Koepsell H (2013) The SLC22 family with transporters of organic cations, anions and zwitterions. Mol Asp Med 34(2–3):413–435. https://doi.org/10.1016/j.mam.2012.10.010

Koepsell H (2021) Update on drug–drug interaction at organic cation transporters: mechanisms, clinical impact, and proposal for advanced in vitro testing. Expert Opin Drug Metab Toxicol 17(6):635–653. https://doi.org/10.1080/17425255.2021.1915284

Lester C, Troutman J, Obringer C et al (2019) Intrinsic relative potency of a series of pyrrolizidine alkaloids characterized by rate and extent of metabolism. Food Chem Toxicol 131:110523. https://doi.org/10.1016/j.fct.2019.05.031

Li W, Zhao L, Le J et al (2015) Evaluation of tetrahydropalmatine enantiomers on the activity of five cytochrome P450 isozymes in rats using a liquid chromatography/mass spectrometric method and a cocktail approach. Chirality 27(8):551–556. https://doi.org/10.1002/chir.22469

Louisse J, Rijkers D, Stoopen G et al (2019) Determination of genotoxic potencies of pyrrolizidine alkaloids in HepaRG cells using the gammaH2AX assay. Food Chem Toxicol 131:110532. https://doi.org/10.1016/j.fct.2019.05.040

Marechal A, Zou L (2013) DNA damage sensing by the ATM and ATR kinases. Cold Spring Harb Perspect Biol. https://doi.org/10.1101/cshperspect.a012716

Merz KH, Schrenk D (2016) Interim relative potency factors for the toxicological risk assessment of pyrrolizidine alkaloids in food and herbal medicines. Toxicol Lett 263:44–57. https://doi.org/10.1016/j.toxlet.2016.05.002

Mimmler M, Peter S, Kraus A et al (2016) DNA damage response curtails detrimental replication stress and chromosomal instability induced by the dietary carcinogen PhIP. Nucleic Acids Res 44(21):10259–10276. https://doi.org/10.1093/nar/gkw791

Moreira R, Pereira DM, Valentao P, Andrade PB (2018) Pyrrolizidine alkaloids: chemistry, pharmacology, toxicology and food safety. Int J Mol Sci. https://doi.org/10.3390/ijms19061668

Müller M, Strand S, Hug H et al (1997) Drug-induced apoptosis in hepatoma cells is mediated by the CD95 (APO-1/Fas) receptor/ligand system and involves activation of wild-type p53. J Clin Invest 99(3):403–413. https://doi.org/10.1172/JCI119174

Nakata T, Matsui T, Kobayashi K, Kobayashi Y, Anzai N (2013) Organic cation transporter 2 (SLC22A2), a low-affinity and high-capacity choline transporter, is preferentially enriched on synaptic vesicles in cholinergic neurons. Neuroscience 252:212–221. https://doi.org/10.1016/j.neuroscience.2013.08.011

Nielsen TL, Rasmussen BB, Flinois JP, Beaune P, Brosen K (1999) In vitro metabolism of quinidine: the (3S)-3-hydroxylation of quinidine is a specific marker reaction for cytochrome P-4503A4 activity in human liver microsomes. J Pharmacol Exp Ther 289(1):31–37

Nigam SK (2015) What do drug transporters really do? Nat Rev Drug Discov 14(1):29–44. https://doi.org/10.1038/nrd4461

Nikolova T, Dvorak M, Jung F et al (2014) The gammaH2AX assay for genotoxic and nongenotoxic agents: comparison of H2AX phosphorylation with cell death response. Toxicol Sci 140(1):103–117. https://doi.org/10.1093/toxsci/kfu066

Prakash AS, Pereira TN, Reilly PE, Seawright AA (1999) Pyrrolizidine alkaloids in human diet. Mutat Res 443(1–2):53–67. https://doi.org/10.1016/s1383-5742(99)00010-1

Rodrigues AC, Curi R, Genvigir FD, Hirata MH, Hirata RD (2009) The expression of efflux and uptake transporters are regulated by statins in Caco-2 and HepG2 cells. Acta Pharmacol Sin 30(7):956–964. https://doi.org/10.1038/aps.2009.85

Rundle S, Bradbury A, Drew Y, Curtin NJ (2017) Targeting the ATR-CHK1 axis in cancer therapy. Cancers (basel). https://doi.org/10.3390/cancers9050041

Ruoss M, Vosough M, Konigsrainer A et al (2020) Towards improved hepatocyte cultures: progress and limitations. Food Chem Toxicol 138:111188. https://doi.org/10.1016/j.fct.2020.111188

Rutz L, Gao L, Kupper JH, Schrenk D (2020) Structure-dependent genotoxic potencies of selected pyrrolizidine alkaloids in metabolically competent HepG2 cells. Arch Toxicol 94(12):4159–4172. https://doi.org/10.1007/s00204-020-02895-z

Schrenk D, Gao L, Lin G et al (2020) Pyrrolizidine alkaloids in food and phytomedicine: occurrence, exposure, toxicity, mechanisms, and risk assessment—a review. Food Chem Toxicol 136:111107. https://doi.org/10.1016/j.fct.2019.111107

Shiloh Y, Ziv Y (2013) The ATM protein kinase: regulating the cellular response to genotoxic stress, and more. Nat Rev Mol Cell Biol 14(4):197–210. https://doi.org/10.1038/nrm3546

Teschke R, Vongdala N, Quan NV, Quy TN, Xuan TD (2021) Metabolic toxification of 1,2-unsaturated pyrrolizidine alkaloids causes human hepatic sinusoidal obstruction syndrome: the update. Int J Mol Sci. https://doi.org/10.3390/ijms221910419

Tu M, Sun S, Wang K et al (2013) Organic cation transporter 1 mediates the uptake of monocrotaline and plays an important role in its hepatotoxicity. Toxicology 311(3):225–230. https://doi.org/10.1016/j.tox.2013.06.009

Tu M, Li L, Lei H et al (2014) Involvement of organic cation transporter 1 and CYP3A4 in retrorsine-induced toxicity. Toxicology 322:34–42. https://doi.org/10.1016/j.tox.2014.04.007

White DL, Saunders VA, Dang P et al (2006) OCT-1-mediated influx is a key determinant of the intracellular uptake of imatinib but not nilotinib (AMN107): reduced OCT-1 activity is the cause of low in vitro

sensitivity to imatinib. Blood 108(2):697–704. https://doi.org/10.1182/blood-2005-11-4687

Zhao M, Li LP, Sun DL et al (2012) Stereoselective metabolism of tetrahydropalmatine enantiomers in rat liver microsomes. Chirality 24(5):368–373. https://doi.org/10.1002/chir.22020

SI Fig. 1

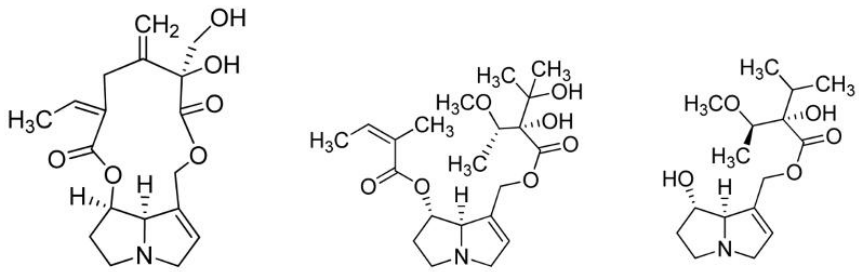

SI Fig. 1: Chemical structures of the three selected PAs, which differ in their degree and type of esterification.

SI Fig. 2

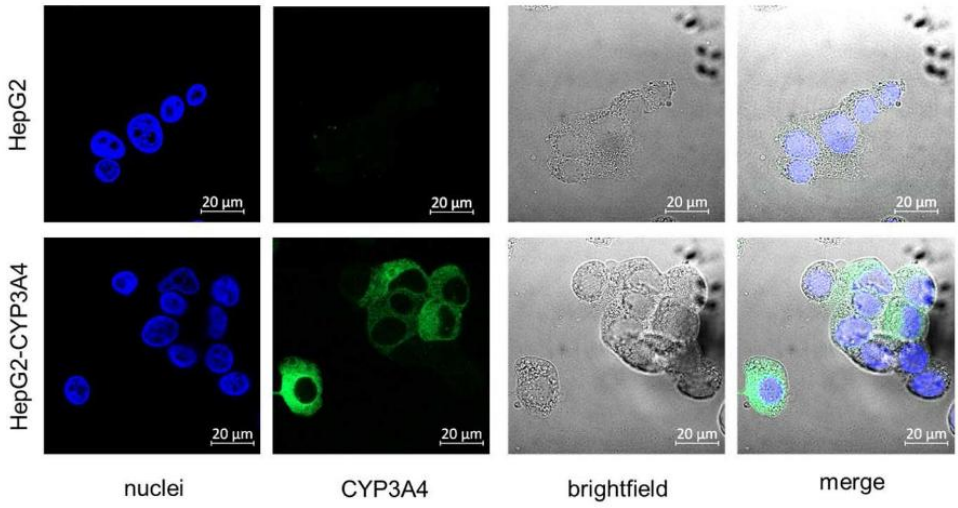

SI Fig. 2: Expression of CYP3A4 in HepG2 and HepG2-CYP3A4 cells. Immunostaining of CYP3A4 in wild-type HepG2 cells and genetically engineered HepG2-CYP3A4 cells. Nuclei were visualized with DAPI staining and cell morphology was assessed using brightfield. Representative confocal images are shown. Scale bar indicates 20 µm.

SI Fig. 3

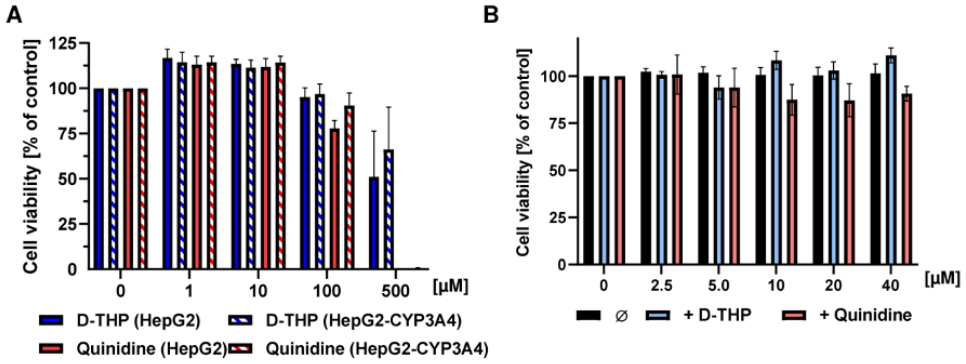

SI Fig. 3: Cytotoxicity of pharmacological OCT1-inhibitors in HepG2 and HepG2-CYP3A4 cells and PA-mediated cytotoxicity in HepG2 cells with or without OCT1-inhibitors. A Viability of HepG2 and HepG2-CYP3A4 cells 24 h after treatment with increasing concentrations of the OCT1 inhibitors D-THP and quinidine. **B** Viability of HepG2 cells 24 h after incubation with increasing concentrations of lasiocarpine with or without OCT1 inhibitors. Solvent (0 µM) was included as negative control. Mean + SEM are shown for each incubation (n=3, each measured as triplicates).

SI Fig. 4

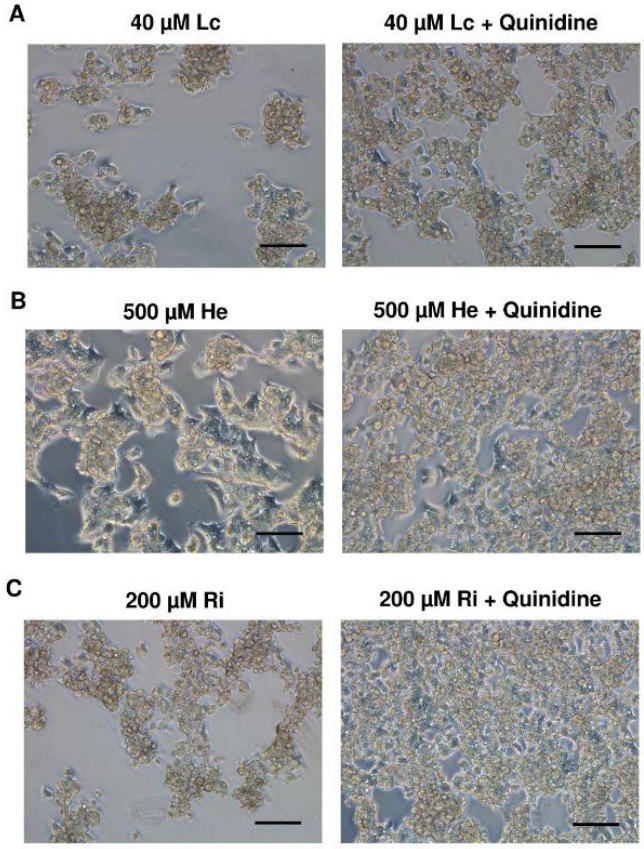

SI Fig. 4: Pharmacological OCT1 inhibition and impact on PA-induced cytotoxicity in HepG2-CYP3A4 cells. A-C Representative microscopic images of HepG2-CYP3A4 cells after 24 h treatment with lasiocarpine (A) heliotrine (B) and riddelliine (C) in the absence or presence of quinidine as OCT1 inhibitor. Scale bar represents 100 µm.

SI Fig. 5

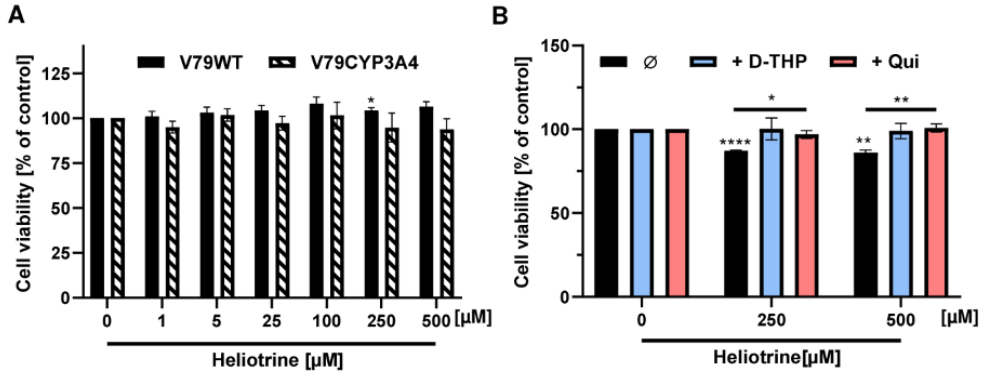

SI Fig. 5: Cytotoxicity of heliotrine in V79 and V79-CYP3A4 cells and impact of OCT1-inhibition. A Viability of V79 and V79-CYP3A4 cells 24h after treatment with increasing concentrations of heliotrine. Solvent (0 µM) was used as negative control. Mean + SEM for each incubation (n≥3, each measured as triplicates). Statistical analyses were performed using unpaired two-tailed Students t-test with respect to the negative control. *P<0.05. **B** Viability of V79-CYP3A4 cells 24 h after incubation with 250 and 500 µM heliotrine in the absence or presence of the OCT1-inhibitors D-THP and quinidine (100 µM each). Solvent (0 µM) was used as negative control. Mean + SEM for each incubation (n=3, each measured as triplicates). Statistical analyses were performed using unpaired two-tailed Students t-test with respect to the negative control or as indicated with a bar. *P<0.05, **P<0.01, ****P<0.0001.

SI Fig. 6

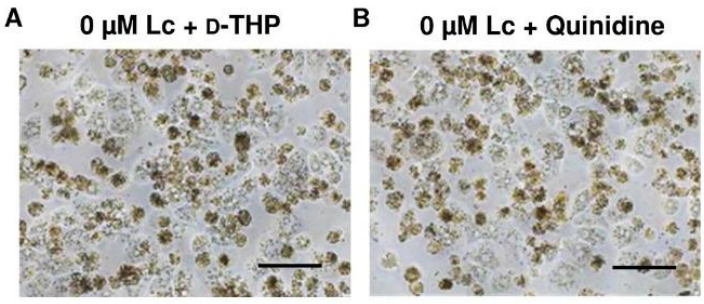

SI Fig. 6: Impact of OCT1-inhibitiors on morphology of primary human hepatocytes. A and **B** Representative microscopic images of primary human hepatocytes after 24 h incubation with solvent (0 µM) in the presence of the OCT1 inhibitors D-THP and Quinidine, respectively. The scale bar represents 100 µm.

SI Fig. 7

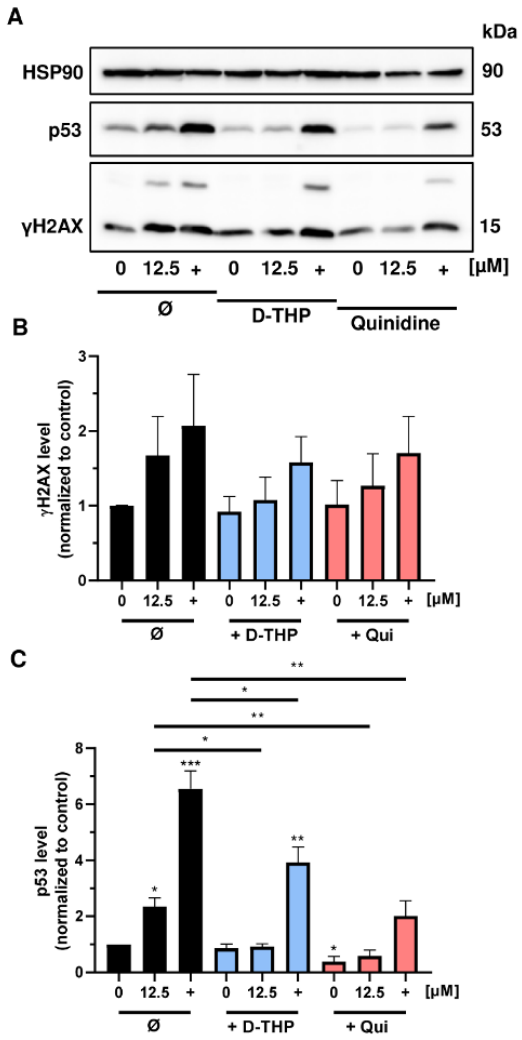

SI Fig. 7: Impact of OCT1-inhibition on the genotoxicity of riddelliine in HepG2-CYP3A4 cells. A Representative western blots of γH2AX and p53 after 24 h treatment with riddelliine. The genotoxic anticancer drug irinotecan was used as a positive control (+) and solvent as a negative control (0 µM). HSP90 served as loading control. **B** and **C**: Densitometric evaluation of γH2AX (B) and p53 (C) after 24 h incubation with lasiocarpine (C) and heliotrine (D) in HepG2-CYP3A4 cells. HSP90 served as loading control. γH2AX level and p53 level relative to the loading control and normalized versus the negative control. Mean + SEM for three independent experiments (n=3). Statistical analyses were performed using unpaired two-tailed Students t-test with respect to the negative control or as indicated with a bar. *P<0.05, **P<0.01, ***P<0.001, ****P<0.0001.

SI Fig. 8

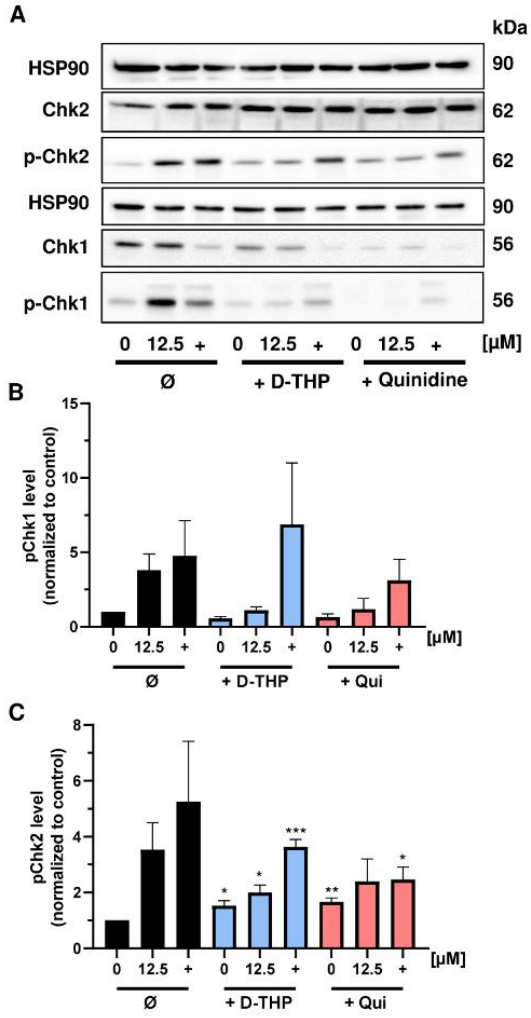

SI Fig. 8: OCT1-inhibition and riddellinne-triggered DNA damage response (DDR). A Representative western blots of (phosphorylated) CHK1 and CHK2 as downstream targets of the apical DDR kinases ATR and ATM after 24 h treatment with riddellinne. The genotoxic anticancer drug irinotecan was used as a positive control (+) and solvent as a negative control (0). Hsp90 served as additional loading control. **B** and **C** Densitometric evaluations of p-Chk1 (S345) and pCHK2 (Thr68) after 24 h incubation with riddellinne in HepG2-CYP3A4 cells. Unphosphorylated CHK1 and CHK2 served as loading controls. pCHK1 and pCHK2 levels relative to the loading control and normalized versus the negative control. Mean + SEM for three independent experiments (n=3). Statistical analyses were performed using unpaired two-tailed Students t-test with respect to the negative control. *P<0.05, **P<0.01, ***P<0.001, ****P<0.0001.

5 Discussion

5.1 Study design

5.1.1 Selected PAs for the studies

Over 660 PAs and their *N*-oxides are identified, whereby only 35 PAs are in point of interest. This goes back to their frequent contamination in food including herbal infusions, tea, food supplements, pollen and honey (Rizzo et al. 2023). The 35 PAs are composed of 21 PAs/ PANOs and their 14 co-eluting isomers, which are regulated in food with maximum levels (EC Regulation 2023/ 915). Notably, the 21 regulated PAs and PANOs accounted for 89% of the total PA content in herbal infusions and 87% in food supplements, whereby the 14 co-eluting isomers contributed significantly to the PA content in honey (36%) and tea (48%) (Rizzo et al. 2023). In recent years, *in vitro* studies using human liver cell models have particularly focused on the structure-dependent toxicity of monoesters, open diesters and cyclic esters, which are included among the 35 PAs (Allemang et al. 2018; Lester et al. 2019; Gao et al. 2020; Rutz et al. 2020). Notably, the human health risk is evaluated for the total PA content in food based on the BMDL value of riddelliine, which is considered critical, as studies show that the toxicity of individual PAs may be underestimated (e.g. heliotrine) or overestimated (e.g. monocrotaline). Merz and Schrenk proposed the implementation of iREP factors to account for the individual toxicity of PAs in risk assessment. However, this approach has not been applied in risk assessment due to insufficient data on toxicity and toxicokinetics (Merz and Schrenk 2016; Schrenk et al. 2022). The 11 PAs that were examined in the first study, in which the structure-dependent toxicity was investigated, are included under the 35 regulated PAs. Furthermore, these 11 PAs were recently the subject of research in pRH and should be investigated in human liver cells as comparison (Gao et al. 2020; Rutz et al. 2020). The results should complement existing studies to support the adoption of iREP factors in risk assessment. Additionally, data on PA toxicity in PHH were collected for the first time, reflecting the results in HepG2-CYP3A4 and highlighting the assessment of PAs based on individual toxicity.

Previous publications mentioned that PAs including retrorsine, senecionine and monocrotaline are transported by influx transporter including OCT1 and Na^+/taurocholate Co-transporting polypeptide into liver cells to exert hepatotoxicity (Tu et al. 2013, 2014; Enge et al. 2021, 2022). However, the impact of OCT1 on the PA transport of monoester, open diester and cyclic diester was not elucidated in human liver cells. In the publication II, three different PAs including riddelliine, lasiocarpine and heliotrine were selected to study the role of OCT1 as influx transporter for a cyclic diester, open diester and monoester, respectively. The selection for the PAs was based on the results from the publication I as well as from previous publications. Riddelliine is described as a moderate cytotoxic and genotoxic PA congener, whereas lasiocarpine showed predominantly a higher toxicity in liver cells. Furthermore, heliotrine

showed surprisingly higher cytotoxic and genotoxic effects compared to other monoester (Allemang et al. 2018; Lester et al. 2019; Louisse et al. 2019; Gao et al. 2020; Rutz et al. 2020; Haas et al. 2023b). By studying the role of OCT1 on the PA transport of riddelliine, lasiocarpine and heliotrine, we wanted to find the differences in their PA toxicity. Furthermore, studies indicate that certain PAs, such as lasiocarpine, activate both CHK1 and CHK2 proteins, as well as the p53 signaling pathway, in liver or TK6 cells (Ebmeyer et al. 2019; Li et al. 2020). The phosphorylation of checkpoint kinases, CHK1 or CHK2, as downstream targets of the apical phosphokinases ATR and ATM indicate a specific DNA damage caused by PAs. The identification of the DNA damage type could help to differentiate between the PAs and their toxicity. So far, the DDR mechanism is still unknown for PAs. Thus, the impact of the OCT1 transport on the PA-induced DDR was investigated for all three PAs in HepG2-CYP3A4 cells.

5.1.2 Selected PA concentrations for the studies and their relevance

In the conducted *in vitro* studies, concentrations ranging from 0.01 to 500 µM were used, depending on the PA and the endpoint to be investigated. The dose ranges of the PAs were tested and adjusted in the *in vitro* cell systems based on the literature (Louisse et al. 2019; Gao et al. 2020; Rutz et al. 2020). The cytotoxicity was determined with maximum concentrations up to 500 µM, as higher solvent content would have led to negative effects on cell viability. It should be noted, that PA concentrations up to 500 µM were predicated on the absence of prior knowledge regarding the cytotoxic potential of PAs in HepG2-CYP3A4 and PHH, thereby requiring investigation. Previous studies have demonstrated that the cytotoxic effects of PAs are structure-dependent, with diesters exhibiting higher toxicity compared to monoesters in pRH and HepaRG cells. However, the cytotoxic effects were relatively low in HepaRG cells and moderate in pRH, which justified testing PA concentrations up to 500 µM in HepG2-CYP3A4 and PHH (Louisse et al. 2019; Gao et al. 2020; Enge et al. 2021). The genotoxicity was determined with PA concentrations, which show minimal to no cytotoxic effects in the cell lines including HepG2-CYP3A4, PHH and V79-CYP3A4 studied. Generally, the cytotoxicity and genotoxicity of the PAs were ascertained in immortalized and genetically modified cell lines (HepG2-CYP3A4 and V79-CYP3A4), wildtype V79 cells as well as in PHH. If a dose-response relationship was evident from the data, the results were converted into relative values. Based on cell viability, EC_{50} values were determined after 24 h and 72 h of PA exposure. The genotoxicity data served as the basis for BMD modelling to determine the relative genotoxic potential of the PAs after 24 h incubation (Haas et al. 2023b, a).

Based on the EC_{50} and BMD values, a potential risk to human health can be assessed considering PA exposure data. Since the genotoxicity of the studied PAs occurred below cytotoxic effects, only the BMDL values are considered. The PAs, retrorsine and lasiocarpine,

exhibited the strongest genotoxic potential with BMDL values of 0.01 µM (γH2AX, HepG2-CYP3A4) and 0.06 µM (γH2AX, PHH). Both BMDL values should be compared with the HBGV of 0.1 µg PA/ kg bw per day as reference point for non-neoplastic damage (BfR 2020). For the comparison, the HBGV has to be calculated for adults (70 kg) and normalized to the liver blood volume (approximately 750 mL) (Schwegler and R. Lucius 2021). The liver blood volume is more appropriate than the whole-body blood volume because PAs are rapidly absorbed in the intestine and transported directly to the liver. Additionally, the bioactivation and primary mode of action of 1,2-unsaturated PAs occur predominantly in the liver (EFSA 2011; Yang et al. 2017). An adapted HBGV of 0.027 µM and 0.023 µM was calculated based on the above-mentioned parameters for retrorsine and lasiocarpine, respectively. The comparison of the estimated BMDL values and the adapted HBGV shows that first genotoxic effects are achieved below the adapted HBGV for non-neoplastic damage with retrorsine, but not with lasiocarpine. According to this example, the risk of non-neoplastic damage cannot be generalized for all PAs based on the NOAEL for riddelliine from the two-year carcinogenicity study; otherwise, the genotoxic potential of PAs may be over- or underestimated. However, the hypothesis is considered as very conservative, since the hypothetical model assumes complete transport of the PAs after oral intake and distribution to the liver, an on-site complete toxification, and without taking safety factors into account. According to calculated scenarios from the BfR, the human PA exposure can exceed the HBGV depending on the food source. For example, the regular intake of plant-based food supplements or high intake of contaminated tea can result in PA intake above 0.1 µg PA/ kg bw per day. Furthermore, MoE values below 10,000 can be reached based on the BMDL value of 73 µg/ kg bw per day for lasiocarpine (BfR 2016).

5.1.3 Selected liver cell models and their attributes

5.1.3.1 HepG2 and HepG2-CYP3A4

HepG2 cells are a cell line derived from the liver tissue of a 15-year-old white male with hepablastoma in the 1980s (Aden et al. 1979). As many other immortalized cell lines, they are commonly used for cancer research, toxicity or metabolism studies, along with other liver cell lines such as Huh7, Hep3B or HepaRG (Arzumanian et al. 2021). However, the cytological and molecular features vary among each category of liver cancer and its respective subtype. This goes back to key mutations in genes such as *CTNNB1*, in gene promoter like TERT or tumor suppressor genes as TP53. HepG2 cells are commonly mutated in the *CTNNB1* gene, which allow an accumulation of beta-catenin due to the loss of original function. This result in cell proliferation and survival (Zeng et al. 2007; Di Masi et al. 2010; Arzumanian et al. 2021). On the other hand, the TP53 gene is unaffected HepG2 compared to other immortalized liver cell lines such as Hep3B. Notably, HepG2 cells lack various phase I and II enzymes, making

them unsuitable for direct testing with 1,2-unsatured PAs (Westerink and Schoonen 2007; Di Masi et al. 2010; Gerets et al. 2012). However, the HepG2 cells can be genetically modified by infection with lentiviral expression vectors, consisting of human CYP3A4 cDNA. The clones with stable CYP3A4 expression are selected with blasticidin to form recombinant cell clones. The working group of Küpper generated a HepG2 cell line with CYP3A4 overexpression, which is comparably to the CYP3A4 activity in human hepatocytes, as shown by real-time PCR and immunofluorescence (Herzog et al. 2015). The clones have to be cultivated in medium supplemented with blasticidin to maintain stable CYP3A4 expression (Herzog et al. 2015). The HepG2-CYP3A4 cells were used previously by Rutz and colleagues and were suitable for studying the PA toxicity. Furthermore, the CYP3A4 isoenzyme is one of the major CYP450 enzymes responsible for PA bioactivation (Ruan et al. 2014a; Rutz et al. 2020). The CYP3A4 protein expression was exclusively demonstrated in the CYP3A4-transfected HepG2 and V79 cell lines via western blot analysis, thereby confirming the metabolic activation of all tested PA (Haas et al. 2023a). However, the expression of transporter is limited in HepG2 cell line compared to human liver tissue. It was shown that HepG2 show significant lower OCT1 expression than PHH (Hilgendorf et al. 2007). However, we could demonstrate OCT1 expression via western blot analysis and compared it with V79-CYP3A4 cells, which showed almost no OCT1 expression. The OCT1 expression correlated with the PA cytotoxicity, showing less cytotoxicity effects caused by PAs than in HepG2-CYP3A4 cells (Haas et al. 2023a).

5.1.3.2 Primary human hepatocytes (pooled)

PHH are considered the gold standard in toxicological and pharmacological research for assessing the ADME (absorption, distribution, metabolism, and excretion) profiles and hepatotoxic effects of various substances. They possess complete metabolic capabilities, express a wide array of influx and efflux transporters, and do not exhibit mutations in key tumor suppressor genes or proto-oncogenes (Fraczek et al. 2013; Ruoß et al. 2020). The CYP3A4 activity in 2D cultured PHH is comparable with the activity in healthy male subjects (Berger et al. 2016). In comparison to other species such as rats or dogs, the expression of CYP450 enzymes or transporters differs. For example, the CYP3A4 enzyme predominantly expressed in humans followed by rats and mice, whereby the latter did not express any CYP3A4 comparable enzyme (Hammer et al. 2021). Furthermore, the OCT1 expression in PHH is lesser than in monkeys but significantly greater than in rats followed by mice and dogs (Morse et al. 2021).

For our studies, we used primary human hepatocytes, which were pooled from five Caucasian donors and successfully cryoconserved with DMSO (supplier: Thermo Fisher Scientific). The use of cryopreserved primary hepatocytes indeed eliminates the need for fresh liver tissues,

which is a big advantage. Furthermore, pooled primary hepatocytes can average out individual differences, leading to more consistent and reliable experimental results (Hengstler et al. 2000). It should be noted, that the metabolic capacity, viability and functionality of human hepatocytes can be affected based on factors such as donor age, gender, pathological status and drug intake (Gómez-Lechón et al. 2004; Konstandi and Johnson 2023). Additionally, the hepatocytes (periportal versus perivenous) can show different functions or vary in their metabolic capability depending on the liver lobule (Jungermann 1986). The donor information of the acquired pooled cryopreserved human hepatocytes from Thermo Fisher Scientifc (Lot No. HPP2434269) is online available and is listed in table 5.1. The majority of donors were female, with an average age of 56 years, ranging from 29 to 69 years. Furthermore, three donors were regular consumers of alcohol and/or tobacco, while only one donor had a documented history of alcohol consumption until the date of death. The three donors died due to drug intoxication, intracerebral haemorrhage and anoxia. In addition, two donors were found to have metastatic tumours and hepatic cellular carcinoma, and the circumstances surrounding their deaths are not known. Additionally, the supplier stated no positive PCR detection for Hepatitis B/C, HIV1&2, HTLV 1&2, CMV or SARS-CoV-2. Given that the donors had a mean age of 56, a history of drug use, or cancer-related diseases, their metabolic capacity may be reduced compared to that of healthy donors.

Table 5.1: Donor information of pooled cryoconserved human hepatocytes from Thermo Fisher Scientic (Lot No. HPP2434269).

Age	Sex	Tobacco history	Alcohol history	Drug history	Cause of death	Other
62	F	No	No	Unknown	N/A	Metastatic tumor
69	F	No	No	Unknown	N/A	HCC
59	F	Yes/ 1 ppd, quit 30 yrs pre-death	Yes/ 1 drink daily	Unknown	Drug intoxication	N/A
61	F	No	No	No	ICH	N/A
29	M	½ pack/ week, quit 18 yrs pre-death	6-8 beers bi-weekly, quit 5 yrs pre-death	Hydrocodone (prescribed) & THC occasionally	Anoxia	N/A

The cultivation of primary cell lines has to be carefully managed and checked before if they are suitable for research. For example, it was previously shown with pRH that a rapid loss in CYP activity was measured over the time after cultivation (Gao et al. 2020). Additionally, primary hepatocytes can dedifferentiate over time, which is why long-timed experiments should be avoided if they are cultured without supplements to extend their functionality. For example,

an increased expression of structural proteins such as actin or tubulin is followed due to the time-dependent decrease of hepatocyte nuclear factors. Thus, PHH do not proliferate compared to immortalized cell lines (Jungermann and Katz 1982; Rowe et al. 2010).

5.2 Consolidated study insights

The present dissertation comprises two publications that address various aspects of the toxicity of PAs in human liver cell models. Both publications provide valuable insights into the structure-dependent cytotoxic and genotoxic effects of 11 PAs, emphasizing the role of OCT1 as an important influx transporter for mono-ester, open di-ester and cyclic di-ester and highlighting their need for refined risk assessment strategies. The figures 5.1-5.2 demonstrate the findings from both publications.

5.2.1 Publication I

The publication I describes the cytotoxic and genotoxic effects of 11 structurally different PAs in HepG2-CYP3A4 cells and PHH. The findings indicated that both cyclic and open diesters exhibit significant cytotoxicity as early as 24 h post-exposure, which further intensifies over 72 h in HepG2-CYP3A4 cells. Based on their cytotoxic potential, it was not possible to determine whether cyclic or open diesters were inherently more cytotoxic. However, among the PAs studied, the open diester, lasiocarpine, exhibited the highest cytotoxicity, followed by cyclic diesters such as seneciphylline and senecionine in HepG2-CYP3A4 cells. The increase in cytotoxicity over time could be attributed to the greater sensitivity of proliferating cells or the cumulative damage sustained by the cells. It should be noted, that monocrotaline as cyclic diester demonstrated no cytotoxicity at 24 h, and exhibited only minimal cytotoxic effects at 72 h with an EC_{50} of 445.7 µM. On the other hand, monoesters, apart from heliotrine, showed no substantial cytotoxic effects at 24 h but displayed low toxicity at 72 h. The cytotoxicity of heliotrine intensified 7.7-fold greater at 72 h, which is comparable to the increase in the cytotoxicity of the diester. However, with regard to the other monoesters, only an EC_{50} value of 189.9 µM could be determined for europine, but not for indicine or lycopsamine.

The PAs exhibited significantly greater cytotoxic effects in HepG2-CYP3A4 cells compared to HepaRG cells, in which the level of toxicity was insufficient to allow for EC_{50} calculation. The HepaRG cells were treated up to 250 µM (Glück et al. 2021) and 400 µM (Louisse et al. 2019) of PA and the cytotoxicity was determined after 24 h of PA exposure. In comparison to our results, lasiocarpine demonstrated the highest cytotoxic potential with an EC_{50} of 12 µM at 24 h, whereas HepaRG cells exhibited only a moderate response even at 250 µM (Louisse et al. 2019; Glück et al. 2021). However, a structure-dependent toxicity pattern was observed in HepaRG cells, with cyclic and open diesters exhibiting the highest cytotoxicity, followed by

monoesters. Notably, monocrotaline demonstrated no cytotoxic effect after 24 h in HepaRG cells, aligning with our findings in HepG2-CYP3A4 cells. Furthermore, heliotrine exhibited greater cytotoxicity than other monoesters, a trend that was also observed in HepG2-CYP3A4 cells.

To further assess the cytotoxic effects of these PAs in a more physiologically relevant system, we examined their impact in PHH, which are widely recognized as the benchmark in pharmaco-toxicokinetic *in vitro* studies of the human liver. Therefore, we assessed the cytotoxicity of six structurally distinct PAs in PHH following 24 h of exposure. Overall, the cytotoxic ranking of PAs in PHH closely mirrored that in HepG2-CYP3A4 cells, showing a structure-dependent toxicity, but with a 3- to 4-fold lower potency. Lasiocarpine exhibited the highest cytotoxic potential, while lycopsamine demonstrated the lowest cytotoxic effects. Interestingly, the PA cytotoxicity was more pronounced in PHH than in HepaRG cells, even though PHH are non-proliferative (Louisse et al. 2019; Glück et al. 2021). Gao and colleagues investigated the cytotoxicity effects of ten PAs in pRH with PA concentrations up to 300 µM after 24 h and 48 h exposure (Gao et al. 2020). Furthermore, they compared the cytotoxicity outcomes after 3 and 24 h of seeding to assess differences in the bioactivation of the PAs as well as the CYP3A activity in pRH. Overall, pRH exhibited lower cytotoxicity levels than PHH, likely due to the absence of cell proliferation, differences in transporter expression and metabolic capacity (Hilgendorf et al. 2007; Gao et al. 2020; Hammer et al. 2021; Morse et al. 2021). The study found that lasiocarpine induced the highest cytotoxicity following 24 h of seeding, whereas senecionine exhibited greater cytotoxicity after 3 h. Furthermore, CYP3A activity, assessed via the 7-Benzoxyresorufin-O-Dealkylase (BROD) assay, was monitored up to 72 hours post-seeding and showed a reduction in BROD activity to below 60% within the first 6 hours (Gao et al. 2020).

The PA genotoxicity was assessed using an *in vitro* test battery, which included the analysis of the DNA damage markers γH2AX and p53 via western blot or immunofluorescence staining, as well as DNA strand break analysis using alkaline comet assay in HepG2-CYP3A4 and PHH. It should be noted, that the genotoxicity was determined with PA concentrations, which show minimal to no cytotoxic effects in the liver cell lines. Overall, the BMDL values derived from γH2AX, p53, and DNA strand break data indicate a structure-dependent genotoxicity of the PAs. In this context, cyclic and open diesters generally exhibited higher genotoxic potentials than monoesters in HepG2-CYP3A4 cells. Moreover, monocrotaline displayed a low genotoxic potential, which was comparable to that of monoesters such as europine and indicine. In contrast, heliotrine demonstrated moderate genotoxicity, exceeding that of monocrotaline and aligning with our cytotoxicity data. The highest genotoxic potential was observed by retrorsine with a BMDL value of 0.01 µM followed by seneciphylline based on the γH2AX data.

Louisse and colleagues investigated the genotoxicity of 37 PAs and PANOs including cyclic diester, open diester and monoester in HepaRG cells by determining the induction of the DNA damage marker γH2AX using the in cell western assay (Louisse et al. 2019). A similar trend was observed in HepaRG cells, wherein cyclic and open diesters exhibited the highest genotoxic potentials, followed by monoesters. However, the BMDL values were significantly higher in HepG2-CYP3A4 cells, possibly due to differences in proliferation rates and other factors that influence the cellular sensitivity. Senecionine followed by seneciphylline and lasiocarpine showed the strongest genotoxic potentials with BMDL values between 3.4 and 4.2 µM. Furthermore, heliotorine exhibited a higher genotoxic potential than monocrotaline in HepaRG cells, aligning with our results in HepG2-CYP3A4 cells. Furthermore, studies in HepG2-CYP3A4 and HepaRG cells assessing micronucleus induction revealed that monocrotaline demonstrates a generally lower genotoxic potential among cyclic diesters and compared to heliotrine, which aligns well with our findings (Allemang et al. 2018; Rutz et al. 2020). As described in chapter 2.3.2 and 2.4.1, monocrotaline is mainly metabolized in rat liver S9 fractions, with minimal lung metabolism and shows higher lung-to-liver pyrrole protein adduct ratios, indicating a primary lung toxicity, which is confirmed by findings in mice and rats (Song et al. 2020; He et al. 2021a).

The p53 marker proved to be a sensitive genotoxicity indicator, allowing for precise potency classification using BMD modelling. Interestingly, monoesters exhibited a higher BMDL range with p53 as an endpoint compared to γH2AX, suggesting a possible variance in genotoxic mechanisms between monoesters and diesters. As previously described, the activation of p53 is in response to DNA damage and is necessary to allow for DNA repair, cell cycle arrest and apoptosis if the DNA damage is too high (see chapter 2.6.2). On one hand, these differences may be attributed to the delayed activation of p53 as part of the DNA damage response or to the lower extent of DNA damage caused by monoesters compared to diesters, suggesting reduced cellular stress. The results align with findings from two studies that demonstrated the upregulation of the p53 pathway by structurally different PAs in HepG2-CYP3A4 cells and in a 28-day feeding study in rats using transcriptome analysis (Ebmeyer et al. 2020; Abdelfatah et al. 2022).

Additionally, DNA strand break analysis using the alkaline comet assay confirmed the structure-dependent genotoxicity of PAs, with results aligning well with those from γH2AX and p53 assessments. The sensitivity of the comet assay allowed for the detection of genotoxic effects even for weak toxic PAs including monocrotaline and lycopsamine with BMDL values of 39.9 and 62.1 µM, respectively. The BMDL value of monocrotaline is by a factor of 36.6 and 6.4 higher compared to the BMDL values of riddelliine and heliotrine, respectively, whereby the BMDL values of europine and monocrotaline were almost similar. This assay effectively detects single-strand breaks (SSBs), double-strand breaks (DSBs), and alkali-labile sites, such

as apurinic/apyrimidinic sites. Moreover, it serves as a supplementary method to detect DNA damage, especially when other genotoxicity assays for endpoints including mutations (e. g. AMES) or clastogenic effects (e. g. micronuclei) yield inconclusive results. Due to its reliability, it is widely used into regulatory genotoxicity testing of pharmaceuticals under ICH S2 (R1) (EMA 2012; Frötschl 2015). It should be noted that DNA strand breaks can result in chromosomal damage and micronuclei formation (see chapter 2.4.3.2). In previous studies, the formation of micronuclei was investigated in HepG2-CYP3A4, HepG2 cells with rifampicin pretreatment, and HepaRG cells (Allemang et al. 2018; Louisse et al. 2019; Rutz et al. 2020; Hadi et al. 2021). The results support a similar ranking of PAs, consistent with our findings that cyclic and open diesters exhibit the highest genotoxic potential. It should be noted that retrorsine exhibited a comparable potency to that of seneciphylline, which was not reported in previous studies. The studies reported that retrorsine was dissolved in a 1:1 mixture of DMSO and acetonitrile, DMSO or water, whereas our stock solution was prepared in ethanol. While this suggests that the chemical stability or solubility of retrorsine was not adversely affected in ethanol, further investigation is needed to determine whether solvent choice influenced the observed genotoxic potency. To date, the chemical stability and solubility of PAs have received limited attention in the literature. Considering these factors is essential for ensuring the accuracy and reliability of genotoxicity assessments.

Given that HepG2-CYP3A4 cells are engineered to express only CYP3A4, further validation in PHH was necessary to account for a full spectrum of metabolic enzymes. Our study confirmed that lasiocarpine and retrorsine were the most potent genotoxic PAs in PHH, with BMDL values of 0.06 and 0.4 µM, respectively. Notably, the genotoxicity levels of the tested PAs in PHH were comparable to those in HepG2-CYP3A4 cells but were significantly higher for monocrotaline and lasiocarpine, likely due to additional metabolic activation via CYP2A6 and CYP3A5 in PHH (Gerets et al. 2012; Berger et al. 2016; Hammer et al. 2021). Furthermore, the transporter expression such as OCT1 is generally higher compared to HepG2 cells, which allow a faster bioactivation and intoxication in PHH (Hilgendorf et al. 2007; Gerets et al. 2012). In addition, a previous study demonstrated that lasiocarpine followed by echimidine, riddelliine, and heliotrine induced the highest levels of DHP-DNA adducts in rat sandwich-culture hepatocytes, which is in line with the results in PHH (Lester et al. 2019). These observations reinforce the relevance of PHH in detecting structure-dependent genotoxicity effects that might not be as pronounced in engineered cell models.

The application of the BMD modelling was critical for categorizing PAs into different potency classes, enabling risk assessment. Our results established a consistent ranking of PAs based on genotoxic potency, with retrorsine being the most potent and lycopsamine the least. Monocrotaline displayed lower BMD values compared to riddelliine, a finding corroborated by previous studies in HepaRG and HepG2-CYP3A4 cells (Allemang et al. 2018; Louisse et al.

2019; Rutz et al. 2020). The incorporation of BMD confidence intervals (BMDL and BMDU) provided a comprehensive approach for comparing PA toxicities across different cellular models. Our integrated approach to PA potency ranking used data from multiple genotoxicity endpoints, demonstrating consistency between HepG2-CYP3A4 cells and PHH. It remains unclear why PAs such as heliotrine or monocrotaline differ in their potency. The discrepancies in PA toxicity may result from metabolic activation, as a previous study using genetically modified TK6 cells have demonstrated that specific PAs, such as riddelliine and lasiocarpine, undergo bioactivation by CYP3A7 and CYP3A5 too, respectively. (Li et al. 2020). Several lines of evidence showed that PAs differ in their induction of DNA damage measured by the DHP-DNA adduct levels or in their potential of chromosomal damage such as micronuclei or chromosomal aberrations (see chapter 2.4.3). Thus, certain PAs preferentially induce DSBs and/or SSBs due to their high reactivity, leading to increased cell death when the level of DNA damage exceeds a critical threshold. It can be suggested that the reactivity of certain PAs, such as lasiocarpine or echimidine, is influenced by the structure of their necine acids, which contain reactive groups such as α,β-unsaturated carbonyl groups. Nevertheless, our findings underscore the importance of chemical structure for the toxic properties of PAs and support the concept of grouping PAs into potency classes, initially proposed by Merz and Schrenk in 2016. However, our findings indicate discrepancies for monocrotaline and echimidine, which do not align with the iREP classifications. Specifically, monocrotaline should be reclassified to potency class 0.1 and echimidine to class 1.0 based on our findings in HepG2-CYP3A4 and PHH. The study's findings support efforts to develop standardized methods for assessing PA toxicity and highlight the importance of including PHH in preclinical toxicology studies. Future studies should focus on refining iREP factors using broader datasets and harmonizing BMD modeling methodologies for improved regulatory acceptance in PA risk assessment.

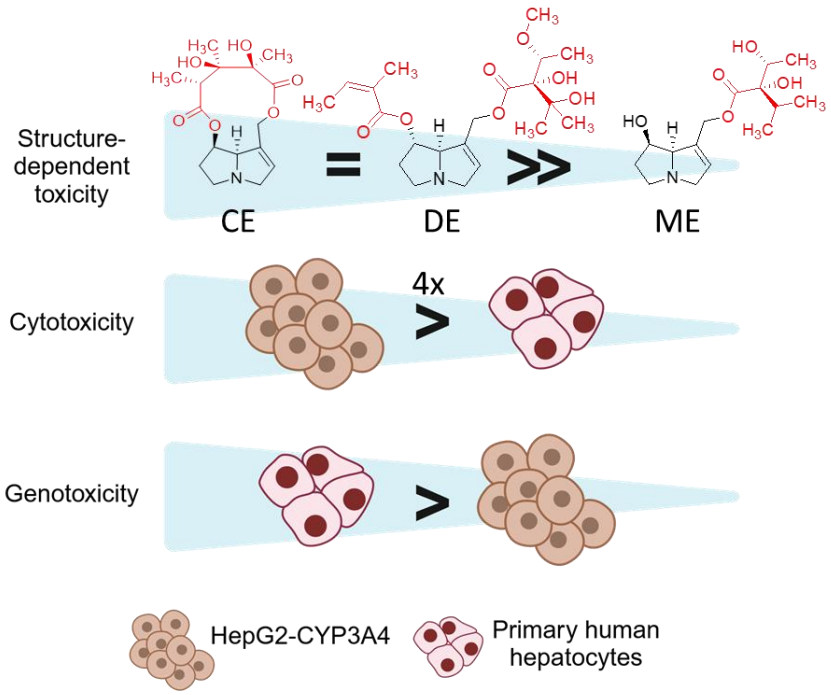

Figure 5.1: Ranking of PAs by toxic potency and liver cell models by sensitivity to PAs. CE: Cyclic diester**; DE:** open diester**; ME:** monoester (created in https://BioRender.com)

5.2.2 Publication II

The publication II underscores the pivotal role of OCT1 in mediating the uptake of structurally diverse PAs including riddelliine (cyclic diester), lasiocarpine (open diester) and heliotrine (monoester) into human liver cells (HepG2-CYP3A4 and PHH), with significant implications for their cytotoxic and genotoxic effects. It is widely known that the role of OCT1 in drug transport, along with its genetic variability, has been associated with variations in drug response and toxicity (Koepsell 2020). Our findings highlighted the critical interplay between OCT1 and CYP3A4 in determining PA toxicity. While wild-type HepG2 cells exhibited no cytotoxic effects in the presence of lasiocarpine, HepG2-CYP3A4 cells showed clear dose-dependent cytotoxicity for all tested PAs, as previously reported in Publication I, underscoring the pivotal role of CYP3A4 in PA bioactivation. Furthermore, our analysis revealed comparable CYP3A4 protein levels in both HepG2-CYP3A4 and V79-CYP3A4 cell models, while HepG2-CYP3A4 cells exhibited higher OCT1 protein expression. This elevated OCT1 expression correlated with increased sensitivity to all tested PAs, strengthen the functional interplay between OCT1 and CYP3A4 in PA toxicity.

In order to investigate the role of OCT1 in PA toxicity, two pharmaceutical inhibitors, D-THP and quinidine, were selected. D-THP serves as a specific OCT1 inhibitor, whereas quinidine acts as a broad-spectrum OCT inhibitor. It is notable that both compounds are substrates of

phase I enzymes, which potentially leads to competition for CYP enzymes. While quinidine is a known substrate of CYP3A4, D-THP exhibits inhibitory effects on CYP2D6 and CYP1A2. (Nielsen et al. 1999; Li et al. 2015a). These inhibitors effectively reduced PA-induced cytotoxicity in HepG2-CYP3A4 and V79-CYP3A4 cells, regardless of PA structure, while exhibiting no cytotoxic effects themselves. Furthermore, D-THP exhibited greater efficacy than quinidine in inhibiting OCT1 and significantly enhanced cell viability.

This aligns with findings from Tu and colleagues, which demonstrated that OCT1 mediates the hepatic uptake of monocrotaline or retrorsine and contributes to their hepatotoxicity in wildtype and genetically modified MDCK cells as well as pRH (Tu et al. 2013, 2014). The investigation revealed a correlation between increased PA toxicity and the presence of CYP3A4, with OCT1 expression further amplifying this effect in MDCK cells. Interestingly, quinidine demonstrated a greater efficacy than D-THP in inhibiting OCT1 and enhanced cell viability in presence of retrorsine in pRH. However, both inhibitors showed the same efficiency in inhibiting OCT1 and improved cell viability in presence of monocrotaline in pRH. Consequently, it can be hypothesised that both PAs were not transported in the same manner into pRH. It should be noted that the OCT1 protein expression in liver tissues of rats are significantly lower compared to those of humans (Wang et al. 2015).

Furthermore, the role of OCT1 in PA toxicity was studied with PAs including retrorsine and senecionine in combination with different pharmacological influx and efflux inhibitors in HepaRG cells (Enge et al. 2021). Quinidine and tetraethylammonium bromide were employed as OCT1 inhibitors and demonstrated comparable inhibitory effects on OCT1, resulting in increased cell viability in the presence of retrorsine but not senecionine. Notably, the inhibitory effect of quinidine was significantly stronger than that of tetraethylammonium bromide in the presence of senecionine. These differences may be attributed to variations in the inhibitory potency of the compounds, with quinidine exhibiting greater efficiency as an OCT1 inhibitor compared to tetraethylammonium bromide.

OCT1 has been identified as a critical influx transporter for PA cytotoxicity in various cell lines; however, its role in PHH remained unclear. In this study, we demonstrated that lasiocarpine is an OCT1 substrate, and competitive inhibition of OCT1 significantly improved cell viability with D-THP, but not with quinidine. As previously noted, quinidine is a substrate for CYP3A4 and may undergo metabolism in PHH, potentially reducing its inhibitory effect on OCT1. Despite this limitation, the involvement of OCT1 in PA-induced cytotoxicity was confirmed in PHH.

Furthermore, we further explored the impact of OCT1 in PA genotoxicity by analyzing the DNA damage markers γH2AX and p53 in HepG2-CYP3A4 cells. OCT1 inhibition significantly reduced PA-induced γH2AX formation and p53 accumulation for all PAs, indicating that OCT1-mediated uptake is essential for PA-triggered genotoxicity. Besides, we examined the

activation of the PA triggered DDR by assessing the phosphorylation of CHK1 and CHK2. These kinases are activated by apical phosphor kinases ATM and ATR and play a critical role in cellular responses to genotoxic stress. It should be noted that the tested PAs (riddelliine, lasiocarpine and heliotrine) significantly increased CHK1 and CHK2 phosphorylation in HepG2-CYP3A4 cells, while OCT1 inhibition reduced their activation. Based on the results, the inhibitory effect of D-THP was generally greater compared to quinidine. Our findings align with previous transcriptomic studies from a 28-day feeding rat study and in PA-exposed HepG2-CYP3A4 cells (Ebmeyer et al. 2020; Abdelfatah et al. 2022). The studies showed an activation of DDR signaling pathways such as p53 and ATM with structurally different PAs. Furthermore, the phosphorylation of CHK1 and CHK2 was previously observed in genetically engineered TK6 cells following treatment with lasiocarpine and riddelliine at concentrations comparable to those used in our study, supporting the consistency of our findings.

The therapeutic potential of OCT1 inhibitors in mitigating PA toxicity is an area of growing interest. For instance, Li and colleagues demonstrated that OCT1 inhibitors like D-THP significantly reduced the hepatotoxicity of nitidine chloride, a quaternary ammonium alkaloid, by limiting its cellular uptake (Li et al. 2014). This aligns with the current study's findings, suggesting that OCT1 inhibitors could serve as a protective strategy against PA-induced liver damage.

In conclusion, this work establishes OCT1 as a critical determinant of PA-induced hepatotoxicity, linking its transport activity to both cytotoxic and genotoxic outcomes. By elucidating the mechanisms underlying PA uptake and toxicity, the study provides a foundation for developing targeted interventions to protect against PA-related liver damage. Further research into the genetic variability of OCT1 and its role in interindividual differences in PA toxicity could enhance our understanding of its clinical implications.

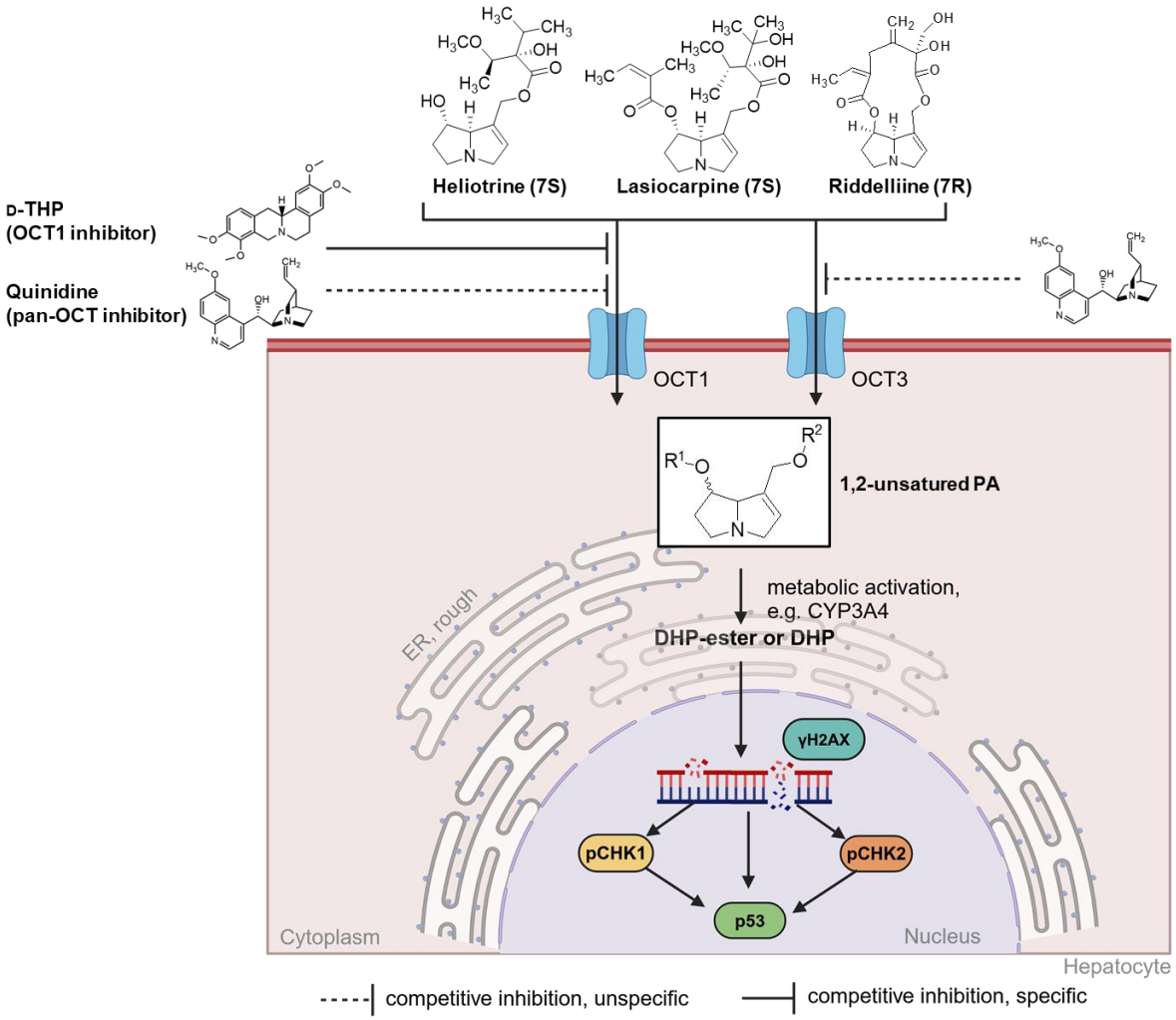

Figure 5.2: Holistic overview of the PA transport and mode of action in the hepatocytes. The PAs including heliotrine, lasiocarpine and riddelliine are transported by OCT1 and/ or OCT3 in hepatocytes. The pharmacological inhibition of OCT1 by D-tetrahydropalmatine (D-THP) and quinidine, which act as an OCT1 and pan-OCT inhibitor, respectively, prevents the OCT-dependent transport of xenobiotics into hepatocytes through competitive inhibition. In the presence of CYP450 enzymes, PA metabolites (DHP ester and DHP) are formed and react with DNA and/or proteins to form adducts in the nucleus. The resulting DNA damage (SSB and/ or DSB) leads to an increase in the DNA damage markers γH2AX and p53, as well as phosphorylated CHK1 and CHK2 levels (created in https://BioRender.com).

6 Conclusion and future perspectives

The subsequent PA research was conducted as a follow-up project to investigate the structure-dependent toxicity of 11 PAs as well as the impact of OCT1 in the transport of structurally different PAs in human cell models including HepG2-CYP3A4 and PHH. Both aspects were elucidated to find the discrepancies between PA individuals within and between degree of esterification.

The first study provides a comprehensive evaluation of the cytotoxic and genotoxic effects of structurally diverse PAs including five cyclic diester, two open diester and four monoester using a combination of HepG2-CYP3A4 cells and PHH, which show similar levels of CYP3A4 enzyme activity. This study clearly demonstrated the structure-dependent toxicity of PAs using an *in vitro* genotoxicity battery that combined three distinct genotoxic endpoints with cytotoxicity assessments. The findings emphasize that cyclic and open diesters exhibit significantly higher cytotoxic and genotoxic potency compared to monoesters, supporting the hypothesis that PA toxicity is intrinsically linked to their chemical structure. The cytotoxicity ranking of PAs revealed that lasiocarpine, followed by seneciphylline, senecionine and retrorsine exhibited the highest cytotoxic potential, while lycopsamine and monocrotaline showed the weakest cytotoxic effects in HepG2-CYP3A4 cells. A similar cytotoxicity ranking was observed in PHH, although the overall potency was notably lower. Notably, retrorsine, seneciphylline, and lasiocarpine demonstrated the highest genotoxic potency in HepG2-CYP3A4 cells, whereas in PHH, the strongest genotoxic effects were observed with lasiocarpine, retrorsine, and riddelliine. Monocrotaline and lycopsamine exhibited the lowest genotoxic effects in both cell models. The potency ranking of PAs based on genotoxicity endpoints was broadly consistent across both HepG2-CYP3A4 cells and PHH, underscoring the reliability of these models for toxicological assessment. In addition, the results of our study indicated the presence of genotoxic effects in PHH, even in the absence of overt cytotoxic effects. The study also provides additional support for the use of relative potency factors in PA risk assessment. Given that PAs are still regulated as a sum parameter regardless of their individual potency, the results of this study highlight the necessity of implementing a structure-based risk assessment approach. However, a definitive explanation for the observed variations in toxicity among congeners, both within and across different degrees of esterification, remains elusive. To address these uncertainties, further analyses are warranted, such as evaluating mutagenicity using the phosphatidylinositol glycan class A (PIG-A) gene mutation assay or investigating DNA adduct formation with and without recovery time. These findings highlight the necessity of assessing PAs individually for risk evaluation, given the significant variability in toxicity across congeners with different esterification patterns.

The second study revealed insights into the role of OCT1 in the uptake and toxicity of structurally different PAs including riddelliine, lasiocarpine and heliotrine in HepG2-CYP3A4, PHH and V79-CYP3A4. In general, the results showed that OCT1 is a key determinant for PA-induced cytotoxicity and genotoxicity. Both cyclic and open-chain diesters, as well as monoester, are substrates for OCT1, highlighting the broad relevance of this transporter in PA toxicity. The use of pharmacological OCT1 inhibitors, D-THP and quinidine, revealed a significant reduction in PA-triggered cytotoxicity in HepG2-CYP3A4 and V79-CYP3A4 cells, indicating that OCT1-mediated transport plays a crucial role in PA cyototoxicity. In PHH, lasiocarpine treatment led to a significant decrease in cell viability, which was largely restored with D-THP co-administration, confirming the protective role of OCT1 inhibition in reducing PA-induced cytotoxicity. Furthermore, the inhibition of OCT1 resulted in a marked decrease in DNA damage markers, such as γH2AX and p53, as well as reduced phosphorylation of the checkpoint kinases CHK1 and CHK2, which are key mediators of the DDR. This finding indicates that OCT1-dependent uptake is a required mechanism for the genotoxic effects of PAs. Another important aspect that requires further exploration is the potential therapeutic application of OCT1 inhibitors as protective agents against PA-induced liver toxicity. Given that pharmacological inhibition of OCT1 significantly reduced both cytotoxic and genotoxic effects, future studies could investigate whether OCT1 inhibitors could be developed into preventive treatments for individuals at risk of PA exposure. However, potential side effects and interactions of such inhibitors with other essential physiological transport functions must be carefully evaluated. Advanced cell models, such as three-dimensional liver organoids or organ-on-a-chip systems, could provide more physiologically relevant insights into PA transport and metabolism. These models may help bridge the gap between in vitro and in vivo studies, offering a more accurate representation of human liver physiology and PA toxicity.

Overall, the studies underscore the critical role of the chemical structure and OCT1-mediated transport in PA toxicity, highlighting the need for structure-based risk assessment approaches. Future research should focus on elucidating the intracellular signal mechanisms underlying toxicity variations among PA congeners and exploring the therapeutic potential of OCT1 inhibitors to mitigate PA-induced toxicity.

In the context of intracellular signaling mechanisms, preliminary experiments utilizing heliotrine in HepG2-CYP3A4 cells provided valuable insights into the PA triggered DDR. The heliotrine triggered DDR was investigated by measuring the downstream targets of ATM, ATR and DNA-PK via western-blot analysis in a time-dependent manner (Figure 6.1, A) as well as with or without the co-administration of pharmaceutical inhibitors against the ATM or ATR (Figure 6.1, B). A key finding was that heliotrine induced significant phosphorylation of checkpoint kinases CHK1 and CHK2 as well as RPA in presence of evaluated γH2AX and p53 levels in HepG2-CYP3A4 cells in a time-dependent manner, reaching its maximum after 8 h (Figure 6.1, A).

The activation of the ATM-CHK2- and ATR-CHK1-axis aligns with previous transcriptomic studies or western-blot results, indicating a robust cellular response to PA-induced DNA damage (Ebmeyer et al. 2019; Li et al. 2020).

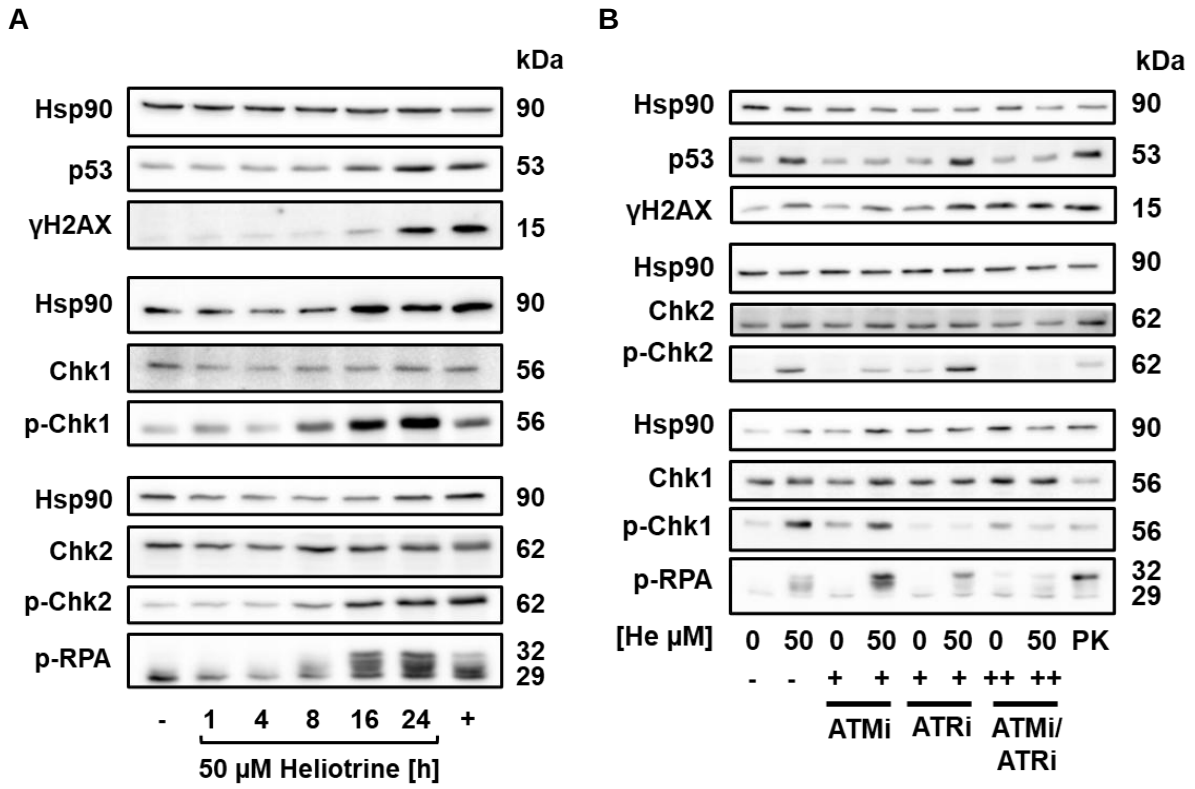

Figure 6.1:Representative western blots of γH2AX, p53, pCHK1, pCHK2 and RPA2 as downstream targets of the apical DDR kinases ATR, ATM as well as DNA-PK after 1-24 h incubation with or without 1-2 µM of each ATM, ATR as well as both inhibitors. Etoposide served as a positive control (+, PK) and solvent as a negative control (-, 0 µM). HSP90, CHK1/ 2 and RPA (29 kDa) served as loading controls.

To further explore the roles of different DDR signaling pathways, pharmacological inhibitors against the apical DDR kinases ATM and ATR were used in co-administration (Figure 6.2, B). Notably, the inhibitors did not affect CHK1/ 2 and RPA32 protein levels, either alone or in combination with PAs, but did suppress the phosphorylation of their downstream targets in response to the respective apical phosphokinase. However, elevated γH2AX and p53 levels were observed due to ATR activity, indicating increased cellular stress. The inhibition of ATM and ATR significantly reduced PA-induced phosphorylation of CHK1 (Ser345) and CHK2 (Thr68), respectively, as well as γH2AX formation and p53 accumulation, highlighting the central role of these kinases in the cellular response to PA-induced DNA damage. For instance, ATR inhibition led to higher pCHK2 levels, suggesting more pronounced DSBs. This aligns with previous studies demonstrating DSB formation in ATR-deficient cells and following ATR inhibition in Caco-2 cells exposed to genotoxic agents (Chanoux et al. 2009; Mimmler et al. 2016). Furthermore, the dual inhibition of ATM and ATR led to no significant increase of pRPA (Thr21), pCHK1 and pCHK2, indicating no influence of DNA-PK in the heliotrine triggered DDR.

Notably, the inhibition of either ATR or ATM resulted in elevated activation of the remaining kinase, accompanied by elevated levels of its downstream targets.

The role of ATR and ATM in the PA-induced DDR has to be investigated on PA structure. The analysis of downstream targets of ATR and ATM. By examining the PA affected cell cycle regulation in presence of pharmacological inhibitors against ATR and ATM could identify which protective role the apical phosphokinases in the PA-induced DDR provide. Abdelfatah and colleagues showed that PAs including riddelliine, monocrotaline, lasiocarpine, echimidine and lycopsamine caused S-phase and G2/M-phase arrest in HepG2-CYP3A4 cells, suggesting a replication fork blockage by bulky lesions and the involvement of p21 in cell cycle regulation. The increase in both S phase and G2/M phase was more pronounced with increasing PA concentrations (Abdelfatah et al. 2022). Besides, the PA-induced cytotoxicity can be investigated in the presence of ATR- and ATM-specific inhibitors to explore their roles in the PA-induced DDR and replication stress. ATR inhibition has been shown to increase DSB due to replication fork collapse, as ATR plays a critical role in stabilizing stalled replication forks and preventing their collapse into DSB (Saldivar et al. 2017). Conversely, ATM inhibition can result in the accumulation of DNA damage and genomic instability by disrupting the recognition and repair of DSB, as ATM is a critical mediator of DSB signaling and repair through pathways such as homologous recombination (Hickson et al. 2004; Shiloh and Ziv 2013). In addition, further research is necessary to determine the role of apical phosphokinases in the PA-induced DDR in relation to the PA structure. This investigation will facilitate the understanding of discrepancies in the PA structure-dependent toxicity. To evaluate the levels of bulky DNA lesions induced by structurally distinct pyrrolizidine alkaloids (PAs), a modified comet assay incorporating replication inhibitors such as hydroxyurea, araC, or aphidicolin could be utilized (Collins et al. 2023). Additionally, a neutral comet assay can be employed to specifically detect DSB providing a comprehensive assessment of DNA damage. Moreover, the role of ATR and ATM in the PA induced DDR can be verified through the analysis their individual protein levels using western blot. Additionally, siRNA-mediated knockdown or plasmid-based silencing in HepG2-CYP3A4 cells, as well as experiments in ATR- and ATM-deficient cell lines, can further confirm the involvement of ATR and ATM in the PA-induced DDR. Besides, phosphoproteomics could also be employed to map downstream targets and repair proteins, providing a comprehensive view of the DDR pathways activated by PAs.

7 References

Abdelfatah S, Naß J, Knorz C, et al (2022) Pyrrolizidine alkaloids cause cell cycle and DNA damage repair defects as analyzed by transcriptomics in cytochrome P450 3A4-overexpressing HepG2 clone 9 cells. Cell Biol Toxicol 38:325–345. https://doi.org/10.1007/s10565-021-09599-9

Abraham RT (2001) Cell cycle checkpoint signaling through the ATM and ATR kinases. Genes Dev 15:2177–2196. https://doi.org/10.1101/gad.914401

Aden DP, Fogel A, Plotkin S, et al (1979) Controlled synthesis of HBsAg in a differentiated human liver carcinoma-derived cell line. Nature 282:615–619

Allemang A, Mahony C, Lester C, Pfuhler S (2018) Relative potency of fifteen pyrrolizidine alkaloids to induce DNA damage as measured by micronucleus induction in HepaRG human liver cells. Food and Chemical Toxicology 121:72–81. https://doi.org/10.1016/j.fct.2018.08.003

Altin J, Bygrave F (1988) Non-parenchymal cells as mediators of physiological responses in liver. Mol Cell Biochem 83:3–14

Arzumanian VA, Kiseleva OI, Poverennaya E V. (2021) The curious case of the HepG2 cell line: 40 years of expertise. Int J Mol Sci 22:. https://doi.org/10.3390/ijms222313135

Avila C, Breakspear I, Hawrelak J, et al (2020) A systematic review and quality assessment of case reports of adverse events for borage (Borago officinalis), coltsfoot (Tussilago farfara) and comfrey (Symphytum officinale). Fitoterapia 142:. https://doi.org/10.1016/j.fitote.2020.104519

Badie C, Itzhaki JE, Sullivan MJ, et al (2000) Repression of CDK1 and Other Genes with CDE and CHR Promoter Elements during DNA Damage-Induced G 2 /M Arrest in Human Cells. Mol Cell Biol 20:2358–2366

Barlow S, Renwick AG, Kleiner J, et al (2006) Risk assessment of substances that are both genotoxic and carcinogenic. Report of an International Conference organized by EFSA and WHO with support of ILSI Europe. Food and Chemical Toxicology 44:1636–1650. https://doi.org/10.1016/j.fct.2006.06.020

Bass TE, Luzwick JW, Kavanaugh G, et al (2016) ETAA1 acts at stalled replication forks to maintain genome integrity. Nat Cell Biol 18:1185–1195. https://doi.org/10.1038/ncb3415

Beagan K, McVey M (2016) Linking DNA polymerase theta structure and function in health and disease. Cellular and Molecular Life Sciences 73:603–615. https://doi.org/10.1007/s00018-015-2078-9

Berger B, Donzelli M, Maseneni S, et al (2016) Comparison of Liver Cell Models Using the Basel Phenotyping Cocktail. Front Pharmacol 7:. https://doi.org/10.3389/fphar.2016.00443

Bermudez VP, Lindsey-Boltz LA, Cesare AJ, et al (2003) Loading of the human 9-1-1 checkpoint complex onto DNA by the checkpoint clamp loader hRad17-replication factor C complex in vitro. Proc Natl Acad Sci U S A 100:1633–1638

BfR (2020) (Bundesinstitut für Risikobewertung). Updated risk assessment on levels of 1,2-unsaturated pyrrolizidine alkaloids (PAs) in foods, BfR Opinion 026/2020 issued 17 June 2020

BfR (2016) (Bundesinstitut für Risikobewertung). Pyrrolizidinalkaloide: Gehalte in Lebensmitteln sollen nach wie vor so weit wie möglich gesenkt werden. Stellungnahme Nr. 030/2016 des BfR vom 28. September 2016. .

Bieging KT, Mello SS, Attardi LD (2014) Unravelling mechanisms of p53-mediated tumour suppression. Nat Rev Cancer 14:359–370. https://doi.org/10.1038/nrc3711

Blackford AN, Jackson SP (2017) ATM, ATR, and DNA-PK: The Trinity at the Heart of the DNA Damage Response. Mol Cell 66:801–817

Boppré M (2011) The ecological context of pyrrolizidine alkaloids in food, feed and forage: An overview. Food Additives and Contaminants - Part A 28:260–281. https://doi.org/10.1080/19440049.2011.555085

Brosseau N, Ramotar D (2019) The human organic cation transporter OCT1 and its role as a target for drug responses. Drug Metab Rev 51:389–407

Bruggeman IM, Van Der Hoeven JCM (1985) Induction of SCEs by some pyrrolizidine alkaloids in V79 Chinese hamster cells co-cultured with chick embryo hepatocytes. Mutat Res 142:209–212

Byun TS, Pacek M, Yee MC, et al (2005) Functional uncoupling of MCM helicase and DNA polymerase activities activates the ATR-dependent checkpoint. Genes Dev 19:1040–1052. https://doi.org/10.1101/gad.1301205

Candrian U, Luethy J, Graf U, Schlatter CH (1984) MUTAGENIC ACTIVITY OF THE PYRROLIZIDINE ALKALOIDS SENECIPHYLLINE AND SENKIRKINE IN DROSOPHILA AND THEIR TRANSFER INTO RAT MILK*. Fd Chem Toxic 22:223–225

Carusillo A, Mussolino C (2020) DNA Damage: From Threat to Treatment. Cells 9:. https://doi.org/10.3390/cells9071665

Chan PC, Mahler J, Bucher JR, et al (1994) TOXICITY AND CARCINOGENICITY OF RIDDELLIINE FOLLOWING 13 WEEKS OF TREATMENT TO RATS AND MICE. Toxicon 32:891–908

Chanoux RA, Yin B, Urtishak KA, et al (2009) ATR and H2AX cooperate in maintaining genome stability under replication stress. Journal of Biological Chemistry 284:5994–6003. https://doi.org/10.1074/jbc.M806739200

Chen L, Liu S, Tao Y (2020) Regulating tumor suppressor genes: post-translational modifications. Signal Transduct Target Ther 5

Chen L, Zhang B, Liu J, et al (2018) Pharmacokinetics and Bioavailability Study of Monocrotaline in Mouse Blood by Ultra-Performance Liquid Chromatography-Tandem Mass Spectrometry. Biomed Res Int 2018:. https://doi.org/10.1155/2018/1578643

Chen L, Zhang Q, Yi Z, et al (2022a) Risk Assessment of (Herbal) Teas Containing Pyrrolizidine Alkaloids (PAs) Based on Margin of Exposure Approach and Relative Potency (REP) Factors. Foods 11:. https://doi.org/10.3390/foods11192946

Chen M, Li L, Zhong D, et al (2016) 9-Glutathionyl-6,7-dihydro-1-hydroxymethyl-5H-pyrrolizine Is the Major Pyrrolic Glutathione Conjugate of Retronecine-Type Pyrrolizidine Alkaloids in Liver Microsomes and in Rats. Chem Res Toxicol 29:180–189. https://doi.org/10.1021/acs.chemrestox.5b00427

Chen T, Mei N, Fu PP (2010) Genotoxicity of pyrrolizidine alkaloids. Journal of Applied Toxicology 30:183–196

Chen Y, Tang Y, Liu P, et al (2023) Species difference in toxicokinetics and safety assessment of senecionine N-oxide in a UDP-glucuronosyltransferase 1A4 humanized mouse model. Chem Biol Interact 380:. https://doi.org/10.1016/j.cbi.2023.110505

Chen Y, Wang WQ, Jia XL, et al (2022b) Firm evidence for the detoxification of senecionine-induced hepatotoxicity via N-glucuronidation in UGT1A4–humanized transgenic mice. Food and Chemical Toxicology 165:. https://doi.org/10.1016/j.fct.2022.113185

Chou MW, Jian Y, Williams LD, et al (2003) Identification of DNA adducts derived from riddelliine, a carcinogenic pyrrolizidine alkaloid. Chem Res Toxicol 16:1130–1137. https://doi.org/10.1021/tx030018y

Chung WG, Miranda CL, Buhler DR (1995) A cytochrome p4502b form is the major bioactivation enzyme for the pyrrolizidine alkaloid senecionine in Guinea pig. Xenobiotica 25:929–939. https://doi.org/10.3109/00498259509046664

Clark AM (1976) NATURALLY OCCURRING MUTAGENS *. Mutat Res 32:361–374

Clark DAM (1959) MUTAGENIC ACTIVITY OF THE ALKALOID HELIOTRINE IN DROSOPHILA. Nature 183:

Colegate SM, Boppré M, Monzón J, Betz JM (2015) Pro-toxic dehydropyrrolizidine alkaloids in the traditional Andean herbal medicine “asmachilca.” J Ethnopharmacol 172:179–194. https://doi.org/10.1016/j.jep.2015.06.012

Collins A, Møller P, Gajski G, et al (2023) Measuring DNA modifications with the comet assay: a compendium of protocols. Nat Protoc 18:929–989

Coon EA, Benarroch EE (2018) DNA damage response selected review and neurologic implications. Neurology 90:367–376. https://doi.org/10.1212/WNL.0000000000004989

Cotta-Ramusino C, McDonald ER, Hurov K, et al (2011) A DNA damage response screen identifies RHINO, a 9-1-1 and topBP1 interacting protein required for ATR signaling. Science (1979) 332:1313–1317. https://doi.org/10.1126/science.1203430

Coulombe RA, Drew GL, Stermitz FR (1999) Pyrrolizidine Alkaloids Crosslink DNA with Actin. Toxicol Appl Pharmacol 154:198–202

D’Arcy MS (2019) Cell death: a review of the major forms of apoptosis, necrosis and autophagy. Cell Biol Int 43:582–592. https://doi.org/10.1002/cbin.11137

Davis AJ, Chi L, So S, et al (2014) BRCA1 modulates the autophosphorylation status of DNA-PKcs in S phase of the cell cycle. Nucleic Acids Res 42:11487–11501. https://doi.org/10.1093/nar/gku824

De Jesus Inacio L, Lanza I, Merlanti R, et al (2020) Discriminant analysis of pyrrolizidine alkaloid contamination in bee pollen based on near-infrared data from lab-stationary and portable spectrometers. European Food Research and Technology 246:2471–2483. https://doi.org/10.1007/s00217-020-03590-0

Deleve LD, Ito Y, Bethea NW, et al (2003a) Embolization by sinusoidal lining cells obstructs the microcirculation in rat sinusoidal obstruction syndrome. Am J Physiol Gastrointest Liver Physiol 284:. https://doi.org/10.1152/ajpgi.00526.2002.-Mechanisms

DeLeve LD, Shulman HM, McDonald GB (2002) Toxic Injury to Hepatic Sinusoids: Sinusoidal Obstruction Syndrome (Veno-Occlusive Disease). Semin Liver Dis 22:

Deleve LD, Wang X, Kanel GC, et al (2003b) Decreased hepatic nitric oxide production contributes to the development of rat sinusoidal obstruction syndrome. Hepatology 38:900–908. https://doi.org/10.1002/hep.1840380416

Deleve LD, Wang X, Tsai J, et al (2003c) Sinusoidal obstruction syndrome (veno-occlusive disease) in the rat is prevented by matrix metalloproteinase inhibition. Gastroenterology 125:882–890. https://doi.org/10.1016/S0016-5085(03)01056-4

Deng J, Wang P, Chen X, et al (2018) FUS interacts with ATP synthase beta subunit and induces mitochondrial unfolded protein response in cellular and animal models. Proc Natl Acad Sci U S A 115:E9678–E9686. https://doi.org/10.1073/pnas.1806655115

Di Masi A, Viganotti M, Antoccia A, et al (2010) Characterization of HUH6, HEP3B, HEPG2 and HLE liver cancer cell lines by WNT/Q- catenin pathway, microrna expression and protein expression profile. Cell Mol Biol 56:. https://doi.org/10.1170/149

Duringer JM, Buhler DR, Craig AM (2004) Comparison of hepatic in vitro metabolism of the pyrrolizidine alkaloid senecionine in sheep and cattle. Am J Vet Res 11:1563–1572. https://doi.org/10.2460/ajvr.2004.65.1563.

Dusemund B, Nowak N, Sommerfeld C, et al (2018) Risk assessment of pyrrolizidine alkaloids in food of plant and animal origin. Food and Chemical Toxicology 115:63–72. https://doi.org/10.1016/j.fct.2018.03.005

Dusemund B, Rietjens IMCM, Cartus A, et al (2017) Pflanzliche Kontaminanten in Lebensmitteln: Vorkommen, Wirkung und Risikobewertung. Bundesgesundheitsblatt Gesundheitsforschung Gesundheitsschutz 60:728–736

Ebmeyer J, Braeuning A, Glatt H, et al (2019) Human CYP3A4-mediated toxification of the pyrrolizidine alkaloid lasiocarpine. Food and Chemical Toxicology 130:79–88. https://doi.org/10.1016/j.fct.2019.05.019

Ebmeyer J, Rasinger JD, Hengstler JG, et al (2020) Hepatotoxic pyrrolizidine alkaloids induce DNA damage response in rat liver in a 28-day feeding study. Arch Toxicol 94:1739–1751. https://doi.org/10.1007/s00204-020-02779-2

EC Regulation 2023/ 915 COMMISSION REGULATION (EU) 2023/915 of 25 April 2023 on maximum levels for certain contaminants in food and repealing Regulation (EC) No 1881/2006, consolidated version: 22.07.2024

EFSA (2011) (European Food Safety Authority: Scientific Panel on Contaminants in the Food Chain (CONTAM)): Scientific Opinion on Pyrrolizidine alkaloids in food and feed. EFSA Journal 9 (11), 2406.

EFSA (2017a) (European Food Safety Authority: Scientific Committee), Update: use of the benchmark dose approach in risk assessment. EFSA Journal 15 (1), 4658

EFSA (2017b) (European Food Safety Authority: Scientific Panel on Contaminants in the Food Chain (CONTAM)): Risks for human health related to the presence of pyrrolizidine alkaloids in honey, tea, herbal infusions and food supplements. EFSA Journal 15 (7), 4908. Wiley-Blackwell Publishing Ltd

Ellison V, Stillman B (2003) Biochemical characterization of DNA damage checkpoint complexes: Clamp loader and clamp complexes with specificity for 5′ recessed DNA. PLoS Biol 1:. https://doi.org/10.1371/journal.pbio.0000033

EMA (2021) (European Medicines Agency)/ Committee on Herbal Medicinal Products (HMPC): Public statement on the use of herbal medicinal products 1 containing toxic, unsaturated pyrrolizidine alkaloids (PAs) including recommendations regarding contamination of herbal medicinal products with PAs, EMA/HMPC/893108/2011 Rev. 1

EMA (2012) ICH guideline S2 (R1) on genotoxicity testing and data interpretation for pharmaceuticals intended for human use. EMA/CHMP/ICH/126642/2008

Enge AM, Kaltner F, Gottschalk C, et al (2021) Active transport of hepatotoxic pyrrolizidine alkaloids in heparg cells. Int J Mol Sci 22:. https://doi.org/10.3390/ijms22083821

Enge AM, Kaltner F, Gottschalk C, et al (2022) Organic Cation Transporter I and Na+/taurocholate Co-Transporting Polypeptide are Involved in Retrorsine- and Senecionine-Induced Hepatotoxicity in HepaRG cells. Mol Nutr Food Res 66:. https://doi.org/10.1002/mnfr.202100800

Estep JE, Lamé MW, Morin D, et al (1990) [14C]MONOCROTALINE KINETICS AND METABOLISM IN THE RAT. Drug metabolism and disposition 19:

Feng J, Wakeman T, Yong S, et al (2009) Protein Phosphatase 2A-Dependent Dephosphorylation of Replication Protein A Is Required for the Repair of DNA Breaks Induced by Replication Stress. Mol Cell Biol 29:5696–5709. https://doi.org/10.1128/mcb.00191-09

Fraczek J, Bolleyn J, Vanhaecke T, et al (2013) Primary hepatocyte cultures for pharmaco-toxicological studies: At the busy crossroad of various anti-dedifferentiation strategies. Arch Toxicol 87:577–610

Franco RS (2012) Measurement of red cell lifespan and aging. Transfusion Medicine and Hemotherapy 39:302–307

Frei H, Luthy J, Brauchli J, et al (1992) STRUCTURE/ACTIVITY RELATIONSHIPS OF THE GENOTOXIC POTENCIES OF SIXTEEN PYRROLIZIDINE ALKALOIDS ASSAYED FOR THE INDUCTION OF SOMATIC MUTATION AND RECOMBINATION IN WING CELLS OF DROSOPHILA MELANOGASTER. Chem-Biol Interactions 83–1992

Frötschl R (2015) Experiences with the in vivo and in vitro comet assay in regulatory testing. Mutagenesis 30:51–57. https://doi.org/10.1093/mutage/geu069

Fu PP (2017) Pyrrolizidine alkaloids: Metabolic activation pathways leading to liver tumor initiation. Chem Res Toxicol 30:81–93

Fu PP, Chou MW, Churchwell M, et al (2010a) High-performance liquid chromatography electrospray ionization tandem mass spectrometry for the detection and quantitation of pyrrolizidine alkaloid-derived DNA adducts in vitro and in viwo. Chem Res Toxicol 23:637–652. https://doi.org/10.1021/tx900402x

Fu PP, Chou MW, Churchwell M, et al (2010b) High-performance liquid chromatography electrospray ionization tandem mass spectrometry for the detection and quantitation of pyrrolizidine alkaloid-derived DNA adducts in vitro and in viwo. Chem Res Toxicol 23:637–652. https://doi.org/10.1021/tx900402x

Fu PP, Xia Q, Lin G, Chou MW (2004) Pyrrolizidine Alkaloids - Genotoxicity, Metabolism Enzymes, Metabolic Activation, and Mechanisms. Drug Metab Rev 36:1–55

Fu PP, Yang Y-C, Xia Q, et al (2002) Pyrrolizidine Alkaloids-Tumorigenic Components in Chinese Herbal Medicines and Dietary Supplements. J Food Drug Anal 10:198–211

Gao L, Rutz L, Schrenk D (2020) Structure-dependent hepato-cytotoxic potencies of selected pyrrolizidine alkaloids in primary rat hepatocyte culture. Food Chem Toxicol 135:. https://doi.org/10.1016/j.fct.2019.110923

Geburek I, Preiss-Weigert A, Lahrssen-Wiederholt M, et al (2020) In vitro metabolism of pyrrolizidine alkaloids – Metabolic degradation and GSH conjugate formation of different structure types. Food and Chemical Toxicology 135:. https://doi.org/10.1016/j.fct.2019.110868

Gerets HHJ, Tilmant K, Gerin B, et al (2012) Characterization of primary human hepatocytes, HepG2 cells, and HepaRG cells at the mRNA level and CYP activity in response to inducers and their predictivity for the detection of human hepatotoxins. Cell Biol Toxicol 28:69–87. https://doi.org/10.1007/s10565-011-9208-4

Giglia-Mari G, Zotter A, Vermeulen W (2011) DNA damage response. Cold Spring Harb Perspect Biol 3:1–19. https://doi.org/10.1101/cshperspect.a000745

Gimmler-Luz MC, Erdtmann B, Balbueno RA (1990) The effect of pyrrolizidine alkaloid integerrimine on the chromosomes of mouse bone marrow cells. Mutat Res 241:297–304

Glück J, Waizenegger J, Braeuning A, Hessel-Pras S (2021) Pyrrolizidine alkaloids induce cell death in human heparg cells in a structure-dependent manner. Int J Mol Sci 22:1–12. https://doi.org/10.3390/ijms22010202

Gómez-Lechón MJ, Donato MT, Castell J V, Jover R (2004) Human Hepatocytes in Primary Culture: The Choice to Investigate Drug Metabolism in Man. Curr Drug Metab 5:443–462

Gorecki L, Andrs M, Korabecny J (2021) Clinical candidates targeting the atr–chk1–wee1 axis in cancer. Cancers (Basel) 13:1–23. https://doi.org/10.3390/cancers13040795

Gottschalk C, Kaltner F, Zimmermann M, et al (2020) Spread of jacobaea vulgaris and occurrence of pyrrolizidine alkaloids in regionally produced honeys from northern Germany: Inter- And intra-site variations and risk assessment for special consumer groups. Toxins (Basel) 12:. https://doi.org/10.3390/toxins12070441

Griffin DS, Segall HJ (1987) Lipid Peroxidation and Cellular Damage caused by the pyrrolizidine alkaloids senecionine, the alkenal trans-4-hydroxy-2-hexenal, and related alkenals. Cell Biol Toxicol 3:

Griffin DS, Segall HJ (1986) Genotoxicity and Cytotoxicity of Selected Pyrrolizidine Alkaloids, A Possible Alkenal Metabolite of the Alkaloids, and Related Alkenals. Toxicol Appl Pharmacol 86:227–234

Günthardt BF, Schönsee CD, Hollender J, et al (2020) “Is there anybody else out there?”-First Insights from a Suspect Screening for Phytotoxins in Surface Water. Chimia (Aarau) 74:129–135. https://doi.org/10.3929/ethz-b-000407110

Guo Y, Xiao D, Yang X, et al (2019) Prenatal exposure to pyrrolizidine alkaloids induced hepatotoxicity and pulmonary injury in fetal rats. Reproductive Toxicology 85:34–41. https://doi.org/10.1016/j.reprotox.2019.02.006

Haahr P, Hoffmann S, Tollenaere MAX, et al (2016) Activation of the ATR kinase by the RPA-binding protein ETAA1. Nat Cell Biol 18:1196–1207. https://doi.org/10.1038/ncb3422

Haas M, Ackermann G, Küpper JH, et al (2023a) OCT1-dependent uptake of structurally diverse pyrrolizidine alkaloids in human liver cells is crucial for their genotoxic and cytotoxic effects. Arch Toxicol 97:3259–3271. https://doi.org/10.1007/s00204-023-03591-4

Haas M, Wirachowski K, Thibol L, et al (2023b) Potency ranking of pyrrolizidine alkaloids in metabolically competent human liver cancer cells and primary human hepatocytes using a genotoxicity test battery. Arch Toxicol 97:1413–1428. https://doi.org/10.1007/s00204-023-03482-8

Hadi NSA, Bankoglu EE, Schott L, et al (2021) Genotoxicity of selected pyrrolizidine alkaloids in human hepatoma cell lines HepG2 and Huh6. Mutat Res Genet Toxicol Environ Mutagen 861–862:. https://doi.org/10.1016/j.mrgentox.2020.503305

Hama JR, Strobel BW (2021) Occurrence of pyrrolizidine alkaloids in ragwort plants, soils and surface waters at the field scale in grassland. Science of the Total Environment 755:. https://doi.org/10.1016/j.scitotenv.2020.142822

Hammer H, Schmidt F, Marx-Stoelting P, et al (2021) Cross-species analysis of hepatic cytochrome P450 and transport protein expression. Arch Toxicol 95:117–133. https://doi.org/10.1007/s00204-020-02939-4

Harper JW, Elledge SJ, Keyomarsi K, et al (1995) Inhibition of Cyclin-dependent Kinases by p21. Mol Biol Cell 6:387–400

Hartmann T, Witte L (1995) Chemistry, Biology and Chemoecology of the Pyrrolizidine Alkaloids. pp 155–233

Hartwig A, Arand M, Epe B, et al (2020) Mode of action-based risk assessment of genotoxic carcinogens. Arch Toxicol 94:1787–1877

He X, Ma L, Xia Q, Fu PP (2016) 7-N-Acetylcysteine-pyrrole conjugate—A potent DNA reactive metabolite of pyrrolizidine alkaloids. J Food Drug Anal 24:682–694. https://doi.org/10.1016/j.jfda.2016.08.001

He X, Xia Q, Woodling K, et al (2017) Pyrrolizidine alkaloid-derived DNA adducts are common toxicological biomarkers of pyrrolizidine alkaloid N-oxides. J Food Drug Anal 25:984–991. https://doi.org/10.1016/j.jfda.2017.09.001

He X, Xia Q, Wu Q, et al (2019) Primary and secondary pyrrolic metabolites of pyrrolizidine alkaloids form DNA adducts in human A549 cells. Toxicology in Vitro 54:286–294. https://doi.org/10.1016/j.tiv.2018.10.009

He X, Xia Q, Zhao Y, Fu PP (2020a) 1-Formyl-7-hydroxy-6,7-dihydro-5 H-pyrrolizine (1-CHO-DHP)-Cysteine Conjugates: Metabolic Formation and Binding to Cellular DNA. Chem Res Toxicol 33:2139–2146. https://doi.org/10.1021/acs.chemrestox.0c00143

He X, Xia Q, Zhao Y, Fu PP (2020b) 1-Formyl-7-hydroxy-6,7-dihydro-5 H-pyrrolizine (1-CHO-DHP)-Cysteine Conjugates: Metabolic Formation and Binding to Cellular DNA. Chem Res Toxicol 33:2139–2146. https://doi.org/10.1021/acs.chemrestox.0c00143

He Y, Lian W, Ding L, et al (2021a) Lung injury induced by pyrrolizidine alkaloids depends on metabolism by hepatic cytochrome P450s and blood transport of reactive metabolites. Arch Toxicol 95:103–116. https://doi.org/10.1007/s00204-020-02921-0

He Y, Ma J, Fan X, et al (2021b) The key role of gut–liver axis in pyrrolizidine alkaloid-induced hepatotoxicity and enterotoxicity. Acta Pharm Sin B 11:3820–3835. https://doi.org/10.1016/j.apsb.2021.07.013

He Y, Shi M, Wu X, et al (2021c) Mutational Signature Analysis Reveals Widespread Contribution of Pyrrolizidine Alkaloid Exposure to Human Liver Cancer. Hepatology 74:2021. https://doi.org/10.1002/hep.31723/suppinfo

He Y, Zhu L, Ma J, Lin G (2021d) Metabolism-mediated cytotoxicity and genotoxicity of pyrrolizidine alkaloids. Arch Toxicol 95:1917–1942

He YQ, Yang L, Liu HX, et al (2010) Glucuronidation, a new metabolic pathway for pyrrolizidine alkaloids. Chem Res Toxicol 23:591–599. https://doi.org/10.1021/tx900328f

Hediger MA, Clémençon B, Burrier RE, Bruford EA (2013) The ABCs of membrane transporters in health and disease (SLC series): Introduction. Mol Aspects Med 34:95–107

Helmy A (2006) Review article: Updates in the pathogenesis and therapy of hepatic sinusoidal obstruction syndrome. Aliment Pharmacol Ther 23:11–25

Hengstler JG, Utesch D, Steinberg P, et al (2000) CRYOPRESERVED PRIMARY HEPATOCYTES AS A CONSTANTLY AVAILABLE IN VITRO MODEL FOR THE EVALUATION OF HUMAN AND ANIMAL DRUG METABOLISM AND ENZYME INDUCTION*

Hermeking H, Lengauer C, Polyak K, et al (1997) 14-3-3r Is a p53-Regulated Inhibitor of G2/M Progression. Mol Cell 1:3–11

Herzog N, Katzenberger N, Martin F, et al (2015) Generation of cytochrome P450 3A4-overexpressing HepG2 cell clones for standardization of hepatocellular testosterone 6β-hydroxylation activity. J Cell Biotechnol 1:15–26. https://doi.org/10.3233/jcb-15002

Hessel S, Gottschalk C, Schumann D, et al (2014) Structure-activity relationship in the passage of different pyrrolizidine alkaloids through the gastrointestinal barrier: ABCB1 excretes

heliotrine and echimidine. Mol Nutr Food Res 58:995–1004. https://doi.org/10.1002/mnfr.201300707

Hickson I, Zhao Y, Richardson CJ, et al (2004) Identification and Characterization of a Novel and Specific Inhibitor of the Ataxia-Telangiectasia Mutated Kinase ATM. Cancer Res 9152–9159

Hilgendorf C, Ahlin G, Seithel A, et al (2007) Expression of thirty-six drug transporter genes in human intestine, liver, kidney, and organotypic cell lines. Drug Metabolism and Disposition 35:1333–1340. https://doi.org/10.1124/dmd.107.014902

Hodgson Ernest (2010) A textbook of modern toxicology, 4th edn. Wiley

Hong HL, Ton T V., Devereux TR, et al (2003) Chemical-specific alterations in ras, p53, and β-catenin genes in hemangiosarcomas from B6C3F1 mice exposed to o-nitrotoluene or riddelliine for 2 years. Toxicol Appl Pharmacol 191:227–234. https://doi.org/10.1016/S0041-008X(03)00165-0

Hosokawa M, Maki T, Satohty T (1990) Characterization of Molecular Species of Liver Microsomal Carboxylesterases of Several Animal Species and Humans

Huan J-Y, Miranda CL, Buhler DR, Cheeke PR (1998) Species differences in the hepatic microsomal enzyme metabolism of the pyrrolizidine alkaloids. Toxicol Lett 99:127–137

Huang RX, Zhou PK (2020) DNA damage response signaling pathways and targets for radiotherapy sensitization in cancer. Signal Transduct Target Ther 5:. https://doi.org/10.1038/s41392-020-0150-x

Huxtable RJ (1990) ACTIVATION AND PULMONARY TOXICITY OF PYRROLIZIDINE ALKALOIDS

IARC (2020) IARC Monographs on the evaluation of the carcinogenic risk of chemicals to man: some naturally occurring substances, vol 10

IARC (1976) IARC Monographs on the evaluation of carcinogenic risk of chemicals to man. In: Some Naturally Occurring Substances, vol 10.

IARC (2002) IARC Monographs on the evaluation of carcinogenic risks to humans. In: Some Traditional Herbal Medicines, Some Mycotoxins, Naphthalene and Styrene, vol 82.

IARC (1987) IARC Monographs on the Evaluation of Carcinogenic Risks to Humans. Suppl. 7: Overall evaluations of carcinogenicity - An updating of IARC Monographs Volumes 1 to 42

IARC (1983) IARC Monogr. Eval. Carcinog. Risk Chem. Humans. In: Some Food Additives, Feed Additives and Naturally Occurring Substances, vol 31

Jackson SP, Bartek J (2009) The DNA-damage response in human biology and disease. Nature 461:1071–1078

JECFA (2020) JECFA (World Health Organization: Joint FAO/WHO Expert Committee on Food Additives) (2020). Safety evaluation of certain food additives and contaminants: prepared by the eightieth meeting of the Joint FAO/WHO Expert Committee on Food Additives (JECFA). Supplement 2: Pyrrolizidine alkaloids Licence: CC BY-NC-SA 3.0 IGO. World Health Organization

Jedlinszki N, Balázs B, Csányi E, Csupor D (2017) Penetration of lycopsamine from a comfrey ointment through human epidermis. Regulatory Toxicology and Pharmacology 83:1–4. https://doi.org/10.1016/j.yrtph.2016.11.015

Jiricny J (2006) The multifaceted mismatch-repair system. Nat Rev Mol Cell Biol 7:335–346. https://doi.org/10.1038/nrm1907

Jung JH, Lee H, Zeng SX, Lu H (2020) RBM10, a new regulator of p53. Cells 9:1–13

Jungermann K (1986) Functional Heterogeneity of Periportal and Perivenous Hepatocytes. Enzyme 35:161–180

Jungermann K, Katz N (1982) Functional Hepatocellular Heterogeneity. Hepatology 2:385S-395S. https://doi.org/10.1002/hep.1840020316

Kaltner F, Rychlik M, Gareis M, Gottschalk C (2020) Occurrence and risk assessment of pyrrolizidine alkaloids in spices and culinary herbs from various geographical origins. Toxins (Basel) 12:. https://doi.org/10.3390/toxins12030155

Kang Y, Han YG, Khim KW, et al (2023) Alteration of replication protein A binding mode on single-stranded DNA by NSMF potentiates RPA phosphorylation by ATR kinase. Nucleic Acids Res 51:7936–7950. https://doi.org/10.1093/nar/gkad543

Kell DB, Oliver SG (2014) How drugs get into cells: tested and testable predictions to help discriminate between transporter-mediated uptake and lipoidal bilayer diffusion. Front Pharmacol 5:. https://doi.org/10.3389/fphar.2014.00231

Kim H-Y, Stermitz FR, Coulombe RA (1995) Pyrrolizidine alkaloid-induced DNA-protein cross-links. Carcinogenesis 16:2691–2697

Kim H-Y, Stermitz FR, Li JK-K, Coulombe RA (1999) Comparative DNA Cross-linking by Activated Pyrrolizidine Alkaloids. Food and Chemical Toxicology 37:619–625

Kisielius V, Hama JR, Skrbic N, et al (2020) The invasive butterbur contaminates stream and seepage water in groundwater wells with toxic pyrrolizidine alkaloids. Sci Rep 10:. https://doi.org/10.1038/s41598-020-76586-1

Koepsell H (2013) Polyspecific organic cation transporters and their biomedical relevance in kidney. Curr Opin Nephrol Hypertens 22:533–538

Koepsell H (2020) Organic cation transporters in health and disease. Pharmacol Rev 72:253–319. https://doi.org/10.1124/pr.118.015578

Kolrep F, Numata J, Kneuer C, et al (2018) In vitro biotransformation of pyrrolizidine alkaloids in different species. Part I: Microsomal degradation. Arch Toxicol 92:1089–1097. https://doi.org/10.1007/s00204-017-2114-7

Konstandi M, Johnson EO (2023) Age-related modifications in CYP-dependent drug metabolism: role of stress. Front Endocrinol (Lausanne) 14:. https://doi.org/10.3389/fendo.2023.1143835

Kowalczykowski SC (2015) An overview of the molecular mechanismsof recombinational DNA repair. Cold Spring Harb Perspect Biol 7

Kozlov S V., Graham ME, Jakob B, et al (2011) Autophosphorylation and ATM activation: Additional sites add to the complexity. Journal of Biological Chemistry 286:9107–9119. https://doi.org/10.1074/jbc.M110.204065

Krupina K, Goginashvili A, Cleveland DW (2021) Causes and consequences of micronuclei. Curr Opin Cell Biol 70:91–99. https://doi.org/10.1016/j.ceb.2021.01.004

Kumagai A, Dunphy WG (2000) Claspin, a Novel Protein Required for the Activation of Chk1 during a DNA Replication Checkpoint Response in Xenopus Egg Extracts. Mol Cell 6:839–849

Lachenmeier DW, Rehm J (2015) Comparative risk assessment of alcohol, tobacco, cannabis and other illicit drugs using the margin of exposure approach. Sci Rep 5:. https://doi.org/10.1038/srep08126

Lamé MW, Jones AD, Morin D, et al (1997) Association of Dehydromonocrotaline with Rat Red Blood Cells

Lee YC, Zhou Q, Chen J, Yuan J (2016) RPA-Binding Protein ETAA1 Is an ATR Activator Involved in DNA Replication Stress Response. Current Biology 26:3257–3268. https://doi.org/10.1016/j.cub.2016.10.030

Nielsen TL, Rasmussen BB, Flinois J, et al (1999) In Vitro Metabolism of Quinidine: The (3S)-3-Hydroxylation of Quinidine Is a Specific Marker Reaction for Cytochrome P-4503A4 Activity in Human Liver Microsomes. J Pharmacol Exp Ther 289:31–37

Leschziner GD, Andrew T, Pirmohamed M, Johnson MR (2007) ABCB1 genotype and PGP expression, function and therapeutic drug response: A critical review and recommendations for future research. Pharmacogenomics Journal 7:154–179

Lester C, Troutman J, Obringer C, et al (2019) Intrinsic relative potency of a series of pyrrolizidine alkaloids characterized by rate and extent of metabolism. Food and Chemical Toxicology 131:. https://doi.org/10.1016/j.fct.2019.05.031

Letsyo E, Adams ZS, Dzikunoo J, Asante-Donyinah D (2021) Uptake and accumulation of pyrrolizidine alkaloids in the tissues of maize (Zea mays L.) plants from the soil of a 4-year-old Chromolaena odorata dominated fallow farmland. Chemosphere 270:. https://doi.org/10.1016/j.chemosphere.2020.128669

Letsyo E, Jerz G, Winterhalter P, et al (2017) Pyrrolizidine alkaloids in floral honeys of tropical Ghana: a health risk assessment. Food Addit Contam Part B Surveill 10:300–310. https://doi.org/10.1080/19393210.2017.1354336

Letsyo E, Madilo FK, Effah-Manu L (2024) Pyrrolizidine alkaloid contamination of food in Africa: A review of current trends and implications. Heliyon 10

Lewis CW, Jin Z, Macdonald D, et al (2017) Prolonged mitotic arrest induced by Wee1 inhibition sensitizes breast cancer cells to paclitaxel. Oncotarget 8:73705–73722

Li J, Zhou M, Lai X, et al (2022) Toxicokinetic and bioavailability studies on retrorsine in mice, and ketoconazole-induced alteration in toxicokinetic properties. Biomedical Chromatography 36:. https://doi.org/10.1002/bmc.5270

Li L, Tu M, Yang X, et al (2014) The contribution of human OCT1, OCT3, and CYP3A4 to nitidine chloride-induced hepatocellular toxicity. Drug Metabolism and Disposition 42:1227–1234. https://doi.org/10.1124/dmd.113.056689

Li LY, Guan Y Di, Chen XS, et al (2021) DNA Repair Pathways in Cancer Therapy and Resistance. Front Pharmacol 11

Li W, Zhao L, Le J, et al (2015a) Evaluation of Tetrahydropalmatine Enantiomers on the Activity of Five Cytochrome P450 Isozymes in Rats Using a Liquid Chromatography / Mass Spectrometric Method and a Cocktail Approach. Chirality 27:551–556. https://doi.org/10.1002/chir.22469

Li X, He X, Chen S, et al (2020) Evaluation of pyrrolizidine alkaloid-induced genotoxicity using metabolically competent TK6 cell lines. Food and Chemical Toxicology 145:. https://doi.org/10.1016/j.fct.2020.111662

Li X, Yang X, Xiang E, et al (2018) Maternal-fetal disposition and metabolism of retrorsine in pregnant rats. Drug Metabolism and Disposition 46:422–428. https://doi.org/10.1124/dmd.117.079186

Li YH, Tai WCS, Xue JY, et al (2015b) Proteomic Study of Pyrrolizidine Alkaloid-Induced Hepatic Sinusoidal Obstruction Syndrome in Rats. Chem Res Toxicol 28:1715–1727. https://doi.org/10.1021/acs.chemrestox.5b00113

Lin T, Zhou L, Chen Z, et al (2023a) Exposure to echimidine impairs the heart development and function of zebrafish larvae. Ecotoxicol Environ Saf 266:. https://doi.org/10.1016/j.ecoenv.2023.115574

Lin T, Zhou L, Chen Z, et al (2023b) Exposure to echimidine impairs the heart development and function of zebrafish larvae. Ecotoxicol Environ Saf 266:. https://doi.org/10.1016/j.ecoenv.2023.115574

Lindahl T (1993) Instability and decay of the primary structure of DNA. Nature 362:709–715

Lindsey-Boltz LA, Kemp MG, Capp C, Sancar A (2015) RHINO forms a stoichiometric complex with the 9-1-1 checkpoint clamp and mediates ATR-Chk1 signaling http://www.tandfonline.com/doi/pdf/10.4161/15384101.2014.967076. Cell Cycle 14:99–108. https://doi.org/10.4161/15384101.2014.967076

Lipinski CA, Lombardo F, Dominy BW, Feeney PJ (2001) Experimental and computational approaches to estimate solubility and permeability in drug discovery and development settings

Lis-Cieplak A, Trześniowska K, Stolarczyk K, Stolarczyk EU (2024) Pyrrolizidine Alkaloids as Hazardous Toxins in Natural Products: Current Analytical Methods and Latest Legal Regulations. Molecules 29

Liu S, Opiyo SO, Manthey K, et al (2012) Distinct roles for DNA-PK, ATM and ATR in RPA phosphorylation and checkpoint activation in response to replication stress. Nucleic Acids Res 40:10780–10794. https://doi.org/10.1093/nar/gks849

Liu X, Pan G (2019) Drug Transporters in Drug Disposition, Effects and Toxicity. Springer

Llovet JM, Kelley RK, Villanueva A, et al (2021) Hepatocellular carcinoma. Nat Rev Dis Primers 7

Long F, Ji J, Wang X, et al (2021) LC–MS/MS method for determination of seneciphylline and its metabolite, seneciphylline N-oxide in rat plasma, and its application to a rat pharmacokinetic study. Biomedical Chromatography 35:. https://doi.org/10.1002/bmc.5145

Louisse J, Rijkers D, Stoopen G, et al (2019) Determination of genotoxic potencies of pyrrolizidine alkaloids in HepaRG cells using the γH2AX assay. Food and Chemical Toxicology 131:. https://doi.org/10.1016/j.fct.2019.05.040

Lu Y, Ma J, Song Z, et al (2018) The role of formation of pyrrole–ATP synthase subunit beta adduct in pyrrolizidine alkaloid-induced hepatotoxicity. Arch Toxicol 92:3403–3414. https://doi.org/10.1007/s00204-018-2309-6

Lu YS, Qiu J, Mu XY, et al (2024) Levels, Toxic Effects, and Risk Assessment of Pyrrolizidine Alkaloids in Foods: A Review. Foods 13

Luo Y, Hurwitz J, Massague J (1995) Cell-cycle inhibition by independent CDK and PCNA binding domains in p21Cip1. Nature 375:159–161

Ma J, Ruan J, Chen X, et al (2019) Pyrrole-Hemoglobin Adducts, a More Feasible Potential Biomarker of Pyrrolizidine Alkaloid Exposure. Chem Res Toxicol 32:1027–1039. https://doi.org/10.1021/acs.chemrestox.8b00369

Maréchal A, Zou L (2013) DNA damage sensing by the ATM and ATR kinases. Cold Spring Harb Perspect Biol 5:. https://doi.org/10.1101/cshperspect.a012716

Maréchal A, Zou L (2015) RPA-coated single-stranded DNA as a platform for post-translational modifications in the DNA damage response. Cell Res 25:9–23. https://doi.org/10.1038/cr.2014.147

Martin PA, Thorburn MJ, Hutchinson S, et al (1972) PRELIMINARY FINDINGS OF CHROMOSOMAL STUDIES ON RATS AND HUMANS WITH VENO-OCCLUSIVE DISEASE. Br J exp Path 53:374–380

Mattocks AR (1986) Chemistry and Toxicology of Pyrrolizidine Alkaloids. Academic Press. London

Mei N, Chou MW, Fu PP, et al (2004a) Differential mutagenicity of riddelliine in liver endothelial and parenchymal cells of transgenic big blue rats. Cancer Lett 215:151–158. https://doi.org/10.1016/j.canlet.2004.06.013

Mei N, Heflich RH, Chou MW, Chen T (2004b) Mutations induced by the carcinogenic pyrrolizidine alkaloid riddelliine in the liver cII gene of transgenic big blue rats. Chem Res Toxicol 17:814–818. https://doi.org/10.1021/tx049955b

Merz KH, Schrenk D (2016) Interim relative potency factors for the toxicological risk assessment of pyrrolizidine alkaloids in food and herbal medicines. Toxicol Lett 263:44–57

Mimmler M, Peter S, Kraus A, et al (2016) DNA damage response curtails detrimental replication stress and chromosomal instability induced by the dietary carcinogen PhIP. Nucleic Acids Res 44:10259–10276. https://doi.org/10.1093/nar/gkw791

Miranda CL, Chung W, Reed RE, et al (1991) Flavin-containing monooxygenase: A major detoxifying enzyme for the pyrrolizidine alkaloid senecionine in guinea pig tissues. Biochem Biophys Res Commun 178:546–552

Mirsalis JC (1987) IN VIVO MEASUREMENT OF UNSCHEDULED DNA SYNTHESIS AND S-PHASE SYNTHESIS AS AN INDICATOR OF HEPATOCARCINOGENESIS IN RODENTS

Mirsalis JC, Steinmetz KL, Blazak WF, Spalding JW (1993) Evaluation of the potential of riddelliine to induce unscheduled DNA synthesis, S-phase synthesis, or micronuclei following in vivo treatment with multiple doses. Environ Mol Mutagen 21:265–271. https://doi.org/10.1002/em.2850210310

Mishra V, Heath RJ (2021) Structural and biochemical features of human serum albumin essential for eukaryotic cell culture. Int J Mol Sci 22

Modrich P (2006) Mechanisms in eukaryotic mismatch repair. Journal of Biological Chemistry 281:30305–30309. https://doi.org/10.1074/jbc.R600022200

Mohty M, Malard F, Abecassis M, et al (2015) Sinusoidal obstruction syndrome/veno-occlusive disease: Current situation and perspectives - A position statement from the European Society for Blood and Marrow Transplantation (EBMT). Bone Marrow Transplant 50:781–789

Mordes DA, Glick GG, Zhao R, Cortez D (2008) TopBP1 activates ATR through ATRIP and a PIKK regulatory domain. Genes Dev 22:1478–1489. https://doi.org/10.1101/gad.1666208

Moreira R, Pereira DM, Valentão P, Andrade PB (2018) Pyrrolizidine alkaloids: Chemistry, pharmacology, toxicology and food safety. Int J Mol Sci 19

Morse BL, Fallon JK, Kolur A, et al (2021) Comparison of Hepatic Transporter Tissue Expression in Rodents and Interspecies Hepatic OCT1 Activity. AAPS Journal 23:. https://doi.org/10.1208/s12248-021-00583-z

Mueller L, Kasper P, Kaufmann G (1992) The clastogenic potential in vitro of pyrrolizidine alkaloids employing hepatocyte metabolism. Mutat Res 282:169–176

Mueller-Tegethoff K, Kasper P, Mueller L (1995) Evaluation studies on the in vitro rat hepatocyte micronucleus assay. Mutat Res 335:293–307

Mueller-Tegethoff K, Kersten B, Kasper P, Mueller L (1997) Application of the in vitro rat hepatocyte micronucleus assay in genetic toxicology testing. Mutat Res 392:125–138

Muetterlein R, Arnold C-G (1993) Investigations Concerning the Content and the Pattern of Pyrrolizidine Alkaloids in Symphytum officinale L. PZ Wissenschaft 119–119

Mulder PPJ, López P, Castelari M, et al (2018) Occurrence of pyrrolizidine alkaloids in animal- and plant-derived food: results of a survey across Europe. Food Addit Contam Part A Chem Anal Control Expo Risk Assess 35:118–133. https://doi.org/10.1080/19440049.2017.1382726

Mulder PPJ, Sánchez PL, These A, et al (2015) Occurrence of Pyrrolizidine Alkaloids in food. Wiley

Mullenders L (2015) DNA damage mediated transcription arrest: Step back to go forward. DNA Repair (Amst) 36:28–35

Nastasi C, Mannarino L, D'incalci M (2020) DNA damage response and immune defense. Int J Mol Sci 21:1–28. https://doi.org/10.3390/ijms21207504

NCI (1978) Bioassay of Lasiocarpine for Possible Carcinogenicity. Carcinogenesis Technical Report Series 39 (NCI-CG-TR-39; DHEW Publication No. (NIH) 78–839)

Nickoloff JA, Sharma N, Taylor L, et al (2022) Nucleases and Co-Factors in DNA Replication Stress Responses. DNA 2:68–85. https://doi.org/10.3390/dna2010006

Nikolova T, Dvorak M, Jung F, et al (2014) The gammaH2AX assay for genotoxic and nongenotoxic agents: comparison of H2AX phosphorylation with cell death response. Toxicol Sci 140:103–117

NTP (2003) Technical Report on the Toxicology and Carcinogenesis Studies of Riddelliine (CAS No. 23246-96-0) in F344/N Rats and B6C3F1 Mice (Gavage Studies). NTP Technical Report Series 508 (NIH Publication No. 03-4442). .

NTP (1987) BIOASSAY OF LASIOCARPINE FOR POSSIBLE CARCINOGENICITY, Technical Report Series No. 39: Lasiocarpine (CASRN 303-34-4)

Pan Y, Ma J, Zhao H, et al (2023) Hepatotoxicity screening and ranking of structurally different pyrrolizidine alkaloids in zebrafish. Food and Chemical Toxicology 178:. https://doi.org/10.1016/j.fct.2023.113903

Peloso M, Minkoumba Sonfack G, Paduano S, et al (2023) Pyrrolizidine Alkaloids in Food on the Italian Market. Molecules 28:. https://doi.org/10.3390/molecules28145346

Pereira TN, Webb RI, Reilly PEB, et al (1998) Dehydromonocrotaline generates sequence-selective N-7 guanine alkylation and heat and alkali stable multiple fragment DNA crosslinks. Nucleic Acids Res 26:5441–5447

Petry TW, Bowden GT, Huxtable RJ, Sipes IG (1984) Characterization of Hepatic DMA Damage Induced in Rats by the Pyrrolizidine Alkaloid Monocrotaline. Cancer Res 44:1505–1509

Prakash AS, Pereira TN, Reilly PEB, Seawright AA (1999) Pyrrolizidine alkaloids in human diet. Mutat Res 443:1999–53

Ramsdell HS, Buhler DR (1987) MICROSOMAL METABOLISM OF PYRROLIZIDINE ALKALOIDS: N-OXIDATION OF SENECIPHYLLINE AND SENECIONINE (Senecio jacobaea; cytochrome P-450; flavin-containing monooxygenase)

Rao R (2009) Endotoxemia and gut barrier dysfunction in alcoholic liver disease. Hepatology 50:638–644. https://doi.org/10.1002/hep.23009

Rizzo S, Celano R, Piccinelli AL, et al (2023) An analytical platform for the screening and identification of pyrrolizidine alkaloids in food matrices with high risk of contamination. Food Chem 406:. https://doi.org/10.1016/j.foodchem.2022.135058

Roeder E (2000) Medicinal plants in China containing pyrrolizidine alkaloids. Pharmazie 10:711–726

Roos WP, Kaina B (2013) DNA damage-induced cell death: From specific DNA lesions to the DNA damage response and apoptosis. Cancer Lett 332:237–248

Roos WP, Thomas AD, Kaina B (2016) DNA damage and the balance between survival and death in cancer biology. Nat Rev Cancer 16:20–33

Roth M, Obaidat A, Hagenbuch B (2012) OATPs, OATs and OCTs: the organic anion and cation transporters of the SLCO and SLC22A gene superfamilies. https://doi.org/10.1111/bph.2011.164.issue-7

Rowe C, Goldring CEP, Kitteringham NR, et al (2010) Network analysis of primary hepatocyte dedifferentiation using a shotgun proteomics approach. J Proteome Res 9:2658–2668. https://doi.org/10.1021/pr1001687

Roy A, Ganguly A, BoseDasgupta S, et al (2008) Mitochondria-dependent reactive oxygen species-mediated programmed cell death induced by 3,3′-diindolylmethane through inhibition of F0F1-ATP synthase in unicellular protozoan parasite Leishmania donovani. Mol Pharmacol 74:1292–1307. https://doi.org/10.1124/mol.108.050161

Ruan J, Liao C, Ye Y, Lin G (2014a) Lack of metabolic activation and predominant formation of an excreted metabolite of nontoxic platynecine-type pyrrolizidine alkaloids. Chem Res Toxicol 27:7–16. https://doi.org/10.1021/tx4004159

Ruan J, Yang M, Fu P, et al (2014b) Metabolic activation of pyrrolizidine alkaloids: Insights into the structural and enzymatic basis. Chem Res Toxicol 27:1030–1039. https://doi.org/10.1021/tx500071q

Rubiolo P, Pieters L, Calomme M, et al (1992) Mutagenicity of pyrrolizidine alkaloids in the Salmonella typhimurium/mammalian microsome system. Mutat Res 281:143–147

Rundle S, Bradbury A, Drew Y, Curtin NJ (2017) Targeting the ATR-CHK1 axis in cancer therapy. Cancers (Basel) 9:. https://doi.org/10.3390/cancers9050041

Ruoß M, Vosough M, Königsrainer A, et al (2020) Towards improved hepatocyte cultures: Progress and limitations. Food and Chemical Toxicology 138

Rutz L, Gao L, Küpper JH, Schrenk D (2020) Structure-dependent genotoxic potencies of selected pyrrolizidine alkaloids in metabolically competent HepG2 cells. Arch Toxicol 94:4159–4172. https://doi.org/10.1007/s00204-020-02895-z

Sahoo S, Aurich MK, Jonsson JJ, Thiele I (2014) Membrane transporters in a human genome-scale metabolic knowledgebase and their implications for disease. Front Physiol 5 MAR

Saldivar JC, Cortez D, Cimprich KA (2017) The essential kinase ATR: Ensuring faithful duplication of a challenging genome. Nat Rev Mol Cell Biol 18:622–636. https://doi.org/10.1038/nrm.2017.67

Sander M, Cadet J, Casciano DA, et al (2004) Proceedings of a workshop on DNA adducts: Biological significance and applications to risk assessment Washington, DC, April 13-14, 2004. In: Toxicology and Applied Pharmacology. pp 1–20

Sanderson BJS, Clark AM (1993) Micronuclei in adult and foetal mice exposed in vivo to heliotrine, urethane, monocrotaline and benzidine. Mutat Res 285:27

Sarkar C, Mondal M, Khanom B, et al (2021) Heliotropium indicum L.: From Farm to a Source of Bioactive Compounds with Therapeutic Activity. Evidence-based Complementary and Alternative Medicine 2021

Schärer OD (2013) Nucleotide excision repair in Eukaryotes. Cold Spring Harb Perspect Biol 5

Schramm S, Köhler N, Rozhon W (2019) Pyrrolizidine alkaloids: Biosynthesis, biological activities and occurrence in crop plants. Molecules 24

Schrenk D, Fahrer J, Allemang A, et al (2022) Novel Insights into Pyrrolizidine Alkaloid Toxicity and Implications for Risk Assessment: Occurrence, Genotoxicity, Toxicokinetics, Risk Assessment-A Workshop Report. Planta Med 88:98–117

Schwegler JS, R. Lucius (2021) Der Mensch - Anatomie und Physiologie, 7th edn. Thieme

Sekiguchi M, Matsushita N (2022) DNA Damage Response Regulation by Histone Ubiquitination. Int J Mol Sci 23:. https://doi.org/10.3390/ijms23158187

Seol JH, Shim EY, Lee SE (2018) Microhomology-mediated end joining: Good, bad and ugly. Mutation Research - Fundamental and Molecular Mechanisms of Mutagenesis 809:81–87

Sharma N, Zhu Q, Wani G, et al (2014) USP3 counteracts RNF168 via deubiquitinating H2A and γh2AX at lysine 13 and 15. Cell Cycle 13:106–114. https://doi.org/10.4161/cc.26814

Shiloh Y, Ziv Y (2013) The ATM protein kinase: Regulating the cellular response to genotoxic stress, and more. Nat Rev Mol Cell Biol 14:197–210

Shumaker RC, Hsu IC, Allen JR (1976) Localisation and tissue effect's of tritiated dehydroretronecine in young rats. J Pathol 119:21–28. https://doi.org/10.1002/path.1711190105

Silva AL, Oliveira JL, do Nascimento RP, et al (2023) Monocrotaline induces acutely cerebrovascular lesions, astrogliosis and neuronal degeneration associated with behavior changes in rats: A model of vascular damage in perspective. Neurotoxicology 94:59–70. https://doi.org/10.1016/j.neuro.2022.10.017

Silva JL, Lima CGS, Rangel LP, et al (2020) Recent synthetic approaches towards small molecule reactivators of p53. Biomolecules 10

Skoryk OD, Horila M V. (2023) Oxidative stress and disruption of the antioxidant defense system as triggers of diseases. Regul Mech Biosyst 14:665–672. https://doi.org/10.15421/022395

Smith HL, Southgate H, Tweddle DA, Curtin NJ (2020) DNA damage checkpoint kinases in cancer. Expert Rev Mol Med 22

Song Z, He Y, Ma J, et al (2020) Pulmonary toxicity is a common phenomenon of toxic pyrrolizidine alkaloids. J Environ Sci Health C Toxicol Carcinog 38:124–140. https://doi.org/10.1080/26896583.2020.1743608

Stegelmeier BL (2011) Pyrrolizidine Alkaloid-Containing Toxic Plants (Senecio, Crotalaria, Cynoglossum, Amsinckia, Heliotropium, and Echium spp.). Veterinary Clinics of North America - Food Animal Practice 27:419–428

Stegelmeier BL, Colegate SM, Brown AW (2016) Dehydropyrrolizidine alkaloid toxicity, cytotoxicity, and carcinogenicity. Toxins (Basel) 8

Stickel F, Seitz HK (2000) The efficacy and safety of comfrey. Public Health Nutr 3:501–508

Sugano K, Kansy M, Artursson P, et al (2010) Coexistence of passive and carrier-mediated processes in drug transport

Sundareson AE (1942) An experimental study of placental permeability to cirrhogenic poisons. J Pathol Bacteriol 54:289–198

Tábuas B, Cruz Barros S, Diogo C, et al (2024) Pyrrolizidine Alkaloids in Foods, Herbal Drugs, and Food Supplements: Chemistry, Metabolism, Toxicological Significance, Analytical Methods, Occurrence, and Challenges for Future. Toxins (Basel) 16

Takanashi H, Umeda M, Hirono I (1980) CHROMOSOMAL ABERRATIONS AND MUTATION IN CULTURED MAMMALIAN CELLS INDUCED BY PYRROLIZIDINE ALKALOIDS. Mutat Res 78:67–77

Tamariz J, Burgueño-Tapia E, Vázquez MA, Delgado F (2018) Pyrrolizidine Alkaloids. In: Alkaloids: Chemistry and Biology. Academic Press Inc., pp 1–314

Tan Y, Zheng S (2023) Clinicopathological characteristics and diagnosis of hepatic sinusoidal obstruction syndrome caused by Tusanqi - Case report and literature review. Open Med 18:. https://doi.org/10.1515/med-2023-0737

Teschke R, Vongdala N, Quan N Van, et al (2021) Metabolic toxification of 1,2-unsaturated pyrrolizidine alkaloids causes human hepatic sinusoidal obstruction syndrome: The update. Int J Mol Sci 22

To YC, Pan Y, Yan X, et al (2024) The toxicokinetic and metabolism of structurally diverse pyrrolizidine alkaloids in rats. J Ethnopharmacol 321:. https://doi.org/10.1016/j.jep.2023.117390

Tu M, Li L, Lei H, et al (2014) Involvement of organic cation transporter 1 and CYP3A4 in retrorsine-induced toxicity. Toxicology 322:34–42. https://doi.org/10.1016/j.tox.2014.04.007

Tu M, Sun S, Wang K, et al (2013) Organic cation transporter 1 mediates the uptake of monocrotaline and plays an important role in its hepatotoxicity. Toxicology 311:225–230. https://doi.org/10.1016/j.tox.2013.06.009

US EPA (1995) (United States Environmental Protection Agency). The Use of the Benchmark Dose Approachin Health Risk Assessment, EPA/630/R-94/007

Valla DC, Cazals-Hatem D (2016) Sinusoidal obstruction syndrome. Clin Res Hepatol Gastroenterol 40:378–385

Van Schendel R, Roerink SF, Portegijs V, et al (2015) Polymerase θ is a key driver of genome evolution and of CRISPR/Cas9-mediated mutagenesis. Nat Commun 6:. https://doi.org/10.1038/ncomms8394

Vlatkovic T, Veldwijk MR, Giordano FA, Herskind C (2022) Targeting Cell Cycle Checkpoint Kinases to Overcome Intrinsic Radioresistance in Brain Tumor Cells. Cancers (Basel) 14:. https://doi.org/10.3390/cancers14030701

Waizenegger J, Braeuning A, Templin M, et al (2018) Structure-dependent induction of apoptosis by hepatotoxic pyrrolizidine alkaloids in the human hepatoma cell line HepaRG: Single versus repeated exposure. Food and Chemical Toxicology 114:215–226. https://doi.org/10.1016/j.fct.2018.02.036

Wang C, Li Y, Gao J, et al (2011) The comparative pharmacokinetics of two pyrrolizidine alkaloids, senecionine and adonifoline, and their main metabolites in rats after intravenous and oral administration by UPLC/ESIMS. Anal Bioanal Chem 401:275–287. https://doi.org/10.1007/s00216-011-5075-3

Wang L, Prasad B, Salphati L, et al (2015) Interspecies variability in expression of hepatobiliary transporters across human, dog, monkey, and rat as determined by quantitative

proteomics. Drug Metabolism and Disposition 43:367–374. https://doi.org/10.1124/dmd.114.061580

Ward JF (1988) DNA Damage Produced by Ionizing Radiation in Mammalian Cells: Identities, Mechanisms of Formation, and Reparability. Prog Nucleic Acid Res Mol Biol 35:

Wehner FC, Thiel PG, Van Rensburg SJ (1979) MUTAGENICITY OF ALKALOIDS IN THE SALMONELLA/MICROSOME SYSTEM. Mutat Res 66:187–190

Westerink WMA, Schoonen WGEJ (2007) Cytochrome P450 enzyme levels in HepG2 cells and cryopreserved primary human hepatocytes and their induction in HepG2 cells. Toxicology in Vitro 21:1581–1591. https://doi.org/10.1016/j.tiv.2007.05.014

Weston PA, Weston LA, Hildebrand S (2013) Metabolic profiling in Echium plantagineum: Presence of bioactive pyrrolizidine alkaloids and napthoquinones from accessions across southeastern Australia. Phytochemistry Reviews 12:831–837

WHO-IPCS (1988) (World Health Organisation-International Programme on Chemical Safety), 1988. Pyrrolizidine alkaloids. Environmental Health Criteria 80. WHO, Geneva, 1-345. Available from http://www.inchem.org/documents/ehc/ehc/ehc080.htm

Widjaja F, Alhejji Y, Rietjens IMCM (2022) The Role of Kinetics as Key Determinant in Toxicity of Pyrrolizidine Alkaloids and Their N-Oxides. Planta Med 88:130–143

Wiedenfeld H (2011) Plants containing Pyrrolizidine Alkaloids-Toxicity and Problems. 28:282–292. https://doi.org/10.1080/19440049.2010.541288ï

Wiedenfeld H, Edgar J (2011) Toxicity of pyrrolizidine alkaloids to humans and ruminants. Phytochemistry Reviews 10:137–151. https://doi.org/10.1007/s11101-010-9174-0

Wiedenfeld H, Roeder E, Bourauel T, Edgar J (2008) Pyrrolizidine Alkaloids - Structure and Toxicity, V&R unipress, Bonn University Press, Goettingen, Germany

Williams L, Chou MW, Yan J, et al (2002) Toxicokinetics of riddelliine, a carcinogenic pyrrolizidine alkaloid, and metabolites in rats and mice. Toxicol Appl Pharmacol 182:98–104. https://doi.org/10.1006/taap.2002.9441

Wilson DM, Bohr VA (2007) The mechanics of base excision repair, and its relationship to aging and disease. DNA Repair (Amst) 6:544–559. https://doi.org/10.1016/j.dnarep.2006.10.017

Xia Q, Chou MW, Kadlubar FF, et al (2003) Human liver microsomal metabolism and DNA adduct formation of the tumorigenic pyrrolizidine alkaloid, riddelliine. Chem Res Toxicol 16:66–73. https://doi.org/10.1021/tx025605i

Xia Q, Chou MW, Lin G, Fu PP (2004) Metabolic formation of DHP-derived DNA adducts from a representative otonecine type pyrrolizidine alkaloid clivorine and the extract of Ligularia hodgsonnii hook. Chem Res Toxicol 17:702–708. https://doi.org/10.1021/tx030030q

Xia Q, He X, Ma L, et al (2018) Pyrrolizidine Alkaloid Secondary Pyrrolic Metabolites Construct Multiple Activation Pathways Leading to DNA Adduct Formation and Potential Liver Tumor Initiation. Chem Res Toxicol 31:619–628. https://doi.org/10.1021/acs.chemrestox.8b00096

Xia Q, Zhao Y, Von Tungeln LS, et al (2013) Pyrrolizidine alkaloid-derived DNA adducts as a common biological biomarker of pyrrolizidine alkaloid-induced tumorigenicity. Chem Res Toxicol 26:1384–1396. https://doi.org/10.1021/tx400241c

Xiao L, Hu L, Chu H, et al (2022) Retrorsine Cooperates with Gut Microbiota to Promote Hepatic Sinusoidal Obstruction Syndrome by Disrupting the Gut Barrier. J Clin Transl Hepatol 10:1086–1098. https://doi.org/10.14218/JCTH.2021.00398

Xiao R, Zhu L, Su Y, et al (2019) Monocrotaline pyrrole induces pulmonary endothelial damage through binding to and release from erythrocytes in lung during venous blood reoxygenation. Am J Physiol Lung Cell Mol Physiol 316:798–809. https://doi.org/10.1152/ajplung.00279.2018.-Monocrotaline

Xiong F, Jiang K, Chen Y, et al (2020) Protein cross-linking in primary cultured mouse hepatocytes by dehydropyrrolizidine alkaloids: Structure–toxicity relationship. Toxicon 186:4–11. https://doi.org/10.1016/j.toxicon.2020.07.015

Xu J, Wang W, Yang X, et al (2019) Pyrrolizidine alkaloids: An update on their metabolism and hepatotoxicity mechanism. Liver Res 3:176–184

Yan CC, Huxtable RJ (1995) Relationship between glutathione concentration and metabolism of the pyrrolizidine alkaloid, monocrotaline, in the isolated, perfused liver. Toxicol Appl Pharmacol 130:132–139. https://doi.org/10.1006/taap.1995.1017

Yan X, Kang H, Feng J, et al (2016) Identification of toxic pyrrolizidine alkaloids and their common hepatotoxicity mechanism. Int J Mol Sci 17:. https://doi.org/10.3390/ijms17030318

Yang M, Ma J, Ruan J, et al (2020) Absorption difference between hepatotoxic pyrrolizidine alkaloids and their N-oxides – Mechanism and its potential toxic impact. J Ethnopharmacol 249

Yang M, Ma J, Ruan J, et al (2019) Intestinal and hepatic biotransformation of pyrrolizidine alkaloid N-oxides to toxic pyrrolizidine alkaloids. Arch Toxicol 93:2197–2209. https://doi.org/10.1007/s00204-019-02499-2

Yang M, Ruan J, Gao H, et al (2017) First evidence of pyrrolizidine alkaloid N-oxide-induced hepatic sinusoidal obstruction syndrome in humans. Arch Toxicol 91:3913–3925. https://doi.org/10.1007/s00204-017-2013-y

Yang NJ, Hinner MJ (2015) Getting across the cell membrane: an overview for small molecules, peptides, and proteins. Methods Mol Biol 1266:29–53

Yang YC, Crowder J, Wardle NJ, et al (2011) 1H NMR study of monocrotaline and its metabolites in human blood. Food and Chemical Toxicology 49:2793–2799. https://doi.org/10.1016/j.fct.2011.07.063

Yang YC, Yan J, Doerge DR, et al (2001) Metabolic activation of the tumorigenic pyrrolizidine alkaloid, riddelliine, leading to DNA adduct formation in vivo. Chem Res Toxicol 14:101–109. https://doi.org/10.1021/tx000150n

Yousefzadeh M, Henpita C, Vyas R, et al (2021) Dna damage—how and why we age? Elife 10:1–17. https://doi.org/10.7554/eLife.62852

Zannini L, Delia D, Buscemi G (2014) CHK2 kinase in the DNA damage response and beyond. J Mol Cell Biol 6:442–457. https://doi.org/10.1093/jmcb/mju045

Zeng G, Apte U, Cieply B, et al (2007) siRNA-mediated β-catenin knockdown in human hepatoma cells results in decreased growth and survival. Neoplasia 9:951–959. https://doi.org/10.1593/neo.07469

Zeng YC, Sobti M, Quinn A, et al (2023) Structural basis of promiscuous substrate transport by Organic Cation Transporter 1. Nat Commun 14:. https://doi.org/10.1038/s41467-023-42086-9

Zha S, Guo C, Boboila C, et al (2011) ATM damage response and XLF repair factor are functionally redundant in joining DNA breaks. Nature 469:250–254. https://doi.org/10.1038/nature09604

Zhao Y, Xia Q, Gamboa Da Costa G, et al (2012) Full structure assignments of pyrrolizidine alkaloid DNA adducts and mechanism of tumor initiation. Chem Res Toxicol 25:1985–1996. https://doi.org/10.1021/tx300292h

Zhou B-BS, Elledge SJ (2000) The DNA damage response: putting checkpoints in perspective. Nature 408:433–439

Zhu L, Xue J, Xia Q, et al (2017) The long persistence of pyrrolizidine alkaloid-derived DNA adducts in vivo: kinetic study following single and multiple exposures in male ICR mice. Arch Toxicol 91:949–965. https://doi.org/10.1007/s00204-016-1713-z

Zhu Y, Zhang S, Shao Y, et al (2024) Regulatory role of oxidative stress in retrorsine – Induced apoptosis and autophagy in primary rat hepatocytes. Ecotoxicol Environ Saf 279:. https://doi.org/10.1016/j.ecoenv.2024.116515

Zou L, Elledge SJ (2003) Sensing DNA damage through ATRIP recognition of RPA-ssDNA complexes. Science (1979) 300:1542–1548. https://doi.org/10.1126/science.1083592

Zou L, Liu D, Elledge SJ, et al (2003) Replication protein A-mediated recruitment and activation of Rad17 complexes

Permissions

Curriculum Vitae

Work experience

05.2023 – present	**Safety Scientist** Kao Germany GmbH, R&D, Darmstadt
04.2014 – 09.2014	**Temporary position, GMP (Chemistry laboratory)** Institute SGS Fresenius, Taunusstein Neuhof
08.2013 – 01.2014	**Practical Part of Advanced Technical College Certificate** Institute of Forensic Medicine, Department of Toxicology, Mainz

Education

2020 – present	**Advanced Training Program for Certification as "Fachtoxikologe/ Fachtoxikologin DGPT"**
2019 – 2025	**PhD (rer. nat.) in Toxicology** University of Kaiserslautern-Landau, Kaiserslautern, Thesis: Investigation of the hepatotoxic potency of selected genotoxic pyrrolizidine alkaloids and the significance of the DNA damage response (submitted)
2017 – 2019	**Master of Science in Food Chemistry** Justus Liebig University, Giessen Thesis: Determination of substance-dependent parameters for toxicokinetic modelling of pyrrolizidine alkaloids using liquid chromatography in combination with mass spectrometry, completed at the federal institute for risk assessment (BfR)
2014 – 2017	**Bachelor of Science in Food Chemistry** Justus Liebig University, Giessen Thesis: Quantitation of vitamin D in a vegetarian meat replacer based on fungal mycelia
2011 – 2013	**Education as a Chemical-Technical Assistant (CTA) and Advanced Technical College Certificate ("Fachholschulreife")** Kerschensteinerschule, Wiesbaden
2005 – 2011	**Secondary School Diploma („Realschulabschluss")** IGS Obere Aar, Taunusstein Hahn

Publication list

[4] A. Lehmann*, M. Haas*, J. Tänzer, G. Hamscher, C. Kloft, A. These*, C. Hethey*, **Characterization of Lipophilicity and Blood Partitioning of Pyrrolizidine Alkaloids and Their *N*-Oxides *in vitro* and in Silico for Toxicokinetic Modeling**, Planta Medica, 2025; DOI: 10.1055/a-2523-3987

*These authors contributed equally to this work

[3] M. Haas, G. Ackermann, J.-H. Küpper, H. Glatt, D. Schrenk, J. Fahrer, **OCT1-dependent uptake of structurally diverse pyrrolizidine alkaloids in human liver cells is crucial for their genotoxic and cytotoxic effects**, Arch. Toxicol.; 2023; PMID: 37676300

[2] M. Haas, K. Wirachowski, L. Thibol, J.-H. Küpper, D. Schrenk, J. Fahrer; **Potency ranking of pyrrolizidine alkaloids in metabolically competent human liver cancer cells and primary human hepatocytes using a genotoxicity test battery**, Arch. Toxicol.; 2023; PMID: 36928417

[1] A. Jiso, P. Demuth, M. Bachowsky, M. Haas, N. Seiwert, D. Heylmann, B. Rasenberger, M. Christmann, L. Dietrich, T. Brunner, Riyanti, T. Schäberle, An. Plubrukarn, J. Fahrer; **Natural Merosesquiterpenes activate the DNA damage response via DNA strand break formation and trigger apoptotic cell death in p53-wild-type and mutant colorectal cancer**; Cancers; 2021; PMID: 34209047

Congress contributions

20.03.2024 – 22.03.2024	**34th Gesellschaft für Umwelt- und Mutationsforschung (GUM) Meeting, Kaiserslautern**
	Poster presentation
28.03.2023 – 29.03.2023	**Regionalverbandstagung Südwest der LchG, Karlsruhe**
	Oral presentation
05.10.2022 – 07.10.2022	**33rd Gesellschaft für Umwelt- und Mutationsforschung (GUM) Meeting, Würzburg**
	Oral presentation
20.09.2022 – 23.09.2022	**IMB/SFB 1361 Conference – Restore, Reorganise, Repurpose: The many faces of DNA repair, Mainz**
	Poster presentation
07.03.2022 – 10.03.2022	**7th German Pharm-Tox Summit 2022, Online**
	Oral presentation
05.09.2021 – 08.09.2021	**69th International Congress and Annual Meeting of the Society for Medicinal Plant and Natural Product Research (GA) Annual Meeting, Online**
	Oral presentation
30.08.2021 – 01.09.2021	**49. Deutscher Lebensmittelchemikertag, Online**
	Poster presentation
24.06.2021 – 25.06.2021	**Jubiläumskongress Phytotherapie 2021, Online**
	Oral presentation
01.03.2021 – 03.03.2021	**6th German Pharm-Tox Summit 2021, Online**
	Oral presentation

Acknowledgements

I would like to express my deepest gratitude to my supervisor, **Prof. Dr. Jörg Fahrer**, for the opportunity to be part of his research group and for his invaluable mentorship, continuous support, and insightful guidance throughout this project. His expertise and encouragement have been instrumental in shaping this work. I also sincerely appreciate the resources and stimulating research environment he provided. It has been an honor to be part of your team as a PhD student!

I am also grateful to **Prof. Dr. Dieter Schrenk** for his valuable advices and support throughout the PA project and for serving as the second examiner of my dissertation. Our scientific discussions were truly inspiring, and I thoroughly enjoyed them.

A special thank you to **Prof. Dr. Stefan Kubik** for his role as chairman in my PhD defense.

Moreover, I sincerely appreciate **Dr. Tina Kostka** for her thoughtful insights, enjoyable coffee breaks, and for being part of the examination committee. Your kindness and support made a meaningful impact.

I extend my heartfelt thanks to my closed colleagues, **Dr. Max, Simon**, **Philipp**, **Gabriel**, **Caro**, **Ann-Kathrin** and **Lea Thibol**, for their collaboration, engaging discussions, and unwavering encouragement. Your shared knowledge and camaraderie made this journey both enriching and enjoyable. I just can't thank you enough for the time we spent together, whether it was in the lab, during coffee and lunch breaks, or at social gatherings. Furthermore, I enjoyed the time with all **new colleagues**, which joined by the end of my time in the working group. I had an absolute blast working with such a great team! Dear **Max**, I truly valued our time as office buddies and miss our light-hearted and amusing moments.

I am also grateful to all the **students**, who contributed to my research and made lab work even more enjoyable. Your support and enthusiasm have significantly enriched the PA project.

Additionally, I sincerely appreciate the funding and guidance provided by the **Kooperation Phytopharmaka** society and its members, whose contributions played a key role in the success of this research.

A special thanks to all **collaboration partners**, which were not previously mentioned, for their contributions to both publications.

Last but not least, I am deeply thankful to my **family, Feyza, Fabio** and **Florian,** for their patience, encouragement, and unwavering belief in me throughout this process. A lovely thank you goes to **Feyza** for her unconditional support in the last years.

Declaration of interest

Hiermit erkläre ich, Manuel Haas, dass ich die vorliegende Dissertation mit dem Titel „Untersuchung der hepatotoxischen Potenz ausgewählter genotoxischer Pyrrolizidinalkaloide und Bedeutung der DNA-Schadensantwort“ (engl.: „*Investigation of the hepatotoxic potency of selected genotoxic pyrrolizidine alkaloids and the significance of the DNA damage response*“) selbstständig verfasst, ausschließlich die in der Arbeit angegebenen Quellen und Hilfsmittel benutzt und alle Mitwirkende an den entsprechenden Ergebnissen explizit zitiert habe.

Die Dissertation wurde ausschließlich beim Fachbereich Chemie der RPTU eingereicht und kein anderes Promotionsverfahren an einer weiteren Hochschule beantragt oder eröffnet. Die erforderlichen Unterlagen für den Promotionsantrag, sowie die Anforderungen zum Promotionsverfahren sind gemäß der geänderten Promotionsordnung vom 07.Oktober 1999 des Fachbereiches Chemie der ehemalig bezeichneten Technischen Universität Kaiserslautern in der vorliegenden Dissertation beachtet und beigefügt worden.

Ort, Datum	Manuel Haas